Aalto University
School of Engineering

Olli-Ville Laukkanen

Low-temperature rheology of bitumen and its relationship with chemical and thermal properties

Thesis submitted for examination for the degree of Master of Science in Technology.

Espoo 4.5.2015
Supervisor: Professor Terhi Pellinen
Advisors: Professor H. Henning Winter
M.Sc. (tech) Timo Blomberg

Aalto University
School of Engineering

Aalto University, P.O. BOX 11000, 00076 AALTO
www.aalto.fi

Abstract of master's thesis

Author Olli-Ville Laukkanen

Title of thesis Low-temperature rheology of bitumen and its relationships with chemical and thermal properties

Degree programme Civil and Environmental Engineering

Major/minor Highway Engineering **Code** Yhd-10

Thesis supervisor Professor Terhi Pellinen

Thesis advisors Professor H. Henning Winter, M.Sc. (tech) Timo Blomberg

Date 4.5.2015 **Number of pages** 115+71 **Language** English

Abstract

The thermal cracking performance of asphalt pavements is largely governed by the properties of the bituminous binder, and thus the low-temperature rheological characterization of bitumen is of great importance. Recently, a novel testing technique has been developed for the measurement of the low-temperature rheological properties of bituminous materials. This testing technique, commonly referred to as the 4-mm DSR, uses a 4-mm parallel plate geometry on a dynamic shear rheometer (DSR) with radial instrument compliance corrections. However, very little data produced by using the 4-mm DSR technique is currently available in the literature.

The primary objective of this study was to examine the low-temperature rheological characteristics of various unmodified bitumens by using the 4-mm DSR technique. In addition, the correlations of the chemical and thermal properties with the low-temperature rheology of bitumen were investigated. The secondary purpose of this thesis was to study physical aging in bitumen.

The 4-mm DSR technique was used to test twenty-seven bitumen samples originating from various crude oil sources and refineries. The chemical properties of the bitumens were described in terms of their molecular weight properties, as measured by gel permeation chromatography (GPC), and aromatic properties, as measured by ultraviolet-visible spectroscopy (UV-vis), infrared spectroscopy (FT-IR) and refractive index (RI) techniques. The thermal properties of the studied bitumens, including the glass transition temperatures (T_g), were determined by differential scanning calorimetry (DSC).

Both horizontal and vertical shifts were needed to produce smooth master curves in the vicinity of T_g. The temperature dependence of horizontal shift factors was shown to accurately follow the Kaelble-WLF equation in the temperature range of T_g-30 K to T_g+115 K. The calculated relaxation time spectra $H(\tau)$ evidenced a transition from small-scale molecular to large-scale cooperative relaxation processes when bitumen was cooled below its T_g. It was shown that the low-temperature rheological properties of bitumen can be fairly accurately predicted from the molecular weight and aromatic properties. Physical aging in bitumen was successfully analyzed by means of time-aging time superposition, and, based on the limited data available, equilibrium is attained in approximately 2-3 days at T_g. However, additional studies are needed to properly assess the effect of physical aging on the low-temperature rheological properties of various bitumens.

Keywords bitumen, rheology, 4-mm DSR, bitumen chemistry, differential scanning calorimetry, physical aging

Aalto-yliopisto
Insinööritieteiden korkeakoulu

Aalto-yliopisto, PL 11000, 00076 AALTO
www.aalto.fi

Diplomityön tiivistelmä

Tekijä Olli-Ville Laukkanen

Työn nimi Bitumin kylmälämpötilareologia ja sen yhteys kemiallisiin ja termisiin ominaisuuksiin

Koulutusohjelma Yhdyskunta- ja ympäristötekniikka

Pää-/sivuaine Tietekniikka **Koodi** Yhd-10

Työn valvoja Professori Terhi Pellinen

Työn ohjaajat Professori H. Henning Winter, DI Timo Blomberg

Päivämäärä 4.5.2015 **Sivumäärä** 115+71 **Kieli** englanti

Tiivistelmä

Asfalttipäällysteen pakkashalkeilu on suuressa määrin riippuvaista bitumisen sideaineen ominaisuuksista, ja siksi bitumin reologinen karakterisointi alhaisissa lämpötiloissa on erittäin tärkeää. Äskettäin bitumin reologisten kylmälämpötilaominaisuuksien mittaamiseen on kehitetty uudenlainen mittaustekniikka. Tässä niin kutsutussa 4-mm DSR -mittaustekniikassa dynaaminen leikkausreometri (DSR) on varustettu 4 mm:n levy-levy-geometrialla, ja mittaustulokset korjataan säteittäisen laitekompliansin suhteen. Tähän mennessä on julkaistu kuitenkin vain hyvin rajallinen määrä 4-mm DSR -tekniikalla tuotettua dataa.

Tämän työn ensisijainen tavoite oli tutkia modifioimattomien bitumien reologisia kylmälämpötilaominaisuuksia 4-mm DSR -tekniikalla. Lisäksi tutkittiin kylmälämpötilaominaisuuksien yhteyttä bitumin kemiallisiin ja termisiin ominaisuuksiin. Työn toissijainen tavoite oli tutkia bitumin fysikaalista vanhenemista.

Tutkimusta varten kerättiin 27 bituminäytettä, jotka olivat peräisin useista raakaöljylähteistä ja öljynjalostamoista, ja näiden näytteiden ominaisuuksia tutkittiin 4-mm DSR -tekniikalla. Bitumien kemiallisia ominaisuuksia kuvattiin geelisuodatuskromatografialla (GPC) mitattujen molekyylipaino-ominaisuuksien avulla, sekä ultravioletti-näkyvän valon spektroskopialla (UV-vis), infrapunaspektroskopialla (FT-IR) ja taitekerroinmittauksilla (RI) määritettyjen aromaattisten ominaisuuksien avulla. Bitumien termisiä ominaisuuksia, mukaan lukien niiden lasisiirtymälämpötiloja (T_g), tutkittiin differentiaalisen pyyhkäisykalorimetrian (DSC) avulla.

Sekä vaaka- että pystysuuntaisten siirtojen käyttö oli tarpeen kunnollisten master-käyrien aikaansaamiseksi T_g:n läheisyydessä. Vaakasiirtokertoimien lämpötilariippuvuuden huomattiin noudattavan tarkasti Kaelble-WLF-yhtälöä lämpötila-alueella T_g-30 K … T_g+115 K. Lasketut relaksaatioaikaspektrit $H(\tau)$ osoittivat siirtymän pienen mittakaavan molekulaarisista relaksaatioprosesseista suuremman mittakaavan relaksaatioprosesseihin tapahtuvan jäähdytettäessä bitumi sen T_g:n alapuolelle. Bitumin reologiset kylmälämpötilaominaisuudet pystyttiin ennustamaan melko tarkasti molekyylipaino- ja aromaattisten ominaisuuksien perusteella. Bitumin fysikaalista vanhenemista analysoitiin onnistuneesti aika-vanhenemisaika-superposition avulla, ja tämän tutkimuksen rajallisten mittaustulosten perusteella kestää noin 2-3 päivää ennen kuin tasapainotila fysikaalisen vanhenemisen suhteen saavutetaan T_g:ssa. Lisätutkimukset ovat kuitenkin tarpeen, jotta fysikaalisen vanhenemisen vaikutusta eri bitumien reologisiin kylmälämpötilaominaisuuksiin voitaisiin kunnolla arvioida.

Avainsanat bitumi, reologia, 4-mm DSR, bitumikemia, differentiaalinen pyyhkäisykalorimetria, fysikaalinen vanheneminen

Acknowledgements

This thesis was commissioned by Nynas Oy and performed in the Department of Polymer Science and Engineering at the University of Massachusetts Amherst. This thesis is a part of a joint research project between Aalto University and Nynas Oy that focuses on the low-temperature rheological characterization of bituminous binders. The thesis supervisor was Professor Terhi Pellinen from Aalto University School of Engineering, and the advisors of the thesis were Professor H. Henning Winter from the University of Massachusetts Amherst and M.Sc. (tech) Timo Blomberg from Nynas Oy. In addition, Ph.D. Hilde Soenen from Nynas NV significantly contributed to the content of this thesis. This thesis was mainly funded by Nynas Oy. The financial support from the Rapal student fund and from the Finnish Association of Civil Engineers is also greatly acknowledged.

I would like to thank Terhi Pellinen not only for supervising my thesis, but also for introducing me to the world of rheological research approximately four years ago. My great thanks go also to H. Henning Winter who kindly invited me to join his research group, and therefore demonstrated great courage in pursuing a new research direction. In addition, I would like to express my sincere gratitude to Timo Blomberg for providing valuable comments on the conducted work and on the thesis manuscript. Enormous thanks also to Hilde Soenen who provided access to the extensive sample set investigated in this thesis and gave valuable comments on the obtained experimental results. Moreover, she is greatly acknowledged for providing all the chemical and thermal characterization data of the investigated bitumens, and also the rheological frequency sweep data measured with the 8-mm and 25-mm parallel plate geometries. I would also like to extend special thanks to Malvern Instruments Ltd for helping in rheometer-related technical issues. In particular, I would like to thank John Casola for providing the 4-mm parallel plate geometry of Malvern Kinexus rheometer used in the experimental section of this thesis, and Philip Rolfe who helped me to improve the quality of the low-temperature rheological data. My humble thanks also to Mike Farrar and Alec Otto Cookman from Western Research Institute (WRI) for fruitful discussions about the low-temperature rheology of bitumen and for providing the test sequence for the 4-mm DSR experiments. Further, my sincere gratitude goes to my co-workers in the Winter group – Ben, Brian, David, Varick and Vijesh – for help in and outside the laboratory. I also want to acknowledge my current and former colleagues in the Highway Engineering research group of Aalto University School of Engineering. Finally, I would like to thank my family and friends for their support and encouragement during my thesis process and throughout my university studies.

Amherst, MA 6.4.2015

Olli-Ville Laukkanen

Table of contents

List of symbols

Symbol	Unit	Name
C_p	[J g^{-1} K^{-1}]	Heat capacity at constant pressure
C_p^g	[J g^{-1} K^{-1}]	Glass heat capacity at constant pressure
C_p^l	[J g^{-1} K^{-1}]	Liquid heat capacity at constant pressure
E_g	[kJ mol^{-1}]	Apparent activation energy for viscous flow at T_g
G^*	[Pa]	Complex modulus in small-amplitude oscillatory shear
$\|G^*\|$	[Pa]	Absolute magnitude of G^*
G'	[Pa]	Storage modulus in small-amplitude oscillatory shear
G'_m	[Pa]	Measured storage modulus in small-amplitude oscillatory shear when using the 4-mm parallel plate geometry
G'_s	[Pa]	Sample storage modulus in small-amplitude oscillatory shear when using the 4-mm parallel plate geometry
G''	[Pa]	Loss modulus in small-amplitude oscillatory shear
G''_m	[Pa]	Measured loss modulus in small-amplitude oscillatory shear when using the 4-mm parallel plate geometry
G''_s	[Pa]	Sample loss modulus in small-amplitude oscillatory shear when using the 4-mm parallel plate geometry
G_e	[Pa]	Equilibrium modulus (= 0 for viscoelastic liquids)
G_g	[Pa]	Glassy modulus in shear
$G(t)$	[Pa]	Relaxation modulus in shear
$H(\tau)$	[Pa]	Relaxation time spectrum
J''	[Pa^{-1}]	Loss compliance in small-amplitude oscillatory shear
$J_{instrument}$	[rad N^{-1} m^{-1}]	Radial instrument compliance
M_n	[g mol^{-1}]	Number-average molecular weight
M_w	[g mol^{-1}]	Weight-average molecular weight
M_w/M_n	[-]	Polydispersity
M_z	[g mol^{-1}]	Z-average molecular weight
M_{z+1}	[g mol^{-1}]	Z+1-average molecular weight

Q	[J]	Amount of heat
R	[J mol^{-1} K^{-1}]	Universal gas constant, 8.314 J mol^{-1} K^{-1}
R^2	[-]	Coefficient of determination
R_p	[m]	Radius of the parallel plate geometry
S	[J K^{-1}]	Entropy
$S(t)$	[Pa]	Flexural creep modulus in the BBR testing
T	[K] or [°C]	Temperature
T_∞	[K]	VFT divergence temperature
T_d	[K]	Defining temperature in the Kaelble-WLF equation
T_g	[K] or [°C]	Glass transition temperature (in this work $T_g = T_{g,mid}$)
$T_{g,onset}$	[K] or [°C]	Onset temperature of the glass transition region
$T_{g,mid}$	[K] or [°C]	Mid-point glass transition temperature
$T_{g,end}$	[K] or [°C]	Endset temperature of the glass transition region
T_r	[K]	Reference temperature in the construction of master curves
$T_{R\&B}$	[°C]	Ring-and-Ball softening point
T_v	[K]	Vogel temperature in the VFT equation
T_β	[K] or [°C]	Temperature of the highest secondary transition
a_T	[-]	Horizontal shift factor in time-temperature superposition
a_{te}	[-]	Horizontal shift factor in time-aging time superposition
b_T	[-]	Vertical shift factor in time-temperature superposition
c_1	[-]	First WLF coefficient
c_1^g	[-]	First WLF coefficient when $T_r = T_g$
c_2	[K]	Second WLF coefficient
c_2^g	[K]	Second WLF coefficient when $T_r = T_g$
h	[m]	Gap between the plates in the parallel plate geometry
k_g	[m^3]	Geometry constant used in the radial instrument compliance correction, $k_g = 2h / \pi R_p^4$ for parallel plate geometry
m	[-]	Dynamic fragility

$m(t)$ or $m_c(t)$	[-]	Logarithmic creep rate in the BBR testing
$m_r(t)$	[-]	Logarithmic creep rate in the 4-mm DSR testing
p	[-]	Significance level
r	[-]	Pearson's correlation coefficient
t	[s]	Time
$tan\ \delta$	[-]	Loss tangent in small-amplitude oscillatory shear
x	various	Viscosity, relaxation time or any other dynamic variable used in the determination of m
ΔC_p	[J g^{-1} K^{-1}]	Heat capacity change at T_g
γ	[-]	Shear strain
γ_0	[-]	Strain amplitude
δ	[°] or [rad]	Phase angle (loss angle) in small-amplitude oscillatory shear
η	[Pa s]	Viscosity
η^*	[Pa s]	Complex viscosity
η'	[Pa s]	Dynamic viscosity (in phase with strain rate)
η''	[Pa s]	Out-of-phase (with strain rate) component of η^*
μ	[-]	Aging time shift rate
v	[m^3 kg^{-1}]	Specific volume
σ	[Pa]	Shear stress
σ_0	[Pa]	Stress amplitude
τ	[s]	Relaxation time
τ_{max}	[s]	The longest relaxation time
ω	[rad s^{-1}] or [Hz]	Angular frequency of oscillation

List of abbreviations

ABCD	Asphalt Binder Cracking Device
AFM	Atomic Force Microscopy
ATR	Attenuated Total Reflection
BBR	Bending Beam Rheometer
C=C	Carbon-carbon double bond
CFS	Cyclic Frequency Sweep
DENT	Double Edge Notch Test
DPF	Dispersed Polar Fluid
DSC	Differential Scanning Calorimetry
DSR	Dynamic Shear Rheometer
DTA	Differential Thermal Analysis
DTT	Direct Tension Test
ETG	Expert Task Group
FHWA	Federal Highway Administration
FT-IR	Fourier Transform Infrared (spectroscopy)
FTT	Fracture Toughness Test
GPC	Gel Permeation Chromatography
IRIS	Interactive Rheology Information Systems
LAS	Linear Amplitude Sweep
LVE	Linear Viscoelastic
MDSC	Modulated Differential Scanning Calorimetry
MSCR	Multiple Stress Creep-Recovery
MYEGA	Mauro-Yue-Ellison-Gupta-Allan (model)
NRMSE	Normalized Root-Mean-Square Error
PAI	Physical Aging Index
PAV	Pressure Aging Vessel
PDA	Photo Diode Array

PDM	Phase Detection Microscopy
Pen	Penetration
PG	Performance Grade
PI	Penetration Index
R&B	Ring-and-Ball (softening point test)
RI	Refractive Index
RTFO	Rolling Thin Film Oven
SAOS	Small-Amplitude Oscillatory Shear
SARA	Saturates, Aromatics, Resins, Asphaltenes (fractions)
SBS	Styrene-Butadiene-Styrene
SENB	Single Edge Notched Beam (test)
SHRP	Strategic Highway Research Program
TB	Torsion Bar
TGA	Thermogravimetric Analysis
THF	Tetrahydrofurane
TRMS	Time-resolved Mechanical Spectroscopy
TRR	Time-resolved rheometry
TTS	Time-Temperature Superposition
UV-vis	Ultraviolet-visible (spectroscopy)
VFT	Vogel-Fulcher-Tammann (equation)
WLF	Williams-Landel-Ferry (equation)
WRI	Western Research Institute
YAG	Yttrium-Aluminum-Garnet
d2s	95 % limits on the difference between two test results
dmm	Decimillimeter; 1/10 mm
vGP	van Gurp-Palmen (plot)

Glossary

4-mm DSR	A testing technique employing 4-mm diameter parallel plate fixture on a dynamic shear rheometer with instrument compliance corrections; used to measure low-temperature rheological properties of bituminous binders
Activation energy for viscous flow	A characteristic of the flow that indicates the amount of energy necessary to make fluid flow
Angell plot	A T_g-normalized Arrhenius plot that is used to study the dynamic fragility of glass-forming materials
Aromaticity	A property of conjugated cycloalkenes in which the stabilization of the molecule is strong due to the ability of the electrons in the p-orbitals to delocalize and act as a framework to create a planar molecule
Bitumen	Virtually involatile, adhesive and waterproofing material derived from crude petroleum, or present in natural asphalt, which is completely or nearly completely soluble in toluene, and very viscous or nearly solid at ambient temperatures
Coefficient of determination	A number that indicates how well data fit a statistical model; in the case of linear model it is the square of the Pearson's correlation coefficient
Cole-Cole plot	A representation where storage and loss parts of a complex quantity are plotted against each other; in this work a plot of G'' vs. G' on linear scales
Cyclic frequency sweeps	Successively repeated frequency sweeps that are used to capture time-dependent changes in viscoelastic properties
Differential scanning calorimetry	A thermoanalytical method that allows the determination of physical changes in a material associated with a heat exchange
Dynamic fragility	A measure of the temperature dependence of dynamic properties at the glass transition temperature; effectively a T_g-normalized activation energy
Dynamic shear rheometer	A laboratory device used to measure the viscoelastic properties of wide range of materials; also called rotational rheometer

Gel permeation chromatography	A type of size exclusion chromatography for obtaining information on the molecular weight distributions of polymeric materials
Glass transition	The reversible transition in amorphous materials (or in amorphous regions within semicrystalline materials) from a hard and relatively brittle state into a molten or rubber-like state
Glass transition temperature	The temperature at which the glass transition occurs
Glassy modulus	The asymptotic value of complex modulus at low temperatures and/or high frequencies where the material behavior is ideally perfectly glassy
Infrared spectroscopy	A subset of absorption spectroscopy that deals with the infrared region of the electromagnetic spectrum
Master curve	A representation of rheological data over a wide range of frequencies or times "reduced" to a reference temperature, T_r; obtained as a result of time-temperature (or time-aging time) superposition
Pearson's (product-moment) correlation coefficient	A measure of the degree of linear dependence between two variables, giving a value between +1 and -1 inclusive, where +1 is the total positive correlation, 0 is no correlation, and -1 is the total negative correlation
Performance grading	A classification system which tests the bitumen for various performance qualities within specific temperature ranges
Physical aging	Structural relaxation of the glassy state toward the metastable equilibrium amorphous state, accompanied by changes in almost all physical properties
Physical hardening	See 'Physical aging'
Radial instrument compliance	Experimental artifact that results in errors in measured rheological data due to the compliances of rheometer transducer and measurement fixture; significant in the measurement of high-viscous materials
Refractive index	A dimensionless number that describes how light, or any other radiation, propagates through that medium

Relaxation time spectrum	A fundamental quantity in the linear theory of viscoelastic materials that gives a macroscopic expression of small-scale structural rearrangements in time
Rheology	The science of the deformation and flow of matter
Shift factor	The amount of horizontal or vertical shifting needed to produce master curves
Size exclusion chromatography	A chromatographic method in which molecules in solution are separated by their size, and in some cases molecular weight; see ‘Gel permeation chromatography’
Stepwise regression	Stepwise regression includes regression models in which the choice of predictive variables is carried out by an automatic procedure
Thermorheological simplicity	Obtains when all contributing retardation or relaxation mechanisms of the material have the same temperature dependence and when stress magnitudes at all times or frequencies have the same temperature dependence
Time-aging time superposition	An equivalent to time-temperature superposition where temperature is replaced by isothermal aging time; used to study physical aging
Time-resolved mechanical spectroscopy	A tool to study time-dependent changes in mechanical properties of materials with changing structure
Time-temperature superposition	A tool for describing the viscoelastic behavior of linear polymers over a broad range of times or frequencies by shifting data obtained at several temperatures to a common reference temperature
Ultraviolet–visible spectroscopy	A commonly used spectrophotometric assay that examines photons in the UV-visible region
Van Gurp-Palmen plot	A plot of the phase angle δ versus the absolute value of the complex modulus $\|G^*\|$

1. Introduction

1.1. Background

The low-temperature rheology of bituminous binders is of great interest because low-temperature cracking is one of the primary asphalt pavement failure modes observed in cold-climate roads [1]. Moreover, binder properties have been found to mainly determine the thermal cracking performance of asphalt pavements, other asphalt mixture properties being of secondary importance [2]. Low-temperature cracking typically occurs during extreme low-temperature weather, usually within a few years after pavement construction. This failure mode is visible in the asphalt pavement as transverse cracks that are caused by the binder's inability to deform to reduce stress. When the stresses exceed the asphalt binder's strength, transverse cracks appear. To reduce the frequency of low-temperature cracking failure, the strength or stress relaxation ability of the binder must be increased. For the asphalt producer, the problem is to know how to blend asphalt components to control the low-temperature properties [3].

Field studies concerned with the monitoring of pavement performance over time are becoming ever more important. However, it is very laborious and time-consuming to extract large amounts of binder from an existing asphalt pavement. To minimize this effort, a binder test that uses only small amounts of material is required. Moreover, quick data acquisition and low sampling and preparation temperatures are needed. For this purpose, a testing method that uses 4-mm parallel plate geometry in a dynamic shear rheometer (DSR) has recently been developed to measure the rheological properties of bituminous binders at low temperatures. This new testing technique is commonly referred to as "4-mm DSR". [4,5]

As is the case with many viscoelastic materials, the rheological properties of bitumen appear to be largely governed by chemical composition and molecular interactions [6-14]. In particular, Lesueur et al. [15] have suggested that the low-temperature rheology of bitumen is related to the asphaltene content. However, most relationships between the rheological and chemical properties of bitumen are also known to be dependent on crude oil source [16]. Moreover, thermal analysis methods have been used in an effort to better understand bitumen rheology [17,18].

The rheological properties of bitumen are known to change with time when held under isothermal conditions at low temperatures [19]. This phenomenon is commonly known as physical aging [20], or physical hardening in asphalt industry [21]. During the last decade or so, a great deal of research has been conducted to assess the effect of the physical aging of bitumen on low-temperature pavement performance [22-25]. It has been shown that the onset of low-temperature cracking can be more reliably predicted when the effect of physical aging on the low-temperature properties of bitumen is taken into account [26]. However, despite the undisputed importance of binder physical aging

for pavement performance, it is still not incorporated in asphalt specifications because of testing time limitations.

1.2. Research problems

A literature review reveals that in the 1990s and 2000s numerous articles were published concerning the low-temperature rheology of bitumen, e.g. [1,15,27-34]. However, the results of the older studies where DSRs have been employed to measure bitumen's low-temperature characteristics are subject to criticism. This is because in these investigations, the data measured with 8-mm parallel plate geometry have been reported without accurate instrument compliance correction. Consequently, the reliability of these test results is rather questionable.

Only during the last few years have asphalt researchers started to use the 4-mm DSR technique and systematic compliance correction to minimize the effect of instrument compliance. Thus, only a rather limited amount of data produced with this testing technique is available in the literature. Moreover, the currently available data have been produced almost exclusively in a single laboratory facility at the Western Research Institute (WRI). In order to assess the suitability of this testing method for the standard testing of bituminous binders, more interlaboratory testing should be conducted. In addition, the techniques used to analyze the low-temperature rheological data of bitumen have been somewhat limited so far, and thus novel techniques need to be introduced to gain more comprehensive understanding of the rheological nature of bitumen at sub-zero temperatures.

Although unmodified bitumens have been tested with the 4-mm DSR technique in a number of studies, e.g. [4,5,35,36], none of them has combined an extensive chemical characterization with the rheological analysis. Even in a larger perspective, very few studies exist that concern the relationship between the chemical and low-temperature mechanical properties of bitumen. During the Strategic Highway Research Program (SHRP) an extensive analysis was conducted to find correlations between the rheological and chemical properties of various unmodified bitumen samples [13]. However, it should be noted that the SHRP binders were collected as "commercial" bitumens used for highway construction and were thus limited in variation of properties to fulfil the contemporary asphalt specifications in the US. Also, a thorough comparative analysis of the thermodynamic and dynamic aspects of bitumen glass transition is yet to be published.

Traditionally, physical aging of bituminous binders has been characterized by conducting creep measurements on the bending beam rheometer (BBR) [37,38]. Although it is expected that physical aging occurs also during 4-mm DSR experiments, currently only very limited information is available concerning this topic [35]. A deeper understanding of physical aging during low-temperature rheological testing of bituminous binders is needed so that its effect on the test results could be quantified and

possibly isolated. Moreover, more comprehensive characterization of physical aging is needed for more accurate predictions of low-temperature pavement performance.

1.3. Aims and structure of the thesis

This thesis attempts to cover some of the knowledge gaps disclosed in Section 1.2 Consequently, this thesis aims to address the following three major topics:

1. Low-temperature rheology of various unmodified bitumens

    - Specifically, it will be investigated whether the thermorheological behavior of bitumen is simple at sub-zero temperatures, and consequently, whether the time-temperature superposition (TTS) principle is applicable. If TTS principle proves to be valid, dynamic master curves will be constructed and an effort will be made to model the temperature dependence of horizontal shift factors. This thesis also aims to introduce concepts and analysis techniques used in the field of glass rheology as novel methods to characterize the dynamics of bitumen at low service temperatures.

2. Correlations of chemical and thermal properties with low-temperature rheological characteristics of bitumen

    - An effort will be made to correlate the molecular weight and aromatic properties of bitumen with its low-temperature rheological behavior. Potentially, the results of such analysis could provide insight into the relation between the structural and low-temperature dynamic properties of bitumen. In addition, possible correlations between the glass transition temperatures (T_g), as measured by differential scanning calorimetry (DSC), and low-temperature rheological properties of bitumen will be investigated. The aim of this analysis is to study whether and how the low-temperature thermodynamic and dynamic properties are related in bitumen.

3. Physical aging of bitumen as studied by the 4-mm DSR technique

    - It will be investigated whether physical aging in bitumen can be effectively quantified by the 4-mm DSR method. Further, the applicability of time-resolved mechanical spectroscopy (TRMS) and time-aging time superposition principle in the analysis of physical aging data will be tested.

This thesis consists of a literature review and laboratory study. In Section 2, the most common production methods and general properties of bitumen are discussed. This discussion considers both chemical, thermal and mechanical characteristics of bitumen. The aim of this section is to provide the reader with the necessary information to understand the generic properties of the materials investigated.

Section 3 describes the basics of oscillatory rheological testing and relevant data analysis. The application of rheological testing in the asphalt industry is also discussed in terms of the performance grading of bituminous binders.

In Section 4, the low-temperature characteristics of bitumen are discussed. Firstly, traditional methods to measure the low-temperature mechanical properties of bitumen are briefly reviewed. After this, the newly proposed 4-mm DSR measurement technique and a method for the radial instrument compliance correction are introduced. The general and asphalt-specific aspects of glass transition and physical aging are discussed throughout the rest of the section.

Section 5 is an introduction to the experimental section of this thesis. The basic physical and thermal properties of the investigated bitumen samples are presented, followed by the description of the characterization techniques used in the laboratory study.

The results of the laboratory study are presented in Section 6, along with relevant analysis. A rheological analysis of the frequency sweep test results is provided in Section 6.1 with emphasis on the low-temperature test results. After this, in Section 6.2, correlations of the chemical and thermal properties of bitumen with its low-temperature rheological characteristics are investigated. In Section 6.3, the physical aging properties of bitumen are briefly studied. The results and observations of Section 6 are further discussed in Section 7.

Section 8 summarizes the findings of this thesis and provides outlook on future work.

1.4. Limitations of the research

This thesis is a part of a joint research project of Aalto University and Nynas Oy. This project mainly concerns the low-temperature rheology of bituminous binders as measured with the 4-mm DSR technique. Because of the large extent of this research project, only selected research findings are presented in this thesis. Research topics that are investigated in the complete research project but are not discussed in this thesis, include:

- The effect of aging on the low-temperature rheological properties of bitumen
- The correlation between the low-temperature rheological and fracture properties of bitumen
- The effect of Styrene-Butadiene-Styrene (SBS) polymer modification on the low-temperature rheological properties of bitumen.

In addition, the application of the 4-mm DSR technique to the characterization of bitumens modified with various polymers, waxes and chemical additives remains to be investigated in future studies. Moreover, the characterization of asphalt mastics and mixtures made with the investigated bitumens is not considered in this research project.

The rheological properties of the investigated bitumens at high and intermediate temperatures are reported elsewhere [6]. Finally, it should be noted that this thesis is mainly concerned with the low-temperature rheological characterization of unmodified bitumens, and that the results from the other characterization techniques employed in this study might not be exhaustively analyzed and presented in this work. Critical discussion of the interpretation of the chemical test results obtained in this study is provided elsewhere [6].

2. Properties of bitumen

2.1. Definition and production of bitumen

According to the current European specifications [39], bitumen is defined as a "virtually involatile, adhesive and waterproofing material derived from crude petroleum, or present in natural asphalt, which is completely or nearly completely soluble in toluene, and very viscous or nearly solid at ambient temperatures". In addition, a toluene solubility of greater than 99% is required for bitumen used in paving applications [40]. This European definition of *bitumen* is equivalent to American definitions of *asphalt* or *asphalt cement* [41]. Also terms *bituminous binder* and *asphalt binder* are used interchangeably.

Before modern oil refining technologies became available at the turn of the 20th century, bitumen was recovered only from natural sources [42]. However, nowadays bitumen is essentially obtained by the distillation of crude oil [43,44], and native bitumen is used only for small and very specific markets, generally as an additive for straight-run bitumen [45]. Atmospheric and vacuum distillation techniques are the main means to refine bitumen for road construction, while solvent refining and visbreaking production techniques are clearly of secondary importance [46]. However, the latter mentioned techniques have recently regained popularity because the current petroleum product demand patterns can only be fulfilled by the inclusion of heavier feedstock, and because the bitumen produced with these techniques is able to satisfy the stringent environmental and quality specifications of today's paving industry [6]. Further, bitumen can be treated in an air blowing unit after production as explained more in detail later in this subsection.

In the following bitumen production techniques relevant for this work are briefly described. For more detailed description of refining processes in general the reader should refer to Robinson [47].

- Distillation of straight-run bitumen: A typical distillation process is depicted in Figure 1. The process begins with the separation of the light components from the crude oil by atmospheric distillation, typically at 350 °C. In the second step, the residue from the atmospheric distillation is further refined at a slightly higher temperature (350–425 °C) under vacuum with pressures of the order of 1–10 kPa (0.01–0.1 bars) [44,48]. Bitumen is then the vacuum residue of the crude oil, corresponding to an equivalent atmospheric cut-point of typically 500 °C [48]. Typically, refiners manufacture only two grades of straight-run bitumen, a soft one and a hard one, and the intermediate grades are obtained by blending [43].

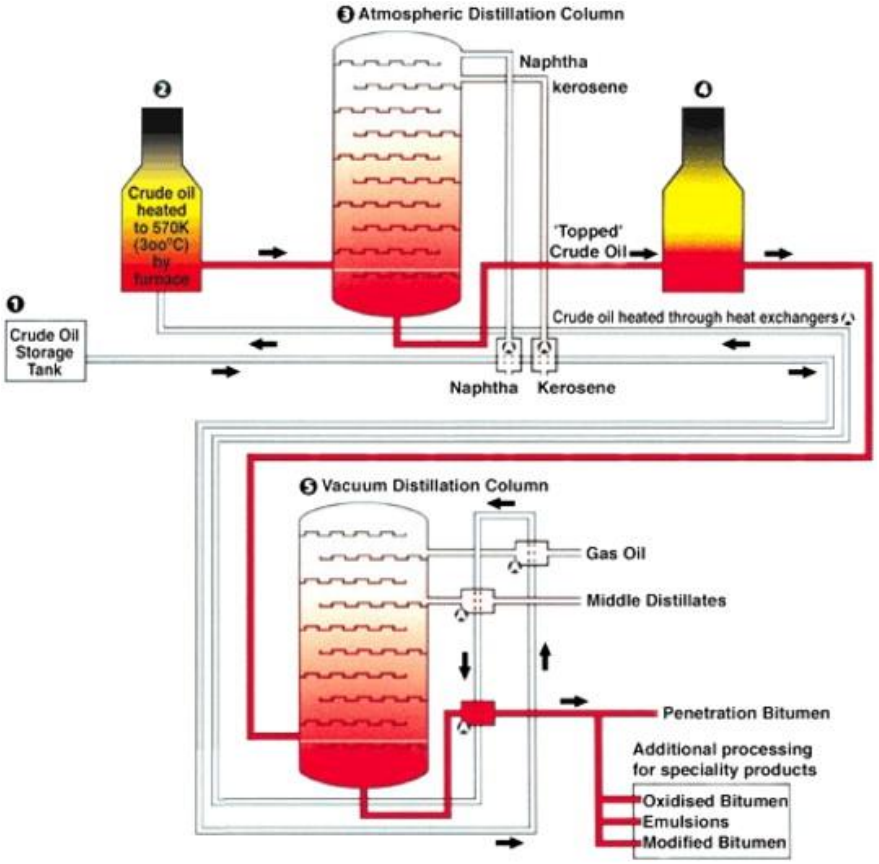

Figure 1. Distillation of bitumen (courtesy of Nynas) [49].

- Solvent deasphalting: In this process, asphaltenes are precipitated by a solvent that is usually a light paraffin (propane, butane, isobutene, pentane or isopentane). The heavy fraction of a crude oil (or soft bitumen) is mixed with the solvent and then left to settle typically at a temperature range of 25–70 °C and a pressure of 120 kPa (12 bars). Bitumen is then the solvent-free precipitate obtained after settling. Further, the soluble part (the deasphalted oil) can be further processed by hydrotreaters, fluid catalytic cracking units, hydrocrackers or fuel-oil blending. The precipitated residue, which is usually obtained as a by-product of lubricant recovery rather than from bitumen production, is often promoted as a blending component for bitumen. [6,48,49]

- Visbreaking: As opposed to physical separation processes, bitumen or bitumen components can also result from conversion processes in which carbon-carbon bonds are broken. Visbreaking is a mild form of thermal cracking operated at 455–510 °C and 0.3–2 MPa (3–20 bars) for a short residence time of 1–3 min. It significantly lowers the viscosity of atmospheric or vacuum residues with the main aim to increase conversion to gas oil and lighter boiling range materials. The residue from visbreaking is placed on the market typically as a bitumen blending component for road paving. [6,48,49]

- Air-blowing: Air-blowing is used to manufacture bitumen from an otherwise too fluid or temperature susceptible crude oil source or to produce very hard bitumens [48-50]. It consists of air-oxidizing the oil (or soft bitumen) for a few hours at 200–275 °C, sometimes in the presence of a catalyst [49]. Mild air blowing produces air-rectified bitumen (also called semi-blown bitumen) that is mainly used in paving applications, while more severe air blowing results in oxidized bitumen for roofing applications [6]. Oxidized bitumens are discarded in road construction because of their high susceptibility to cracking [45].

Finally, it should be mentioned that when several processes are applied to one or more crude oils, the resultant bitumen blends may have properties clearly superior to those obtained when only one manufacturing process is used [51]. Thus, blending of different bitumen types or grades in various proportions is used to obtain specific technical specifications for paving materials [6].

2.2. Chemical properties and microstructure of bitumen

Bitumen is a complex chemical mixture of molecules that are predominantly hydrocarbons of different molecular sizes with a small amount of structurally analogous heterocyclic species (heteroatoms) and functional groups containing e.g. sulphur, nitrogen and hydrogen atoms [52]. Given the concentration of polar molecules, functional groups generally do not amount for more than a few 0.1 mol/l for straight-run bitumens [13]. Bitumen contains also trace quantities of metals such as vanadium, nickel, iron, magnesium and calcium, which occur in the form of inorganic salts and oxides or in porphyrine structures [53]. Elementary analysis of bitumens manufactured from a variety of crude oils shows that most bitumens are mainly comprised of carbon, hydrogen, sulphur, oxygen and nitrogen, see Table 1.

Table 1. Elementary analysis of the core SHRP bitumens (data from [54]).

Bitumen code		AAA-1	AAB-1	AAC-1	AAD-1	AAF-1	AAG-1	AAK-1	AAM-1
Origin		Canada	USA	Canada	USA	USA	USA	Venezuela	USA
C	wt.%	83.9	82.3	86.5	81.6	84.5	85.6	83.7	86.8
H	wt.%	10	10.6	11.3	10.8	10.4	10.5	10.2	11.2
H+C	wt.%	93.9	92.9	97.8	92.4	94.9	96.1	93.9	98
H/C	Molar	1.43	1.55	1.57	1.59	1.48	1.47	1.46	1.55
O	wt.%	0.6	0.8	0.9	0.9	1.1	1.1	0.8	0.5
N	wt.%	0.5	0.5	0.7	0.8	0.6	1.1	0.7	0.6
S	wt.%	5.5	4.7	1.9	6.9	3.4	1.3	6.4	1.2
V	ppm	174	220	146	310	87	37	1480	58
Ni	ppm	86	56	63	145	35	95	142	36
M_n [a]	g/mol	790	840	870	700	840	710	860	1300

[a] The values of M_n were measured by Vapor Pressure Osmometry in toluene and pyridine at 60 °C [55].

This elemental composition results in the formation of a wide range of molecules, which are typically divided into four SARA (Saturates, Aromatics, Resins, Asphaltenes) fractions based on their size and solubility in polar, aromatic or non-polar solvents [49]. Hereby, the molecular weights increase from the saturates (300 to 2000 g/mol) to the asphaltenes (1000 to 10000 g/mol) [44]. Likewise, the aromaticity and heteroatom content increase from the saturates to the asphaltenes in the same order [53]. Due to these characteristics in the molecular composition, bitumen is sometimes referred to as a "molecular cocktail" [56].

The relative distribution of carbon atoms in bitumen is typically 28-40 % aromatic and 60-72 % aliphatic [57]. The majority of aromatic carbons are associated with polycondensed heteronuclear aromatic clusters, but also some single phenyl ring compounds with alkane substituents are possible. Structurally, the aliphatic carbons are associated with normal, branched and cyclic alkanes. These alkane structural units can either be attached to a condensed aromatic cluster or exist independently (e.g. paraffin waxes). [58]

The molecular interactions (hydrogen bonding, π-π interactions, etc.) in a complex molecular system such as asphalt are extensive. At any given temperature, these interactions will tend to control the molecular motions of the constituents in asphalt. However, translational and rotational motions of the whole molecule within the asphalt matrix at room temperature and below are not expected to occur at any appreciable rate. [58]

In a recent paper, Redelius and Soenen [7] showed that the mechanical properties of bitumen are governed by molecular interactions, of which the dispersive London forces and aromatic π-π interactions seem to be most important. They also proposed that the largest and most aromatic molecules in bitumen have the strongest interactions and thus the largest influence on the viscosity of bitumen. In another recent article, Soenen and Redelius [6] suggested that the elasticity of bituminous binders is related to the presence of polyaromatic structures.

There are three main theories that attempt to explain the microstructure of bitumen. Probably the most widely accepted one of these models is the colloidal model which claims that bitumen is a colloidal dispersion of asphaltenes into an oily matrix constituted by saturates, aromatics and resins (which make up the maltene fraction) [15,49,59]. On the other hand, Dispersed Polar Fluid (DPF) model describes bitumen as a single-phase system, i.e. a simple homogenous liquid [14,60]. The third model, the so-called "Nynäs Bitumen Solubility Model" [61], is based on mutual solubility of solvents and incorporates information about cohesion, molecular volume, dispersive and polar interactions as well as hydrogen bonding.

2.3. Thermal properties of bitumen

There are at least three analysis techniques that have been used to study the thermal properties of bituminous binders: Differential Scanning Calorimetry (DSC), Differential Thermal Analysis (DTA) and Thermogravimetric Analysis (TGA). However, only the most popular one of these methods, DSC, is introduced in this subsection, because it was the only thermal analysis technique that was utilized during the experimental part of this study.

DSC is a thermoanalytical method that allows the determination of physical changes in a material associated with a heat exchange. In practice, the difference in the amount of heat required to increase the temperature of a sample and reference is measured as a function of temperature while they are maintained at (nearly) the same temperature [62]. DSC has shown promising results in analyzing bitumen as it can be used to measure quantities related to physical changes like glass transition and phase transitions such as melting and crystallization [63]. Furthermore, chemical reactions and heat capacity can be measured [64,65]. If wax is present in bitumen, DSC can further indicate the melting and crystallization points of wax, and, if the melting enthalpy of pure wax is known, the results could be used to determine wax content [66].

The heat flow measured by a DSC is a function of the heating rate, sample heat capacity, and any endo- or exothermic events occurring in the sample. This is summarized as follows:

$$\frac{\mathrm{d}Q}{\mathrm{d}t} = C_p \frac{\mathrm{d}T}{\mathrm{d}t} + \mathrm{f}(t,T) \tag{1}$$

where $\mathrm{d}Q/\mathrm{d}t$ = total heat flow [J s^{-1}]
C_p = heat capacity [J K^{-1}]
$\mathrm{d}T/\mathrm{d}t$ = heating rate [K s^{-1}]
$\mathrm{f}(t,T)$ = kinetic component [J s^{-1}]

The first term on the right side of the equation is the heat flow contribution due to heat capacity and heating the sample. Because there is a shift in heat capacity at the glass transition, this term contains information about the glass transition. The second term on the right is the kinetic component that arises from the time dependence of crystallization, melting and/or chemical reactions. [3]

An example of a DSC thermogram for bitumen containing natural wax is presented in Figure 2. This thermogram was produced by first cooling and then heating the bitumen sample. The glass transition temperature T_g manifests itself as a broad step change in the

baseline of the heating curve, and in this specific case its value is determined to be -20.8 °C. In addition, the melting and crystallization enthalpies of bitumen wax can be retrieved from the heating and cooling curves, respectively. In Figure 2, these enthalpies are calculated from the red-shaded areas between the heat flow curves and the extrapolated baselines; in this special case, the values of heating and cooling enthalpy are calculated to be 6.0 J/g and 1.34 J/g, respectively. The onset and endset temperatures of the aforementioned thermal events can also be defined from the DSC thermogram as shown in the figure.

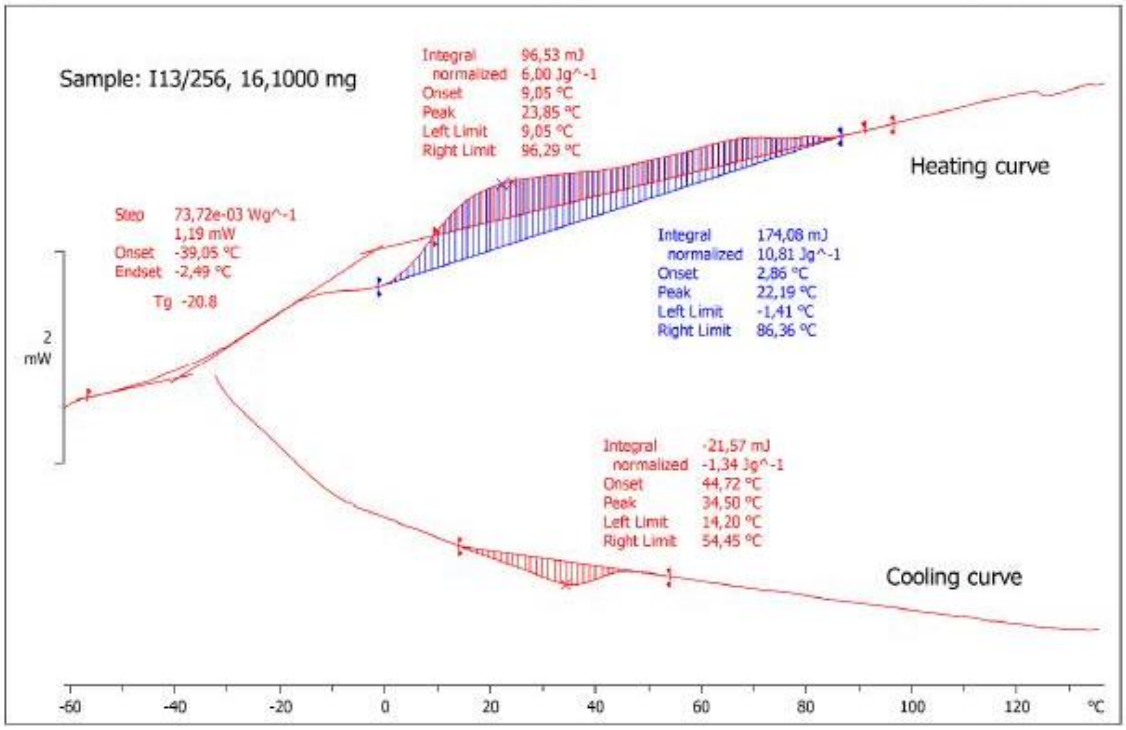

Figure 2. Typical DSC thermogram for bitumen containing natural wax (endothermic is up on this graph).

Bitumen is known to exhibit a glass transition around -20 °C, although it varies in a very wide range from +5 °C down to -40 °C depending essentially on the crude origin and somewhat less on the refining process [3,67-70]. However, one should note that glass transition does not occur at a single temperature in bitumen, but over a range of temperatures. The transition range typically spans 30 to 45 K, and -20 °C corresponds to the typical midpoint value [3]. Further, Masson et al. [71] have suggested that bitumen does not actually exhibit only one T_g, but four distinct T_gs that arise from different amorphous phases in bitumen. More detailed information about the glass transition phenomenon is provided in Section 4.3.

The waxes naturally present in bitumen are known to have a much wider crystallization and melting point range than the synthetic waxes used as flow improvers in warm-mix

asphalts. Lesueur [49] stated that natural bitumen waxes crystallize typically at temperatures starting from 90 °C down to the glass transition temperature. Correspondingly, the melting point range of these waxes is typically nearly 100 K wide, cf. Figure 2. The large widths of the aforementioned temperature ranges are due to the varying molecular structures of the natural waxes.

2.4. Physical properties of bitumen

Bitumen is a viscoelastic liquid that exhibits Newtonian flow behavior at high temperatures (typically above 60 °C), viscoelastic behavior at intermediate temperatures (typically between -20 °C and 60 °C), and glassy, brittle behavior at low temperatures (typically below -20 °C). For practical purposes, its engineering properties have traditionally been characterized with the penetration and softening point tests [44].

The consistency of bitumen is measured by the penetration test [72]. In this test, a needle of specified dimensions is allowed to penetrate a sample of bitumen under a load of 100 g for 5 seconds. The test is performed at a fixed temperature of 25 °C (or at 15 °C when soft bitumens are tested). The penetration (Pen) is defined as the distance travelled by the needle into the bitumen sample, and it is measured in tenths of a millimeter (decimillimeter, dmm). The lower is the value of penetration, the harder is the bitumen, and vice versa. This test is the basis of European bitumen classification system in which bitumens are divided into different penetration classes [40,73].

The consistency of bitumen at high in-service temperatures can be measured by determining its Ring-and-Ball (R&B) softening point [74]. In this test, a steel ball (weighting 3.5 g) is placed on a sample of bitumen contained in a brass ring that is then suspended in a water or glycerin bath. Water is used for bitumen with a softening point of 80 °C or below, and glycerin is used for softening points greater than 80 °C. When the bath temperature is raised at the rate of 5 K/min, the bitumen softens and eventually deforms slowly with the ball through the ring. At the moment the bitumen and steel ball touch a base plate 25 mm below the ring, the temperature of the water is recorded. The recorded temperature is designated the Ring-and-Ball softening point of the bitumen.

The temperature susceptibility of bitumen can be described with the penetration index (PI) that was introduced by Pfeiffer and Van Doormaal in 1936 [75]. The PI is calculated from the penetration and softening point values as follows (assuming the penetration test temperature of 25 °C):

$$\mathrm{PI} = \frac{1952 - 500 \log \mathrm{Pen} - 20 T_{R\&B}}{50 \log \mathrm{Pen} - T_{R\&B} - 120} \tag{2}$$

where $T_{R\&B}$ = Ring-and-Ball softening point [°C]

The higher is the value of the PI, the less temperature-susceptible is the bitumen, and vice versa. It was observed that blown bitumens have typically PI > +1 when straight-run bitumens have −1 < PI < +1 and solvent-deasphalted bitumens have −2 < PI < +2 [75,76]. In general, the PI varies between −2.6 and 8 when including all types of bitumen (including blown ones), but typically lies between −2 and +2 for paving grade bitumens [77]. The PI proved a rather powerful indicator for classifying bitumen rheological behavior; in particular, Van der Poel [77] showed that bitumens with the same PI have similar rheological master curves.

Other empirical test methods of bitumen include capillary viscosity tests and Fraass breaking point test [44]. Capillary viscosity is measured to determine the flowability of bitumen at pavement mixing and compaction temperatures (typically 135-165 °C and 80-160 °C, respectively). In turn, Fraass breaking point test is used to describe the cracking behavior of bitumen at very low temperatures (as low as -30 °C). Sometimes also penetration and PI values have been used to estimate the low-temperature properties of bitumen [78].

3. Rheological characterization and its application in asphalt industry

3.1. Oscillatory rheological testing

Oscillatory testing is the most common way to characterize rheological properties of viscoelastic materials with a DSR. The basic principle of an oscillatory test is to induce a sinusoidal shear deformation in the sample and measure the resulting stress response. The time scale of the measurement is determined by the frequency of oscillation, ω, of the shear deformation. In a typical experiment, the sample is placed between two plates, as shown in Figure 3(a). While the bottom plate remains stationary, a motor rotates the top plate, thereby imposing a time dependent strain $\gamma(t) = \gamma_0 \cdot \sin(\omega t)$ on the sample. Simultaneously, the time dependent stress $\sigma(t)$ is quantified by measuring the torque that is required to produce the desired deformation in the test sample. Examples of strain inputs and stress outputs for an elastic solid, a viscous fluid and a viscoelastic material are shown in Figure 3(b).

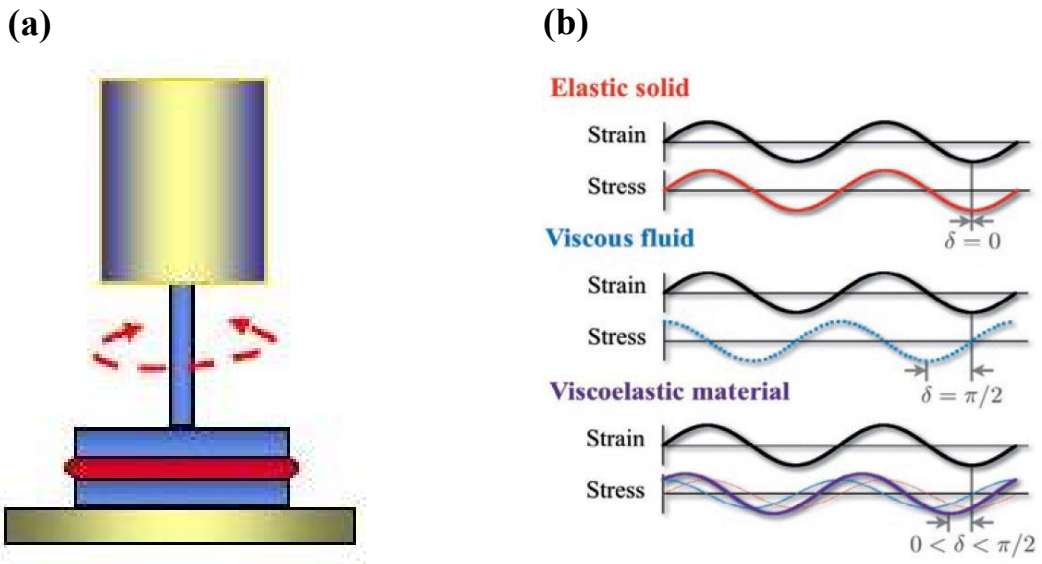

Figure 3. (a) Parallel plate geometry of a DSR, and (b) schematic stress response to oscillatory strain deformation for an elastic solid, a viscous fluid and a viscoelastic material. Figure (a) courtesy of TA Instruments, figure (b) from [79].

In most cases, oscillatory testing is performed within the linear viscoelastic (LVE) region where the values of viscoelastic material parameters are, by definition, independent of the applied stress or strain. This type of testing is generally known as small-amplitude oscillatory shear (SAOS) testing. The material functions in SAOS relevant for this study are defined in Table 2 and presented in the complex plane in Figure 4.

Table 2. Definitions of selected SAOS material functions [80,81].

Material function	Symbol	Definition	Unit	Physical meaning
Complex modulus	G^*	$G'+iG''$	Pa	a measure of the total resistance of the system to strain in a cyclic deformation
Loss angle (phase angle)	δ	$\sigma(t)=\sigma_0\sin(\omega t+\delta)$	rad or °	a measure of the energy dissipation per cycle of sinusoidal deformation
Storage modulus	G'	$\lvert G^*\rvert\cos\delta$	Pa	a measure of the energy stored and recovered per cycle of sinusoidal deformation
Loss modulus	G''	$\lvert G^*\rvert\sin\delta$	Pa	a measure of the energy dissipated or lost as heat per cycle of sinusoidal deformation
Loss tangent	$\tan\delta$	G''/G'	-	a measure of the ratio of energy lost to energy stored in a cyclic deformation

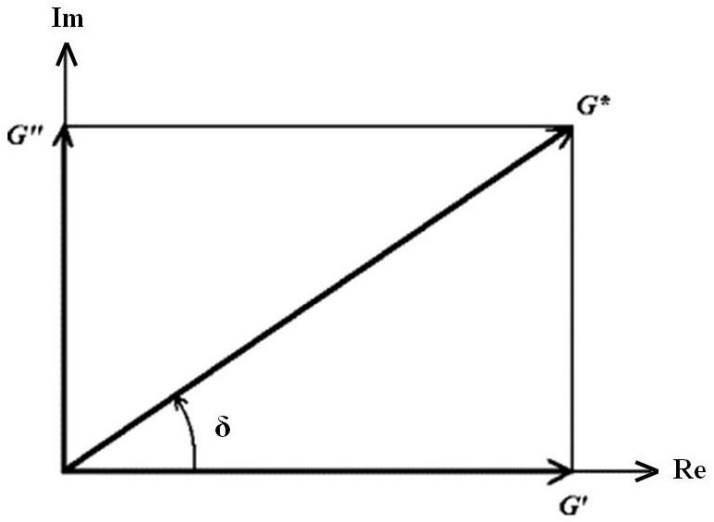

Figure 4. Representation of selected SAOS material functions on a complex plane.

3.2. Master curve construction and relaxation time spectrum

In many occasions, the rheological behavior of a material needs to be characterized at very long loading times or modeled at various temperatures. For this purpose, it is often necessary to utilize the time-temperature superposition (TTS) principle [82]. It essentially states that the effect of increasing the loading time (or decreasing the

frequency) on the mechanical properties of a material is equivalent to that of raising the temperature [83]. Further, when data at several temperatures have been obtained, TTS can be used to generate a "master curve" showing the rheological behavior at a "reference temperature" that covers many decades of time or frequency. A material to which this technique is applicable is said to be "thermorheologically simple". An illustrative example of master curve construction is given in Figure 5.

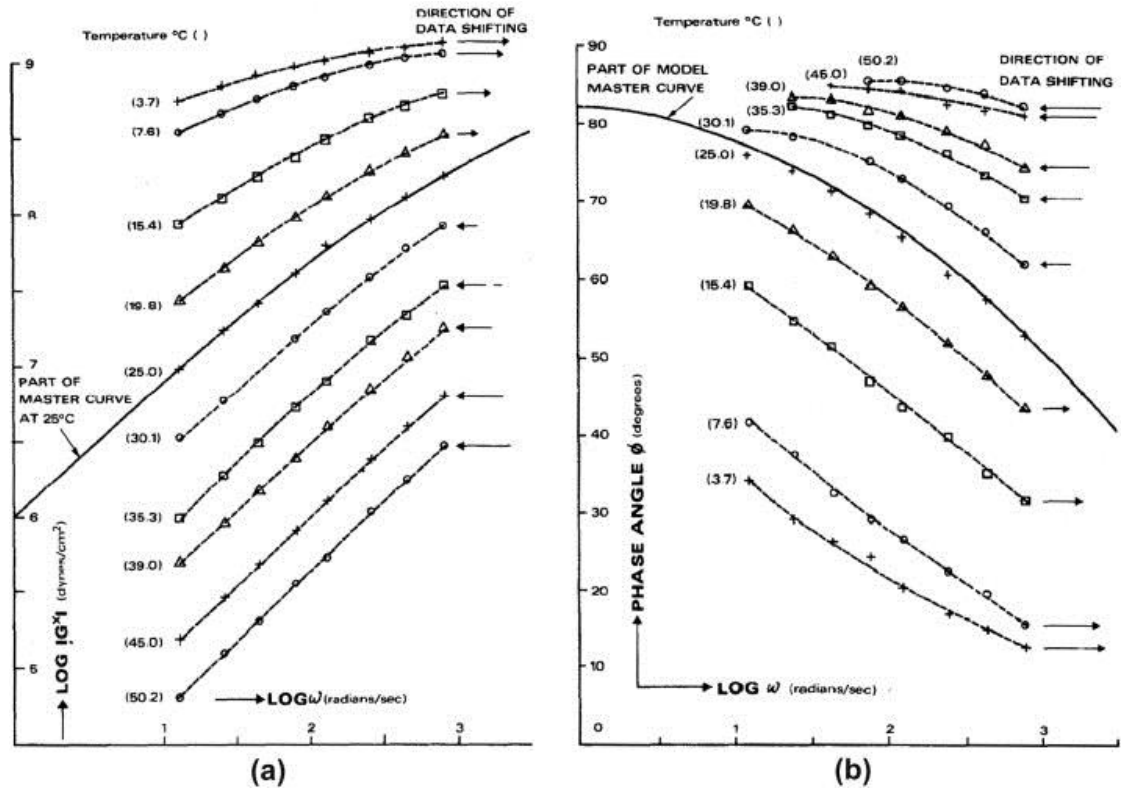

Figure 5. Illustrative example of the construction of (a) $|G^*|$ and (b) δ master curves [84].

As a result of the master curve construction, horizontal and vertical shift factors – a_T and b_T, respectively – are obtained based on the amount of shifting that is required to relocate isothermal frequency sweep curves on a single master curve at each measurement temperature. Shift factors can be used to assess the temperature dependence of viscoelastic functions [85], and the temperature dependence of horizontal shift factors is often modeled with the Williams-Landel-Ferry (WLF) [86], Arrhenius-type and Vogel-Fulcher-Tammann (VFT) [87-89] equations, among others. Moreover, the Kaelble modification of the WLF equation [90], the Mauro-Yue-Ellison-Gupta-Allan (MYEGA) model [91] (also known as the Topological constraint theory [92]) and the parabolic model [93-97], among others, have been used to model horizontal shift factors especially at low temperatures, i.e. near and below T_g [98].

From the aforementioned models, the Kaelble modification of the WLF equation (Equation 3) is of the greatest interest for us. This is because it is capable of modeling horizontal shift factors over a very wide temperature range, both above and below T_g [99]. Hereafter, this equation will be simply referred to as the Kaelble-WLF equation.

$$\log a_T = -\frac{c_1(T - T_d)}{c_2 + |T - T_d|} \tag{3}$$

where c_1 = WLF constant [-]
c_2 = WLF constant [K]
T_d = defining temperature [K]

At T_d there is an inflection point in the plot of log a_T vs. T that marks a change in the curvature of the shift factor curve [99]. Note that this equation deviates from the WLF equation only by the inclusion of a magnitude term in the denominator of the right hand side fraction (assuming that the reference temperature T_r is set at T_d). Hence, above T_d the Kaelble curve is identical to the WLF curve, but below T_d it slowly approaches a horizontal asymptote whereas the WLF curve approaches a vertical asymptote at $T = T_d$-c_2 (see Figure 6). It is also noteworthy to mention that, according to Rowe and Sharrock [99], the T_d produced by the Kaelble analysis produces a numerical value very close to that of the defining temperature as prescribed in the SHRP work conducted by Christensen and Anderson [100].

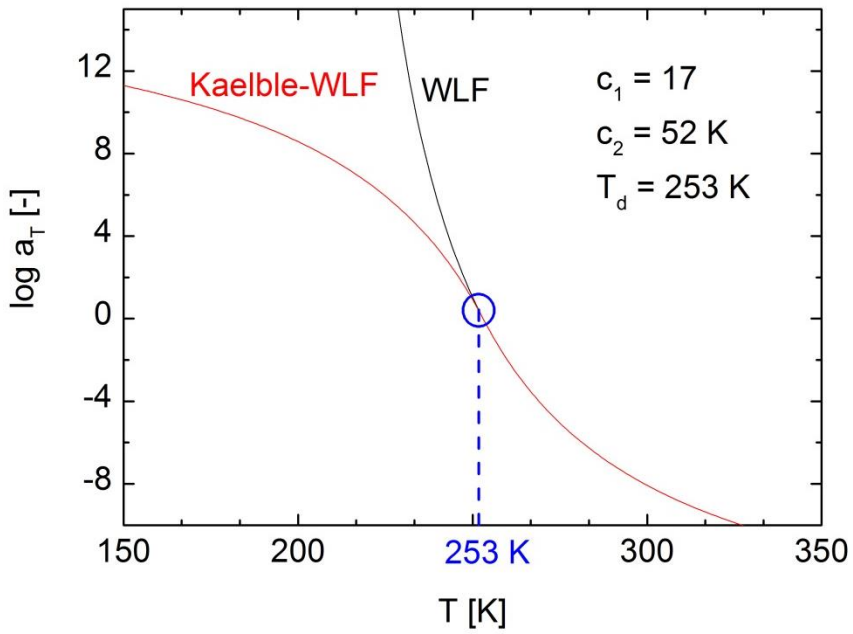

Figure 6. Illustrative example of the shapes of shift factor curves according to the WLF equation and its Kaelble modification.

However, Equation 3 is difficult to apply to data since the form of the equation implies that the defining temperature and the reference temperature are the same. This difficulty can be overcome by introducing a constant term that separates T_d from T_r:

$$\log a_T = -c_1 \left(\frac{T - T_d}{c_2 + |T - T_d|} - \frac{T_r - T_d}{c_2 + |T_r - T_d|} \right) \tag{4}$$

It is well known [101,102] that the WLF equation is identical to the VFT equation. Here it is also observed that, in the glassy region ($T \leq T_d$), it is possible to write the Kaelble-WLF equation in the form that is similar to the VFT equation. If a sufficiently low reference temperature is selected so that $T_r \leq T_d$, Equation 4 can be rewritten as:

$$\ln a_T = B \frac{T_r - T}{(T - T_v)(T_r - T_v)} \tag{5}$$

where $B = \ln(10) c_1 c_2$

T_v = Vogel temperature = $c_2 + T_d$

The derivation of Equation 5 from Equation 4 is presented in Appendix A.

Time-temperature shifted dynamic data is often used to calculate the relaxation time spectrum $H(\tau)$. The relationship between $H(\tau)$ and linear dynamic data is described by the following equations:

$$G'(\omega) = G_e + \int_0^{\tau_{max}} \frac{\mathrm{d}\tau}{\tau} H(\tau) \frac{(\omega\tau)^2}{1 + (\omega\tau)^2} \tag{6}$$

$$G''(\omega) = \int_0^{\tau_{max}} \frac{\mathrm{d}\tau}{\tau} H(\tau) \frac{\omega\tau}{1 + (\omega\tau)^2} \tag{7}$$

where G_e = equilibrium modulus (= 0 for viscoelastic liquids) [Pa]
τ = relaxation time [s]
τ_{max} = the longest relaxation time [s]

$H(\tau)$ is a macroscopic expression of small-scale structural rearrangements in time. Relaxation processes at short τ refer to small-scale rearrangements in a test material, whereas long-time relaxation depends on the large-scale rearrangement processes of material constituents. Thus, $H(\tau)$ may exhibit any functional shape depending whether short or long-time structural rearrangements dominate the stress [103]. However, most importantly, the linear viscoelastic behavior of any material is fully described by $H(\tau)$ [104].

3.3. Performance grading of bituminous binders

During the last few decades, the suitability of the aforementioned empirical test methods for the performance characterization of bituminous binders has impaired due to the increased popularity of bitumen modification [105,106]. This is because the introduction of modifiers makes bitumen rheology more complex [107], resulting in poor correlations between empirical test results and bitumen performance in asphalt pavements [106,108]. Hence, fundamental rheological test methods were introduced in the SHRP program for the use in the classification of road bitumens [109].

The classification system developed during the SHRP program is based on the division of bituminous binders into different performance grades (PG). The original specifications for performance grading were adopted in the USA in the early 1990s [110]. In the PG system the binder is said to be PG H-L, where H is the limiting high

temperature and -L is the limiting low temperature [111]. The limiting high temperature corresponds to the temperature at which the inverse of the viscous compliance, $1/J'' = G^*/\sin\delta$, of the unaged binder becomes inferior to 1 kPa when measured at an angular frequency of 10 rad s^{-1} [112]. The grades are defined by 6 °C steps starting from 46 °C up to 82 °C. The limiting high temperature can be thought of as the temperature above which the risk of rut formation becomes critical for an asphalt mixture made with the corresponding binder [49].

Correspondingly, the limiting low temperature corresponds to the temperature at which the flexural creep modulus of the binder, $S(t)$, becomes superior to 300 MPa at a loading time of 60 s, or at which the logarithmic creep rate, $m(t)$, falls below 0.300, whichever is higher [113]. Low-temperature testing is performed with a BBR on the rolling thin film oven (RTFO) and then pressure aging vessel (PAV) aged binder from −10 °C down to −46 °C with 6 °C decrements. The limiting temperature stated in the paving grade is in fact 10 °C lower than that of the creep test: for example, if the binder has a creep modulus of 300 MPa at −12 °C and 60 s, its limiting low temperature is −22 °C. This is because it has been claimed that typical time-temperature shift factors for bitumen show that a 2-h loading time, which is characteristic for daily temperature changes, is equivalent to a 60-s loading time at a 10 °C higher temperature [21]. However, some criticism on this assumption was set forward by Basu et al. [114]. The limiting low temperature can be thought of as the temperature below which the risk of cracking becomes critical for an asphalt mixture made with the corresponding binder [49].

More recently, new rheological testing methods, like the Multiple Stress Creep-Recovery (MSCR) test [115], the Linear Amplitude Sweep (LAS) test [116-118] and the 4-mm DSR technique [5] (described more in detail in Section 4.2), have been developed to replace the rheological test methods developed during the SHRP program. In addition, modeling work has been conducted to characterize the rheological behavior of bituminous binders on a more fundamental level. Perhaps the most notable recent development in the rheological modeling of bituminous materials has been the introduction of the 2S2P1D and 1S2P1D models for bituminous mixtures and binders, respectively [119]. However, the theory and application of these models is out of the scope of this work and thus, for brevity, will not be described in detail herein.

4. Low-temperature characteristics of bitumen

4.1. Traditional techniques for the characterization of the low-temperature rheological properties of bitumen

It has been shown that the low-temperature performance of asphalt pavements is largely controlled by the low-temperature rheology of bituminous binders. Therefore, a better understanding of the low-temperature rheological characteristics of bituminous binders is needed to predict thermal cracking and thus, to improve the low-temperature performance of asphalt pavements [5]. Traditionally, there have been two methods for measuring the low-temperature rheological properties of bituminous binders: BBR for measuring flexural creep stiffness and stress relaxation rate [120] and torsion bar (TB) on the DSR for measuring dynamic shear modulus and phase angle under oscillatory shear loading [121]. It should be noted that various fracture tests have also been developed to characterize the low-temperature properties of bituminous binders, e.g. Fraass breaking point test, direct tension test (DTT), double edge notch test (DENT), single edge notched beam (SENB) test, asphalt binder cracking device (ABCD) test and fracture toughness test (FTT) [122]. However, the fracture characterization of bitumen is out of the scope of this work, and hence the aforementioned test methods will not be discussed in detail herein.

However, both BBR and TB methods require relatively large amounts of material for testing and relatively high specimen preparation temperatures. In addition, TB method has practical problems related to specimen loading and holding that can significantly affect the test results. These disadvantages make it difficult to analyze samples from field studies that require a test method that uses only small amounts of material and produces data quickly. The aforementioned factors led some asphalt researchers to develop a novel low-temperature testing technique for a DSR as discussed in the following.

4.2. 4-mm DSR technique and the correction for radial instrument compliance

Recently, researchers at WRI developed a novel method to measure the low-temperature rheological properties of bituminous binders. This experimental technique introduces the use of 4-mm parallel plate geometry in a DSR, combined with the systematic correction of radial instrument compliance [5]. To date, this 4-mm DSR technique has been successfully used to measure the low-temperature rheological properties of various types of asphalt binders (unaged and aged, neat and modified, etc.) [4,5,9,35,36,123-133] and other bituminous materials such as emulsion residues [134-136]. Furthermore, an AASHTO standard draft of this test method has been prepared (see Appendix B) and is currently under evaluation.

In the 4-mm DSR technique the binder specimen is sandwiched between two 4-mm-diameter parallel plates that are separated from each other by a 1.75-mm gap, see Figure 7. A small plate diameter and a large gap are used to minimize radial instrument compliance effects [137-139]. Radial instrument compliance implies that the true strain on the sample is lower than the measured strain due to the compliances of rheometer transducer and measurement fixture [138]. However, even when using the aforementioned specimen dimensions, the measured values of rheological parameters are influenced by compliance effects. Hence, it is necessary to systematically correct the measurement results for radial instrument compliance.

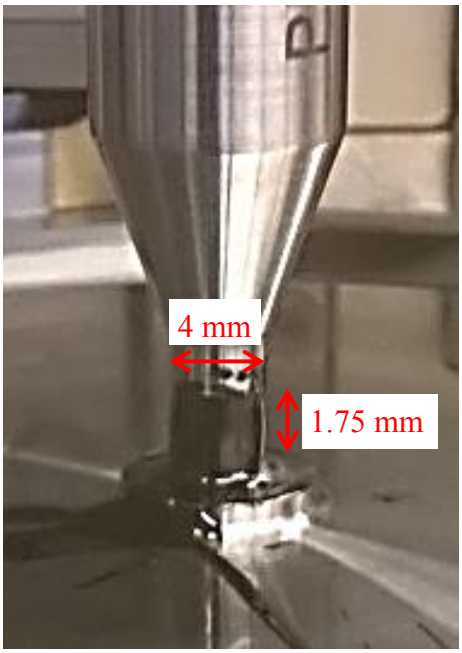

Figure 7. 4-mm parallel plate set-up for a DSR.

There are a few methods available in the literature for the correction of radial instrument compliance errors [140-142]. Out of these methods, the one developed by Schröter et al. [141] is probably the most popular one. Moreover, this correction method is endorsed by the AASHTO standard draft for the 4-mm DSR technique. The derivation of the instrument compliance correction according to Schröter et al. is presented in Appendix B. The compliance corrections for storage modulus, loss modulus and phase angle are as follows:

$$G'_s = \frac{G'_m\left(1 - \frac{J_{\text{instrument}}}{k_g}G'_m\right) - \frac{J_{\text{instrument}}}{k_g}G''^2_m}{(1 - \frac{J_{\text{instrument}}}{k_g}G'_m)^2 + (\frac{J_{\text{instrument}}}{k_g}G''_m)^2} \tag{8}$$

$$G_s'' = \frac{G_m''}{(1 - \frac{J_{\text{instrument}}}{k_g} G_m')^2 + (\frac{J_{\text{instrument}}}{k_g} G_m'')^2} \quad (9)$$

$$\tan \delta = \frac{G_m''}{G_m' \left(1 - \frac{J_{\text{instrument}}}{k_g} G_m'\right) - \frac{J_{\text{instrument}}}{k_g} G_m''^2} \quad (10)$$

where G'_s = storage modulus of the sample [Pa]
G''_s = loss modulus of the sample [Pa]
tan δ = loss tangent of the sample [-]
G'_m = measured storage modulus [Pa]
G''_m = measured loss modulus [Pa]
$J_{instrument}$ = instrument compliance [rad N^{-1} m^{-1}]
k_g = geometry constant [m^3]

Note that in the special case of the parallel plate geometry, the geometry constant k_g is calculated as follows:

$$k_g = \frac{2h}{\pi R_p^4} \quad (11)$$

where h = gap between the plates [m]
R_p = radius of the plates [m]

In most of the studies, the radial instrument compliance is assumed to be constant, i.e. independent of the angular frequency and temperature. However, some researchers have pointed out that the radial instrument compliance of single-head (stress-controlled) rheometers is actually frequency-dependent [35,142]. The extent of frequency dependence varies from one rheometer model to the other, and is presumably dependent at least on the instrument inertia and/or a response time of the force rebalance transducer controlled by the servo loop [35].

In 2011, Sui et al. [4] proposed a new low-temperature performance grading method for bituminous binders that utilized the 4-mm DSR technique. By testing eleven binders, they observed a strong linear correlation between BBR and 4-mm DSR data. This led them to conclude that the 4-mm DSR technique could be used as an alternative to the BBR measurement to obtain the low-temperature performance grade of bituminous

binders. Based on the aforementioned linear correlation, they suggested that the criterion S(60 s, low PG temp + 10 °C) ≤ 300 MPa should be replaced with the criterion G(7200 s, low PG temp) ≤ 160 MPa, and the criterion m_c(60 s, low PG temp + 10 °C) ≥ 0.300 be replaced with the criterion m_r(7200 s, low PG temp) ≥ 0.26 when 4-mm DSR technique is used to determine the low-temperature performance grade. Finally, they tested four additional binders to validate that the low-temperature performance grades obtained with BBR and DSR techniques were comparable.

More recently, the data collected by Sui et al. [4] were revisited and modifications to the previously proposed low-temperature grading criteria were suggested [35]. The modified criteria are determined at 60 seconds and 10 °C higher than the PG temperature, rather than at 7200 seconds and at the PG temperature. Again, critical values of $G(t)$ and $m_r(t)$ were obtained from the linear correlation between BBR and 4-mm DSR data: G(60 s, low PG temp + 10 °C) ≤ 143 MPa and m_r(60 s, low PG temp + 10 °C) ≥ 0.28. However, it should be noted that a rather limited number of binders was used to validate the correlation between BBR and 4-mm DSR data, and that this binder set contained only two modified binders [143].

4.3. Glass transition

The glass transition is a fundamental property of amorphous materials, including bitumen. Below the glass transition temperature, T_g, there is insufficient thermal energy in a material to allow large-amplitude molecular motion. Without this motion and the viscous flow it allows, the approach to a thermodynamic equilibrium is slow. This slow approach to equilibrium is called physical aging, which is covered more in detail in Section 4.4. The transition is manifested by changes in the slope of primary thermodynamic quantities such as specific volume and enthalpy, and by step changes in secondary quantities such as thermal expansion coefficient and specific heat capacity. [3]

The glass transition has been studied extensively in polymer sciences because it marks a distinct change in mechanical and other material properties as a function of temperature and, thus, is important for tailoring product properties. Numerous excellent texts have been written containing large sections about the glass transition and its relation to physical and mechanical properties of polymeric and other materials, e.g. [144-150]. There are three main theoretical developments that have been applied to explain the glass transition phenomenon: the free-volume theory, the kinetic theory and the thermodynamic theory. These theories are not discussed in detail in this work, but more comprehensive information of their development is available in the book of Sperling [146]. In general, T_g increases with the stiffness, polarity, aromaticity and molecular weight of the repeat molecular structure within the amorphous phase [151].

It is important to recognize that the glass transition depends on the thermal history of a sample, especially on the cooling or heating rate. If the cooling rate in the DSC measurement is decreased, also the measured value of T_g decreases, and vice versa

[152-154]. The heating/cooling rates of DSC measurements are not standardized in the asphalt industry, but a heating rate of 10 K/min is probably most commonly used in the determination of the T_g of bitumen (and also of other glass-forming materials [155]).

Usually a single T_g is reported for bitumen, with a typical value being approximately -20 °C. However, as mentioned already in Section 2.3, Masson et al. [71] were actually able to define four distinct T_gs for bitumen with a modulated DSC (MDSC). They claimed that these are the T_gs of four different amorphous phases in bitumen: (1) the maltene phase, (2) the asphaltene phase, (3) the maltene–asphaltene interfacial region of mixed composition likely rich in resins (the so-called "interphase") and (4) the phase rich in flexible paraffinic segments. The glass transition of the maltenes is the most intense one, and thus the single T_g value usually reported for bitumens is most often associated with the glass transition of the maltene phase [3]. Interestingly, by using cryogenic atomic force microscopy (AFM) and phase detection microscopy (PDM), Masson et al. [156] detected collections of quasi-circular domains of 20–400 nm below the T_g of the maltenes. These domains, called "the salphase" by the authors, were found to be composed of unfrozen material phases with low T_g. This kind of nanophase separation and partial freezing-in are commonly observed in glass-forming materials [145].

It is also worth noting that, since the molecular compositions of different amorphous phases of bitumen are not homogeneous, their glass transition regions are relatively broad compared to the glass transition regions of typical single-component systems [3]. This possesses a problem for the determination of T_g since the glass transition does not manifest itself as a sharp step change in the heat flow curve of DSC measurement but rather as a broad change in the baseline. Two different methods are widely used to define the exact value of T_g: the "derivative method" (e.g. [71,156,157]) and the "mid-point method" (e.g. [3,63]). The mid-point method was used to determine the T_gs of the investigated bitumens in this work, and thus the principle of this method is briefly described in Appendix G.

In addition, besides DSC, there exist various other analysis techniques that have been employed to detect the glass transition event [155]. These techniques include e.g. thermal (e.g. heat capacity) [158], physical (e.g. specific volume) [159], mechanical (e.g. dynamic modulus) [160] and electrical (e.g. ionic conductivity) [161] characterization techniques, amongst others. In mechanical sense, T_g denotes the temperature at which, upon cooling, an amorphous material goes from a viscous fluid behavior to a hard, stiff, glassy state, or vice versa upon heating [162]. From rheological experiments, the "dynamic glass transition temperature" can be defined in principle in four different ways [83,163]:

(1) The temperature at which G' or η attains a certain value

(2) The temperature at which tan δ has its maximum value

(3) The temperature at which G'' has its maximum value

(4) The temperature at which *G'* has its greatest variation with frequency.

It should be noted that in all the above definitions T_g necessarily depends upon the time or frequency of the rheological measurement [83]. Although the definition (2) is very common in the literature, Illers and Baur, alongside with Boyer [164], stated that it would be more practical to use the definition (3) as the definition of the dynamic glass transition temperature. Bitumen does not exhibit peak in tan δ, but its value decreases monotonically when temperature is decreased. This is why the definition (3) has most often been used to determine the dynamic glass transition temperature for bitumen.

There are two rheological parameters that have been widely used to characterize the temperature dependence of dynamics in glass-forming materials: the dynamic fragility m and the apparent activation energy E_g at T_g. The concept of dynamic fragility was originally developed by Angell [165,166], and it is used to quantify the degree of deviation from the Arrhenius behavior [167]. More practically, it can be used to characterize how rapidly rheological properties change with temperature as T_g is approached [101]. Thus, in general, it has nothing to do with the fragility of glasses in the common sense, i.e. breaking easily or being brittle. Instead, Angell's pristine interpretation of the dynamic fragility was related to molecular pictures for dynamics or thermodynamics in the liquid [145]. The dynamic fragility is defined according to Equation 12, and graphically it is equal to the slope of the T_g-normalized Arrhenius plot of x, the so-called Angell plot, at T_g (see Figure 8).

$$m = \left[\frac{\mathrm{d}\log x}{\mathrm{d}\left(\frac{T_g}{T}\right)}\right]_{T=T_g} \tag{12}$$

where x = viscosity, relaxation time or any other dynamic variable

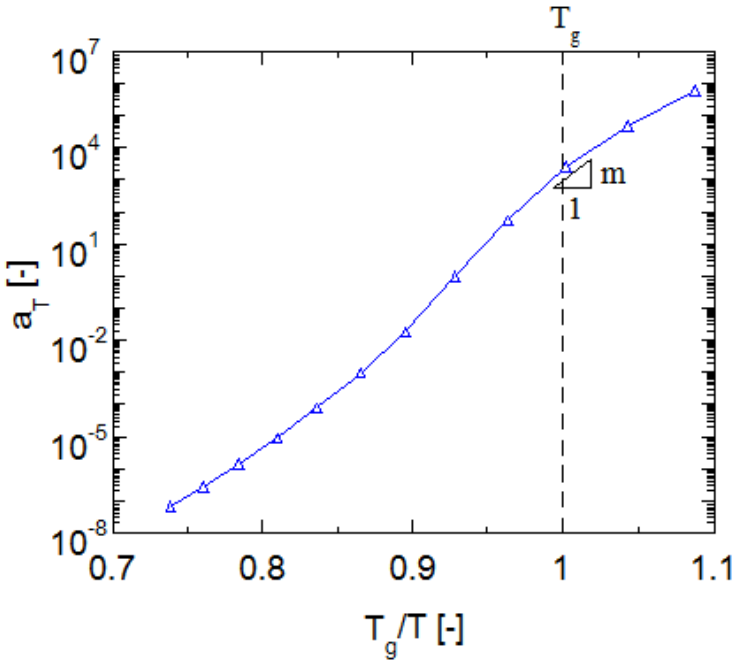

Figure 8. Graphical definition of the dynamic fragility parameter *m* in the Angell plot.

In asphalt research, the concept of dynamic fragility was earlier applied by Zhai and Salomon [168] and Qin et al. [9].

For example, Williams et al. [169-172] and, more recently, Ferrer et al. [173], Roland et al. [174-177] and McKenna et al. [101,178,179] showed the promise of using the apparent activation energy for viscous flow at T_g, E_g, for classifying material behaviors. E_g is defined as the slope of the logarithmic viscosity or relaxation time (or any other dynamic variable) vs. $1/T$ at T_g, see Figure 9. Importantly, the dynamic fragility is effectively a T_g-normalized activation energy:

$$E_g = \ln 10 \, RT_g m \tag{13}$$

where R = universal gas constant, 8.314 J mol^{-1} K^{-1}

McKenna [178] reported that E_g varies as T_g^2 for many polymers, metals, hydrogen bonding liquids and ionic glass-formers, and as T_g for many small molecule organics and inorganic network glass-formers.

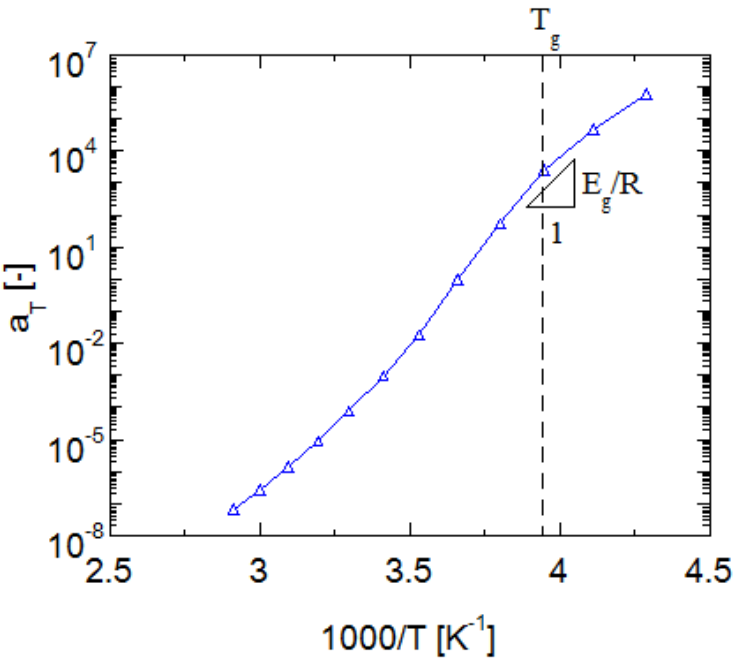

Figure 9. Graphical definition of the apparent activation energy E_g at T_g in the Arrhenius plot.

4.4. Physical aging

According to Struik [20], physical aging is a gradual continuation of the glass formation that sets in around T_g. Below T_g, the volume, enthalpy and entropy of a physically aging material are greater than they would be in the equilibrium state, see Figure 10. From another perspective, Donth [145] defined physical aging to be structural relaxation so far below T_g that it cannot be described by main transition modes alone. Irrespective of the definition, physical aging results in the change of specific temperature-dependent material properties, and this change is always in the same direction as upon cooling through the glass transition range [20]. In terms of rheological properties, this means that the material becomes stiffer, more elastic, and more brittle during physical aging.

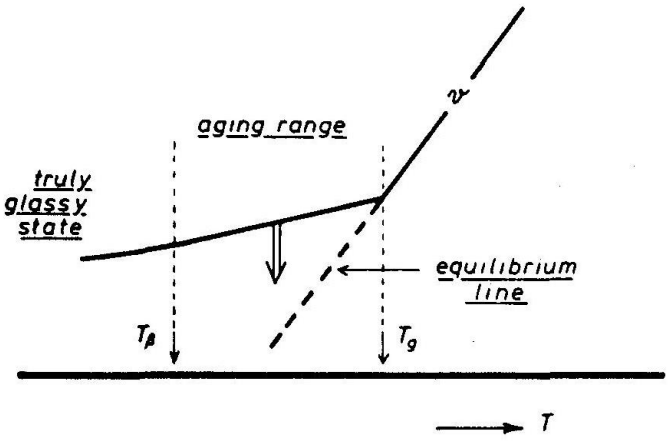

Figure 10. Concept of physical aging according to Struik [20]. T_g is the glass transition temperature, T_β is the temperature of the highest secondary transition, and v is the specific volume.

Physical aging in bitumen was first investigated by Struik [20], and later extensive studies on this topic have been conducted e.g. during the SHRP study [21]. The SHRP researchers called this phenomenon *physical hardening* to emphasize its reversible nature and to avoid confusion with oxidation aging, which is used in the asphalt literature and is not reversible. The term *reversible aging* has also been widely used to emphasize the reversible nature of this phenomenon [24]. In this work, the original nomenclature proposed by Struik [20] (involving the term *physical aging*) is used because some of the analysis techniques and definitions used in this work are adopted directly from her groundbreaking work. Moreover, it should be mentioned that this terminology has been established earlier also in asphalt research [180]. The author wants to emphasize that physical aging does not involve any chemical changes. In the nomenclature of Struik, the high-temperature aging, during which also chemical changes occur, is correspondingly termed *chemical aging*.

In the classical experiments of Struik [20,181,182], the existence and effect of physical aging was quantified mainly by performing creep experiments at various aging times. However, in rheological experiments, physical aging can also be conveniently detected by monitoring the increase in the complex modulus (and the decrease in the phase angle) over time under isothermal conditions. For more advanced analysis, frequency sweeps can be performed at different aging times, and the results analyzed with the time-aging time superposition technique [183,184]. This superposition is similar to the time-temperature superposition; the frequency sweep curves measured at different aging time are superimposed, and as a result of shifting, shift factors are obtained. Moreover, as demonstrated by O'Connell and McKenna [185], time-aging time superposition analysis can be used to determine the aging time that is required for the material to attain equilibrium conditions in terms of physical aging.

In contrast to the physical aging of most amorphous materials, Anderson and Marasteanu [186] stated that the physical aging of bituminous binders occurs both above and below T_g, and that the rate of physical aging peaks at T_g. However, in a more recent study by Tabatabaee et al. [38], the broadness of bitumen's glass transition was taken into account, and a conclusion was made that physical aging becomes relatively insignificant beyond the limits of the glass transition region. Moreover, they observed that the rate of physical aging peaks at T_g and is generally the higher the broader is the glass transition region. They claimed that the highest physical aging rate appears at T_g since the molecular free volume level has the highest deviation from the two linear "non-transition" states at this material-specific temperature (see Figure 11). Many studies [18,21,68,186,187] have also found that the rate of physical aging above and below T_g increases with increasing content of crystallizable fractions (waxes). This has led some researchers to conclude that the crystallization of waxes is responsible for physical aging in bitumen. In addition, the internal structuring of highly polar fractions and the collapse of free volume have been offered as possible mechanisms of physical aging [188].

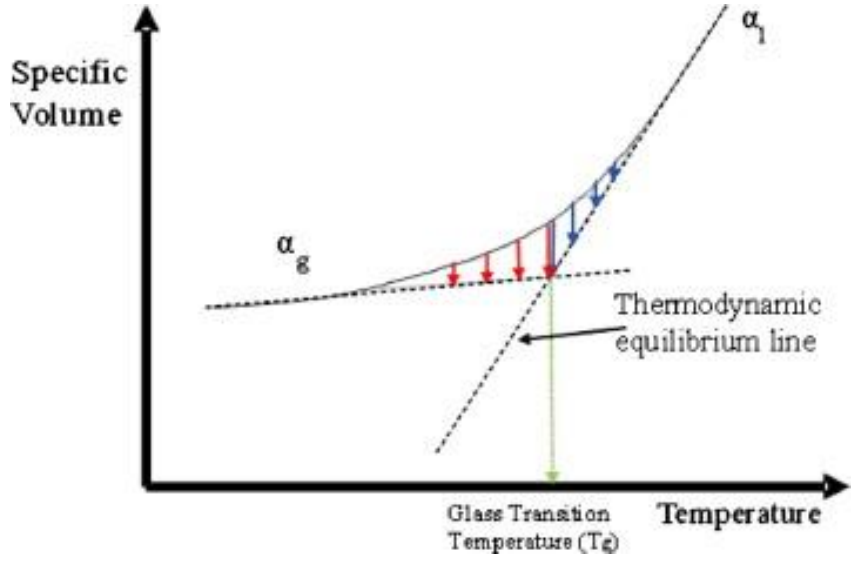

Figure 11. Schematic of material behavior in glass transition region according to Tabatabaee et al. [38]. Note also that in this drawing the slope of specific volume vs. temperature changes gradually in glass transition region as opposed to Figure 10. This is a more realistic representation of the broad glass transition in bituminous binders.

Physical aging also plays an important role in terms of asphalt pavement performance. Hesp et al. [22-25] have found significant evidence that physical aging is able to explain vast differences in pavement performance between adjacent contracts of identical design, climate and age. In general, it has been found that only binders with high colloidal stability are able to sustain low temperatures without physical aging and thus prevent premature and excessive cracking of asphalt pavement [189].

5. Experimental

5.1. Materials

Twenty-seven unaged bitumens were investigated in this study. Details about the production method were available for some of the bitumens while the others were commercial bitumens, collected across Europe and originating from various crude oil sources and refineries. Straight-run, solvent-deasphalted, visbroken, air-rectified and oxidized binders are included. If a blend of products was used, it is indicated as blend. If nothing is indicated, it means that the exact preparation mode of the bitumen is not known. None of these bitumen samples is modified by polymers or by special chemicals.

An overview of the bitumens is given in Table 3, together with the empirical properties (penetration at 25 °C and R&B softening point temperature). In this table, the bitumens are ranked according to their penetration value. It should be noted that the low PG temperatures reported are determined from the 4-mm DSR measurements using the criteria $G(60\text{ s}) \leq 143$ MPa and $m_r(60\text{ s}) \geq 0.28$ at the low PG temperature + 10 °C. An overview of the thermal properties of the investigated bitumens is given in Table 4. For convenience, $T_{g,mid}$ value is referred to as the T_g of bitumen later in this work.

Table 3. Empirical properties of the investigated bitumen samples.

Sample	Production method	Pen [dmm]	$T_{R\&B}$ [°C]	PI [-]	PG grade [a]
B-1	SR followed by oxidation	5	104.5	2.57	88-XX
B-2	SD	5	74.2	-0.74	88-XX
B-3	-	12	65.0	-0.86	82-XX
B-4	VB	15	64.2	-0.64	82-XX
B-5	-	15	62.6	-0.90	82-XX
B-6	SR	20	62.2	-0.49	82-XX
B-7	SR followed by air-rectification	25	61.5	-0.21	82-XX
B-8	Blend: SD + SR	27	55.5	-1.22	70-XX
B-9	-	27	61.5	-0.06	82-XX
B-10	VB	38	54.3	-0.80	70-XX
B-11	-	42	51.3	-1.27	70-22
B-12	-	51	49.1	-1.39	64-XX
B-13	VB	52	49	-1.37	64-16
B-14	VB followed by air-rectification	52	49.8	-1.17	64-16
B-15	-	53	49.9	-1.10	64-XX
B-16	-	61	47.7	-1.34	64-XX
B-17	-	62	50	-0.69	64-XX
B-18	SR	64	47.7	-1.23	64-28
B-19	VB	67	46.8	-1.36	58-16
B-20	-	70	46.1	-1.46	58-XX
B-21	VB	80	45.8	-1.20	58-XX
B-22	-	81	45.5	-1.25	58-XX
B-23	-	107	43.5	-1.09	58-XX
B-24	VB	187	38.5	-1.03	52-XX
B-25	SR	187	36.9	-1.80	52-XX
B-26	VB	190	39.2	-0.63	52-XX
B-27	-	200	37.7	-1.11	52-XX

SR = straight-run
SD = solvent-deasphalted
VB = visbroken
AR = air-rectified
[a] the low PG grades are reported only for five bitumens that were RTFO- and PAV-aged. 4-mm DSR technique was used to determine the critical low temperatures

Table 4. An overview of the thermal properties of the investigated bitumen samples determined from the DSC heating scan. See Appendix G for the definitions of the parameters listed in the table.

Sample	$T_{g,onset}$ [°C]	$T_{g,mid}$ [°C]	$T_{g,end}$ [°C]	ΔC_p [J g^{-1} K^{-1}]	Melting enthalpy [J g^{-1}]	Cold crystallization of waxes upon heating
B-1	-28	-10	8	0.42	0	-
B-2	-15	2	18	0.43	0	-
B-3	-18	-4	11	0.32	1.39	-
B-4	-43	-14	14	0.58	5.55	X
B-5	-27	-10	8	0.45	2.07	-
B-6	-28	-10	9	0.52	0	-
B-7	-34	-22	-4	0.46	0	-
B-8	-32	-14	5	0.45	2.73	X
B-9	-43	-23	-3	0.48	3.51	X
B-10	-47	-27	-7	0.51	5.41	X
B-11	-35	-18	-1	0.38	2.77	X
B-12	-39	-21	-2	0.44	6	X
B-13	-42	-25	-9	0.32	6.8	X
B-14	-42	-23	-5	0.38	6.16	X
B-15	-41	-22	-3	0.48	4.96	X
B-16	-37	-22	-7	0.40	4.86	X
B-17	-42	-27	-12	0.38	6.34	X
B-18	-32	-20	-7	0.40	0	-
B-19	-44	-26	-8	0.37	7.59	X
B-20	-38	-20	-2	0.41	3.76	X
B-21	-44	-24	-4	0.42	7.09	X
B-22	-35	-24	-13	0.34	2.44	-
B-23	-45	-24	-4	0.47	4	X
B-24	-41	-27	-14	0.44	5.36	X
B-25	-37	-26	-15	0.46	0	-
B-26	-45	-38	-30	0.22	9.63	-
B-27	-45	-31	-17	0.40	6.07	X

5.2. Characterization methods

The investigated bitumen samples were submitted to extensive rheological, chemical and thermal characterization. The testing matrix is shown in Table 5. Note that RTFO+PAV aged bitumens were investigated only by the 4-mm DSR technique; all the other tests were performed on unaged bitumens. Further, the data resulting from the 4-mm DSR experiments were used only to determine the low PG grade (see Table 3). The details of the different test methods employed in this study are described in the following.

Table 5. Testing matrix used in this study.

Test method	Rheological				Chemical				Thermal
	4-mm DSR		8-mm & 25-mm DSR	Physical aging experiments	GPC	UV-vis	FT-IR	RI	DSC
	unaged	RTFO +PAV							
B-1	X		X		X	X	X	X	X
B-2	X		X		X	X	X	X	X
B-3	X		X		X	X	X	X	X
B-4	X		X		X	X	X		X
B-5	X		X		X	X	X		X
B-6	X		X		X	X	X	X	X
B-7	X		X		X	X	X	X	X
B-8	X		X		X	X	X	X	X
B-9	X		X		X	X	X		X
B-10	X		X		X	X	X	X	X
B-11	X	X	X		X	X	X		X
B-12	X		X		X	X	X		X
B-13	X	X	X		X	X	X	X	X
B-14	X	X	X		X	X	X	X	X
B-15	X		X		X	X	X		X
B-16	X		X		X	X	X		X
B-17	X		X		X	X	X		X
B-18	X	X	X		X	X	X	X	X
B-19	X	X	X		X	X	X		X
B-20	X		X		X	X	X		X
B-21	X		X	X	X	X	X	X	X
B-22	X		X		X	X	X		X
B-23	X		X		X	X	X	X	X
B-24	X		X		X	X	X	X	X
B-25	X		X		X	X	X	X	X
B-26	X		X		X	X	X	X	X
B-27	X		X		X	X	X	X	X

Rheological characterization

Rheological experiments were performed with a stress-controlled dynamic shear rheometer (Malvern Kinexus Pro). The rheometer was equipped with a Peltier plate and active hood to minimize radial and vertical thermal gradients in the test specimen. This temperature control system was capable of controlling temperature to within ±0.01 K. A Julabo CF41 refrigerated circulator was used to remove heat from the rheometer during the low-temperature measurements. A parallel-plate geometry with a diameter of 4 mm was used, and the test results were corrected for radial instrument compliance as described in the AASHTO standard draft (Appendix B). This standard draft was also followed in the specimen preparation. The radial compliance and thermal expansion of the measuring system were determined prior to the rheological experiments, see Appendices C and D, respectively.

Frequency sweep experiments were performed in a strain-controlled mode within the LVE region (the strain amplitude was varied between 0.075 % and 0.01 % depending on the measurement temperature, see Appendix B). The oscillation frequency was swept from the highest (10 Hz) to the lowest (0.01 Hz) due to a better strain control. Frequency sweeps were conducted at temperatures from 10 °C to -40 °C with 10 K decrements. However, it was observed that the stiffest bitumen samples (Pen ≤ 15) slipped on the rheometer plates at -40 °C (or even at -30 °C in the case of bitumen B-2). Consequently, this data were omitted from the analysis. Details of the measurement procedure are provided in Appendix B. The repeatability of the test results is analyzed briefly in Appendix E.

Cyclic frequency sweeps (CFS) were carried out to study physical aging in bitumen sample B-21 (T_g = -24 °C as defined from DSC measurement). This sample was selected for the analysis since it was expected to exhibit significant physical aging due to its high content of crystallizable fractions and broad T_g range. CFS measurements were carried out in a strain-controlled mode at a constant strain amplitude of 0.01 % that is known not to disrupt the micro-structuring associated with physical aging [35]. The oscillation frequency was repeatedly ramped from 10 Hz to 0.1 Hz under isothermal conditions. Experiments were conducted at five different temperatures; at T_g, and 5 K and 10 K above and below this temperature. To ensure the thermal equilibrium of the test specimens, they were allowed to stabilize at the testing temperature 15 minutes prior to the start of the measurement. The duration of a single frequency sweep was approximately 510 s (= 8.5 min), and the total duration of the CFS measurement was approximately 7.4×10^5 s (≈ 206 h or 8.6 d) at T_g, and 1.0×10^5 s (≈ 28 h or 1.2 d) at the other measurement temperatures. A new specimen was prepared for each measurement at a different temperature.

In addition, another rheometer was used to obtain frequency sweep data at intermediate and high temperatures. The rheometer was a stress-controlled Paar Physica MCR 500, equipped with a double Peltier temperature control system (having an accuracy of ±0.01 K). These frequency sweeps were measured in a frequency range from 0.01 up to 10 Hz; 8-mm parallel plates were used from 0 °C to 50 °C, and 25-mm parallel plates were

used from 40 °C to 90 °C. For the hardest binders (Pen < 15), 8-mm plates were used from 0 °C to 60 °C and 25-mm plates from 50 °C to 90 °C. The strain amplitude levels were fixed as follows: 0.05 % when using 8-mm plates and 1 % when using 25-mm plates. The gap was set at 2 mm for the 8-mm plate tests and at 1 mm for the 25-mm plate tests. A consistency analysis between the rheological data measured with 4-mm parallel plates of Malvern Kinexus Pro and 8-mm parallel plates of Paar Physica MCR 500 is presented in Appendix F.

Size exclusion chromatography

In size exclusion chromatography, also referred to as gel permeation chromatography (GPC), a mixture of molecules is separated based on the volume of the molecules. In this project, an Alliance 2690 Separator module was used and two detectors were available, a differential refractometer (RI) detector and a Waters 996 photo diode array (PDA) detector. In the PDA detector, the concentration of absorbing substances in the eluent is continuously monitored using UV-visible light absorption (UV-vis); a wavelength variation from 200 to 610 nm was used.

Two separate GPC tests were conducted: one for the molecular weight determination and one for the UV-vis absorption. For the molecular weight determination, a set of two identical mix bed columns was used (PL gel 5 um mixed-D columns 300 mm×7.5 mm; pore size 100, 500, 1000, 10000 Å), combined with the RI detector. Calibration for molecular weight was performed with narrow polystyrene standards, see Appendix H. The values of different apparent molecular weights (M_n, M_w, M_z, M_{z+1}) and polydispersities (M_w/M_n) were calculated from the test data as described in Appendix I (note that the word "apparent" is used here to emphasize the effect of associations and interactions on the measured molecular weights [6]). Further, obtained GPC profiles were divided into different fractions based on retention times; this procedure is also presented in Appendix I. To measure the UV-vis absorptions, the PDA detector was used, and the GPC columns consisted of 3 Jordi columns with pore sizes of, respectively, 100, 500 and 1000 Å. In both cases, the eluent was tetrahydrofurane (THF), the injected volume was 10 µl, and the binder concentration in the THF eluent was kept at 0.8 % (±0.025 %). The measured absorption level changes in a linear way with changes in the concentration of the THF solution or changes in the injected volume. This was observed at all wavelengths.

A test using six repeats showed a repeatability standard deviation for the absorption areas of 0.8 % at 210 nm and 2.4 % at 570 nm. Each repeat consisted of preparing a new solution and injection in the GPC. As these variations are small, error bars were in most cases not used. It should be noted that these repeats, as well as the actual measurements, were recorded in a short time interval; comparing tests over longer time intervals may result in larger deviations.

Infrared spectroscopy

Infrared spectroscopy (FT-IR) with attenuated total reflection (ATR) was applied; a Nicolet IS 10 with a diamond cell (smart-orbit) was used. The great advantage of ATR is the possibility to measure a wide variety of solid and liquid samples without complex sample preparation.

The ATR prism consists of an IR transparent material with a high refractive index. The infrared beam enters the ATR crystal so that it is totally reflected at the crystal to sample interface. Due to its wavelike properties, the light is not reflected directly on the boundary surface but by a very small layer within the optically less dense sample. The fraction of the infrared wave that reaches into the sample is called the evanescent wave. Its penetration depth depends on the wavelength, the refractive indices of ATR crystal and sample and the angle of the entering infrared beam. In those spectral regions where the sample absorbs energy, the evanescent wave will be attenuated. After one or several internal reflections, the IR beam exits the ATR crystal and is directed to the IR detector. In the equipment used in this study, the IR beam is reflected only once. Provided a good contact between sample and ATR crystal is obtained, penetration depths for a diamond cell typically vary between 0.5–5 μm between wavenumber 4000 and 500 cm^{-1}.

In this study, a background is taken before each sample measurement to improve the repeatability. Bitumen is heated and a drop of material is poured on the prism. To obtain good contact between sample and prism, a small sample press is used. To account for small variations in penetration depths of the IR beam, a common procedure is to use peak ratios. This procedure was applied to the area integration at 1600 cm^{-1}, see Appendix J. As it did not influence the observed trends, absolute areas were used.

Refractive index

The Abbemat 500 refractometer from Anton Paar, used in this study, calculates the refractive index from a measurement of the angle for total internal reflection, also called the critical angle. For this purpose, the sample is placed on top of the measuring prism. This prism is illuminated from different angles by a light source. For any angle of incidence less than the critical angle, part of the incident light will be transmitted and part will be reflected. The reflected beam is detected by a sensor array. From this, the critical angle for total reflection is calculated and used to determine the refractive index (RI) of the sample. This method of detecting the angle of total reflection can be used to measure the refractive index. It also allows the measurement of optically dense and strongly absorbing samples, like bitumen. In this test, bitumen is first heated to 100 °C, from where a drop can be poured onto the prism. The refractive index of materials varies with wavelength of the incident light and with temperature. In the Abbemat refractometer, temperature can be controlled between 20 and 80 °C, with an accuracy of up to 0.03 K, using Peltier elements. The incident wavelength is fixed at 589±0.2 nm using a LED light source. The prism material is YAG (yttrium-aluminum-garnet). Repeated measurements on the same bitumen indicate a repeatability standard deviation

of 0.0002, which is well below the variation in refractive index observed between the binders. For each repeat, a new specimen of bitumen was placed onto the prism. In this project, the refractive index was determined on 16 bitumens at the temperatures of 20 °C, 50 °C and 80 °C.

Calorimetric measurements

All bitumen samples were investigated by DSC in order to have an idea about the presence of natural wax in these binders. The calorimeter used in this study was a Mettler Toledo DSC1. First, cooling scans were conducted from 140 °C to -60 °C followed by heating scans in the same temperature region. Scanning rates were 10 K/min both upon cooling and heating. T_gs of the investigated bitumens were determined from the data using the mid-point method, and the melting enthalpies were calculated by extrapolating the baseline derived from the melt, see Appendix G.

5.3. Rheological data analysis

rSpace software (version 1.60, Malvern Instruments Ltd) was used for the acquisition of the rheological data measured with the Malvern Kinexus rheometer. The data were transferred to an Excel template that was used to correct the data for radial instrument compliance. The Interactive Rheology Information Systems (IRIS, version 2013) software, developed by Winter and coworkers [190], was used for advanced rheological data analysis and plotting.

6. Results and analysis

6.1. Frequency sweep measurements

van Gurp-Palmen plots

A convenient way to analyze frequency sweep test results without any data manipulation is to plot them in a plot of the phase angle δ versus the absolute value of the complex modulus $|G^*|$. In literature this plot is widely known as the van Gurp-Palmen (vGP) plot [85,191,192] (in asphalt industry this plot is also termed the Black diagram [193]). One of the main uses of this plot is to investigate the validity of thermorheological simplicity; if the effect of b_T on the magnitude of the complex modulus is negligible, the frequency sweep data measured at different temperatures will superpose without shifting if the material is thermorheologically simple [82].

The frequency sweep data measured with the 4-mm parallel plate geometry in the temperature range of 10 °C to -40 °C are shown in the vGP plot in Figure 12. Data for each bitumen sample appear as a smooth curve in this plot, and thus all the investigated materials can be concluded to be thermorheologically simple at low temperatures (≤ 10 °C). However, as reported earlier by Soenen and Redelius [6], deviations from thermorheological simplicity are observed at higher temperatures in many of the samples that contain a significant amount of natural wax. This well-known characteristic of waxy bitumens is attributed to the gradual melting of natural wax when the temperature is increased [6,194]. This distinct difference in the vGP plots of waxy and non-waxy bitumens is demonstrated in Figure 13 where the frequency sweep data measured both at low and high temperatures are shown for the non-waxy bitumen B-18 and for the waxy bitumen B-21.

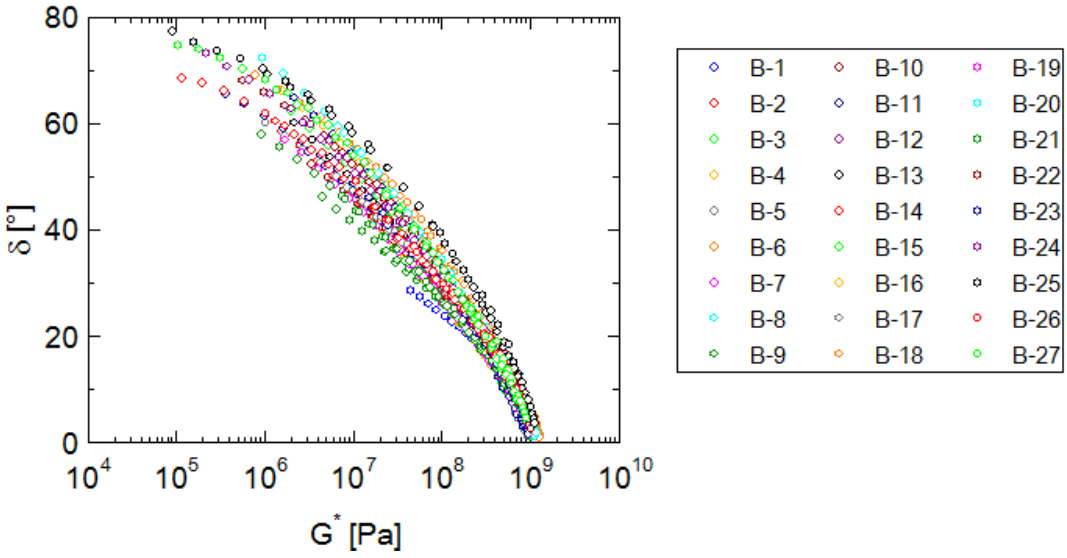

Figure 12. Low-temperature frequency sweep data of all the investigated bitumens plotted in the vGP plot.

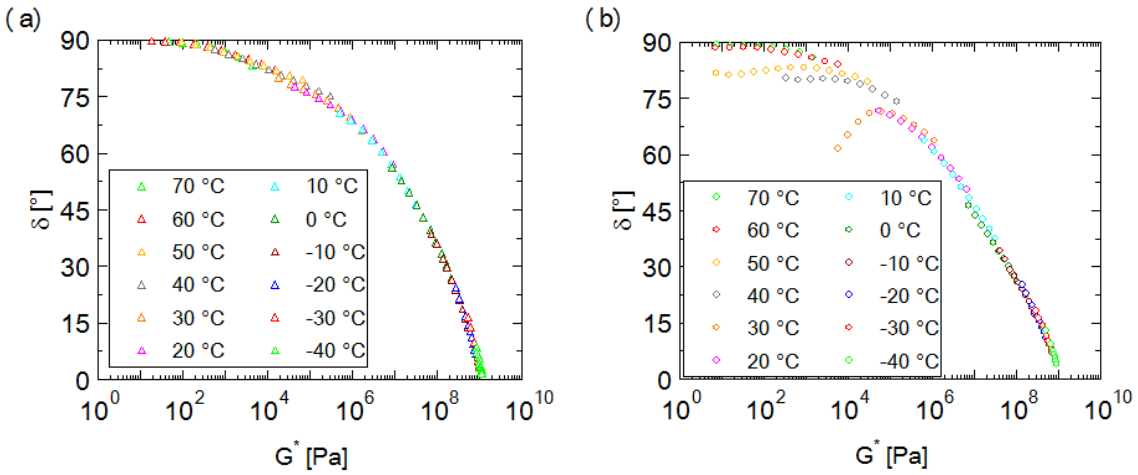

Figure 13. vGP plots for (a) non-waxy bitumen B-18 and (b) waxy bitumen B-21.

Furthermore, the glassy modulus G_g can be conveniently estimated from the vGP plot. G_g is the asymptotic value of complex modulus at low temperatures and/or high frequencies where the material behavior is ideally perfectly glassy. In the vGP plot this corresponds to the complex modulus value at the intersection of the data curve and x-axis. It is already evident from Figure 12 that the curves of all bitumen samples tend to collapse on a single curve at high stiffness values, evidencing the existence of an approximately constant G_g value for all unmodified bitumens. For more accurate estimation of G_g values, a magnification of the high-stiffness end of the vGP plot is provided in Figure 14. Based on this graph, the G_g values of the investigated bitumens can be estimated to vary in the range of 1-1.35 GPa. This result is in agreement with the G_g values of bitumen obtained with torsion bar (TB) and 4-mm parallel plate geometries

elsewhere in the literature [5,9,21,195]. Moreover, this value is also typical for other amorphous organic materials such as polymers [81].

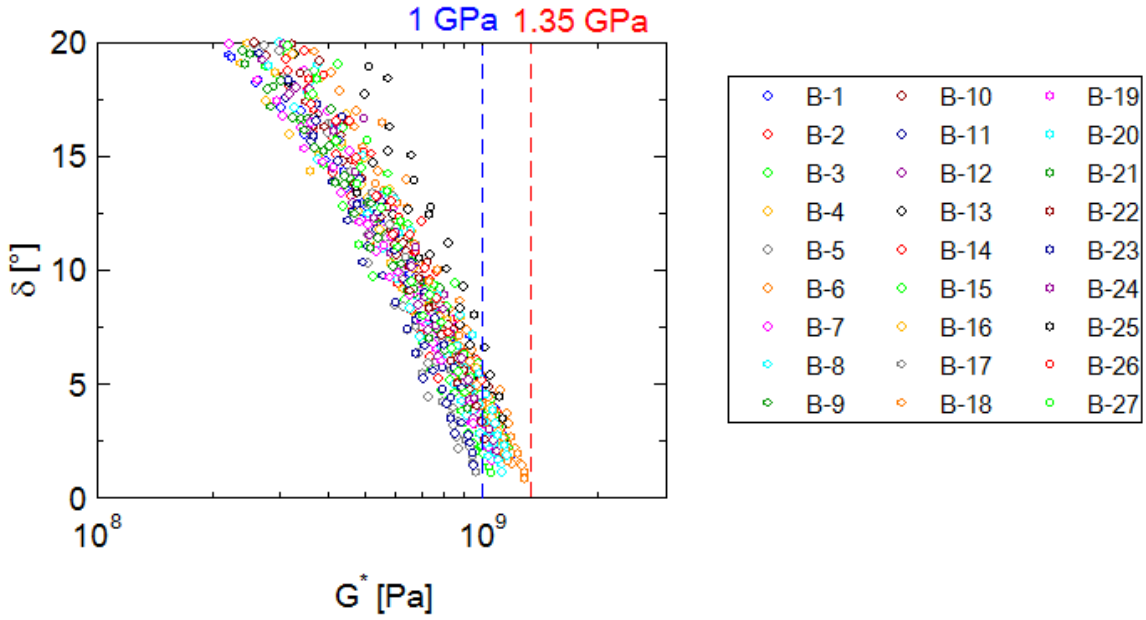

Figure 14. Estimation of the variation in the G_g values of the investigated bitumens.

Based on the limited repeatability analysis of Appendix E, the measured values of G_g are expected to be within ±7 % of the true values. Hence, the observed variation in the G_g values can be at least partly attributed to the differences in material properties rather than to experimental errors. In other words, the G_g of bitumen appears to be very slightly dependent on the crude oil source and/or production method. In particular, the low-temperature rheological behavior of the non-waxy straight-run bitumens (samples B-6, B-18 and B-25) appeared to be peculiar. The curves corresponding to these three bitumens are marked with red symbols in Figure 15, whereas the other bitumens are plotted with blue symbols. The curves of the non-waxy straight-run bitumens plot clearly on the more liquid-like side of the diagram than the curves of the other bitumens on average; i.e., the curves corresponding to the non-waxy straight-run bitumens appear above the other curves in Figure 15. This seems to be true also at the lowest temperatures (at the lower right corner of the plot), evidencing the fact that the G_g of non-waxy straight-run bitumens are higher than the G_g of bitumens produced with different processes. At this moment, it is not clear, what is the actual chemical or structural property of non-waxy straight-run bitumens that causes their G_g to be relatively high. It should be also mentioned that the non-waxy straight-run bitumens that were also air-rectified are not distinguishable in the vGP plot in the same way as the non-air-rectified ones, i.e., in this case, air-rectification appears to shift the curve to the more elastic side of the vGP plot and to lower G_g.

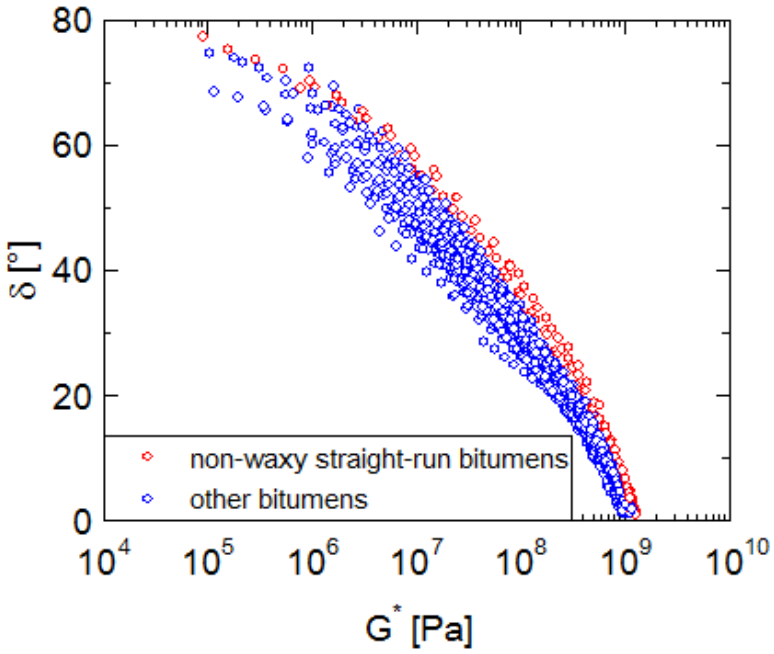

Figure 15. Comparison of the low-temperature rheological behavior of the non-waxy straight-run bitumens (B-6, B-18 and B-25) and other bitumens.

In the past, when the low-temperature rheological data were not easily accessible, a plot of the absolute value of the complex modulus $|G^*|$ versus the logarithm of $(1+\tan \delta)$ was used to estimate the G_g of bitumen [196-199]. It was claimed that the advantage of this plot compared to the vGP plot is that it allows more of the rheological data to be used in the estimation of G_g since the relationship between the $|G^*|$ and $\log(1+\tan \delta)$ appears to be linear over several decades of modulus values. Figure 16 shows the data from Figure 12 replotted in the $|G^*|$ vs. $\log(1+\tan \delta)$ plot. It can be seen that near G_g (at the top left corner of the plot) the curves tend to bend downward, and thus the value of G_g is overestimated if linearity is assumed. Therefore, the estimation of G_g by the low-temperature extrapolation of the intermediate-temperature data in the $|G^*|$ vs. $\log(1+\tan \delta)$ plot is discouraged.

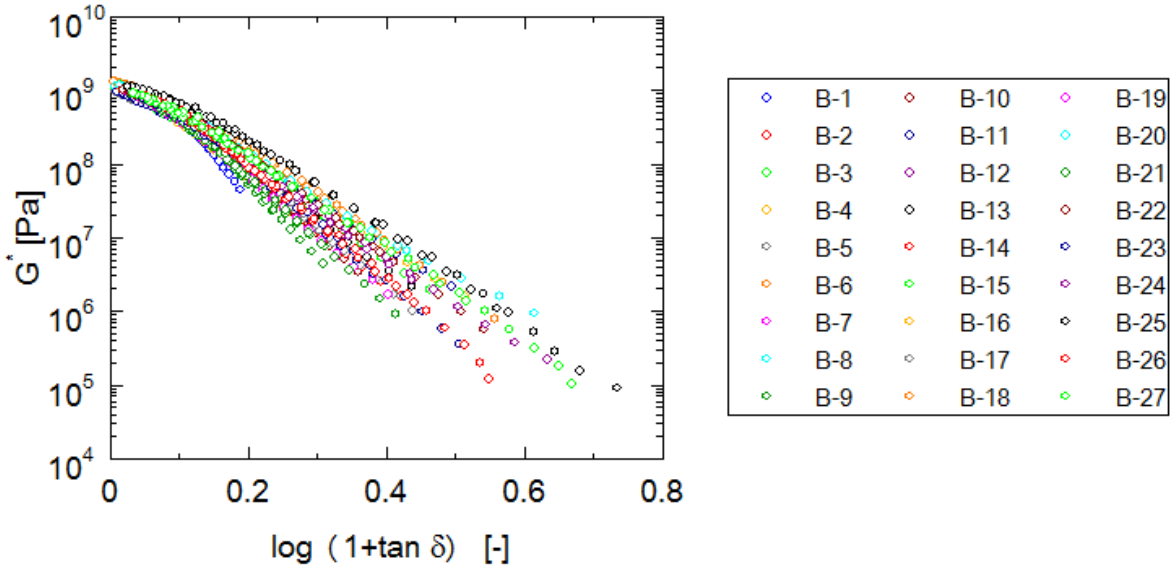

Figure 16. Estimation of G_g using the $|G^*|$ vs. log(1+tan δ) plot.

Master curves and shift factors

For further analysis of the frequency sweep test results, master curves of the dynamic material functions (storage G' and loss G'' moduli, as well as the loss tangent tan δ) were built by applying the TTS principle. The master curves were constructed by horizontal shifting of the isothermal frequency sweep data. Smooth master curves are obtained for the bitumen samples that did not contain a significant amount of natural wax, see Figure 17(a). However, the master curves of some of the samples that contained a significant amount of natural wax appeared to be not very smooth, see Figure 17(b). These imperfections in the shape of the master curves are apparent at the low-frequency (high-temperature) end of the master curves, as could have been expected based on the analysis of the vGP plots. Thus, it can be concluded that smooth master cannot always be obtained for waxy bitumens, as also observed by e.g. Lesueur et al. [15].

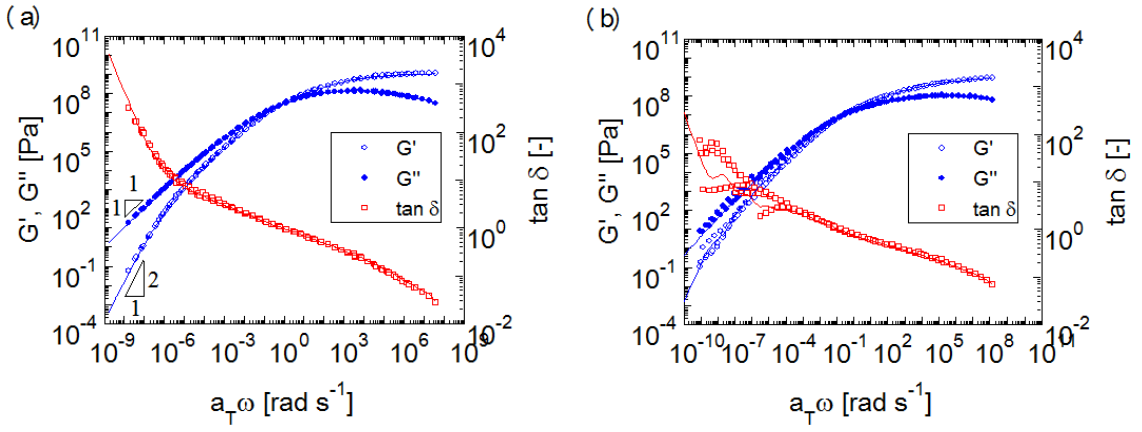

Figure 17. Master curves of (a) non-waxy bitumen B-18 and (b) waxy bitumen B-21, T_r = 0 °C. The lines represent the fits of the generalized Maxwell model.

Horizontal shift factors a_T derived from the master curve construction are observed to follow accurately the Kaelble-WLF temperature dependence (Equation 4). The normalized root-mean-square errors (NRMSE) of these fits were less than 1 % for all the bitumen samples investigated. As an example, the horizontal shift factors and the corresponding Kaelble-WLF fit of bitumen B-18 are shown in Figure 18. Note that here the reference temperature is set to be equal to the T_g of the bitumen sample, as defined by DSC (in this case T_g = -20 °C). The values of the Kaelble-WLF parameters for all the investigated bitumens are listed in Table 6. It is noteworthy that for all the bitumen samples T_d is approximately 5-30 K higher than T_g. Earlier, Rowe and Sharrock [99] assumed that T_d is approximately equal to T_g for bitumen.

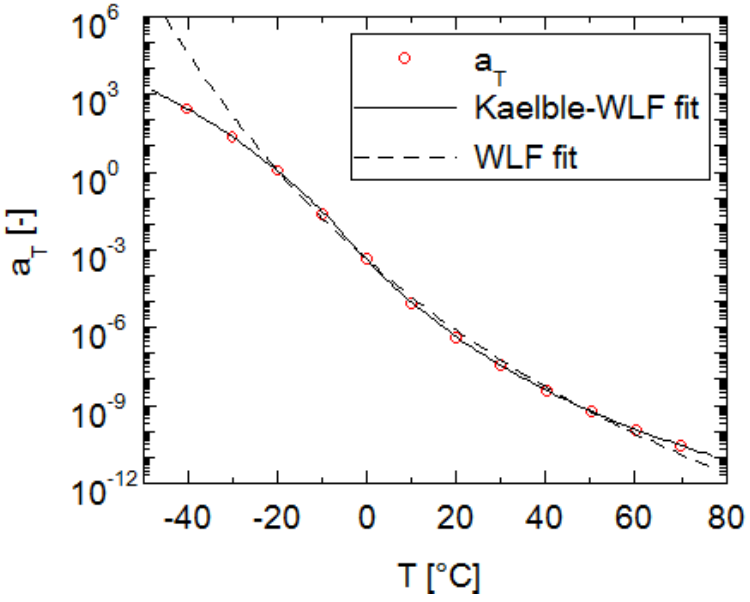

Figure 18. Kaelble-WLF fit to the horizontal shift factors of bitumen B-18. The WLF fit is shown for comparison purposes.

Table 6. The values of the Kaelble-WLF parameters (see Equation 4) and the normalized root-mean-square errors of the model fits. The superscript "g" denotes that $T_r = T_g$.

Sample	c_1^g [-]	c_2^g [K]	$T_r = T_g$ [K]	T_d [K]	NRMSE [%]
B-1	27.0	139.0	263	270.1	0.66
B-2	19.8	92.9	275	281.3	0.61
B-3	19.3	91.2	269	273.0	0.83
B-4	26.3	130.3	259	268.6	0.61
B-5	18.5	87.8	263	274.5	0.59
B-6	18.3	86.8	264	273.5	0.60
B-7	19.2	99.8	251	270.5	0.35
B-8	17.4	79.5	259	272.3	0.56
B-9	20.1	102.3	250	271.1	0.25
B-10	22.6	122.0	246	270.9	0.94
B-11	18.4	92.8	255	269.9	0.43
B-12	19.2	90.0	252	271.4	0.50
B-13	23.5	117.9	248	267.9	0.62
B-14	19.6	95.9	250	268.9	0.81
B-15	17.2	78.7	251	270.9	0.74
B-16	18.5	89.0	251	270.1	0.47
B-17	20.7	109.0	246	268.2	0.40
B-18	17.2	86.2	253	268.8	0.29
B-19	21.4	105.2	247	270.3	0.72
B-20	17.8	83.4	253	268.7	0.61
B-21	31.9	173.6	249	266.0	0.48
B-22	18.3	94.3	249	267.7	0.30
B-23	20.4	111.9	249	267.0	0.63
B-24	17.9	91.2	246	267.3	0.73
B-25	16.5	88.6	247	265.4	0.34
B-26	21.9	130.0	236	267.5	0.59
B-27	17.8	95.6	242	265.9	0.53

The frequency sweep data measured at low temperatures (with 4-mm parallel plate geometry) were also investigated separately from the frequency sweep data measured at higher temperatures (with 8-mm and 25-mm parallel plate geometries). This was done in order to obtain more detailed information of the dynamic properties near the glass transition. The low-temperature master curves obtained by only horizontal shifting for bitumen B-18 are presented in Figure 19(a). It is observed that although the tan δ curves superimpose very accurately, the shift is not perfect for the *G'* and *G''* curves at the lowest temperatures. This indicates that also vertical shifting is needed to produce smooth master curves of all dynamic material functions. Indeed, the result of shifting is

more satisfying when vertical shifting is also performed, see Figure 19(b). The horizontal and vertical shift factors used to construct the master curves in Figure 19(b) are plotted against temperature in Figure 19(c). For all the investigated bitumens vertical shifting is needed to produce smooth master curves of *G'* and *G''* at low temperatures. However, it should be noted that in all cases the vertical shift factors deviated just slightly from one, i.e. the amount of vertical shifting was only minor.

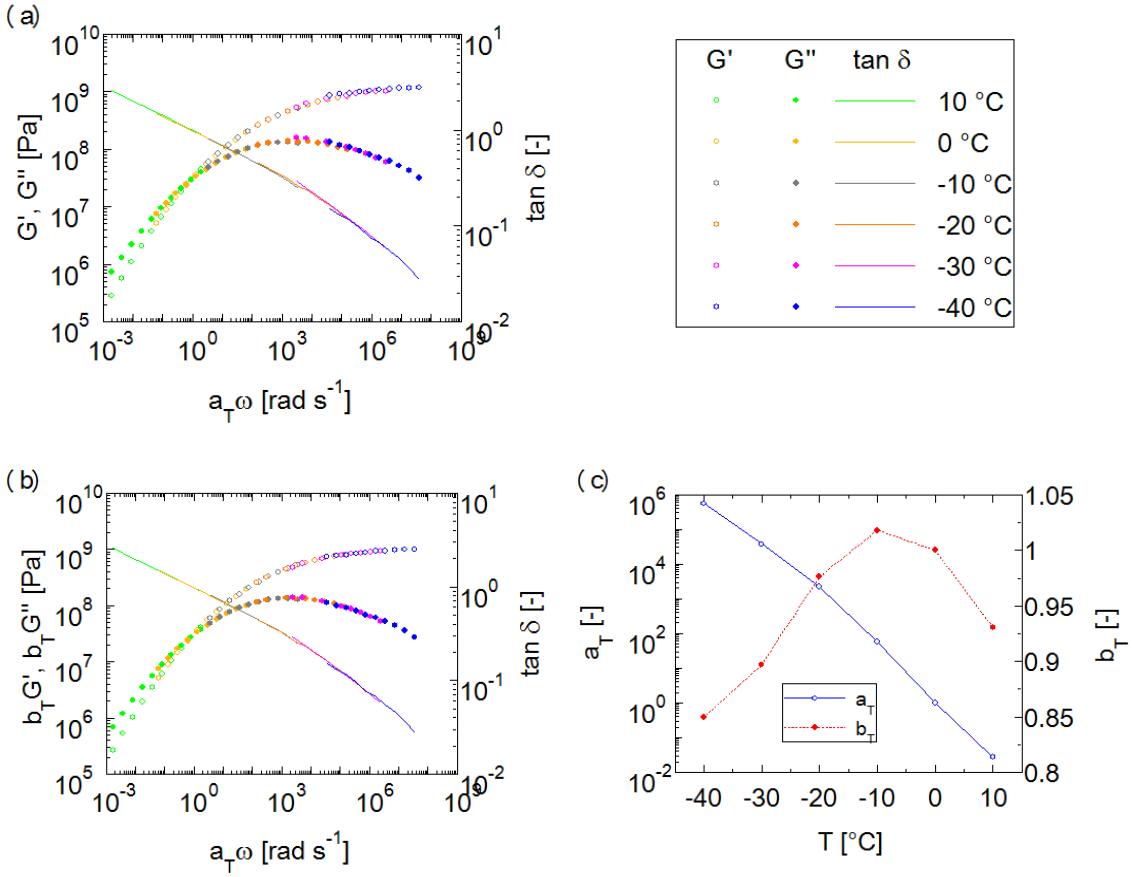

Figure 19. Low-temperature master curves for bitumen B-18 produced (a) by only horizontal shifting and (b) by both horizontal and vertical shifting. The horizontal and vertical shift factors used to construct the master curves in part (b) are shown in part (c). The lines in part (c) are to guide the eye only. In all parts T_r = 0 °C.

The vertical shift factors are typically ignored or mentioned only in passing in the literature due to their relatively small magnitudes compared with the magnitudes of horizontal shift factors, or because the nature of the shift is not always clearly understood [184,185]. However, deep in the glassy state where the response is less pronounced, the application or not of vertical shifts can have a significant effect on the horizontal shift factors [81,200]. O'Connell and McKenna proposed that one possible explanation for the need of vertical shifting is densification [184]. Further discussion on this topic is provided in Section 7.

Finally, the author wants to emphasize that although vertical shifting is needed to produce perfectly smooth master curves at low temperatures, mere horizontal shifting should be performed when both high- and low-temperature frequency sweep data are used to construct master curves. This is because the use of vertical shifting is not justified for the high-temperature data of bitumen (the Cole-Cole curves are temperature-independent at high temperatures, see discussion in the next subsection), and thus the application of vertical shift factors might lead to errors in the calculation of horizontal shift factors. In other words, the slight unsmoothness of the master curves at low temperatures is expected to be a smaller disadvantage than the incorrect values of horizontal shift factors at high temperatures. Therefore, shift factors obtained from the mere horizontal shifting of isothermal frequency sweep data are used in the later analysis.

Cole-Cole plots

The Cole-Cole representation was initially developed to model dielectric relaxation properties [201], but later on it has also been used to describe mechanical relaxation processes especially in the glassy state [202]. Essentially, the Cole-Cole plot is a representation where storage and loss parts of a complex quantity are plotted against each other. Various types of plots have been referred to as the Cole-Cole plot in rheology, most commonly the plots of loss modulus vs. storage modulus (G'' vs. G') or out-of-phase component of the complex viscosity η^* vs. dynamic viscosity (η'' vs. η') on a linear or double-logarithmic scale. In this work, G' and G'' are plotted against each other on linear scales in order to emphasize the low-temperature rheological behavior.

The low-temperature frequency sweep data of bitumen B-18 is shown in Figure 20(a). It is obvious that the data measured at the lowest temperatures do not superimpose very well. This is known to be an indication that vertical shifting is needed to obtain smooth master curves, i.e. the TTS principle to hold [203-206]. Indeed, when the vertically shifted frequency sweep data of Figure 19(b) is depicted in the Cole-Cole plot in Figure 20(b), a smooth curve appears. This confirms the observation made earlier in the text that vertical shifting is needed to produce single master curves from the low-temperature frequency sweep data of bitumen. It is worth noting that in the Cole-Cole plot isothermal curves are shifted in 45° direction when vertical shift factors are applied.

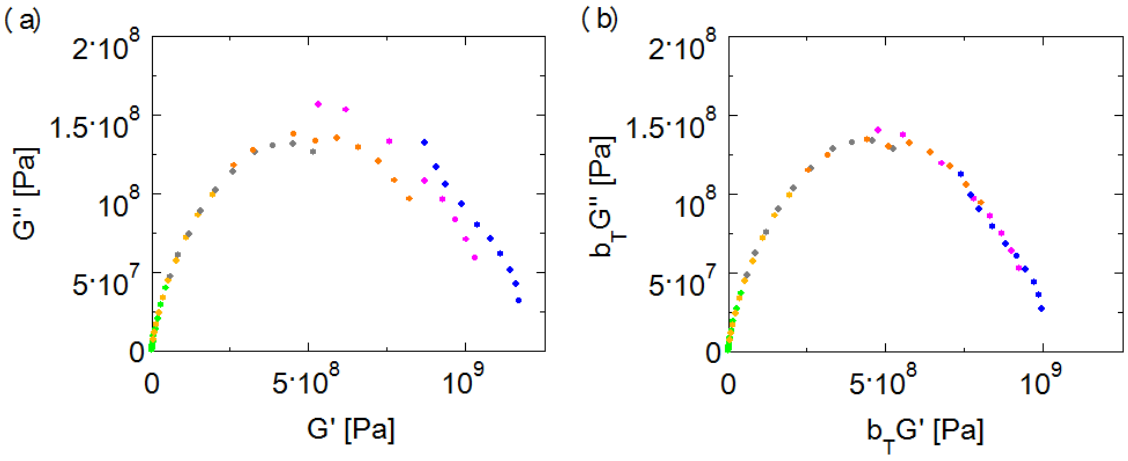

Figure 20. Cole-Cole plots of the frequency sweep data that (a) have not been vertically shifted during master curve construction, and (b) have been vertically shifted during master curve construction.

Temperature dependence of viscoelastic properties

The temperature dependence of viscoelastic properties at T_g can be expressed in terms of dynamic fragility m and apparent activation energy E_g at T_g. The values of these parameters are calculated from the values of the Kaelble-WLF parameters according to Equations 14 and 15. The derivation of these equations is presented in Appendix K.

$$m = \frac{c_1^g c_2^g T_g}{\left(c_2^g + |T_d - T_g|\right)^2} \tag{14}$$

$$E_g = \frac{ln(10) c_1^g c_2^g R T_g^2}{\left(c_2^g + |T_d - T_g|\right)^2} \tag{15}$$

The values of m and E_g are listed for all the investigated bitumens in Table 7. The values of m and E_g vary in the ranges of 26-52 and 115-271 kJ mol^{-1}, respectively. The values of m reported here are significantly higher than the value of 16 reported by Qin et al. [9]. Still, the reported values of m are relatively low compared to most other glass-forming liquids [101,145], and thus bitumen can be regarded to be a relatively strong glass-former.

Table 7. Values of the glass transition temperature, dynamic fragility and apparent activation energy at T_g for the investigated bitumens.

Sample	T_g [K] [a]	m [-]	E_g [kJ mol^{-1}]
B-1	263	46	231
B-2	275	51	267
B-3	269	52	271
B-4	259	45	223
B-5	263	44	221
B-6	264	45	225
B-7	251	34	162
B-8	259	42	207
B-9	250	34	162
B-10	246	31	147
B-11	255	38	184
B-12	252	36	176
B-13	248	36	171
B-14	250	36	170
B-15	251	35	167
B-16	251	36	171
B-17	246	32	153
B-18	253	36	176
B-19	247	34	159
B-20	253	38	185
B-21	249	38	181
B-22	249	34	161
B-23	249	33	159
B-24	246	32	148
B-25	247	32	150
B-26	236	26	115
B-27	242	29	133

[a] as measured by DSC

In order to analyze the temperature dependences of the viscoelastic properties of the investigated bitumens over a wider temperature range, the horizontal shift factors are shown in the Angell plot in Figure 21. This plot is a convenient way to study the rheology of materials near the glass transition since the temperatures on the x-axis of the plot are T_g-normalized. Generally speaking, there are no large differences in the temperature dependences as the curves fall almost on a single curve. Only waxy bitumen B-26 appears to be somewhat less temperature-sensitive than the rest of the bitumens, as also evidenced by its high PI value. However, despite T_g-normalized temperature dependencies appear to be relatively similar among the investigated bitumens over a wide range of temperatures, significant differences are observed near T_g. This conclusion can also be made based on the varying values of m, see Table 7. It is

not yet clear if and how the low-temperature performance of bitumen in paving applications is influenced by its temperature sensitivity near T_g, but this is certainly an interesting topic for future investigations.

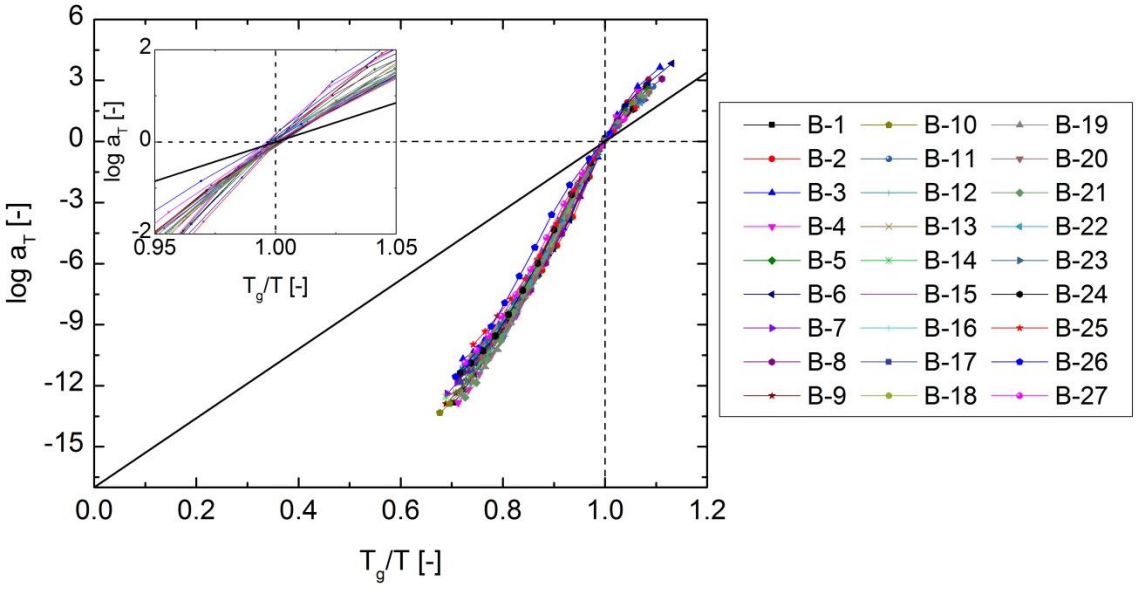

Figure 21. Angell plot of the horizontal shift factors for the investigated bitumens. The inset shows a magnification of the main figure in the vicinity of the glass transition temperature. The solid straight line corresponds to the Arrhenius temperature dependence, $m = 17$.

Characteristics of the relaxation time spectra

The characteristics of the relaxation time spectrum $H(\tau)$ near the glass transition have been earlier described for colloidal and molecular glasses, e.g. [103,207]. Winter [103] concluded that the relaxation patterns of these two classes of glasses are similar near the glass transition, and that they both can be described with a power-law relaxation time spectrum with positive exponent. Here the $H(\tau)$ of the investigated bitumens are calculated from the dynamic master curves using the method of Baumgaertel and Winter [208,209]. As an example, the $H(\tau)$ of bitumen B-18 is shown in Figure 22. In the calculation of this spectrum frequency sweep data measured both at high and low temperatures are utilized. At long τ (corresponding to high temperatures) the spectrum is characterized by a slope of approximately -1, whereas at short τ (corresponding to low temperatures) the spectrum has a slope of approximately 0.16. This overall shape of $H(\tau)$ is characteristic for all the bitumens investigated.

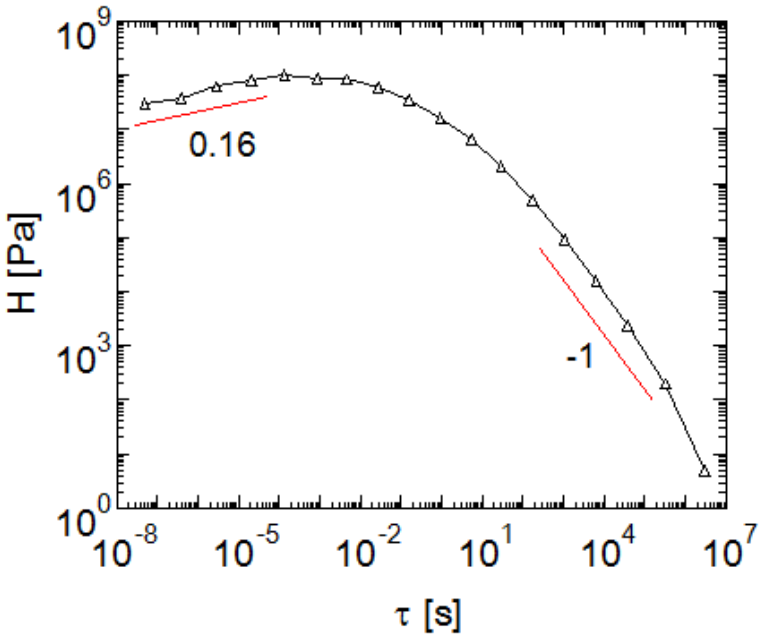

Figure 22. $H(\tau)$ of bitumen B-18 calculated numerically from the data of Figure 17(a).

In order to gain more detailed information of the evolution of the slope of $H(\tau)$ at low temperatures, the spectrum is calculated separately for each frequency sweep measured at or below 0 °C. These $H(\tau)$ are depicted in Figure 23 for bitumen B-18. It can be seen that above T_g the slope of $H(\tau)$ is negative suggesting that the stress is dominated by rearrangement of the small molecules. On the contrary, below T_g, $H(\tau)$ has a positive slope indicating that few molecules can rearrange by themselves or involve small groups of molecules while most relaxation processes require large-scale cooperation of molecular groups [103]. In between, at T_g, the slope of $H(\tau)$ equals to zero representing the transition from small-scale to large-scale relaxation processes upon cooling. These general features of the shape of $H(\tau)$ were observed to be characteristic for all the investigated bitumen samples.

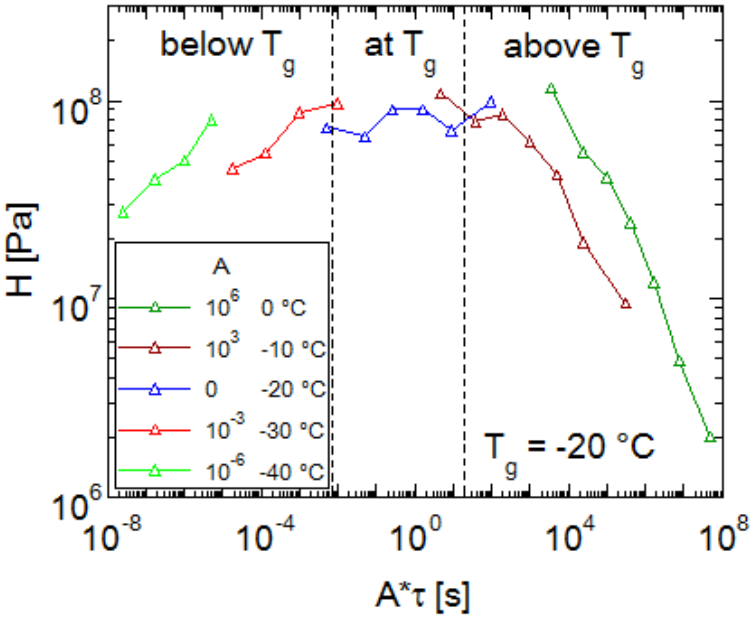

Figure 23. $H(\tau)$ calculated from individual frequency sweeps measured near T_g for bitumen B-18. The spectra corresponding to the frequency sweep data measured above and below T_g have been horizontally shifted to aid visual inspection of the data.

6.2. Correlations of low-temperature rheology with chemical and thermal properties

Correlations between low-temperature rheology and molecular weight characteristics

The Pearson's correlation coefficients (r) for the linear correlations between different molecular weight parameters (M_n, M_w, M_z, M_{z+1}, M_w/M_n) and low-temperature stiffness (G^*) and elasticity (δ) are shown in Tables 8 and 9, respectively. The correlations are not shown for G^* and δ measured at -40 °C since the stiffest bitumen samples were observed to slip during rheological experiments at this very low temperature.

Table 8. Pearson's correlation coefficients (*r*) for the correlations between molecular weight characteristics and *G** at low temperatures.

M_n	10 °C	0 °C	-10 °C	-20 °C	-30 °C
10 Hz	0.44	0.49	0.53	0.52	0.49
1 Hz	0.40	0.45	0.50	0.52	0.51
0.1 Hz	0.36	0.40	0.47	0.50	0.51
0.01 Hz	0.33	0.36	0.43	0.47	0.49

M_w	10 °C	0 °C	-10 °C	-20 °C	-30 °C
10 Hz	0.27	0.29	0.32	0.34	0.39
1 Hz	0.24	0.26	0.30	0.32	0.38
0.1 Hz	0.23	0.23	0.26	0.29	0.36
0.01 Hz	0.23	0.21	0.23	0.26	0.33

M_z	10 °C	0 °C	-10 °C	-20 °C	-30 °C
10 Hz	0.16	0.18	0.21	0.24	0.33
1 Hz	0.14	0.14	0.18	0.22	0.31
0.1 Hz	0.13	0.12	0.14	0.18	0.28
0.01 Hz	0.15	0.11	0.12	0.14	0.24

M_{z+1}	10 °C	0 °C	-10 °C	-20 °C	-30 °C
10 Hz	0.02	0.03	0.08	0.12	0.23
1 Hz	0.02	0.01	0.04	0.09	0.20
0.1 Hz	0.02	0.00	0.01	0.05	0.16
0.01 Hz	0.04	-0.01	-0.01	0.01	0.11

M_w/M_n	10 °C	0 °C	-10 °C	-20 °C	-30 °C
10 Hz	0.16	0.17	0.20	0.23	0.32
1 Hz	0.14	0.14	0.16	0.20	0.30
0.1 Hz	0.13	0.12	0.13	0.16	0.25
0.01 Hz	0.15	0.10	0.11	0.13	0.22

Table 9. Pearson's correlation coefficients (r) for the correlations between molecular weight characteristics and δ at low temperatures.

M_n	10 °C	0 °C	-10 °C	-20 °C	-30 °C
10 Hz	-0.44	-0.46	-0.51	-0.52	-0.54
1 Hz	-0.43	-0.44	-0.48	-0.50	-0.51
0.1 Hz	-0.43	-0.43	-0.45	-0.47	-0.48
0.01 Hz	-0.43	-0.44	-0.45	-0.46	-0.44

M_w	10 °C	0 °C	-10 °C	-20 °C	-30 °C
10 Hz	-0.30	-0.26	-0.28	-0.29	-0.35
1 Hz	-0.34	-0.27	-0.26	-0.27	-0.31
0.1 Hz	-0.40	-0.30	-0.25	-0.25	-0.28
0.01 Hz	-0.47	-0.35	-0.27	-0.24	-0.24

M_z	10 °C	0 °C	-10 °C	-20 °C	-30 °C
10 Hz	-0.19	-0.14	-0.16	-0.18	-0.26
1 Hz	-0.23	-0.15	-0.14	-0.15	-0.21
0.1 Hz	-0.29	-0.19	-0.14	-0.13	-0.18
0.01 Hz	-0.37	-0.25	-0.16	-0.13	-0.14

M_{z+1}	10 °C	0 °C	-10 °C	-20 °C	-30 °C
10 Hz	-0.01	0.01	-0.02	-0.06	-0.16
1 Hz	-0.04	0.01	0.01	-0.02	-0.10
0.1 Hz	-0.10	-0.01	0.02	0.01	-0.06
0.01 Hz	-0.17	-0.06	0.01	0.02	-0.01

M_w/M_n	10 °C	0 °C	-10 °C	-20 °C	-30 °C
10 Hz	-0.16	-0.11	-0.12	-0.15	-0.24
1 Hz	-0.21	-0.12	-0.10	-0.12	-0.18
0.1 Hz	-0.29	-0.16	-0.10	-0.09	-0.15
0.01 Hz	-0.38	-0.23	-0.12	-0.09	-0.10

It is apparent from Tables 8 and 9 that only relatively weak linear correlations between the molecular weight parameters and low-temperature stiffness and elasticity can be observed. Moreover, visual inspection of the correlation plots did not indicate any strong nonlinear relations between the rheological and molecular properties either. However, it is notable from the tables that almost all the correlations between the molecular weight parameters and G^* are positive, while almost all the correlations between the molecular weight parameters and δ are negative. Furthermore, the fact that the strongest correlations are observed for the *number-average* molecular weight M_n indicates that smaller molecules play a more important role in the low-temperature rheology than larger molecules. This is in contrary to the high-temperature rheological

properties of bitumen that have been observed to correlate more strongly with the abundance of larger molecules, e.g. [210,211]. Examples of the weak correlations between M_n and the low-temperature rheological properties are depicted in Figure 24.

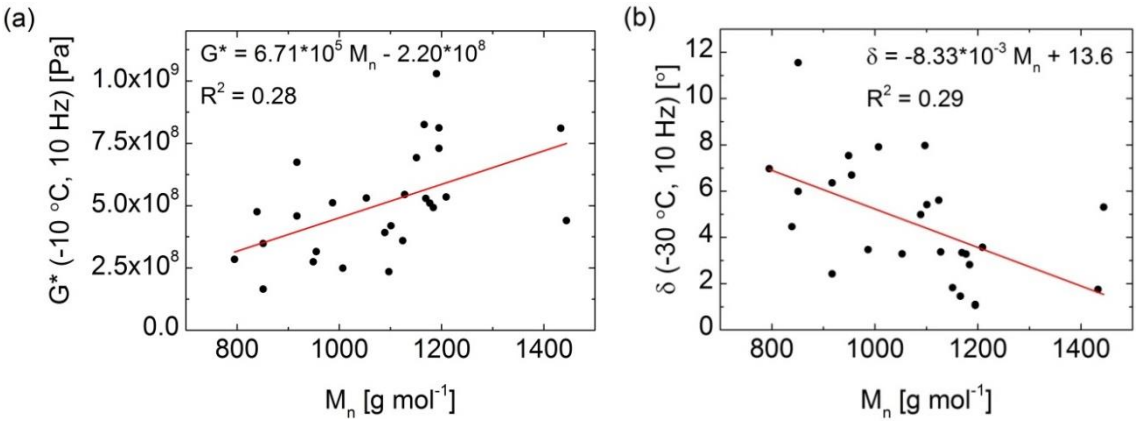

Figure 24. Examples of the weak correlations between M_n and (a) G^* and (b) δ.

Another way to study the importance of small molecules on the low-temperature rheological properties is to investigate the correlation between the small molecular size (SMS) content and the rheological parameters. The relevant correlation plots are shown in Figure 25. The temperature and frequency at which G^* and δ have been measured are the same as in Figure 24. Weak correlations between the small-molecule content and rheological parameters are found, and, as expected, the correlation is negative for G^* and positive for δ. In other words, the bitumens that have a high small-molecule content tend to be, on average, softer and less elastic at low temperatures than the bitumens with lower small-molecule content.

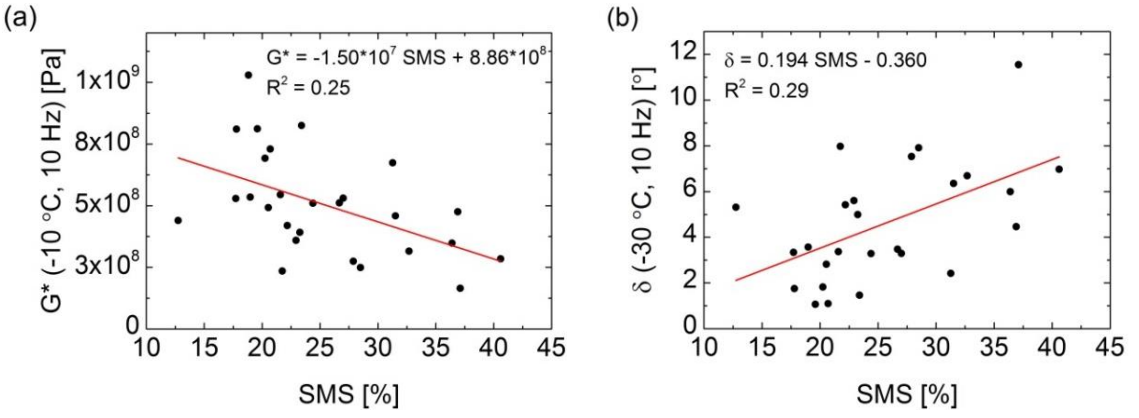

Figure 25. Correlations between the small-molecule content (SMS) and (a) G^* and (b) δ of the investigated bitumens. The temperature and frequency at which G^* and δ have been measured are the same as in Figure 24.

Correlations between low-temperature rheology and aromaticity

In this study, three testing methods were used to determine average levels of aromaticity in bitumen; these are the C=C absorption in FT-IR, the RI measurements and the UV-vis absorption. However, all these methods are only qualitative as they fail to identify the exact structure of the hydrocarbons. A detailed discussion about the interpretation and limitations of these testing techniques is provided by Soenen and Redelius [6]. In the following analysis only the rheological properties measured at low temperatures with the 4-mm parallel plate geometry are considered. The correlations between aromaticity and high- and intermediate-temperature rheological properties have already been reported by Soenen and Redelius [6].

The *r* values from the linear regression analysis between the aromaticity parameters and low-temperature rheological properties are listed in Tables 10-15. RI exhibits a moderate positive correlation with the stiffness (G^*) and a strong negative correlation with the elasticity (δ) of bitumen at selected testing conditions. However, the correlations become weaker with decreasing temperature and increasing frequency. On the contrary, the strength of the correlations is only slightly dependent on the temperature at which RI is measured; correlations are only a little bit stronger at 80 °C than at 50 °C or at 20 °C. For brevity, only the correlations for the RI values measured at 80 °C are shown in Tables 10 and 11.

Even stronger correlations are found between aromaticity and low-temperature rheology are observed when C=C and UV-vis absorptions are used as measures of aromaticity. In the case of UV-vis absorptions, the correlations are highly dependent on the wavelength, and the highest correlations appear at the wavelengths between 380 nm and 450 nm. At these wavelengths, the correlations with the elasticity of bitumen are as high as R^2 = 0.81. However, again the correlations are relatively weak for the rheological properties measured at the lowest temperatures. In Tables 14 and 15 the correlations with rheological parameters are shown, for brevity, only for the UV-vis absorption values measured at 380 nm, 410 nm and 450 nm. To illustrate the strong relationship between the aromaticity and elasticity of bitumen, the strongest linear correlations between different aromaticity parameters and δ are shown in Figure 26.

Table 10. Pearson's correlation coefficients (*r*) for the correlations between refractive index RI measured at 80 °C and G^*.

	10 °C	0 °C	-10 °C	-20 °C	-30 °C
10 Hz	0.60	0.60	0.55	0.48	0.34
1 Hz	0.58	0.59	0.57	0.51	0.37
0.1 Hz	0.55	0.58	0.58	0.55	0.42
0.01 Hz	0.53	0.55	0.58	0.57	0.46

Table 11. Pearson's correlation coefficients (r) for the correlations between refractive index RI measured at 80 °C and δ.

	10 °C	0 °C	-10 °C	-20 °C	-30 °C
10 Hz	-0.78	-0.72	-0.62	-0.49	-0.31
1 Hz	-0.81	-0.77	-0.69	-0.58	-0.43
0.1 Hz	-0.83	-0.80	-0.75	-0.65	-0.51
0.01 Hz	-0.83	-0.82	-0.77	-0.70	-0.60

Table 12. Pearson's correlation coefficients (r) for the correlations between C=C absorption from FT-IR and G^*.

	10 °C	0 °C	-10 °C	-20 °C	-30 °C
10 Hz	0.59	0.60	0.59	0.54	0.46
1 Hz	0.57	0.59	0.59	0.56	0.46
0.1 Hz	0.54	0.57	0.59	0.57	0.48
0.01 Hz	0.52	0.54	0.58	0.58	0.51

Table 13. Pearson's correlation coefficients (r) for the correlations between C=C absorption from FT-IR and δ.

	10 °C	0 °C	-10 °C	-20 °C	-30 °C
10 Hz	-0.74	-0.66	-0.57	-0.47	-0.34
1 Hz	-0.79	-0.72	-0.63	-0.54	-0.42
0.1 Hz	-0.83	-0.76	-0.68	-0.60	-0.49
0.01 Hz	-0.85	-0.80	-0.72	-0.63	-0.54

Table 14. Pearson's correlation coefficients (r) for the correlations between UV-vis absorptions and G^*. For brevity, the correlations are shown only for the UV-vis absorptions measured at 380 nm, 410 nm and 450 nm (these wavelengths were observed to correlate most strongly with G^*).

UV-vis at 380 nm	10 °C	0 °C	-10 °C	-20 °C	-30 °C
10 Hz	0.68	0.68	0.63	0.54	0.39
1 Hz	0.65	0.68	0.66	0.59	0.44
0.1 Hz	0.61	0.66	0.68	0.63	0.50
0.01 Hz	0.56	0.62	0.68	0.66	0.55

Table 14. Continued.

UV-vis at 410 nm	10 °C	0 °C	-10 °C	-20 °C	-30 °C
10 Hz	0.74	0.74	0.74	0.71	0.63
1 Hz	0.72	0.73	0.73	0.71	0.63
0.1 Hz	0.69	0.71	0.73	0.72	0.63
0.01 Hz	0.67	0.69	0.72	0.71	0.63

UV-vis at 450 nm	10 °C	0 °C	-10 °C	-20 °C	-30 °C
10 Hz	0.62	0.63	0.64	0.62	0.58
1 Hz	0.59	0.61	0.62	0.62	0.57
0.1 Hz	0.57	0.59	0.61	0.61	0.55
0.01 Hz	0.56	0.56	0.59	0.60	0.55

Table 15. Pearson's correlation coefficients (r) for the correlations between UV-vis absorptions and δ. For brevity, the correlations are shown only for the UV-vis absorptions measured at 380 nm, 410 nm and 450 nm (these wavelengths were observed to correlate most strongly with δ).

UV-vis at 380 nm	10 °C	0 °C	-10 °C	-20 °C	-30 °C
10 Hz	-0.82	-0.76	-0.66	-0.54	-0.40
1 Hz	-0.85	-0.81	-0.72	-0.62	-0.49
0.1 Hz	-0.87	-0.84	-0.78	-0.69	-0.57
0.01 Hz	-0.86	-0.86	-0.81	-0.73	-0.64

UV-vis at 410 nm	10 °C	0 °C	-10 °C	-20 °C	-30 °C
10 Hz	-0.81	-0.74	-0.68	-0.61	-0.52
1 Hz	-0.85	-0.78	-0.71	-0.65	-0.55
0.1 Hz	-0.89	-0.82	-0.75	-0.69	-0.59
0.01 Hz	-0.90	-0.86	-0.78	-0.71	-0.61

UV-vis at 450 nm	10 °C	0 °C	-10 °C	-20 °C	-30 °C
10 Hz	-0.71	-0.64	-0.58	-0.52	-0.44
1 Hz	-0.77	-0.68	-0.61	-0.55	-0.47
0.1 Hz	-0.82	-0.72	-0.64	-0.58	-0.50
0.01 Hz	-0.86	-0.78	-0.68	-0.60	-0.51

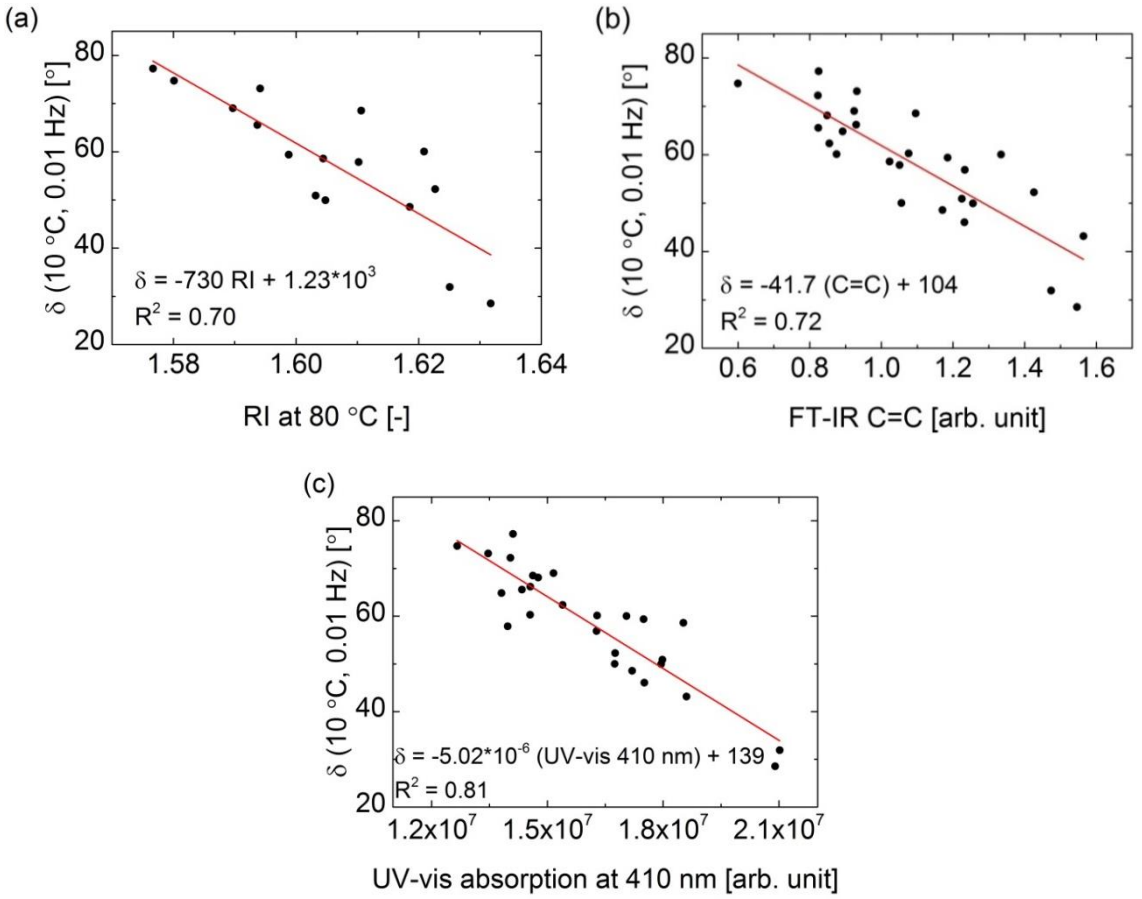

Figure 26. Correlations of δ with (a) RI, (b) C=C absorption from FT-IR and (c) UV-vis absorption at 410 nm.

The finding that the correlation between the aromaticity and elasticity of bitumen is very strong at intermediate temperatures but becomes weaker at lower temperatures is not new; already Soenen and Redelius pointed this out in their article [6]. They speculated that this may be due to the fact that other molecular interactions, for example those between polar groups, start to play a role at low temperatures. One could also argue that the weakening of the correlations with decreasing temperature is due to experimental errors. However, the author wants to remark that the correlations found at 0 °C and 10 °C are comparable to those reported by Soenen and Redelius [6], thus indicating a good quality of the low-temperature rheological data measured in this study. In addition, the repeatability analysis presented in Appendix E indicates a very good repeatability of δ values (or tan δ values, equivalently) at all measurement temperatures. On the other hand, however, it should be noted that differences in the rheological response of different bitumens appear to be only marginal at the lowest measurement temperatures (see, for example, Figure 12). In other words, low-temperature rheology is found to be rather insensitive to the type of bitumen. Therefore, even modest experimental errors may have a significant influence on the quality of the correlations at low temperatures.

Soenen and Redelius [6] also pointed out that bitumen waxes can significantly distort the correlations between aromatic and elastic properties. Therefore, it is investigated here whether the correlations between δ and different aromaticity parameters could be improved by taking account the wax content (melting enthalpy) of the bitumens. Interestingly, it is observed that the addition of wax content as a regression parameter enhanced the correlation with δ from $R^2 = 0.70$ (Figure 26(a)) to $R^2 = 0.90$ (Figure 27). However, the relations of C=C and UV-vis absorptions with δ do not improve significantly when melting enthalpy is introduced as an additional model parameter.

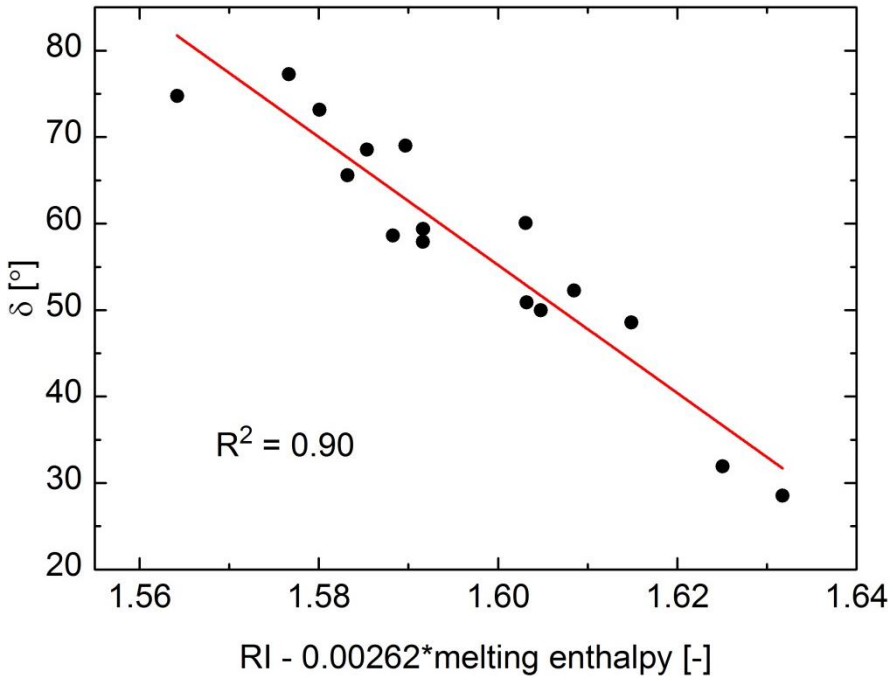

Figure 27. Relation of RI measured at 80 °C and wax content with δ.

In addition, Soenen and Redelius [6] mentioned that the relation between aromaticity and δ improved slightly at low temperatures when a factor of M_n was added. Thus, it is also tempting to test if the correlations between aromaticity and low-temperature rheological properties can be improved by incorporating also molecular weight parameters into the linear regression model. Stepwise linear regression analysis was performed with Statistix software (version 9.0, Analytical Software) using different aromaticity (RI, C=C absorption, UV-vis absorptions) and molecular weight parameters (M_n, M_w, M_z, M_{z+1}, M_w/M_n) as the potential variables of the model. A decision was made to use RI, as measured at 80 °C, as a measure of aromaticity in the linear regression models since it was observed that, together with the different molecular weight parameters, it produced models with the highest R^2 values. The stepwise process was started from the empty model and the significance level of $p < 0.05$ was used both for the entry and removal of the variables from the regression model. A relatively low significance level is used to keep the regression models as simple as possible.

Table 16. Results of the stepwise regression analysis for the linear correlations of RI and molecular weight parameters with G^*.

		RI	M_n	M_w	M_z	M_{z+1}	M_w/M_n	Constant	R^2
10 °C	10 Hz	5.262×10^{9}	1.085×10^{6}	-	-3.067×10^{4}	-	-	-9.274×10^{9}	0.75
	1 Hz	5.096×10^{9}	4.974×10^{5}	-	-	-	-	-8.591×10^{9}	0.55
	0.1 Hz	6.567×10^{9}	-	-	-	-	-	-1.044×10^{10}	0.30
	0.01 Hz	3.459×10^{9}	-	-	-	-	-	-5.505×10^{9}	0.28
0 °C	10 Hz	5.486×10^{9}	1.598×10^{6}	-	-	-2.355×10^{4}	-	-9.937×10^{9}	0.81
	1 Hz	6.549×10^{9}	1.428×10^{6}	-	-4.148×10^{4}	-	-	-1.159×10^{10}	0.77
	0.1 Hz	5.873×10^{9}	1.293×10^{6}	-1.504×10^{5}	-	-	-	-1.032×10^{10}	0.70
	0.01 Hz	1.036×10^{10}	-	-	-	-	-	-1.646×10^{10}	0.30
-10 °C	10 Hz	5.788×10^{9}	2.055×10^{6}	-	-	-2.898×10^{4}	-	-1.054×10^{10}	0.80
	1 Hz	5.922×10^{9}	2.025×10^{6}	-	-	-3.018×10^{4}	-	-1.089×10^{10}	0.82
	0.1 Hz	5.818×10^{9}	1.868×10^{6}	-	-	-2.951×10^{4}	-	-1.070×10^{10}	0.80
	0.01 Hz	6.942×10^{9}	1.610×10^{6}	-	-4.942×10^{4}	-	-	-1.237×10^{10}	0.76
-20 °C	10 Hz	8.007×10^{9}	1.471×10^{6}	-	-	-	-	-1.320×10^{10}	0.62
	1 Hz	5.376×10^{9}	2.221×10^{6}	-	-	-3.034×10^{4}	-	-9.894×10^{9}	0.77
	0.1 Hz	6.079×10^{9}	2.282×10^{6}	-	-	-3.343×10^{4}	-	-1.126×10^{10}	0.81
	0.01 Hz	6.224×10^{9}	2.126×10^{6}	-	-	-3.277×10^{4}	-	-1.150×10^{10}	0.81
-30 °C	10 Hz	5.464×10^{9}	1.364×10^{6}	-	-	-	-	-8.349×10^{9}	0.50
	1 Hz	6.532×10^{9}	1.529×10^{6}	-	-	-	-	-1.066×10^{10}	0.55
	0.1 Hz	8.281×10^{9}	1.649×10^{6}	-	-	-	-	-1.392×10^{10}	0.59
	0.01 Hz	9.719×10^{9}	1.633×10^{6}	-	-	-	-	-1.650×10^{10}	0.62

Table 17. Results of the stepwise regression analysis for the linear correlations of RI and molecular weight parameters with δ.

		RI	M_n	M_w	M_z	M_{z+1}	M_w/M_n	Constant	R^2
10 °C	10 Hz	-4.969×10^{2}	-7.333×10^{-2}	-	-	1.175×10^{-3}	-	9.017×10^{2}	0.91
	1 Hz	-6.005×10^{2}	-7.225×10^{-2}	-	-	1.051×10^{-3}	-	1.076×10^{3}	0.92
	0.1 Hz	-6.595×10^{2}	-6.560×10^{-2}	-	-	7.369×10^{-4}	-	1.175×10^{3}	0.92
	0.01 Hz	-6.975×10^{2}	-4.397×10^{-2}	-	-	-	-	1.230×10^{3}	0.91
0 °C	10 Hz	-3.495×10^{2}	-6.849×10^{-2}	-	-	1.166×10^{-3}	-	6.487×10^{2}	0.88
	1 Hz	-4.612×10^{2}	-7.244×10^{-2}	-	-	1.232×10^{-3}	-	8.380×10^{2}	0.91
	0.1 Hz	-5.634×10^{2}	-7.518×10^{-2}	-	-	1.224×10^{-3}	-	1.012×10^{3}	0.92
	0.01 Hz	-6.337×10^{2}	-7.279×10^{-2}	-	-	1.017×10^{-3}	-	1.133×10^{3}	0.93
-10 °C	10 Hz	-1.982×10^{2}	-5.554×10^{-2}	-	-	8.930×10^{-4}	-	3.850×10^{2}	0.83
	1 Hz	-2.897×10^{2}	-6.359×10^{-2}	-	-	1.073×10^{-3}	-	5.438×10^{2}	0.87
	0.1 Hz	-3.979×10^{2}	-6.928×10^{-2}	-	-	1.193×10^{-3}	-	7.281×10^{2}	0.90
	0.01 Hz	-4.919×10^{2}	-7.694×10^{-2}	-	-	1.316×10^{-3}	-	8.933×10^{2}	0.91
-20 °C	10 Hz	-9.215×10^{1}	-4.164×10^{-2}	-	-	5.986×10^{-4}	-	1.973×10^{2}	0.73
	1 Hz	-1.630×10^{2}	-5.161×10^{-2}	-	-	8.053×10^{-4}	-	3.234×10^{2}	0.80
	0.1 Hz	-2.441×10^{2}	-6.004×10^{-2}	-	-	9.925×10^{-4}	-	4.653×10^{2}	0.84
	0.01 Hz	-3.258×10^{2}	-6.939×10^{-2}	-	-	1.195×10^{-3}	-	6.099×10^{2}	0.88
-30 °C	10 Hz	-7.460×10^{1}	-2.283×10^{-2}	-	-	-	-	1.534×10^{2}	0.52
	1 Hz	-1.700×10^{2}	-2.913×10^{-2}	-	-	-	-	3.181×10^{2}	0.55
	0.1 Hz	-1.643×10^{2}	-5.359×10^{-2}	-	-	8.421×10^{-4}	-	3.272×10^{2}	0.73
	0.01 Hz	-2.530×10^{2}	-6.191×10^{-2}	-	-	1.041×10^{-3}	-	4.810×10^{2}	0.79

It is clear from Tables 16 and 17 that the incorporation of molecular weight parameters into the linear regression model significantly increases the predictability of low-temperature rheological properties. The R^2 values for the prediction of G^* are equal or larger than 0.50 at all the tested temperature-frequency combinations except the measurement points at the highest measurement temperatures and lowest frequencies. Further, the low-temperature elasticity is even more accurately predictable from the aromatic and molecular properties of bitumen than is the low-temperature stiffness (as could be expected already by comparing the R^2 values in Tables 10 and 11). The regression models for δ have R^2 values superior to 0.73 at all testing conditions except at the lowest temperature and highest frequencies. In most cases the R^2 values are as high as between 0.80-0.93. Considering the great variation in the properties of the studied bitumens and the small number of variables used to construct each regression model (none of the models contain more than two molecular weight parameters as variables), the predictability of low-temperature elasticity from aromatic and molecular weight properties can be considered to be very good. Examples of the strong correlations between the measured and predicted values of G^* and δ are illustrated in Figure 28.

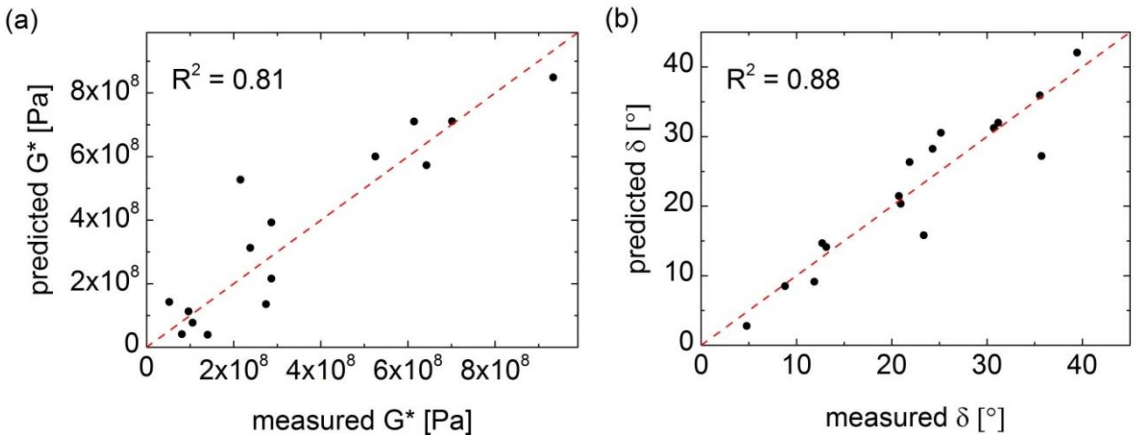

Figure 28. Cross-plots of the measured and predicted values of (a) G^* and (b) δ at -20 °C and 0.01 Hz. The predicted values are obtained from the relevant linear regression models of Tables 16 and 17. The dashed lines are the lines of equality.

Finally, it is worth noting that M_n is the molecular weight parameter that is most often used in the regression models of Tables 16 and 17. This again highlights the moderate importance of relatively small molecules on the low-temperature rheological properties of bitumen. Further, it is observed that the coefficients for the RI and M_n parameters are systematically positive in the linear regression models for G^* and systematically negative in the linear regression models for δ. In other words, bitumens with higher aromaticity and higher M_n are expected to be, on average, stiffer and more elastic at low temperatures than bitumens with lower aromaticity and lower M_n. Notably, Redelius and Soenen [7] have found out that also the zero-shear viscosity at 90 °C increases with

increasing aromaticity and increasing molecular weight. Finally, also the contribution of larger molecules is found to be statistically significant in many cases, as evidenced by the presence of M_{z+1} parameter in most of the regression models.

Correlations between low-temperature rheology and thermal properties

The low-temperature performance of bitumen is commonly evaluated by its dynamic glass transition temperature, that is, the temperature at which G'' attains its maximum value at a predefined frequency (see Section 4.3). Similarly to many other authors [212-216], the dynamic glass transition temperature is defined at a frequency of 1 Hz in this study. To compare the thermodynamic and dynamic aspects of the glass transition, the glass transition temperatures defined from DSC and rheological measurements are cross-plotted in Figure 29. It can be observed that the correlation between the thermal and dynamic glass transition temperatures is very strong, R^2 = 0.91. Furthermore, the data points plot near the equality line, implying that similar glass transition temperatures are obtained by these two methods.

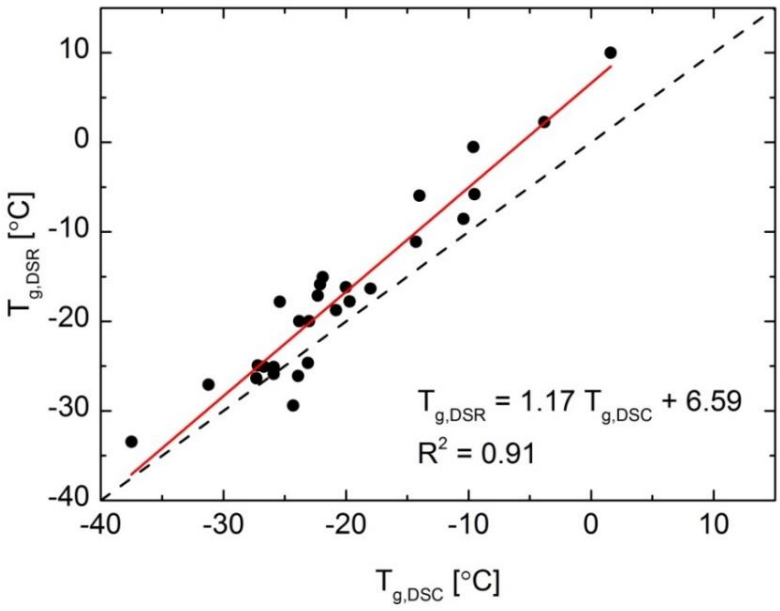

Figure 29. Comparison of the glass transition temperatures measured by DSC and rheology. The solid line represents the linear fit, and the dashed line is the line of equality.

It is also of interest to study if the T_gs defined by DSC correlate with low-temperature rheological properties at fixed temperatures. Therefore, Pearson's correlation coefficients r were calculated for the correlations between T_g and different rheological parameters (G^*, δ, G', G'') measured at various low temperatures. The results of this correlation analysis are displayed in Table 18. It is observed that the correlations with T_g

are strongly positive for G^* and G', and strongly negative for δ at all temperature-frequency combinations. On the other hand, in the case of G'', the correlation is positive at higher temperatures and/or lower frequencies, but negative at lower temperatures and/or higher frequencies.

Table 18. Pearson's correlation coefficients (r) for the correlations between T_g (as defined by DSC) and different rheological parameters at low temperatures.

G^*	10 °C	0 °C	-10 °C	-20 °C	-30 °C
10 Hz	0.91	0.95	0.95	0.90	0.79
1 Hz	0.86	0.93	0.96	0.93	0.86
0.1 Hz	0.80	0.89	0.95	0.95	0.90
0.01 Hz	0.74	0.84	0.93	0.96	0.93

δ	10 °C	0 °C	-10 °C	-20 °C	-30 °C
10 Hz	-0.85	-0.89	-0.91	-0.91	-0.90
1 Hz	-0.81	-0.85	-0.89	-0.91	-0.91
0.1 Hz	-0.77	-0.82	-0.87	-0.90	-0.90
0.01 Hz	-0.69	-0.79	-0.85	-0.88	-0.89

G'	10 °C	0 °C	-10 °C	-20 °C	-30 °C
10 Hz	0.90	0.95	0.95	0.90	0.79
1 Hz	0.85	0.93	0.96	0.93	0.86
0.1 Hz	0.78	0.88	0.95	0.95	0.91
0.01 Hz	0.71	0.81	0.92	0.96	0.93

G''	10 °C	0 °C	-10 °C	-20 °C	-30 °C
10 Hz	0.94	0.63	-0.53	-0.89	-0.92
1 Hz	0.94	0.90	0.30	-0.69	-0.88
0.1 Hz	0.88	0.94	0.77	-0.03	-0.67
0.01 Hz	0.79	0.92	0.92	0.60	-0.03

Figure 30 illustrates the observed strong correlations between T_g and different rheological properties measured at selected temperatures and frequencies. It should be noted that the shown plots are just examples and that the correlations are significantly dependent on the temperature and frequency at which the rheological properties are measured. Further, one should realize that the correlation equations only represent simple linear fits to the data measured in this study, and they cannot be used for predictive purposes in all cases. For example, the linear fits indicate that G^* and G' are negative when $T_g \lesssim$ -33 °C, and that δ and G'' are negative when $T_g \gtrsim$ -2 °C. This is, of

course, physically impossible, and demonstrates the limitations of the linear regression models. A logarithmic fit to the δ data is shown in Figure 30(b) for more realistic and accurate predictions (in this model the predicted value of δ is always positive). It is also noteworthy to mention that a relatively strong linear correlation (R^2 = 0.75) is observed between the logarithm of penetration and T_g.

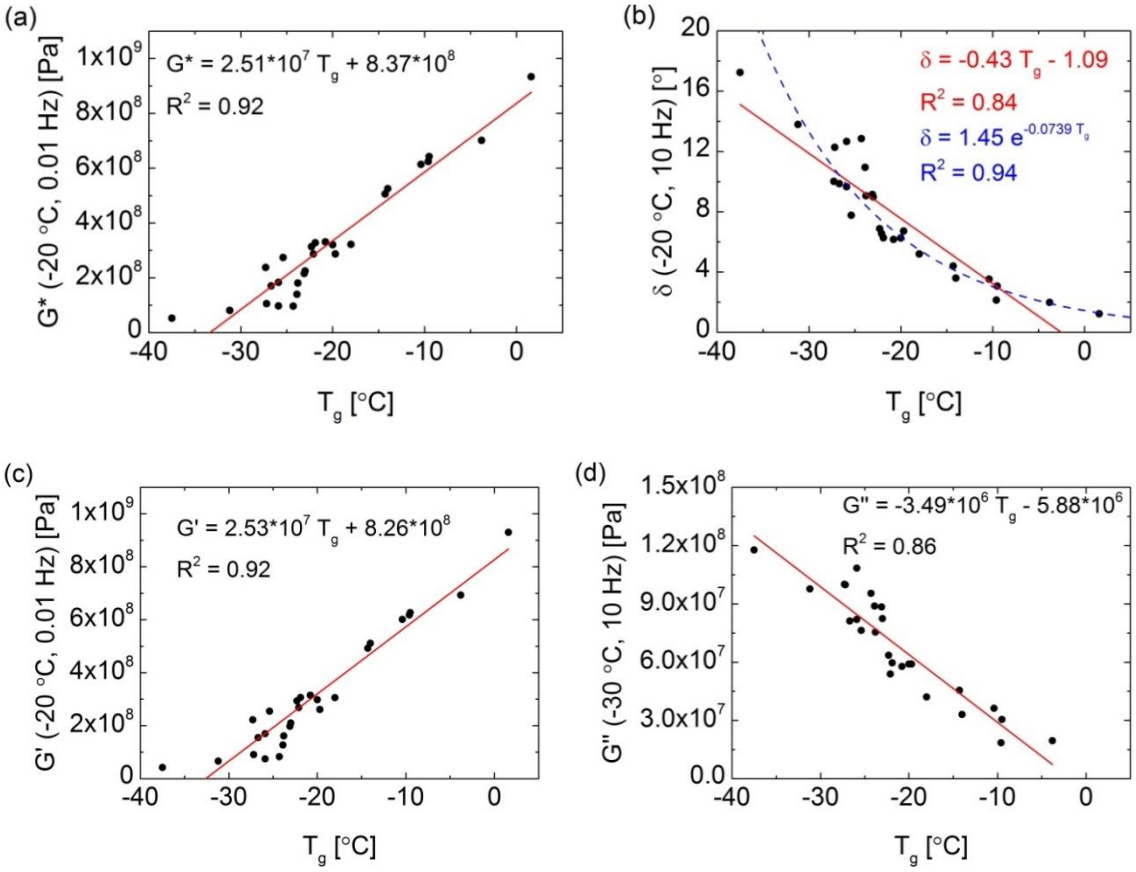

Figure 30. Examples of the strong correlations between T_g and (a) G^*, (b) δ, (c) G' and (d) G''. The temperature and frequency at which each rheological property has been measured is indicated in the y-axis label. Different colors are used in part (b) to distinguish the linear and logarithmic fit curves and corresponding equations from each other.

However, although these regression models are not rigorously correct, they can be used to study the general effect of T_g on the low-temperature rheological behavior of bitumen when testing is conducted at a fixed temperature. Moreover, as the low T_g of bitumen is generally considered to be an advantageous property for the low-temperature performance of asphalt pavement [18], the observed trends in the relationships noted above can be interpreted in terms of low-temperature pavement performance (however, it should be noted that also physical aging arguably plays a very important role when it comes to the low-temperature performance of asphalt pavements. The effect of physical

aging will be discussed in the following sections). As the correlations of G^* and G' with T_g are positive, it can be concluded that the high values of these material properties are disadvantageous for the low-temperature performance in asphalt pavements (when comparison is made at a fixed temperature and frequency). On the contrary, the negative correlations of δ and G'' with T_g imply that high values of these rheological parameters are desired at low temperatures. This makes sense since it is understandable that viscous properties are needed to make bitumen able to relax at low temperatures and consequently prevent the thermal cracking of asphalt pavement. However, it should be still emphasized that the temperatures and frequencies at which the correlations are evaluated in Figure 30 are somewhat arbitrarily chosen, and are not necessarily related to the lowest temperatures at which the investigated bitumens are designed to perform.

One way to compare the thermal and dynamic aspects of the glass transition is to plot the dynamic fragility m as a function of T_g. This is done in Figure 31(a) for the investigated bitumens. Note that in this case T_gs are expressed in Kelvins following the general custom. A very strong linear correlation (R^2 = 0.94) is observed between m and T_g, the slope of m with respect to T_g being about 0.74. Practically speaking, this means that the material with higher T_g tends to behave in a more fragile fashion at the glass transition. In other words, the temperature dependence of rheological properties at T_g is the smaller the lower is T_g. This finding is quite surprising because, as far as the author knows, no such a result has been reported earlier in the asphalt literature.

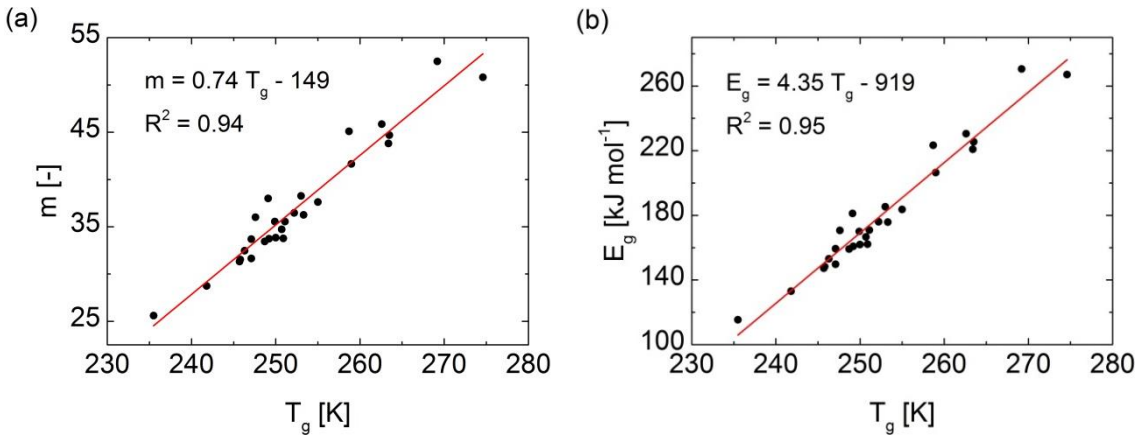

Figure 31. (a) Dynamic fragility m and (b) apparent activation energy E_g at T_g vs. glass transition temperature T_g for the investigated bitumens.

Also, when the apparent activation energy E_g at T_g is plotted against T_g, a very strong linear correlation (R^2 = 0.95) appears, see Figure 31(b). The slope of E_g with respect to T_g is about 4.35. This slope is considerably smaller than that reported by Qin and McKenna [101] for various other small-molecule organic glass-formers (the slope of 1.78); i.e., the temperature dependence of dynamics at T_g appears to be much more dependent on the value of T_g in bitumen than in many other small-molecule organics.

However, it is not yet clearly understood why some particular classes of glass-formers show linear dependence of E_g on T_g [178]. In particular, it should be mentioned that the molecular weights of the investigated bitumens were not observed to correlate with their T_g, m or E_g values.

Finally, the possible relationships between thermodynamic and dynamic glass transition behaviors are discussed through the concepts of thermodynamic and dynamic fragilities. Here the measure of thermodynamic fragility is selected to be the heat capacity change ΔC_p at T_g. This parameter is calculated from the DSC results as described in Appendix G, and its values are plotted against dynamic fragility parameter m in Figure 32. No clear correlation between these two fragility parameters can be observed, maybe partly because of the difficulties in the determination of ΔC_p when the cold crystallization of waxes occurs upon heating of a bitumen sample (see Appendix G for details). This result is consistent with the finding of Huang and McKenna [217], who observed no significant correlation between thermodynamic and dynamic fragilities of small molecule organic glasses (when using the ratio of the liquid to glassy heat capacities at T_g, C_p^l/C_p^g, as a measure of thermodynamic fragility). Although the correlation might look different if different thermodynamic fragility parameters (like the heat capacity ratio, C_p^l/C_p^g, or the rate of change of the T_g-scaled excess entropy, $d(\Delta S(T_g)/\Delta S(T))/d(T_g/T)$ at $T=T_g$) were used, the investigation of these correlations is out of the scope of this work.

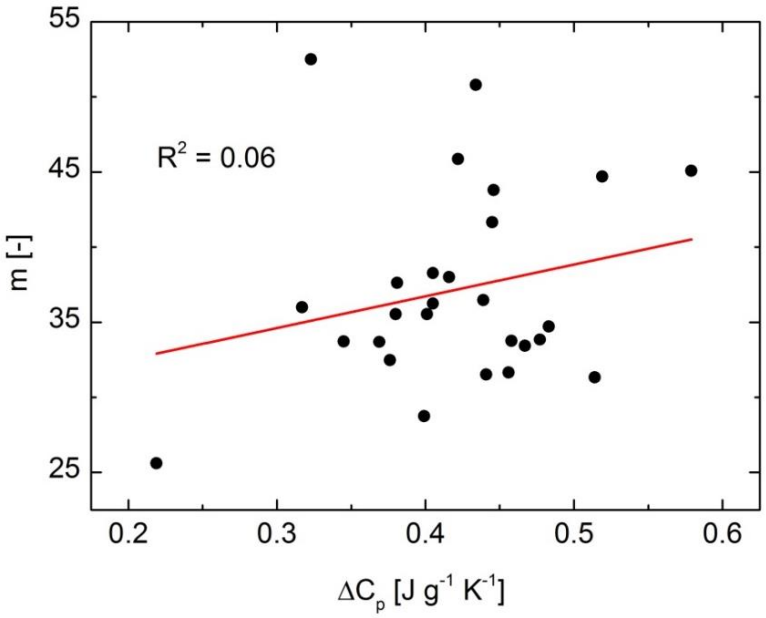

Figure 32. Dynamic fragility m vs. thermodynamic fragility ΔC_p for the investigated bitumens.

In conclusion, although evidence of the relation between the thermodynamic and dynamic signatures of the glass transition can be found (the strong linear correlations between m and T_g and between E_g and T_g), the fundamental understanding of this coupling is still imperfect. Therefore, the author feels that more detailed thermal studies need to be conducted before any definitive conclusions can be drawn regarding this issue.

6.3. Physical aging experiments

The physical aging characteristics of bitumen B-21 were characterized by means of time-resolved mechanical spectroscopy (TRMS), also known as time-resolved rheometry (TRR). This analysis technique utilizes data from the cyclic frequency sweep (CFS) measurements as described in the article by Mours and Winter [218]. CFS measurements were used instead of creep measurements to monitor the development of viscoelastic properties during physical aging because this technique allows continuous monitoring of not only the stiffness (G^*) of the sample but also its elasticity (δ).

As an example, the evolution of G^* with the isothermal aging time at T_g is shown at various frequencies in Figure 33. It should be noted that $t = 0$ s is set to be the moment at which the CFSs are initiated, i.e. the duration of the thermal equilibrium period is not included in the physical aging time presented on the x-axis of the graph. The absolute rate of stiffening appears to be similar at each frequency, as evidenced by the approximately constant vertical spacing of the curves on a linear scale. Further, at relatively short aging times ($< 3\times10^4$ s or 8.3 h) the curves are fairly linear when plotted on a lin-log scale. After this, the rate of stiffening appears to decrease, and after approximately 2×10^5 s ($\approx$ 56 h or 2.3 d) the curves completely plateau at all frequencies. In other words, an equilibrium state at which no significant physical aging occurs anymore is reached after a couple of days of isothermal annealing at T_g.

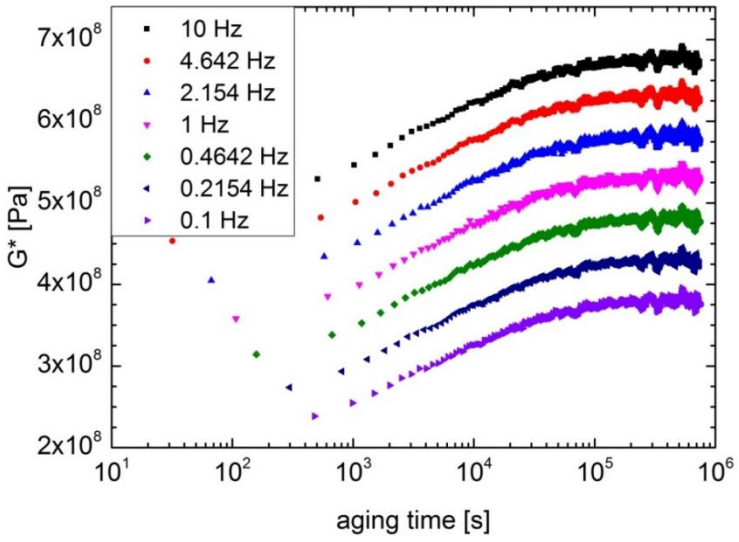

Figure 33. Evolution of G^* with physical aging time at various frequencies for bitumen B-21. The aging temperature is equal to the T_g of the bitumen, -24 °C.

Further, a time-aging time superposition method can be used to further analyze the data from physical aging experiments. Figures 34(a) and 34(b) show the frequency sweep data of bitumen B-21 at various aging times at T_g before and after horizontal shifting, respectively. Note that no vertical shifting of the curves was needed to produce smooth master curves, even though Kriz et al. [180] claimed that this would be required. Consequently, the aging time shift factors a_{te} are obtained from the shifting process and plotted against aging time in Figure 34(c). It is confirmed from this plot that steady-state conditions are reached after 2-3 days of isothermal annealing at T_g, i.e. a_{te} become independent of aging time after this point [185]. This result is consistent with the findings of Lu and Isacsson [219], who concluded that it takes normally 1-2 days in the temperature range of -15 °C to -35 °C before bitumen attains an equilibrium state where no further hardening occurs.

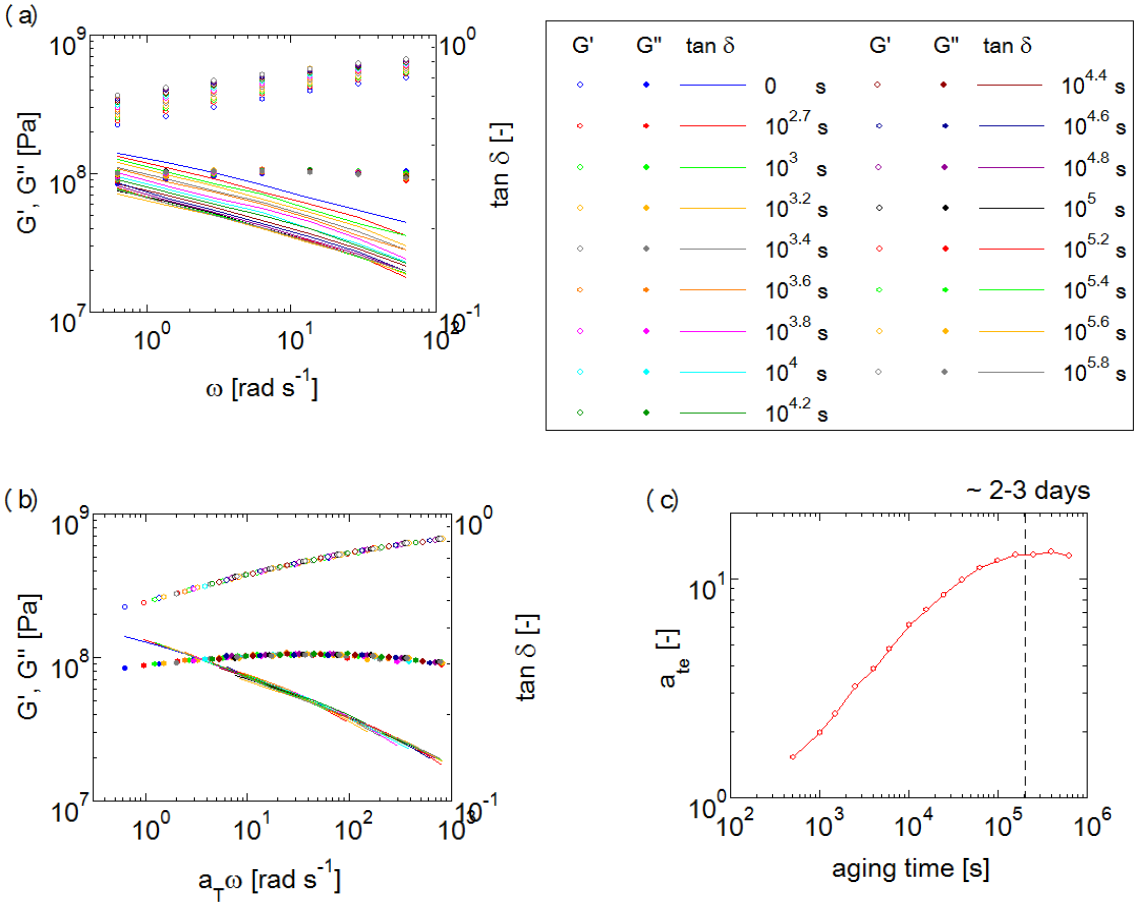

Figure 34. Analysis of physical aging data by means of TRMS coupled with time-aging time superposition analysis. (a) original (unshifted) data, (b) horizontally shifted data, and (c) the time dependence of the aging time shift factors. The data are from the same measurement as in Figure 33. The solid line in part (c) is only to guide the eye.

To study the temperature dependence of the rate of physical aging, CFS experiments were conducted also 5 K and 10 K above and below the T_g of bitumen B-21. The data from these measurements were analyzed using the time-aging time superposition principle described above. The results of this analysis are summarized in Figure 35(a) where the time dependence of aging time shift factors is shown at each measurement temperature. It is found that the rate of physical aging is only moderately dependent on temperature, and that the slope of the log (a_{te}) vs. log (aging time) curve, which is defined by Struik [20] as the aging time shift rate μ, is between 0.35 and 0.45 depending on the aging temperature. The slope is the steepest at the temperatures nearest to T_g, indicating that the rate of physical aging is highest at T_g. It is also notable that no plateau can be observed at the temperatures other than T_g. However, it is believed that equilibrium state would be reached also at these temperatures if the testing time was longer. Figure 35(b) shows the temperature dependence of aging time shift factors at three arbitrarily chosen aging times. This graph further underlines the fact that in bitumen B-21 the rate of physical aging is highest near T_g, especially when long aging times are considered.

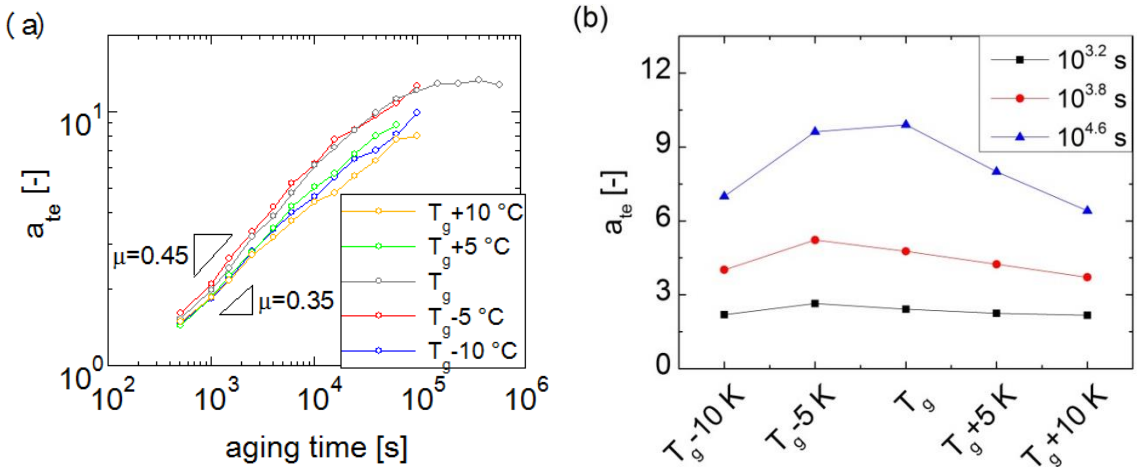

Figure 35. (a) Time dependence of aging time shift factors at various temperatures near T_g. The slopes of the curves represent the aging time-shift rate μ. (b) Temperature dependence of aging time shift factors at three arbitrary aging times. The solid lines are only to guide the eye.

For convenience of comparison, the rate of physical aging is also quantified in terms of the increase in the complex modulus with time. Here the ratio of the complex moduli measured at specific aging time and at the start of the physical aging experiment is called physical aging index (PAI) (Equation 16). The PAIs measured at 0.1 Hz and at different aging times and temperatures are shown in Figure 36. The lowest of the measured It is observed that PAI values are the highest at the highest physical aging temperature of T_g+10 K (-14 °C). However, based on Figure 35(a), the rate of physical aging is the lowest at this temperature. This discrepancy between the analysis results

can most likely be explained by the fact that at this temperature the complex modulus values are furthest away from the glassy modulus value (≈ 1 GPa). Therefore, the complex modulus values are able to increase more at higher aging temperatures than at lower aging temperatures, resulting in higher PAI values. On the contrary, there is no such limiting value for horizontal shift factors at low temperatures (at least in the experimental range of the present study), and hence large time-aging time shifts can be obtained even at the lowest aging temperatures.

$$\mathrm{PAI} = \frac{G^*_{\text{after physical aging}}}{G^*_{\text{before physical aging}}} \tag{16}$$

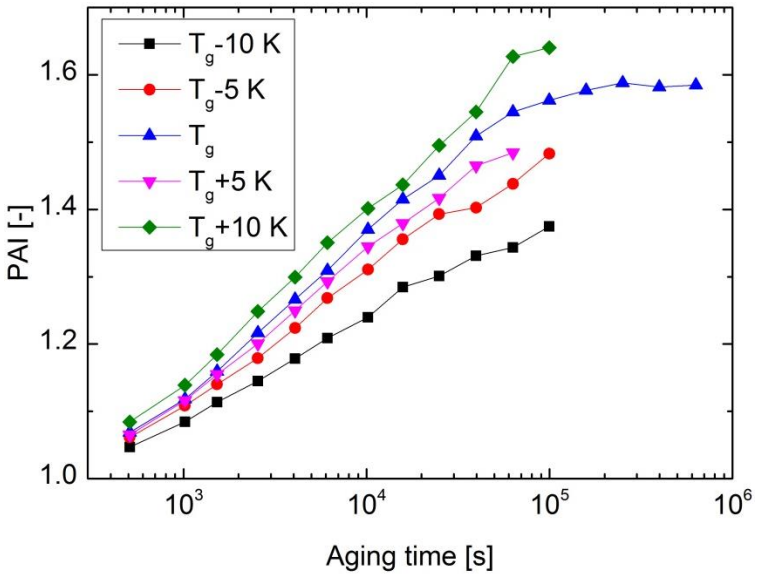

Figure 36. Evolution of physical aging index (PAI) with aging time at various temperatures. The G^* values have been measured at the oscillation frequency of 0.1 Hz.

One interesting question regarding physical aging is whether it changes the value of the glassy modulus G_g. Probably the most convenient way to answer this question is to plot the frequency sweep data measured at various aging times in the vGP plot. In this way, G_g at various aging times can be estimated from the x-axis interception as described in subsection "van Gurp-Palmen plots" of Section 6.1. The dynamic physical aging data measured at T_g (the data of Figure 34) are shown in the vGP plot in Figure 37. It can be seen that the curves corresponding to the data measured at different aging times superimpose, the only change with increasing aging time being the movement of the data points closer to the x-axis. This implies that G_g does not change during physical aging, but the magnitude of G^* and δ approach the ideal glassy state (where δ = 0°) identically.

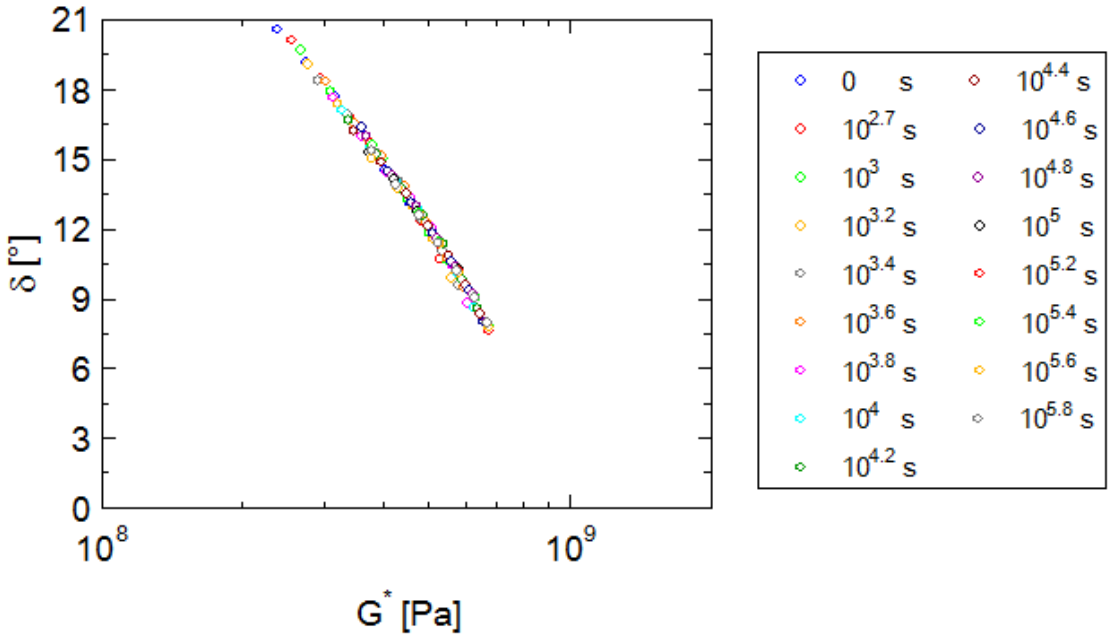

Figure 37. Physical aging data presented in the vGP plot to assess the effect of physical aging on the value of G_g.

It is also of interest to study whether the Cole-Cole plot (*G''* vs. *G'*) of bitumen is influenced by physical aging. Figure 38 shows the Cole-Cole plot of bitumen B-21 at various aging times; the data are the same as that presented in Figures 34 and 37. It is clear that the shape of the Cole-Cole curve does not show any distinct evolution with aging time. This, as discussed in subsection "Cole-Cole plots" of Section 6.1, is an indication that no vertical shifting is needed to produce smooth dynamic master curves, and confirms the observation made already earlier during the time-aging time superposition analysis.

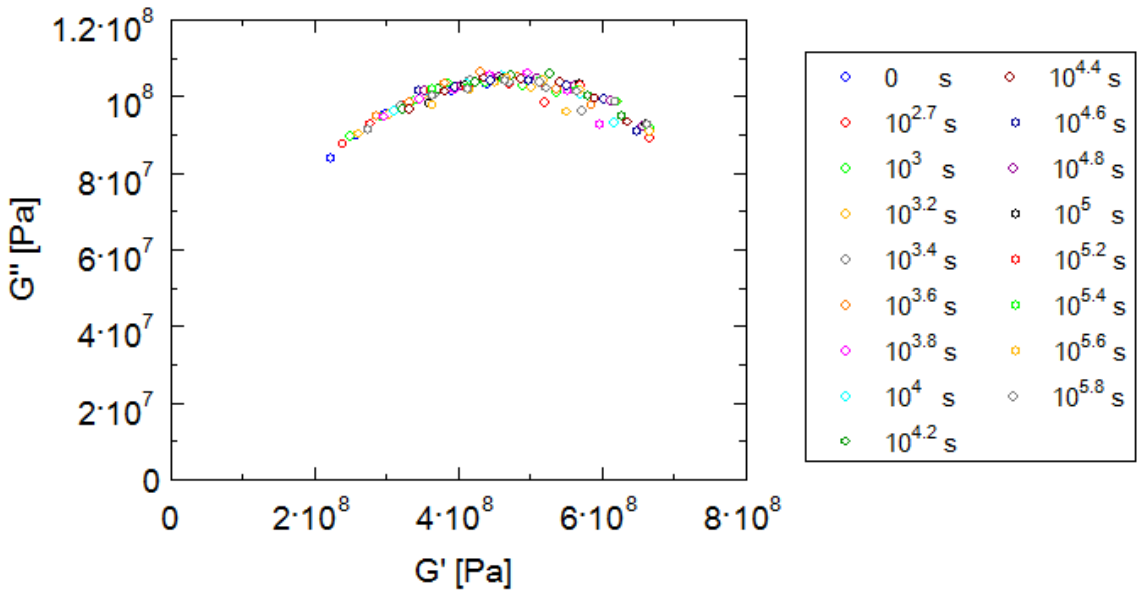

Figure 38. Cole-Cole plot of the physical aging data.

7. Discussion

The vGP plots in Section 6.1 provided evidence that all the investigated bitumens behave in a thermorheologically simple way at low temperatures (≤ 10 °C), i.e. in the glass transition region of the bitumens. This indicates that no significant chemical or physical changes (like phase segregation or crystallization) occur in bitumen in this temperature range. It is notable that this applies also to waxy bitumens that exhibit clear deviations from thermorheological simplicity at higher temperatures (due to wax melting or crystallization). Moreover, it is clear from the results of Qin et al. [130] that thermorheological simplicity holds also in the glass transition region of Sasobit wax modified bitumens. However, in polymer rheology there are also examples of materials whose thermorheological simplicity breaks down in the vicinity of the glass transition [220,221]. Van Gurp and Palmen [85] stated that, in general, both energetically and entropically induced relaxations play a role in the glass transition region, and therefore thermorheological simplicity will not hold. However, even after a comprehensive literature review, it appears that the fundamentals of the structural changes that can induce observable thermorheological complexity in the vicinity of the glass transition are still not completely understood. Therefore, the investigation of this phenomenon remains very experimental for the present, and no firm conclusions about the structural evolution at the glass transition can be drawn based on this analysis.

In many cases, vertical shifting is used purely as a fitting parameter in an attempt to achieve a superposition that "looks OK". This empirical procedure is sometimes used, unintentionally or intentionally, to disguise the failure of TTS by averaging the discrepancy over the entire frequency range. On the other hand, the apparent need to use vertical shifting in the master curve construction may also arise from experimental errors. For the aforementioned reasons, if both horizontal and vertical shifting are carried out by experimental fitting, the results may lack of any physical significance and be questionable [82]. Consequently, a method is needed that can be used to assess the need of vertical shifting without any data manipulation. In the literature, both vGP and Cole-Cole plots (that only involve plotting of the original, unshifted measurement data) have been used for this purpose [82,203-206]. In this study, however, the need for vertical shifts was apparent only from the Cole-Cole plots where the isothermal curves did not overlap sufficiently at the lowest measurement temperatures (see Figure 20(a)). It is speculated that the discrepancies in the curves indicative of the need of vertical shifting are more easily observable on the linear scales of the Cole-Cole plot than on the logarithmic G^* scale of the vGP plot. Therefore, it is recommended that the Cole-Cole plot be used to assess the need of vertical shifting in the master curve construction.

As indicated above, it is not yet clearly understood which physical phenomenon causes the need for vertical shifting. Some researchers, like O'Connell and McKenna [184], have proposed this to be due to the densification. In asphalt research, the temperature-dependent changes in the density of a network of secondary forces and in the mutual solubility of the various chemical compounds have been offered as possible explanations for the apparent need of vertical shifting [21]. Further, when considering

the results presented in Section 6.3 of this work, a question arises if physical aging could also be responsible for the vertical shift. However, the fact that no vertical shifting is needed to produce smooth master curves from the data of physical aging experiments (see Figure 34) does not support the idea that the vertical shift is caused by physical aging. Moreover, the physical aging data appear to fall on a single curve in the Cole-Cole plot (see Figure 38), whereas the unshifted data from the temperature-frequency sweep measurements showed temperature-dependent behavior in this plot (the Cole-Cole plot is very similar for bitumen B-21 as for bitumen B-18, see Figure 20(a)). Based on the aforementioned observations, it is clear that the need of vertical shifting in the master curve construction is not induced by physical aging.

As mentioned in subsection "Master curves and shift factors" of Section 6.1, the temperature dependence of horizontal shift factors can be accurately described with the Kaelble-WLF equation that is able to predict the non-divergence of the dynamics below T_g (the departure from the WLF-VFT behavior). It is remarkable to find that the temperature dependence of viscoelastic functions can be modeled over a wide temperature range that extends both above and below T_g. This is a property that is, at least to the best knowledge of the author, non-existent in any other equation describing the temperature dependence of shift factors. In this study, the applicability of the Kaelble-WLF equation was confirmed in the temperature range from approximately T_g-30 K to T_g+115 K. Notably, this covers the whole in-service temperature range of asphalt pavements.

The physical meaning of the T_d parameter of the Kaelble-WLF equation is also of great interest. This is the temperature at which there is an inflection point in the log a_T vs. T curve. Consequently, this means that the slope of the aforementioned curve is steepest at this temperature, i.e. the temperature dependence of viscoelastic functions is highest. Now, if also the dynamic glass transition temperature is defined to be the temperature at which mechanical properties have the highest variation with temperature (this is basically the definition (4) of Section 4.3), T_d can be introduced as a new definition of the dynamic glass transition temperature. What is most interesting is that, this definition of the dynamic glass transition temperature is completely independent of the time or frequency of the rheological measurement, as opposed to all the previous definitions of this characteristic temperature.

During the last decades, McKenna and coworkers have investigated a great number of glass-forming liquids, and in many of them they have observed non-diverging time scales below T_g [222]. In other words, the temperature dependence of the equilibrium shift factors has been found to deviate strongly from the singular behavior expected from the VFT or WLF dependence obtained in equilibrium and above the nominal T_g (cf. Figure 18). Considering the accumulating evidence for non-diverging time scales in glass-forming liquids, it is not surprising at all that also bitumen exhibits such a behavior. These recent observations also challenge the classical free volume theory which has been widely employed to describe glass transition dynamics and which states that the time scales diverge at finite temperatures above absolute zero.

In many materials viscoelastic properties have been observed to follow, a bit surprisingly, Arrhenius-type temperature dependence below T_g [185,223-229]. In general, the Arrhenius behavior has been found to be valid at temperatures as low as 15-20 K below T_g. However, the data of this study do not appear to follow Arrhenius behavior at this temperature range (the Arrhenius plots of horizontal shift factors not shown here for brevity). Rather, the sub-T_g temperature dependence of bitumen showed similar characteristics to that of amber [230]. In other words, both of these materials form an S-shaped curve in the log a_T vs. T plot (cf. Figure 18 of this work and Figure 3 of Ref. [230]).

It is also of interest to determine the temperature at which a departure from the WLF-VFT behavior occurs. This is achieved by the fitting of the Kaelble-WLF equation since T_d parameter directly represents this deviation temperature. As mentioned already in subsection "Master curves and shift factors" of Section 6.1, T_d values are 5-30 K higher than nominal T_g values for the investigated bitumen samples. On the contrary, a majority of the glass-forming liquids investigated in the literature show departure from the WLF-VFT behavior at or below nominal T_g [222,225,226]. This "discrepancy" between the findings in the literature and those reported here is presumed to be partly due to the broad glass transition of bitumen; signatures of non-diverging time scales are seen in dynamic data already above the nominal T_g because the upper end of the glass transition region extends typically 15-20 K above the mid-point T_g (see Table 4). Secondly, it is expected that T_d would be shifted to a slightly lower temperature (by not more than a few degrees) if the test specimen was physically aged to equilibrium state. The impact of physical aging on the above analysis is discussed briefly in the following paragraph.

At this point, it should be mentioned that the results of this study must be considered only as qualitative indications of the non-divergent time scales below T_g. This is because the low-temperature rheological experiments in this study were not conducted in equilibrium conditions (after sufficiently long physical aging time, see the discussion in Section D of Ref. [226]) due to time restrictions. However, Zhao et al. [230] showed that a radical departure from the WLF-VFT behavior can be observed even after prolonged physical aging – in their case in 20-million-year-old amber. In addition, based on the results of this study, it seems unlikely that physical aging would change the values of horizontal shift factors so much that they would eventually (after sufficiently long physical aging time) end up on the curve corresponding to the WLF-VFT behavior. The aforementioned findings support the conjecture of non-divergent time scales below T_g in bitumen and other glass-formers. However, further studies need to be conducted in order to verify this hypothesis.

As discussed in subsection "Characteristics of the relaxation time spectra" of Section 6.1, the slope of $H(\tau)$ of bitumen appears to be negative on the liquid side of the glass transition, approximately zero at the glass transition, and positive on the glass side of the glass transition. These generic features provide an insight into the development of bitumen microstructure near the glass transition as explained in the following (see also

Figure 39). Above T_g, small-scale molecular rearrangements dominate the relaxation behavior as the movement of molecules relative to each other is possible in the liquid (unfrozen) state. However, when the material is cooled in the glass transition region, the fractions of bitumen having high T_g (alkylated and cycloalkylated aromatic rings according to Masson and Polomark [231]) start to freeze, and the intermolecular motion becomes gradually more and more restricted. In the vicinity of the main glass transition of bitumen, also alkylated cyclopentanes and cyclohexanes start to experience glass transition [157,232]. This results in the further reduction of local molecular mobility. At the nominal T_g (as determined by DSC), both the small-scale molecular motions and large-scale cooperative motions have a significant contribution to the relaxation behavior as evidenced by the nearly constant $H(\tau)$ in Figure 23. Therefore, it is expected that at this temperature the microstructure of bitumen is characterized by the mixture of the islands of mobility and cooperativity shells (details of the theory of the islands of mobility and cooperativity shells are provided in Section 2.2 of Ref. [145]). When bitumen is cooled further below the nominal T_g, the remaining alkylated cyclopentanes and cyclohexanes experience glass transition. As a consequence, the relative amount of the islands of mobility decreases and that of cooperativity shells increases, respectively. Further, this results in the domination of large-scale cooperative relaxation processes, as evidenced by the positive slope of $H(\tau)$ in this temperature region. In the glassy region, the slope of $H(\tau)$ is rather gradual (approximately 0.16), and this is speculated to be partly due to the existence of the islands of mobility even far below the nominal T_g. Indeed, Masson et al. [156] observed domains of unfrozen material in bitumen samples that were cooled down to -55 °C. This unfrozen material was called “the salphase” by the authors, and it was believed to be composed of amorphous and low-molecular-weight alkanes or alkyl segments.

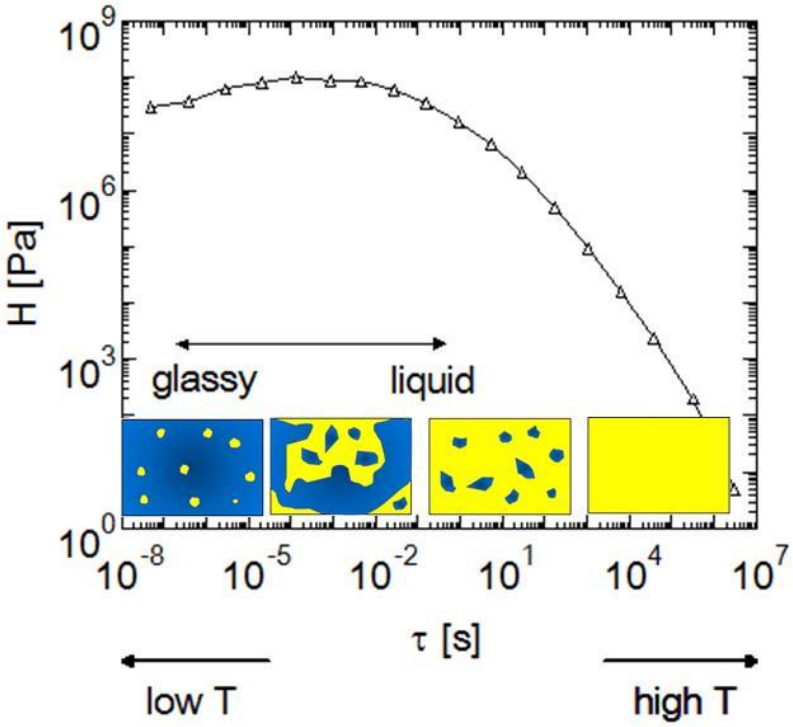

Figure 39. Schematic of the relationship between the structural evolution due to glass transitions of different bitumen fractions and the shape of $H(\tau)$. The yellow and blue areas in the inset figures represent liquid and glassy phases, respectively.

Strong correlations between T_g (as defined by DSC) and low-temperature rheological properties (as measured at fixed temperatures and frequencies) were found in subsection "Correlations between low-temperature rheology and thermal properties" of Section 6.2. The presence of such correlations can be qualitatively explained by using the concept depicted in Figure 40. Generally speaking, the horizontal location of the curves is roughly dependent on the T_g of bitumen: when bitumen has a low T_g, all the curves in Figure 40 shift to the left, and vice versa. One manifestation of this relationship between the horizontal location of the rheological curves and T_g can be seen in Figure 29 where a strong correlation between the thermal and dynamic glass transition temperatures is shown (note that dynamic T_g is practically defined by the location of the G'' peak on the temperature axis). Although this concept is only approximate (e.g. because the shapes of the rheological curves are not perfectly identical for different bitumens), it is able to qualitatively explain the correlations observed between the T_g and low-temperature rheological characteristics of bitumen (see Table 18 and Figure 30). For example, it was observed in Table 18 that the correlation between T_g and G'' is positive at higher temperatures / lower frequencies, but negative at lower temperatures / higher frequencies. In the part (d) of Figure 40 the effect of T_g on the magnitude of G'' is studied at two arbitrary temperatures T_1 and T_2 (so that $T_1 > T_2$). It is obvious from the figure that at the higher of these two temperatures, T_1, G'' values increase with increasing T_g (producing a positive correlation between these parameters), whereas the opposite is observed at the lower temperature of T_2 (leading to a negative correlation

between G'' and T_g). In a similar way, the other correlations of Table 18 and Figure 30 can be qualitatively explained using Figure 40.

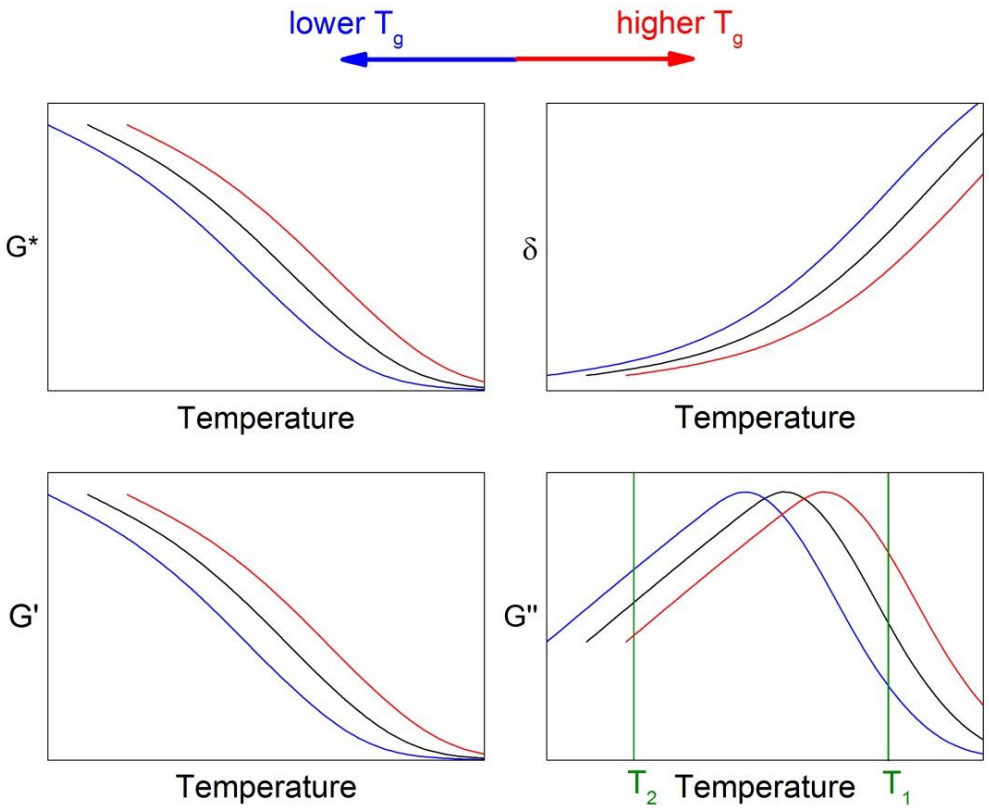

Figure 40. Schematic representation of the relationship between T_g and the location of the rheological curves on the temperature axis. Only low-temperature parts of the curves are shown. The scales on all the axes are linear. Black color represents a "reference" rheological response, blue color the rheological response of a bitumen with lower T_g, and red color the rheological response of a bitumen with higher T_g.

In this study, physical aging was shown to cause significant time-dependent changes in the rheological properties of bitumen. For example, by comparing the test results presented in Sections 6.1 and 6.3, it is concluded that 24 hours of physical aging has a similar effect on the rheological properties as 5-9 °C reduction in the testing temperature. This is equivalent to the loss of one or even two low-temperature PG grades. However, it should be pointed out that in this study the physical aging properties of only a single bitumen were investigated due to time constraints, and this particular bitumen was expected to exhibit exceptionally pronounced physical aging.

Multiple studies suggest that physical aging should be taken into account in order to predict the low-temperature field performance of bitumen more reliably [22-25]. However, the main challenge in the laboratory characterization of physical aging is that it is very time-consuming to do. Unlike in the case of high-temperature chemical aging,

there is no way to accelerate the physical aging process artificially in the laboratory (by increasing the severity of the testing conditions). Moreover, unlike in the TB or BBR testing, it is not possible to load the test specimen into the measurement device without heating it. This makes it very difficult or even impossible to physically age the test specimen outside DSR prior to the testing. This is clearly a disadvantage of the 4-mm DSR technique compared to the TB or BBR techniques in which test specimens can be physically aged prior to the loading into the measurement device (i.e. the test specimen can be kept in cold storage and then quickly transferred to a pre-cooled measurement device). Despite these challenges to take physical aging effects into account in the 4-mm DSR testing, this testing technique is often preferred over the other possible measurement techniques because of its easiness, quick execution and small sample size.

Finally, it should be emphasized that physical aging occurs also during the temperature-frequency sweep testing (Section 6.1). Since there is no practical way to eliminate the effect of physical aging during the testing, the most powerful way to ensure the test repeatability and reproducibility is simply to standardize the duration of each part of the test sequence (thermal equilibrium times, the durations of frequency sweeps). In addition, measurement temperatures and the direction of frequency sweeps (from the highest to the lowest frequency or vice versa) should be always the same in order to obtain repeatable test results. It is also important to establish a standard method for preparing test specimens for 4-mm DSR testing as the thermal and loading history of the test specimen may have a significant influence on the low-temperature rheological properties of bitumen. In this study, experimental errors were minimized by following a well-defined specimen preparation and testing procedure; only the sample loading temperature was varied depending on the stiffness of the bitumen sample (see Appendix B for details).

8. Summary, concluding remarks and outlook

8.1. Summary and concluding remarks

This study investigated the low-temperature rheological properties of various unmodified bitumens, their correlation with chemical and thermal properties, and the influence of physical aging on them. Twenty-seven bitumen samples collected across Europe and originating from various refineries were included in the investigation. The low-temperature rheological properties of the bitumens were characterized by using the 4-mm parallel plate geometry on a DSR with instrument compliance correction. Correspondingly, the 8-mm and 25-mm parallel plate geometries were used to complement the rheological analysis at intermediate and high in-service temperatures, respectively. The chemical characterization of the bitumens consisted of the molecular weight determination by GPC and aromatic characterization by UV-vis spectroscopy, FT-IR spectroscopy and refractive index measurements. The thermal properties of the bitumens were investigated by means of DSC.

It was observed that all the investigated bitumens, regardless of the wax content, exhibited thermorheologically simple behavior at low service temperatures (≤ 10 °C). However, in the vicinity of the glass transition vertical shifting is needed to obtain smooth master curves. The need for vertical shifts can be assessed by plotting frequency sweep data in the plot of G'' vs. G' on linear scales (the Cole-Cole plot). Further, it was concluded that the vertical shifts are not, at least solely, caused by the physical aging of the test specimen during the experiment. The glassy moduli, G_g, of the investigated bitumens varied in the range of 1-1.35 GPa. Interestingly, samples B-6, B-18 and B-25, which all were non-waxy straight-run bitumens, were observed to exhibit more liquid-like behavior at low temperatures than the other bitumens and have relatively high G_g values.

It was found that the temperature dependence of horizontal shift factors can be accurately modeled with the Kaelble-WLF equation over a very wide temperature range, at least from T_g-30 K to T_g+115 K. Interestingly, the T_d parameter of this equation can be used as a frequency-independent definition of the dynamic glass transition temperature as it marks the temperature at which the temperature dependence of viscoelastic behavior is largest. Moreover, it is notable that this model predicts the existence of non-divergent time scales below T_g.

The $H(\tau)$ of all the investigated bitumens were observed to have the same generic shape: above T_g the spectrum has a negative slope, at T_g the slope approximately equals to zero, and below T_g the slope is positive. In physical terms, this indicates that small-scale molecular rearrangements dominate the relaxation behavior above T_g, i.e. when bitumen is (mainly) in liquid state. On the contrary, the dominance of longer τ below T_g indicates that large-scale cooperative motions are the main relaxation mechanism in the glassy state. Correspondingly, the zero slope at the nominal T_g (as defined by DSC) represents

a transition state in which material relaxes both through small-scale molecular and large-scale cooperative rearrangements.

It was found that both the low-temperature stiffness and elasticity of bitumen can be predicted fairly accurately by linear regression models that incorporate information both about the molecular weight and aromatic properties of bitumen. In addition, strong correlations were observed between the T_g (as determined by DSC) and low-temperature rheological properties of the investigated bitumens. In particular, it was observed that the lower is T_g, the lower is the temperature sensitivity of viscoelastic properties at T_g. However, more advanced thermal analysis techniques are needed to develop fundamental understanding of the coupling between the dynamic and thermodynamic aspects of the glass transition.

Physical aging in bitumen was successfully characterized by means of TRMS. It was found that time-aging time superposition is applicable, and only horizontal shifting is needed to superimpose rheological data obtained at different aging times. Based on the limited data of this study, physical aging continues for approximately 2-3 days before equilibrium conditions are attained. Although it would be highly important to take physical aging effects into account in the low-temperature rheological testing of bituminous binders, there does not seem to be an easy and quick way to do that using the 4-mm DSR technique.

In summary, this thesis reported a set of low-temperature rheological data that is perhaps the most extensive in the present asphalt literature. Based on the obtained results, the 4-mm DSR technique seems to be viable method for measuring the low-temperature rheological properties of bitumen as long as the test specimens are carefully prepared. Novel techniques for analyzing the low-temperature rheological data of bitumen were introduced, some of which are adopted from the field of glass rheology. In the author's vision, this thesis serves as a foundation for future studies that more try to relate the low-temperature rheological properties of bitumen more explicitly to the thermal cracking performance of corresponding asphalt mixtures and pavements.

8.2. Outlook

As mentioned in Section 1.4, this thesis presents only a part of the results produced during the joint research project of Aalto University and Nynas Oy. The rest of the results of this project will be reported in the future publications. These publications will address the effects of aging and SBS polymer modification on the low-temperature rheology of bitumen, and the possible relationships between the low-temperature rheology and fracture properties of bitumen. In addition, the correlations between the 4-mm DSR and BBR test results will be investigated as a part of this project. The repeatability and reproducibility of the 4-mm DSR testing technique will be evaluated in detail in the forthcoming round robin test organized by the Federal Highway Administration (FHWA) Asphalt Binder Expert Task Group (ETG).

Future work should also further investigate and model the relaxation time spectrum of bitumen in the vicinity of the glass transition. It is expected that the extremely broad distribution of molecular size and composition in bitumen averages relaxation processes in a way that will generate basic patterns which might be universal to all types of polydisperse glasses. This is remarkable since the glasses investigated and modeled so far in the rheological literature have been almost exclusively monodisperse in nature. Also, the modeling of the low-temperature rheological data of bitumen with the 1S2P1D model is a fascinating topic for future research.

In the future, it would be also interesting to study the low-temperature rheological properties of bitumens modified with other additives than SBS polymer. For example, chemical modification with thiourea and some reactive prepolymers has shown great promise in improving the low-temperature performance of bitumen [233-237]. Moreover, some lightweight oil products have been shown to improve the thermal cracking resistance of bitumen [238]. The author feels that it would be intriguing to investigate especially modified bitumens of the aforementioned types with the 4-mm DSR technique. In addition, it would be interesting to try to extend the 4-mm DSR technique to the low-temperature rheological characterization of mastics.

In this work, the physical aging characterization of bitumen was very limited in extent. Therefore, a more comprehensive study, including a number of bitumens with varying origins and compositions, should be conducted to confirm the observations made in this study and to investigate the dependence of the physical aging characteristics of bitumen on its chemical properties. These investigations should result in predictive equations that can be used to quickly and easily estimate the effect of physical aging on the rheological properties (cf. Ref. [38]). Finally, although being time-consuming, it would be of interest to study the low-temperature rheological properties of various bitumens after extended physical aging and how they relate with the chemical and thermal properties. It should be noted, however, that it might be more appropriate to use TB or BBR testing method instead of the 4-mm DSR technique in this type of investigation (see the discussion at the end of Section 7).

References

[1] Isacsson U, & Zeng H. 1998. Cracking of asphalt at low temperature as related to bitumen rheology. Journal of Materials Science; Vol. 33; pp. 2165-2170.

[2] Fabb T. 1974. The influence of mix composition, binder properties and cooling rate on asphalt cracking at low temperatures. Association of Asphalt Paving Technologists Proc; Vol. 43; pp. 285-331.

[3] Turner TF, Branthaver JF. 1997. DSC studies of asphalts and asphalt components. In: Usmani A, (Ed.). Asphalt science and technology. New York; Marcel Dekker; pp. 59-101.

[4] Sui C, Farrar MJ, Harnsberger PM, Tuminello WH, & Turner TF. 2011. New Low-Temperature Performance-Grading Method. Transportation Research Record: Journal of the Transportation Research Board; Vol. 2207; pp. 43-48.

[5] Sui C, Farrar MJ, Tuminello WH, & Turner TF. 2010. New technique for measuring low-temperature properties of asphalt binders with small amounts of material. Transportation Research Record: Journal of the Transportation Research Board; Vol. 2179; pp. 23-28.

[6] Soenen H, & Redelius P. 2014. The effect of aromatic interactions on the elasticity of bituminous binders. Rheologica Acta; Vol. 53; pp. 741-754.

[7] Redelius P, & Soenen H. 2015. Relation between bitumen chemistry and performance. Fuel; Vol. 140; pp. 34-43.

[8] Jennings P, Pribanic JA, Raub M, Smith J, & Mendes T. 1993. Advanced high performance gel permeation chromatography methodology. Report No.SHRP-A630; National Research Council; Washington, DC.

[9] Qin Q, Schabron JF, Boysen RB, & Farrar MJ. 2014. Field aging effect on chemistry and rheology of asphalt binders and rheological predictions for field aging. Fuel; Vol. 121; pp. 86-94.

[10] Sultana S, & Bhasin A. 2014. Effect of chemical composition on rheology and mechanical properties of asphalt binder. Construction and Building Materials; Vol. 72; pp. 293-300.

[11] Wang Y, Wen Y, Zhao K, Chong D, & Wei J. 2014. Connections between the Rheological and Chemical Properties of Long-Term Aged Asphalt Binders. Journal of Materials in Civil Engineering; doi: http://dx.doi.org/10.1061/(ASCE)MT.1943-5533.0001214.

[12] Petersen JC, & Glaser R. 2011. Asphalt oxidation mechanisms and the role of oxidation products on age hardening revisited. Road Materials and Pavement Design; Vol. 12; pp. 795-819.

[13] Branthaver JF, Petersen J, Robertson R, Duvall J, Kim S, Harnsberger P et al. 1993. Binder characterization and evaluation.Volume 2: Chemistry. Report No.SHRP-A-368; National Research Council; Washington D. C.

[14] Petersen JC, Robertson R, Branthaver J, Harnsberger P, Duvall J, Kim S et al. 1994. Binder characterization and evaluation. Volume 1. Report No.SHRP-A-367; National Research Council; Washington D. C.

[15] Lesueur D, Gerard J, Claudy P, Letoffe J, Planche J, & Martin D. 1996. A structure-related model to describe asphalt linear viscoelasticity. Journal of Rheology; Vol. 40; pp. 813-836.

[16] Yut I, & Zofka A. 2014. Correlation between rheology and chemical composition of aged polymer-modified asphalts. Construction and Building Materials; Vol. 62; pp. 109-117.

[17] Mouazen M, Poulesquen A, & Vergnes B. 2011. Correlation between thermal and rheological studies to characterize the behavior of bitumen. Rheologica Acta; Vol. 50; pp. 169-178.

[18] Planche J, Claudy P, Létoffé J, & Martin D. 1998. Using thermal analysis methods to better understand asphalt rheology. Thermochimica Acta; Vol. 324; pp. 223-227.

[19] Bahia HU. 1991. Low-temperature isothermal physical hardening of asphalt cements. PhD thesis; Pennsylvania State University.

[20] Struik L. 1977. Physical aging in amorphous polymers and other materials. PhD thesis; Delft University of Technology.

[21] Anderson DA, Christensen DW, Bahia HU, Dongre R, Sharma M, Antle CE et al. 1994. Binder characterization and evaluation, volume 3: Physical characterization. Report No.SHRP-A-369; National Research Council; Washington, DC.

[22] Erskine J, Hesp S, & Kaveh F. 2012. Another look at accelerated aging of asphalt cements in the pressure aging vessel. Proceedings of the 5th Eurasphalt and Eurobitumen Congress; June 13-15, 2012; Istanbul, Turkey; Paper P5EE-202.

[23] Hesp S, Genin S, Scafe D, Shurvell H, & Subramani S. 2009. Five Year Performance Review of a Northern Ontario Pavement Trial: Validation of Ontario's Double-Edge-Notched Tension (DENT) and Extended Bending Beam Rheometer (BBR) Test Methods. Proceedings of the Annual Conference of the Canadian Technical Asphalt Association; Vol. 54; pp. 99-126.

[24] Hesp SA, Iliuta S, & Shirokoff JW. 2007. Reversible aging in asphalt binders. Energy & Fuels; Vol. 21; pp. 1112-1121.

[25] Hesp SA, Soleimani A, Subramani S, Phillips T, Smith D, Marks P et al. 2009. Asphalt pavement cracking: analysis of extraordinary life cycle variability in eastern and northeastern Ontario. International Journal of Pavement Engineering; Vol. 10; pp. 209-227.

[26] Dongré R. 2007. Low temperature cracking. Presentation at NA Norsk Asfaltforening in Oslo.

[27] Edwards Y, Tasdemir Y, & Isacsson U. 2006. Rheological effects of commercial waxes and polyphosphoric acid in bitumen 160/220—low temperature performance. Fuel; Vol. 85; pp. 989-997.

[28] Edwards Y, & Redelius P. 2003. Rheological effects of waxes in bitumen. Energy & Fuels; Vol. 17; pp. 511-520.

[29] Lu X, & Isacsson U. 1997. Rheological characterization of styrene-butadiene-styrene copolymer modified bitumens. Construction and Building Materials; Vol. 11; pp. 23-32.

[30] Lu X, & Isacsson U. 1998. Chemical and rheological evaluation of ageing properties of SBS polymer modified bitumens. Fuel; Vol. 77; pp. 961-972.

[31] Lu X, Isacsson U, & Ekblad J. 1998. Low-temperature properties of styrene–butadiene–styrene polymer modified bitumens. Construction and Building Materials; Vol. 12; pp. 405-414.

[32] Lu X, & Isacsson U. 2000. Artificial aging of polymer modified bitumens. Journal of Applied Polymer Science; Vol. 76; pp. 1811-1824.

[33] Lu X, & Isacsson U. 2000. Modification of road bitumens with thermoplastic polymers. Polymer Testing; Vol. 20; pp. 77-86.

[34] Lu X, & Isacsson U. 2001. Effect of binder rheology on the low-temperature cracking of asphalt mixtures. Road Materials and Pavement Design; Vol. 2; pp. 29-47.

[35] Farrar M, Sui C, Salmans S, & Qin Q. 2014. Determining the Low Temperature Rheological Properties of Asphalt Binder Using a Dynamic Shear Rheometer (DSR). Topical report FP 08 prepared by Western Research Institute for the Federal Highway Administration, Contract DTFH61-07-D-00005, Fundamental Properties of Asphalts and Modified Asphalts, III.

[36] Farrar M, Grimes RW, Sui C, Planche J, Huang S, Turner TF et al. 2012. Thin Film Oxidative Aging and Low Temperature Performance Grading Using Small Plate Dynamic Shear Rheometry: An Alternative to Standard RTFO, PAV, and BBR. Proceedings of the 5th Eurasphalt and Eurobitumen Congress; June 13-15, 2012; Istanbul, Turkey; Paper 05EE-467.

[37] Rowe G, & Anderson D. 2013. Lecture 5: Creep - S(t), BBR. Rheobit workshop organized by Asphalt Institute; 12.-14. June 2013; Stockholm, Sweden. pp. 23-26.

[38] Tabatabaee HA, Velasquez R, & Bahia HU. 2012. Predicting low temperature physical hardening in asphalt binders. Construction and Building Materials; Vol. 34; pp. 162-169.

[39] European Committee for Standardization. 2014. EN 12597: Bitumen and bituminous binders – Terminology.

[40] European Committee for Standardization. 2009. EN 12591: Bitumen and bituminous binders – Specifications for paving grade bitumens.

[41] Krishnan JM, & Rajagopal K. 2003. Review of the uses and modeling of bitumen from ancient to modern times. Applied Mechanics Reviews; Vol. 56; pp. 149-214.

[42] Lay MG. 1992. Ways of the World: A History of the World's Roads and of the Vehicles that Used Them. New Jersey; Rutgers University Press.

[43] Corbett L. 1965. Manufacture of petroleum asphalt. Bituminous materials: asphalts, tars and pitches; Vol. 2; pp. 81-122.

[44] Read J, Whiteoak D. 2003. The shell bitumen handbook. 5th ed. London, UK; Thomas Telford.

[45] Bardesi A, Brule B, Corte J, Diani E, Gerritsen A, Lefevre G et al. 1999. Use of modified bituminous binders, special bitumens and bitumens with additives in pavement applications. Technical Committee Flexible Roads (C8) World Road Association (PIARC).

[46] Youtcheff JS, & Jones D. 1994. Guideline for asphalt refiners and suppliers. Report No.SHRP A-686; National Research Council; Washington, DC.

[47] Robinson PR. 2006. Petroleum processing overview. In: Hsu CS, Robinson P, (Ed.). Practical Advances in Petroleum Processing. New York; Springer; pp. 1-78.

[48] Speight JG. 1980. The chemistry and technology of petroleum. New York; Marcel Dekker.

[49] Lesueur D. 2009. The colloidal structure of bitumen: Consequences on the rheology and on the mechanisms of bitumen modification. Advances in Colloid and Interface Science; Vol. 145; pp. 42-82.

[50] Krchma L, & Gagle D. 1974. A USA history of asphalt refined from crude oil and its distribution. Association of Asphalt Paving Technologists Proc; Vol. 43; pp. 25-88.

[51] Oyekunle L. 2006. Certain relationships between chemical composition and properties of petroleum asphalts from different origin. Oil & Gas Science and Technology-Revue de l'IFP; Vol. 61; pp. 433-441.

[52] Redelius P. 2004. Bitumen solubility model using Hansen solubility parameter. Energy & Fuels; Vol. 18; pp. 1087-1092.

[53] Peralta EJF. 2009. Study of the interaction between bitumen and rubber. MSc thesis; University of Minho.

[54] Mortazavi M, & Moulthrop JS. 1993. The SHRP materials reference library. Report No.SHRP-A-646; National Research Council; Washington, DC.

[55] American Society for Testing and Materials. 1992, Reapproved 2007. ASTM D2503-92: Standard test method for relative molecular mass (molecular weight) of hydrocarbons by thermoelectric measurement of vapor pressure.

[56] Stangl K, Jäger A, & Lackner R. 2007. The effect of styrene-butadiene-styrene modification on the characteristics and performance of bitumen. Monatshefte für Chemie-Chemical Monthly; Vol. 138; pp. 301-307.

[57] Soenen H. Personal communication. February 17, 2015.

[58] Netzel DA. 2006. Apparent activation energies for molecular motions in solid asphalt. Energy & Fuels; Vol. 20; pp. 2181-2188.

[59] Pfeiffer JP, & Saal R. 1940. Asphaltic bitumen as colloid system. The Journal of physical chemistry; Vol. 44; pp. 139-149.

[60] Christensen D, & Anderson D. 1991. Rheological evidence concerning the molecular architecture of asphalt cements. Proceedings chemistry of bitumen; Vol. 2; pp. 568-595.

[61] Redelius P. 2000. Solubility parameters and bitumen. Fuel; Vol. 79; pp. 27-35.

[62] Höhne G, Hemminger W, Flammersheim H. 2003. Differential scanning calorimetry. Berlin, Germany; Springer.

[63] Soenen H, Besamusca J, Fischer HR, Poulikakos LD, Planche J, Das PK et al. 2014. Laboratory investigation of bitumen based on round robin DSC and AFM tests. Materials and Structures; Vol. 47; pp. 1205-1220.

[64] International Organization for Standardization. 2009. ISO 11357-1: Plastics-Differential scanning calorimetry, DSC.

[65] American Society for Testing and Materials. 2008. ASTM 1356-08: Standard Test Method for Assignment of the Glass Transition Temperatures by Differential Scanning Calorimetry.

[66] American Society for Testing and Materials. 2012. ASTM D 3418-12: Standard Test Method for Transition Temperatures and Enthalpies of Fusion and Crystallization of Polymers by Differential Scanning Calorimetry.

[67] Claudy P, & King GN. 1992. Caracterisation des bitumes routiers par analyse calorimetrique differentielle (ACD). Analyse thermo-optique (ATO). Correlation entre proprietes physiques et resultats ACD. Bulletin des Laboratoires des Ponts et Chaussées; Vol. Issue 177; pp. 45-51.

[68] Claudy P, Letoffe J, King G, & Plancke J. 1992. Characterization of asphalts cements by thermomicroscopy and differential scanning calorimetry: Correlation to classic physical properties. Fuel science & technology international; Vol. 10; pp. 735-765.

[69] Jiménez-Mateos JM, Quintero LC, & Rial C. 1996. Characterization of petroleum bitumens and their fractions by thermogravimetric analysis and differential scanning calorimetry. Fuel; Vol. 75; pp. 1691-1700.

[70] Schmidt R, & Santucci L. 1966. A practical method for determining the glass transition temperature of asphalts and calculation of their low temperature viscosities. Assoc Asphalt Paving Technol Proc; Vol. 35; pp. 61-90.

[71] Masson J, Polomark G, & Collins P. 2005. Glass transitions and amorphous phases in SBS–bitumen blends. Thermochimica Acta; Vol. 436; pp. 96-100.

[72] European Committee for Standardization. 2007. EN 1426: Bitumen and bituminous binders. Determination of needle penetration.

[73] European Committee for Standardization. 2006. EN 13924: Bitumen and bituminous binders. Specifications for hard paving grade bitumens.

[74] European Committee for Standardization. 2007. EN 1427: Bitumen and bituminous binders: Determination of the softening point, Ring and Ball method.

[75] Pfeiffer JP, & Van Doormaal P. 1936. The rheological properties of asphaltic bitumen. Journal of the Institute of Petroleum Technologists; Vol. 22; pp. 414-440.

[76] Barth EJ. 1962. Asphalt; science and technology. New York; Gordon and Breach Science Publishers.

[77] Van der Poel C. 1954. A general system describing the visco-elastic properties of bitumens and its relation to routine test data. Journal of Applied Chemistry; Vol. 4; pp. 221-236.

[78] de Bats FT, & van Gooswilligen G. 1989. Practical rheological characterization of paving grade bitumens. Proceedings of 4th Eurobitume Symposium; October. 4–6, 1989; Madrid, Spain; .

[79] Weitz D, Wyss H, & Larsen R. 2007. Oscillatory rheology: Measuring the viscoelastic behaviour of soft materials. GIT laboratory journal Europe; Vol. 11; pp. 68-70.

[80] Colby RH. 2013. Official symbols and nomenclature of The Society of Rheology. Journal of Rheology; Vol. 57; pp. 1047-1055.

[81] Ferry JD. 1980. Viscoelastic properties of polymers. 3rd ed. New York, NY; John Wiley & Sons.

[82] Dealy J, & Plazek D. 2009. Time-temperature superposition—a users guide. Rheol.Bull; Vol. 78; pp. 16-31.

[83] Christensen R. 1982. Theory of viscoelasticity: an introduction. 2nd ed. New York, NY; Academic Press.

[84] Dickinson E, & Witt H. 1974. The dynamic shear modulus of paving asphalts as a function of frequency. Transactions of The Society of Rheology; Vol. 18; pp. 591-606.

[85] van Gurp M, & Palmen J. 1998. Time-temperature superposition for polymeric blends. Rheology Bulletin; Vol. 67; pp. 5-8.

[86] Williams ML, Landel RF, & Ferry JD. 1955. The temperature dependence of relaxation mechanisms in amorphous polymers and other glass-forming liquids. Journal of the American Chemical Society; Vol. 77; pp. 3701-3707.

[87] Vogel H. 1921. Das temperaturabhängigkeitsgesetz der viskosität von flüssigkeiten. Physikalische Zeitschrift; Vol. 22; pp. 645-646.

[88] Fulcher GS. 1925. Analysis of recent measurements of the viscosity of glasses. Journal of the American Ceramic Society; Vol. 8; pp. 339-355.

[89] Tammann G, & Hesse W. 1926. Die Abhängigkeit der Viscosität von der Temperatur bie unterkühlten Flüssigkeiten. Zeitschrift für anorganische und allgemeine Chemie; Vol. 156; pp. 245-257.

[90] Kaelble DH. 1985. Computer Aided Design of Polymers and Composites. New York, NY; Marcel Dekker; pp. 145-147.

[91] Mauro JC, Yue Y, Ellison AJ, Gupta PK, & Allan DC. 2009. Viscosity of glass-forming liquids. Proceedings of the National Academy of Sciences of the United States of America; Vol. 106; pp. 19780-19784.

[92] Mauro JC. 2011. Topological constraint theory of glass. American Ceramic Society Bulletin; Vol. 90; pp. 31.

[93] Chandler D, & Garrahan JP. 2010. Dynamics on the Way to Forming Glass: Bubbles in Space-Time. Annual Review of Physical Chemistry; Vol. 61; pp. 191-217.

[94] Elmatad YS, Chandler D, & Garrahan JP. 2009. Corresponding states of structural glass formers. The Journal of Physical Chemistry B; Vol. 113; pp. 5563-5567.

[95] Elmatad YS, Chandler D, & Garrahan JP. 2010. Corresponding states of structural glass formers. II. The Journal of Physical Chemistry B; Vol. 114; pp. 17113-17119.

[96] Elmatad YS. 2011. Fragile-to-strong crossover in supercooled liquids remains elusive. Proceedings of the National Academy of Sciences of the United States of America; Vol. 108; pp. E230; author reply E231.

[97] Garrahan JP, & Chandler D. 2003. Coarse-grained microscopic model of glass formers. Proceedings of the National Academy of Sciences of the United States of America; Vol. 100; pp. 9710-9714.

[98] Zhao J. 2014. Dynamics below the glass transition temperature and viscoelastic and calorimetric investigation of different fossil resins. PhD thesis; Texas Tech University.

[99] Rowe GM, & Sharrock M. 2011. Alternate shift factor relationship for describing temperature dependency of viscoelastic behavior of asphalt materials. Transportation Research Record: Journal of the Transportation Research Board; Vol. 2207; pp. 125-135.

[100] Christensen DW, & Anderson DA. 1992. Interpretation of dynamic mechanical test data for paving grade asphalt cements. Journal of the Association of Asphalt Paving Technologists; Vol. 61; pp. 67-116.

[101] Qin Q, & McKenna GB. 2006. Correlation between dynamic fragility and glass transition temperature for different classes of glass forming liquids. Journal of Non-Crystalline Solids; Vol. 352; pp. 2977-2985.

[102] Liu C, He J, Keunings R, & Bailly C. 2006. New linearized relation for the universal viscosity-temperature behavior of polymer melts. Macromolecules; Vol. 39; pp. 8867-8869.

[103] Winter HH. 2013. Glass transition as the rheological inverse of gelation. Macromolecules; Vol. 46; pp. 2425-2432.

[104] Winter HH. 1997. Analysis of dynamic mechanical data: inversion into a relaxation time spectrum and consistency check. Journal of Non-Newtonian Fluid Mechanics; Vol. 68; pp. 225-239.

[105] Yildirim Y. 2007. Polymer modified asphalt binders. Construction and Building Materials; Vol. 21; pp. 66-72.

[106] Isacsson U, & Lu X. 1995. Testing and appraisal of polymer modified road bitumens—state of the art. Materials and Structures; Vol. 28; pp. 139-159.

[107] García-Morales M, Partal P, Navarro F, Martínez-Boza F, & Gallegos C. 2004. Linear viscoelasticity of recycled EVA-modified bitumens. Energy & Fuels; Vol. 18; pp. 357-364.

[108] Isacsson U, & Lu X. 1999. Laboratory investigations of polymer modified bitumens. Journal of the Association of Asphalt Paving Technologists; Vol. 68; pp. 35-63.

[109] Anderson DA, & Kennedy TW. 1993. Development of SHRP binder specification. Journal of the Association of Asphalt Paving Technologists; Vol. 62; pp. 481-507.

[110] Kennedy TW, Huber GA, Harrigan ET, Cominsky RJ, Hughes CS, Von Quintus H et al. 1994. Superior performing asphalt pavements (Superpave): The product of the SHRP asphalt research program. Report No.SHRP-A-410; National Research Council; Washington, DC.

[111] American Association of State Highway and Transportation Officials. 2010. AASHTO M 320-10: Standard Specification for Performance Graded Asphalt Binder.

[112] American Association of State Highway and Transportation Officials. 2012. AASHTO T 315-12: Determining the Rheological Properties of Asphalt Binder Using a Dynamic Shear Rheometer (DSR).

[113] American Association of State and Highway Transportation Officials. 2012. AASHTO T 313-12: Standard Method of Test for Determining the Flexural Creep Stiffness of Asphalt Binder Using the Bending Beam Rheometer (BBR).

[114] Basu A, Marasteanu MO, & Hesp SA. 2003. Time-temperature superposition and physical hardening effects in low-temperature asphalt binder grading. Transportation Research Record: Journal of the Transportation Research Board; Vol. 1829; pp. 1-7.

[115] D'Angelo J, Kluttz R, Dongre RN, Stephens K, & Zanzotto L. 2007. Revision of the Superpave High Temperature Binder Specification: The Multiple Stress Creep Recovery Test. Journal of the Association of Asphalt Paving Technologists; Vol. 76; pp. 123-162.

[116] Hintz C, Velasquez R, Johnson C, & Bahia H. 2011. Modification and Validation of Linear Amplitude Sweep Test for Binder Fatigue Specification. Transportation Research Record: Journal of the Transportation Research Board; Vol. 2207; pp. 99-106.

[117] Hintz C, & Bahia H. 2013. Simplification of Linear Amplitude Sweep Test and Specification Parameter. Transportation Research Record: Journal of the Transportation Research Board; Vol. 2370; pp. 10-16.

[118] Johnson CM. 2010. Estimating asphalt binder fatigue resistance using an accelerated test method. PhD thesis; University of Wisconsin–Madison.

[119] Olard F, & Di Benedetto H. 2003. General "2S2P1D" model and relation between the linear viscoelastic behaviours of bituminous binders and mixes. Road Materials and Pavement Design; Vol. 4; pp. 185-224.

[120] Anderson DA, Christensen D, Dongre R, Sharma M, Runt J, & Jordhal P. 1990. Asphalt behavior at low service temperatures. Report No.FHWA-RD-88-078; U.S. Department of Transportation, Federal Highway Administration, Research, Development, and Technology, Turner-Fairbank Highway Research Center; Washington, DC.

[121] Soleimani A. 2009. Use of dynamic phase angle and complex modulus for the low temperature performance grading of asphalt cements. MSc thesis; Queen's University.

[122] Rowe G, & Anderson D. 2013. Lecture 12: Fracture of Asphalt Binders. Rheobit workshop organized by Asphalt Institute; 12.-14. June 2013; Stockholm, Sweden.

[123] Farrar MJ, Planche JP, Grimes RW, Qin Q. 2014. The Universal Simple Aging Test (USAT): Simulating short-and long term hot and warm mix oxidative aging in the laboratory. In: Kim YR, (Ed.). Asphalt Pavements. London, UK; Taylor & Francis Group; pp. 79-87.

[124] Farrar MJ, Hajj EY, Planche J, & Alavi MZ. 2013. A method to estimate the thermal stress build-up in an asphalt mixture from a single-cooling event. Road Materials and Pavement Design; Vol. 14; pp. 201-211.

[125] Farrar MJ, Turner TF, Planche J, Schabron JF, & Harnsberger PM. 2013. Evolution of the Crossover Modulus with Oxidative Aging. Transportation Research Record: Journal of the Transportation Research Board; Vol. 2370; pp. 76-83.

[126] Huang SC, Pauli AT, Qin Q. 2014. Physicochemical characteristics of RAP binder blends. In: Kim YR, (Ed.). Asphalt Pavements. London, UK; Taylor & Francis Group; pp. 277-285.

[127] Huang S, & Turner TF. 2013. Aging Characteristics of RAP Modified Binders–Rheological Properties. Transportation Research Board 92nd Annual Meeting; January 13-17, 2013; Washington, DC; No. 13-4226.

[128] Huang S, & Turner TF. 2013. Aging Characteristics of RAP Blend Binders: Rheological Properties. Journal of Materials in Civil Engineering; Vol. 26; pp. 966-973.

[129] Huang S, Pauli AT, Grimes RW, & Turner F. 2014. Ageing characteristics of RAP binder blends–what types of RAP binders are suitable for multiple recycling? Road Materials and Pavement Design; Vol. 15; pp. 113-145.

[130] Qin Q, Farrar MJ, Pauli AT, & Adams JJ. 2014. Morphology, thermal analysis and rheology of Sasobit modified warm mix asphalt binders. Fuel; Vol. 115; pp. 416-425.

[131] Reinke G, Ryan M, Engber S, & Herlitzka D. 2013. Techniques for Accelerating Recovery of Asphalt Emulsion Residues at 60 C by Using Thin Film Procedures and Test Methods Suited to the Limited Amount of Residue Obtained to Characterize the Recovered Binder. Transportation Research E-Circular: Progress Toward Performance-Graded Emulsified Asphalt Specifications; Vol. E-C182; pp. 90-114.

[132] Farrar M, Grimes RW, Turner TF, & Planche J. 2014. The Universal Simple Aging Test (USAT) and Low Temperature Performance Grading Using Small Plate Dynamic Shear Rheometry: An Alternative to Standard RTFO, PAV, and BBR for HMA and WMA. Topical report FP14 prepared by Western Research Institute for the Federal Highway Administration, Contract No. DTFH61-07-D-00005, Fundamental Properties of Asphalts and Modified Asphalts, III.

[133] Farrar MJ, Grimes RW, Wiseman S, & Planche JP. 2013. Asphalt Pavement – Micro-sampling and Micro-extraction Methods. Topical report FP 09 prepared by Western Research Institute for the Federal Highway Administration, Contract DTFH61-07-D-00005, Fundamental Properties of Asphalts and Modified Asphalts, III.

[134] Farrar MJ, Qin Q, Grimes RW, Planche J, Boysen R, Loveridge J et al. 2014. Field Sampling and Testing of Death Valley Chip Seal Emulsion Residue: A Case Study. Transportation Research E-Circular; Vol. E-C182; pp. 68-89.

[135] Farrar MJ, Salmans SL, & Planche J. 2013. Recovery and Laboratory Testing of Asphalt Emulsion Residue. Transportation Research Record: Journal of the Transportation Research Board; Vol. 2370; pp. 69-75.

[136] Salmans S, Farrar M, Sui C, & Planche J. 2013. Emulsions. Topical report FP18 prepared by Western Research Institute for the Federal Highway Administration, Contract No. DTFH61-07-D-00005, Fundamental Properties of Asphalts and Modified Asphalts, III.

[137] Gottlieb M, & Macosko C. 1982. The effect of instrument compliance on dynamic rheological measurements. Rheologica Acta; Vol. 21; pp. 90-94.

[138] Liu C, Yao M, Garritano RG, Franck AJ, & Bailly C. 2011. Instrument compliance effects revisited: linear viscoelastic measurements. Rheologica Acta; Vol. 50; pp. 537-546.

[139] Mackay M, & Halley P. 1991. Technical Note: Angular compliance error in force rebalance torque transducers. Journal of Rheology; Vol. 35; pp. 1609-1614.

[140] Rides M, Olusanya A. 1996. Appendix A.2. Compliance Correction. In: Olusanya A, (Ed.). A Comparison of Techniques for Monitoring the Cure of Adhesives. MTS Adhesives Project 5, Measurements for Optimising Adhesives Processing Report 10, NPL Report CMMT(B104). Teddington, Middlesex, UK; National Physical Laboratory; pp. 33-39.

[141] Schröter K, Hutcheson S, Shi X, Mandanici A, & McKenna G. 2006. Dynamic shear modulus of glycerol: Corrections due to instrument compliance. The Journal of chemical physics; Vol. 125; pp. 214507.

[142] Franck A. 2006. Understanding instrument compliance correction in oscillation. TA Instruments Product Note APN 013.

[143] Farrar MJ. 2015. Personal communication. January 21, 2015.

[144] Donth E. 1992. Relaxation and thermodynamics in polymers: glass transition. 1st ed. Berlin, Germany; Akademie Verlag.

[145] Donth E. 2001. The glass transition: relaxation dynamics in liquids and disordered materials. Berlin, Germany; Springer.

[146] Sperling LH. 2005. Introduction to physical polymer science. 4th ed. Hoboken, NJ; John Wiley & Sons.

[147] Turi E. 1981. Thermal characterization of polymeric materials. New York; Academic Press.

[148] Van Krevelen D. 1990. Properties of polymers. 3rd ed. Amsterdam, the Netherlands; Elsevier.

[149] Wunderlich B. 1990. Thermal Analysis. New York; Academic Press.

[150] Wunderlich B. 2005. Basics of thermal analysis. In: Wunderlich B, (Ed.). Thermal Analysis of Polymeric Materials. Berlin, Germany; Springer; pp. 71-188.

[151] Shen M, & Eisenberg A. 1970. Glass transitions in polymers. Rubber Chemistry and Technology; Vol. 43; pp. 95-155.

[152] Montserrat S, Calventus Y, & Hutchinson J. 2005. Effect of cooling rate and frequency on the calorimetric measurement of the glass transition. Polymer; Vol. 46; pp. 12181-12189.

[153] Brüning R, & Samwer K. 1992. Glass transition on long time scales. Physical Review B; Vol. 46; pp. 11318.

[154] Moynihan C, Macedo P, Montrose C, Gupta P, DeBolt M, Dill J et al. 1976. Structural relaxation in vitreous materials. Annals of the New York Academy of Sciences; Vol. 279; pp. 15-35.

[155] Hutchinson JM. 2009. Determination of the glass transition temperature. Journal of thermal analysis and calorimetry; Vol. 98; pp. 579-589.

[156] Masson JF, Leblond V, Margeson J, & Bundalo-Perc S. 2007. Low-temperature bitumen stiffness and viscous paraffinic nano-and micro-domains by cryogenic AFM and PDM. Journal of microscopy; Vol. 227; pp. 191-202.

[157] Masson J, Polomark G, & Collins P. 2002. Time-dependent microstructure of bitumen and its fractions by modulated differential scanning calorimetry. Energy & Fuels; Vol. 16; pp. 470-476.

[158] Wunderlich B. 1981. The basis of thermal analysis. In: Turi EA, (Ed.). Thermal characterization of polymeric materials. New York, NY; Academic Press Inc; pp. 91-234.

[159] Kovacs AJ. 1964. Transition vitreuse dans les polymères amorphes. Etude phénoménologique. Fortschritte der Hochpolymeren-Forschung; Vol. 3/3; pp. 394-507.

[160] McCrum NG, Read BE, Williams G. 1967. Anelastic and dielectric effects in polymeric solids. New York, NY; Wiley.

[161] Hutchinson J, Ingram M, & Robertson A. 1992. The effects of pressure and densification on ionic conductivities in silver iodomolybdate glasses. Philosophical Magazine B; Vol. 66; pp. 449-461.

[162] Eisenberg A. 1984. The Glassy State and the Glass Transition. In: Mark JE, (Ed.). Physical Properties of Polymers. Washington, DC; American Chemical Society; pp. 55-95.

[163] Rieger J. 2001. The glass transition temperature T_g of polymers—Comparison of the values from differential thermal analysis (DTA, DSC) and dynamic mechanical measurements (torsion pendulum). Polymer Testing; Vol. 20; pp. 199-204.

[164] Boyer RF. 1977. Transitions and relaxations. In: Mark HF, Bikales NM, (Ed.). Encyclopedia of Polymer Science and Technology: Plastics, Resins, Rubbers, Fibers. New York, NY; Wiley Interscience; pp. 745-839.

[165] Angell C. 1985. Strong and fragile liquids. In: Ngai KL, Wright GB, (Ed.). Relaxations in complex systems. Springfield, VA; National Technical Information Service, US Dept. of Commerce; pp. 3-11.

[166] Angell C. 1985. Spectroscopy simulation and scattering, and the medium range order problem in glass. Journal of Non-Crystalline Solids; Vol. 73; pp. 1-17.

[167] Böhmer R, Ngai K, Angell C, & Plazek D. 1993. Nonexponential relaxations in strong and fragile glass formers. The Journal of chemical physics; Vol. 99; pp. 4201-4209.

[168] Zhai H, & Salomon D. 2005. Evaluation of low-temperature properties and the fragility of asphalt binders with non-Arrhenius viscosity-temperature dependence. Transportation Research Record: Journal of the Transportation Research Board; Vol. 1901; pp. 44-51.

[169] Williams G. 1964. Complex dielectric constant of dipolar compounds as a function of temperature, pressure and frequency. Part 1.—General relations and a consideration of models for relaxation. Transactions of the Faraday Society; Vol. 60; pp. 1548-1555.

[170] Williams G. 1964. Complex dielectric constant of dipolar compounds as a function of temperature, pressure and frequency. Part 2.—The α–relaxation of polymethyl acrylate. Transactions of the Faraday Society; Vol. 60; pp. 1556-1573.

[171] Williams G. 1965. Dipole relaxation of polypropylene oxide as a function of frequency, temperature and pressure. Transactions of the Faraday Society; Vol. 61; pp. 1564-1577.

[172] Williams G, & Watts DC. 1971. Molecular motion in solid amorphous polymers. The dielectric relaxation of a poly-nonyl methacrylate and poly-n-lauryl methacrylate as a function of frequency, temperature and applied pressure. Transactions of the Faraday Society; Vol. 67; pp. 2793-2801.

[173] Ferrer ML, Lawrence C, Demirjian BG, Kivelson D, Alba-Simionesco C, & Tarjus G. 1998. Supercooled liquids and the glass transition: Temperature as the control variable. The Journal of chemical physics; Vol. 109; pp. 8010-8015.

[174] Paluch M, Casalini R, & Roland CM. 2002. Relative contributions of thermal energy and free volume to the temperature dependence of structural relaxation in fragile glass-forming liquids. Physical Review B; Vol. 66; pp. 092202.

[175] Pawlus S, Casalini R, Roland C, Paluch M, Rzoska S, & Ziolo J. 2004. Temperature and volume effects on the change of dynamics in propylene carbonate. Physical Review E; Vol. 70; pp. 061501.

[176] Roland C, & Casalini R. 2003. Temperature dependence of local segmental motion in polystyrene and its variation with molecular weight. Journal of Chemical Physics; Vol. 119; pp. 1838-1842.

[177] Roland C, Paluch M, Pakula T, & Casalini R. 2004. Volume and temperature as control parameters for the dielectric α relaxation of polymers and molecular glass formers. Philosophical Magazine; Vol. 84; pp. 1573-1581.

[178] McKenna GB. 2009. A brief discussion: Thermodynamic and dynamic fragilities, non-divergent dynamics and the Prigogine–Defay ratio. Journal of Non-Crystalline Solids; Vol. 355; pp. 663-671.

[179] Zhao J, & McKenna GB. 2014. The apparent activation energy and dynamic fragility of ancient ambers. Polymer; Vol. 55; pp. 2246-2253.

[180] Kriz P, Stastna J, & Zanzotto L. 2008. Physical aging in semi-crystalline asphalt binders. Journal of the Association of Asphalt Paving Technologists; Vol. 77; pp. 795-826.

[181] Struik L. 1976. Physical aging in amorphous glassy polymers. Annals of the New York Academy of Sciences; Vol. 279; pp. 78-85.

[182] Struik L. 1977. Physical aging in plastics and other glassy materials. Polymer Engineering & Science; Vol. 17; pp. 165-173.

[183] Bradshaw R, & Brinson L. 1997. Physical aging in polymers and polymer composites: An analysis and method for time-aging time superposition. Polymer Engineering & Science; Vol. 37; pp. 31-44.

[184] O'Connell P, & McKenna G. 1997. Large deformation response of polycarbonate: Time-temperature, time-aging time, and time-strain superposition. Polymer Engineering & Science; Vol. 37; pp. 1485-1495.

[185] O'Connell PA, & McKenna GB. 1999. Arrhenius-type temperature dependence of the segmental relaxation below Tg. The Journal of chemical physics; Vol. 110; pp. 11054-11060.

[186] Anderson DA, & Marasteanu MO. 1999. Physical hardening of asphalt binders relative to their glass transition temperatures. Transportation Research Record: Journal of the Transportation Research Board; Vol. 1661; pp. 27-34.

[187] Claudy P, Letoffe JM, Rondelez F, Germanaud L, King G, & Planche JP. 1992. A new interpretation of time-dependent physical hardening in asphalt based on DSC and optical thermoanalysis. Division of Fuel Chemistry, American Chemical Society, Preprints of Papers, 204th ACS National Meeting, Washington, DC; Vol. 37; pp. 1408-1426.

[188] Bahia H, & Anderson D. 1992. Physical hardening of paving grade asphalts as related to compositional characteristics. Division of Fuel Chemistry, American Chemical Society, Preprints of Papers, 204th ACS National Meeting, Washington, DC;
.

[189] Wright L, Kanabar A, Moult E, Rubab S, & Hesp S. 2011. Oxidative aging of asphalt cements from an Ontario pavement trial. International Journal of Pavement Research and Technology; Vol. 4; pp. 259-267.

[190] Winter HH, & Mours M. 2006. The cyber infrastructure initiative for rheology. Rheologica Acta; Vol. 45; pp. 331-338.

[191] Trinkle S, & Friedrich C. 2001. Van Gurp-Palmen-plot: a way to characterize polydispersity of linear polymers. Rheologica Acta; Vol. 40; pp. 322-328.

[192] Trinkle S, Walter P, & Friedrich C. 2002. Van Gurp-Palmen plot II–classification of long chain branched polymers by their topology. Rheologica Acta; Vol. 41; pp. 103-113.

[193] Teugels W. 2000. The Black diagram, only a rheological data presentation? Proceedings of the 2nd Eurasphalt and Eurobitume Congress; 20-22 September 2000; Barcelona, Spain; .

[194] Soenen H, De Visscher J, Vanelstraete A, & Redelius P. 2006. Influence of thermal history on rheological properties of various bitumen. Rheologica Acta; Vol. 45; pp. 729-739.

[195] Kriz P, Stastna J, & Zanzotto L. 2008. Glass transition and phase stability in asphalt binders. Road Materials and Pavement Design; Vol. 9; pp. 37-65.

[196] Dobson G. 1967. An apparatus for measuring the dynamic elastic properties of bitumens. Journal of scientific instruments; Vol. 44; pp. 375-378.

[197] Dobson G, Jongepier RD, Monismith C, Puzinauskas V, Busching H, & Warden WD. 1969. The dynamic mechanical properties of bitumen. Proceedings of the Association of Asphalt Paving Technologists; Vol. 38; pp. 123-135.

[198] Airey G, Hunter A, & Rahimzadeh B. 2002. The influence of geometry and sample preparation on dynamic shear rheometer testing. Proceedings of the Fourth European Symposium on Performance of Bituminous and Hydraulic Materials in Pavements; 11-12 April 2002; Nottingham, UK; .

[199] Airey GD. 2002. Use of black diagrams to identify inconsistencies in rheological data. Road Materials and Pavement Design; Vol. 3; pp. 403-424.

[200] Markovitz H. 1975. Superposition in rheology. Journal of Polymer Science: Polymer Symposia; Vol. 50; pp. 431-456.

[201] Cole KS, & Cole RH. 1941. Dispersion and absorption in dielectrics I. Alternating current characteristics. The Journal of chemical physics; Vol. 9; pp. 341-351.

[202] Friedrich C, & Braun H. 1992. Generalized Cole-Cole behavior and its rheological relevance. Rheologica Acta; Vol. 31; pp. 309-322.

[203] Hatzikiriakos SG. 2000. Long chain branching and polydispersity effects on the rheological properties of polyethylenes. Polymer Engineering & Science; Vol. 40; pp. 2279-2287.

[204] Mavridis H, & Shroff R. 1992. Temperature dependence of polyolefin melt rheology. Polymer Engineering & Science; Vol. 32; pp. 1778-1791.

[205] Guedes RM. 2011. A viscoelastic model for a biomedical ultra-high molecular weight polyethylene using the time–temperature superposition principle. Polymer Testing; Vol. 30; pp. 294-302.

[206] Macaubas P, & Demarquette N. 2002. Time-temperature superposition principle applicability for blends formed of immiscible polymers. Polymer Engineering & Science; Vol. 42; pp. 1509-1519.

[207] Winter HH, Siebenbürger M, Hajnal D, Henrich O, Fuchs M, & Ballauff M. 2009. An empirical constitutive law for concentrated colloidal suspensions in the approach of the glass transition. Rheologica Acta; Vol. 48; pp. 747-753.

[208] Baumgaertel M, & Winter H. 1989. Determination of discrete relaxation and retardation time spectra from dynamic mechanical data. Rheologica Acta; Vol. 28; pp. 511-519.

[209] Baumgaertel M, & Winter H. 1992. Interrelation between continuous and discrete relaxation time spectra. Journal of Non-Newtonian Fluid Mechanics; Vol. 44; pp. 15-36.

[210] Kim KW, Kim K, Doh YS, & Amirkhanian SN. 2006. Estimation of RAP's binder viscosity using GPC without binder recovery. Journal of Materials in Civil Engineering; Vol. 18; pp. 561-567.

[211] Zhao S, Bowers B, Huang B, & Shu X. 2013. Characterizing rheological properties of binder and blending efficiency of asphalt paving mixtures containing RAS through GPC. Journal of Materials in Civil Engineering; Vol. 26; pp. 941-946.

[212] Baldino N, Gabriele D, Rossi CO, Seta L, Lupi FR, & Caputo P. 2012. Low temperature rheology of polyphosphoric acid (PPA) added bitumen. Construction and Building Materials; Vol. 36; pp. 592-596.

[213] Navarro FJ, Partal P, Martínez-Boza FJ, & Gallegos C. 2010. Novel recycled polyethylene/ground tire rubber/bitumen blends for use in roofing applications: thermo-mechanical properties. Polymer Testing; Vol. 29; pp. 588-595.

[214] Gallagher KP, Bahia HU, Guerra JD, & Keating J. 1996. Influence of air-blowing on the performance-related properties of paving asphalt. Transportation Research Record: Journal of the Transportation Research Board; Vol. 1535; pp. 29-35.

[215] Izquierdo M, Navarro F, Martínez-Boza F, & Gallegos C. 2013. Effects of MDI–PPG molecular weight on the thermorheological behaviour of MDI–isocyanate based bituminous foams. Journal of Industrial and Engineering Chemistry; Vol. 19; pp. 704-711.

[216] Starck P, & Löfgren B. 2007. Influence of de-icing agents on the viscoelastic properties of asphalt mastics. Journal of Materials Science; Vol. 42; pp. 676-685.

[217] Huang D, & McKenna GB. 2001. New insights into the fragility dilemma in liquids. The Journal of chemical physics; Vol. 114; pp. 5621-5630.

[218] Mours M, & Winter H. 1994. Time-resolved rheometry. Rheologica Acta; Vol. 33; pp. 385-397.

[219] Lu X, & Isacsson U. 2000. Laboratory study on the low temperature physical hardening of conventional and polymer modified bitumens. Construction and Building Materials; Vol. 14; pp. 79-88.

[220] Plazek DJ. 1965. Temperature dependence of the viscoelastic behavior of polystyrene. The Journal of physical chemistry; Vol. 69; pp. 3480-3487.

[221] Zorn R, McKenna GB, Willner L, & Richter D. 1995. Rheological investigation of polybutadienes having different microstructures over a large temperature range. Macromolecules; Vol. 28; pp. 8552-8562.

[222] McKenna GB, & Zhao J. 2015. Accumulating evidence for non-diverging time-scales in glass-forming fluids. Journal of Non-Crystalline Solids; Vol. 407; pp. 3-13.

[223] Alegria A, Guerrica-Echevarria E, Goitiandia L, Telleria I, & Colmenero J. 1995. α-Relaxation in the Glass Transition Range of Amorphous Polymers. 1. Temperature Behavior across the Glass transition. Macromolecules; Vol. 28; pp. 1516-1527.

[224] Koh YP, & Simon SL. 2013. Enthalpy recovery of polystyrene: does a long-term aging plateau exist? Macromolecules; Vol. 46; pp. 5815-5821.

[225] Shi P, Schach R, Munch E, Montes H, & Lequeux F. 2013. Glass transition distribution in miscible polymer blends: from calorimetry to rheology. Macromolecules; Vol. 46; pp. 3611-3620.

[226] Shi X, Mandanici A, & McKenna GB. 2005. Shear stress relaxation and physical aging study on simple glass-forming materials. The Journal of chemical physics; Vol. 123; pp. 174507.

[227] Simon S, Sobieski J, & Plazek D. 2001. Volume and enthalpy recovery of polystyrene. Polymer; Vol. 42; pp. 2555-2567.

[228] Zhao J, & McKenna GB. 2012. Temperature divergence of the dynamics of a poly (vinyl acetate) glass: Dielectric vs. mechanical behaviors. The Journal of chemical physics; Vol. 136; pp. 154901.

[229] Champion D, Le Meste M, & Simatos D. 2000. Towards an improved understanding of glass transition and relaxations in foods: molecular mobility in the glass transition range. Trends in Food Science & Technology; Vol. 11; pp. 41-55.

[230] Zhao J, Simon SL, & McKenna GB. 2013. Using 20-million-year-old amber to test the super-Arrhenius behaviour of glass-forming systems. Nature communications; Vol. 4; Article no. 1783.

[231] Masson J, & Polomark G. 2001. Bitumen microstructure by modulated differential scanning calorimetry. Thermochimica Acta; Vol. 374; pp. 105-114.

[232] Claudy P, Letoffe J, King G, Planche J, & Brule B. 1991. Characterization of paving asphalts by differential scanning calorimetry. Fuel Science & Technology International; Vol. 9; pp. 71-92.

[233] Cuadri AA, Partal P, Navarro FJ, García Morales M, Gallegos C, Lepe AP et al. 2012. Bitumen chemical modification by thiourea: rheological behaviour at low in-service temperatures and microstructure. Proceedings of the 5th Eurasphalt and Eurobitumen Congress; 13-15 June 2012; Istanbul, Turkey; Paper O5EE-478.

[234] Cuadri AA, García-Morales M, Navarro FJ, Airey GD, & Partal P. 2013. End-performance evaluation of thiourea-modified bituminous binders through viscous flow and linear viscoelasticy testing. Rheologica Acta; Vol. 52; pp. 145-154.

[235] Cuadri A, García-Morales M, Navarro F, & Partal P. 2012. Enhancing the viscoelastic properties of bituminous binders via thiourea-modification. Fuel; Vol. 97; pp. 862-868.

[236] Cuadri A, Partal P, Navarro F, García-Morales M, & Gallegos C. 2011. Influence of processing temperature on the modification route and rheological properties of thiourea dioxide-modified bitumen. Energy & Fuels; Vol. 25; pp. 4055-4062.

[237] Cuadri A, Partal P, Navarro F, García-Morales M, & Gallegos C. 2011. Bitumen chemical modification by thiourea dioxide. Fuel; Vol. 90; pp. 2294-2300.

[238] Lehtimäki H. 2012. Asfalttirouheen elvyttäminen keveillä öljytuotteilla (In English: Lightweight oil products as rejuvenators for reclaimed asphalt pavement). MSc thesis; Aalto University.

List of appendices

Appendix A. Derivation of the VFT form of the Kaelble-WLF equation in the glassy region

The Kaelble-WLF equation is as follows:

$$\log a_T = -c_1 \left(\frac{T - T_d}{c_2 + |T - T_d|} - \frac{T_r - T_d}{c_2 + |T_r - T_d|} \right) \tag{A1}$$

Equation A1 can be rewritten in the following form:

$$\ln a_T = -c_1 \ln 10 \left(\frac{T - T_d}{c_2 + |T - T_d|} - \frac{T_r - T_d}{c_2 + |T_r - T_d|} \right) \tag{A2}$$

This derivation is limited to the situation where $T \leq T_d$, i.e. to the description of the temperature dependence of the shift factors in the glassy region. In addition, the reference temperature is selected to be sufficiently low so that $T_r \leq T_d$. In this case:

$$\ln a_T = -c_1 \ln 10 \left(\frac{T - T_d}{c_2 + T_d - T} - \frac{T_r - T_d}{c_2 + T_d - T_r} \right) \tag{A3}$$

Here the Vogel temperature T_v is defined as follows:

$$T_v = c_2 + T_d \tag{A4}$$

By substituting Equation A4 into Equation A3, the shift factor function can be rewritten in the following form:

$$\ln a_T = -c_1 \ln 10 \left(\frac{T - T_d}{T_v - T} - \frac{T_r - T_d}{T_v - T_r} \right) \tag{A5}$$

After simplification, Equation A5 can be expressed as:

$$\ln a_T = \ln 10\, c_1 c_2 \frac{T_r - T}{(T_r - T_v)(T - T_v)} \tag{A6}$$

By using the following notation:

$$B = \ln 10\, c_1 c_2 \tag{A7}$$

Equation A6 can be written as follows:

$$\ln a_T = B \frac{T_r - T}{(T_r - T_v)(T - T_v)} \tag{A8}$$

Appendix B. Specimen preparation and measurement protocol in the 4-mm DSR testing

In this study, the 4-mm DSR experiments were conducted according to the latest version of the AASHTO standard draft "Standard Method of Test for Determining the Low Temperature Rheological Properties of Asphalt Binder Using a Dynamic Shear Rheometer (DSR)". This standard draft is reprinted later in this appendix. However, in this study, some modifications/refinements were made to the standard procedure after preliminary test runs. These modifications/refinements are described in the following:

- Paragraph 10.1.: Only the stiffest of the investigated bitumens were annealed in an oven in order to avoid the high-temperature aging of the test samples. Instead, a heated spoon was used to curve the test specimens out of the airtight metal cans in which the test samples were stored. In this way, the whole sample was not heated multiple times if replicate measurements were needed to be performed. However, the stiffest bitumens were annealed in an oven in order to prepare the test specimen into the rheometer without excessive heating of the spoon that was used to curve the test specimen from the bulk sample. The annealing temperatures and times varied depending on the stiffness of the bitumen sample. However, excessive annealing temperatures and prolonged annealing times were avoided to prevent the high-temperature aging of the test samples.

- Paragraph 10.2.: The gap was zeroed at 0 °C. Because the thermal expansion of the measuring system was determined accurately (see Appendix D), this modification was not expected to have any influence on the test results.

- Paragraph 10.3.: The preheating temperature was varied depending on the stiffness of the bitumen sample. In this way, a good adhesion between the test specimen and the plates was ensured in all cases without causing the specimen to flow out of the gap during the specimen preparation sequence due to low viscosity. For all the bitumens, the preheating temperature was adjusted to be slightly higher than the Ring-and-Ball softening point temperature in order to remove the effects of steric hardening. The preheating temperatures used in this study are listed in Table B1.

- Paragraph 10.8.: The test specimen was cooled down to 30 °C at a rate of 2 K/min. A controlled cooling rate was used to maximize test reproducibility.

- Paragraph 10.9.: In this study, the conditioning time at 30 °C was 15 min. This modification was not expected to have any influence on the test results.

- Paragraph 11.2.: In this study, the conditioning time at the test temperatures was 15 min. It was confirmed by additional tests that thermal equilibrium is reached

within 15 minutes from the moment when the temperature reading of the rheometer attains its target value. Furthermore, as of writing, there is discussion going on about whether the thermal equilibrium time could be significantly reduced [B1].

- Paragraph 11.3.: Stress sweeps were not performed in this study. Instead, fixed strain amplitude levels were used in the frequency sweep testing. The temperature-dependent strain levels used in the 4-mm DSR experiments (adapted from the proposal of Farrar et al. [B1]) are listed in Table B2. Additional strain sweep testing was performed to confirm that the strain levels were well within the LVE range of the investigated bitumens.

- Paragraph 11.4.: Frequency sweeps were performed in the range from 10 Hz to 0.01 Hz with 3 measurement points per decade. The same frequency range and data point density were used in the intermediate- and high-temperature frequency sweep measurements.

- Paragraph 11.5.: The test specimen was always cooled at a rate of 2 K/min in order to maximize test reproducibility.

Table B1. Preheating temperatures used in the specimen preparation.

Sample	Pen [dmm]	$T_{R\&B}$ [°C]	Preheating temperature [°C]
B-1	5	104.5	110
B-2	5	74.2	90
B-3	12	65	70
B-4	15	64.2	70
B-5	15	62.6	70
B-6	20	62.2	70
B-7	25	61.5	70
B-8	27	55.5	70
B-9	27	61.5	70
B-10	38	54.3	60
B-11	42	51.3	60
B-12	51	49.1	60
B-13	52	49	60
B-14	52	49.8	60
B-15	53	49.9	60
B-16	61	47.7	60
B-17	62	50	60
B-18	64	47.7	60
B-19	67	46.8	60
B-20	70	46.1	60
B-21	80	45.8	60
B-22	81	45.5	60
B-23	107	43.5	60
B-24	187	38.5	50
B-25	187	36.9	50
B-26	190	39.2	50
B-27	200	37.7	50

Table B2. Strain amplitude levels used in the 4-mm DSR experiments.

Test temperature [°C]	Strain amplitude [%]
10	0.075
0	0.075
-10	0.02
-20	0.01
-30	0.01
-40	0.01

Standard Method of Test for

Determining the Low Temperature Rheological Properties of Asphalt Binder Using a Dynamic Shear Rheometer (DSR)

AASHTO Designation: T XXX-12

1. SCOPE

1.1. This test method covers the determination of the dynamic shear modulus and phase angle of asphalt binder when tested in dynamic (oscillatory) shear using parallel plate test geometry at low (-40 to 0°C) temperature. This test method is intended for determining the linear viscoelastic properties of asphalt binders as required for specification testing and is not intended as a comprehensive procedure for the full characterization of the viscoelastic properties of asphalt binder.

1.2. This standard is appropriate for unaged material, and material aged in accordance with T 240 and R 28.

1.3. This standard may involve hazardous materials, operations, and equipment. This standard does not purport to address all of the safety concerns associated with its use. It is the responsibility of the user of this procedure to establish appropriate safety and health practices and to determine the applicability of regulatory limitations prior to use.

2. REFERENCED DOCUMENTS

2.1. AASHTO Standards:

- M 315 Standard Test Method for Determining the Rheological Properties of Asphalt Binder Using a Dynamic Shear Rheometer
- M 320, Performance-Graded Asphalt Binder
- R 28, Accelerated Aging of Asphalt Binder Using a Pressurized Aging Vessel (PAV)
- R 29, Grading or Verifying the Performance Grade (PG) of an Asphalt Binder
- T 40, Sampling Bituminous MaterialsT315, Determining the Rheological Properties of Asphalt Binder Using a Dynamic Shear Rheometer (DSR)
- T 240, Effect of Heat and Air on a Moving Film of Asphalt Binder (Rolling Thin-Film Oven Test)

2.2. ASTM Standards:

- D 7175, Standard Test Method for Determining the Rheological Properties of Asphalt Binder Using a Dynamic Shear Rheometer

3. TERMINOLOGY

3.1. Definitions:

3.1.1. asphalt binder—an asphalt-based cement that is produced from petroleum residue either with or without the addition of non-particulate organic modifiers.

3.2. Descriptions of Terms Specific to This Standard:

3.2.1. annealing—heating the binder until it is sufficiently fluid to remove the effects of steric hardening.

3.2.2. complex shear modulus (G*)—ratio calculated by dividing the absolute value of the peak-to-peak shear stress, τ, by the absolute value of the peak-to-peak shear strain, γ.

3.2.3. calibration—process of checking the accuracy and precision of a device using NIST-traceable standards and making adjustments to the device where necessary to correct its operation or precision and accuracy.

3.2.4. dummy test specimen—a specimen formed between the dynamic shear rheometer (DSR) test plates from asphalt binder or other polymer to measure the temperature of the asphalt binder held between the plates. The dummy test specimen is used solely to determine temperature corrections.

3.2.5. loading cycle—a unit cycle of time for which the test sample is loaded at a selected frequency and stress or strain level.

3.2.6. phase angle *(δ)*—the angle in radians between a sinusoid ally applied strain and the resultant sinusoidal stress in a controlled-strain testing mode, or between the applied stress and the resultant strain in a controlled-stress testing mode.

3.2.7. loss shear modulus (G″)—the complex shear modulus multiplied by the sine of the phase angle expressed in degrees. It represents the component of the complex modulus that is a measure of the energy lost (dissipated during a loading cycle).

3.2.8. storage shear modulus (G′)—the complex shear modulus multiplied by the cosine of the phase angle expressed in degrees. It represents the in-phase component of the complex modulus that is a measure of the energy stored during a loading cycle.

3.2.9. parallel plate geometry—refers to a testing geometry in which the test sample is sandwiched between two relatively rigid parallel plates and subjected to oscillatory shear.

3.2.10. oscillatory shear—refers to a type of loading in which a shear stress or shear strain is applied to a test sample in an oscillatory manner such that the shear stress or strain varies in amplitude by about zero in a sinusoidal manner.

3.2.11. linear viscoelastic—within the context of this specification refers to a region of behavior in which the dynamic shear modulus is independent of shear stress or strain.

3.2.12. portable thermometer—is an electronic device that consists of a temperature detector (probe containing a thermocouple or resistive element), required electronic circuitry, and readout system.

3.2.13. reference thermometer—a NIST–traceable liquid-in-glass or electronic thermometer that is used as a laboratory standard.

3.2.14. temperature correction—difference in temperature between the temperature indicated by the DSR and the test specimen as measured by the portable thermometer inserted between the test plates.

3.2.15. thermal equilibrium—is reached when the temperature of the test specimen mounted between the test plates is constant with time.

3.2.16. verification—process of checking the accuracy of a device or its components against an internal laboratory standard. It is usually performed within the operating laboratory.

3.2.17. steric hardening—see molecular association.

3.2.18. physical hardening— structural relaxation below the glass transition temperature.

3.2.19. normal force— the force perpendicular to the surface of the parallel plates.

3.2.20. molecular association—a process where associations occur between asphalt binder molecules during storage at ambient temperature. Often called steric hardening in the asphalt literature, molecular associations can increase the dynamic shear modulus of asphalt binders. The amount of molecular association is asphalt specific and may be significant even after a few hours of storage.

4. SUMMARY OF TEST METHOD

4.1. Test specimens 1.75 mm by 4 mm or 2.00 mm by 8 mm are formed between 4 and 8 mm diameter parallel metal plates, respectively. During testing, one of the parallel plates is oscillated with respect to the other at pre-selected frequencies and rotational deformation amplitudes (strain control) (or torque amplitudes (stress control). A strain or stress sweep is required at each isotherm to insure testing in the linear viscoelastic range.

4.2. The test specimen is maintained at the test temperature to within ±0.1°C by positive heating and cooling of the upper and lower plates or by enclosing the upper and lower plates in a thermally controlled environment or test chamber. Test temperatures are between -40 and 0°C.

4.3. The complex modulus (G*) and phase angle (δ) are calculated automatically as part of the operation of the rheometer using proprietary computer software supplied by the equipment manufacturer.

5. SIGNIFICANCE AND USE

5.1. The test method is a significant benefit to low temperature rheological testing in several ways: (1) the method includes a procedure to measure instrument compliance; (2) testing as low as -40°C is achievable by way of a correction for machine compliance; (3) when using 4mm diameter plates, only 25mg of binder is required for a test (note: in actual practice 150 mg for sample loading and trimming is required, but that is about 100 times less than required under AASHTO T313 to prepare 1 beam) ; (4) a commercial dynamic shear rheometer is a more precise instrument than a bending beam rheometer; (5) intermediate test temperatures are achievable: for 4 mm and 8 mm diameter plates, approximately 0 to 30°C and 0 to 45°C, respectively.

5.2. Test temperatures are related to the low temperatures experienced by the pavement in the geographical area for which the asphalt binder is intended to be used. Master curves of G* and δ curves at selected temperatures can be developed employing time-temperature superposition. The master curves can be used to calculate low temperature performance-related criteria in accordance with M 320.

6. APPARATUS

6.1. The dynamic shear rheometer, environmental chamber and control and data acquisition system shall meet the requirements of T315. Test plates shall be 4.00 ± 0.01 mm or 8.00 ± 0.01mm in diameter, stainless steel or aluminum with smooth ground surface. In addition, the rheometer shall be equipped with a normal force sensor.

Note 1—When measuring low temperature properties by DSR, errors due to instrument compliance need to be corrected. For older DSR's, without updated software to do the real-time online instrument compliance corrections, one can use the method in Appendix 17. For updated DSR the real-time online instrument compliance correction is made by pre-inputting the instrument compliance value into the software. Regardless of the way the correction is performed, the value of instrument compliance is the most important factor. How to measure the instrument compliance is covered in Appendix 18.

7. HAZARDS

7.1. Standard laboratory caution should be used in handling the hot asphalt binder when preparing test specimens.

8. PREPARATION OF APPARATUS

8.1. Prepare the apparatus for testing in accordance with the manufacturer's recommendations. Specific requirements will vary for different DSR models and manufacturers.

8.2. Inspect the surfaces of the test plates and discard any plates with jagged or rounded edges or deep scratches. Clean any asphalt binder residue from the plates with an organic solvent such as mineral oil, mineral spirits, a citrus-based solvent, or toluene. Remove any remaining solvent residue by wiping the surface of the plates with a cotton swab or a soft cloth dampened with acetone. If necessary, use a dry cotton swab or soft cloth to ensure that no moisture condenses on the plates.

8.3. Mount the cleaned and inspected test plates on the test fixtures and tighten firmly.

9. VERIFICATION AND CALIBRATION

9.1. Verify the DSR and its components at least every six months and when the DSR or plates are newly installed, when the DSR is moved to a new location, or when the accuracy of the DSR or any of its components is suspect in accordance with T315.

10. PREPARING TEST SAMPLES

10.1. Anneal the asphalt binder in a forced draft oven at 70°C. For relatively large amounts of material such as an RTFO-PAV aged sample (50 g) in a standard PAV pan, an annealing time of about 30 min. is required. For smaller amounts of binder (<10 g) only 15 minutes is required. For very small amounts (<`1 g) an argon blanket should be used to prevent oxidation.

10.2. While the sample is being annealed, carefully clean and dry the surfaces of the test plates so that the specimen will adhere to both plates uniformly and strongly. Heat the rheometer oven or Peltier plates to 30°C and stabilize at this temperature for about 20 min. Zero the gap in accordance with [Preparation of Apparatus].

10.3. Move the plates apart to 5 mm and preheat the plates to ~ 60°C to improve the adhesion between the asphalt and the plates.

10.4. Transfer the annealed hot asphalt to the lower fixed plate using a metal spatula or other tools.

10.5. Immediately after the transferring, move the test plates together until approaching the desired testing gap plus the gap closure to create the bulge: (1) 4 mm diameter plates - the desired testing gap is 1.75 mm and the closure gap for the bulge is 0.120 mm; (2) 8 mm diameter plates - the desired testing gap is 2.00 mm and the closure gap for the bulge is 0.150 mm).

10.6. Trim excess asphalt binder by moving a heated trimming tool around the edges of the plates so that the asphalt binder is flush with the outer diameter of the plates.

Use a magnifying lens, external light source and mirror to observe the entire surface of the trimmed sample and insure a uniform trimmed surface.

10.7. Close the chamber door and heat the sample to the preheating temperature (~60°C) for about 5 min.

10.8. Cool the system down to 30°C and decrease the gap by the amount of closure gap (0.120 mm for 4 mm plates, and .150 mm for 8 mm plats).

10.9. Condition the sample at 30°C for 20 min.

11. PROCEDURE

11.1. After conditioning the specimen for 20 minutes at 30°C the measuring system shall then be cooled to the target testing temperature and stabilized at the testing temperature for 20 min when testing binder for compliance with M 320.

Note 2—When changing temperature, the metallic rheometer parts and measurement geometries thermally expand or contract causing an expansion or contraction of the gap. The change in the gap due to system thermal expansion or contraction must be compensated for to keep the gap constant. To compensate and keep the gap constant a correction factor must be determined and the gap adjusted for changes in temperature as discussed Appendix 19.

Note 3—Even with the gap correction performed manually or automatically to compensate for system thermal expansion or contraction, the sample will expand or contract with change in temperature causing changes in the sample shape and generation of normal force. This is particularly true at test temperatures close to or below the glass transition temperature of the test materials. In some cases the build-up in thermal stress may be sufficient to damage the normal force transducer. To keep a uniform sample shape as well as to avoid machine damage, the moving plate has to be adjusted to compensate for build up in normal force due to sample expansion or contraction. The normal force should be monitored when changing temperature and the gap adjusted beyond the necessary adjustment for system expansion or contraction to keep the normal force at zero. In no case should the normal force exceed 20 grams during cooling or heating. If performed manually, this adjustment in the gap to keep the normal force at zero causes a very slight error in the gap, but it is small enough that it can be neglected. Some rheometers can maintain the normal force at zero and any slight change in the gap is accounted for eliminating the slight error when the correction is manually performed.

11.2. After cooling to the test temperature, which typically takes about 3 to 5 minutes, condition the sample at the test temperature for 20 minutes. A specific time of 20 minutes is specified to keep the extent of physical hardening at low temperature uniform during testing.

11.3. After the 20 minute conditioning period, perform a strain or stress sweep test (a strain sweep if the rheometer is strain controlled or a stress sweep if the rheometer

is stress controlled) to determine the linear viscoelastic region and select an appropriate linear stain. After the strain or stress sweep test is finished, a plot of G*, G' and G" should be developed in the instrument software. Examine the plot for regions in which all three of these variables form a flat (slope of 0) line. It is in this linear viscoelastic region of all three variables where the percent strain or stress for the frequency sweep should be selected. In some cases, the entire plot may be linear, only a small region linear, or no linearity may be observed. Some instruments can be programmed to perform the strain or stress sweep and select an appropriate strain or stress level (usually the mid-point of the linear region) automatically.

11.4. Perform a frequency sweep test in a frequency range of 0.1 to 50 rad/s using the linear strain or stress determined in step 11.3. There will be 15 steps in the frequency sweep as shown in Table 1.

Table 1—Frequency Sweep Steps

Frequency rad/s														
0.10	0.15	0.25	0.39	0.63	1.00	1.58	2.51	3.98	6.31	10.00	15.85	25.12	39.81	50.00

11.5. Cool the sample to the next isotherm repeating steps 11.2 through 11.4.

12. INTERPRETATION OF RESULTS

12.1. The two frequency sweeps performed at, PG+10°C and PG+20°, are used to develop a storage modulus G'(ω) master curve using time-temperature superposition at a reference temperature of PG+10°C. The relaxation modulus G(t) curve is then determined thru interconversion. The slope (m_r) and magnitude G(t) for M 320 are determined from the relaxation modulus master curve at 60 seconds. Appendix 20 provides further discussion and an example of the process to determine m_r and G(t) at 60 seconds.

13. REPORT

13.1. **REPORT** TS-X T XXX-X AASHTO

13.2. Mr(60 sec) to one decimal place and G(60 sec) to the nearest whole number

14. PRECISION AND BIAS

14.1. To be determined upon results of inter-laboratory testing.

15. KEYWORDS

15.1. Dynamic shear rheometer; DSR; storage modulus; relaxation modulus, asphalt binder.

16. REFERENCES

16.1. Olusanya, A., "A Comparison of Techniques for Monitoring the Cure of Adhesives," MTS Adhesives Project 5, Measurements for Optimizing Adhesives Processing Report 10, NPL Report CMMT(B104) National Physical Laboratory, Teddington, Middlesex, UK, ISSN 1361-4061, November 1996.

16.2. Franck, A. J., TA Instruments, Understanding Instrument Compliance Correction in Oscillation, APN013, November 2006 Version 1.

16.3. Schröter, K., S. A. Hutcheson, X. Shi, A. Mandanici, and G. B. McKenna, Dynamic Shear Modulus of Glycerol: Corrections Due to Instrument Compliance. J. Chem. Phys., 125, 214507, 2006.

16.4. Hutcheson, S. A., and G. B. McKenna, The measurement of mechanical properties of glycerol, m-toluidine, and sucrose benzoate under consideration of corrected rheometer compliance: An in-depth study and review. J. Chem. Phys., 129, 074502, 2008.

16.5. Sui, C., M. J. Farrar, W. H. Tuminello, and T. F. Turner, New Technique for Measuring Low-Temperature Properties of Asphalt Binders with Small Amounts of Material. Transportation Research Record 2179, 23-28, 2010.

16.6. Christensen, R. M. Theory of Viscoelasticity – an Introduction, Academic Press, New York, 1982.

17. APPENDIXES

17.1. (Mandatory Information)

A1. INSTRUMENT COMPLIANCE CORRECTION

A1.1. Scope:

A1.1.1. This is a mathematical method for correcting errors due to instrument compliance and is applicable to the data collected on a DSR that does not have a real-time online instrument compliance correction function.

A1.2. Mathematical methodology:

For low temperature rheological measurements, the stiffness of the test material could be comparable to that of the instrument so instrument compliance can't be neglected in order to obtain reliable results. The measured data has to be properly corrected by taking the instrument compliance into account.

In 1996, Rides and Olusanya proposed an instrument compliance correction for oscillatory shear rheometry (Olusanya 1996). Franck proposed a similar correction in 2006.

Schroter et al. (2006) and Hutcheson and McKenna (2008) demonstrated that error from not properly taking into account rheometer compliance can be quite significant and that the resulting inaccuracies in the determined mechanical properties can result in mistakes in material modeling, design, and theory.

Sui et al. (2010) were the first to apply an instrument compliance correction to asphalt binder low temperature oscillatory shear measurements (~ 5°C to -40°C) using parallel plate geometry.

A1.2.1. Dynamic data correction

When the rheological measurements are on stiff samples or at low temperatures, the actual measured angular displacement (θ_m) includes the sample angular displacement (θs) and the machine or tool angular displacement (θ_t).

$$\theta_m = \theta_s + \theta_t \quad (1)$$

The torsional stiffness K is related to the angular displacement θ and the torque M as follows:

$$K = \frac{M}{\theta} \quad (2)$$

Under the applied torque M,

$$\frac{1}{K_m} = \frac{1}{K_s} + \frac{1}{K_t} \quad (3)$$

Where K_m is the measured stiffness, K_s is the sample stiffness and K_t represents the machine or fixture tool stiffness.

By rearranging Equation (3), the sample stiffness can be obtained as

$$K_s = \frac{K_m K_t}{K_t - K_m} \quad (4)$$

To convert the torsional stiffness (K) into shear modulus (G), the geometry constant or the geometry conversion factor (k_g) needs to be introduced.

$$K = {}^{G}/_{k_g} \quad (5)$$

For example, for the parallel plate fixture geometry with plate radius R and gap between plates of h,

$$k_g = \frac{2h}{\pi R^4} \quad (6)$$

Due to the viscoelastic characteristics of samples, both the measured and sample stiffness and moduli are in the complex form, while the fixture tool only has the real part value by assuming the tool material is purely elastic.

So the machine or tool compliance (J_{tool}) can be simply expressed as

$$J_{tool} = \frac{1}{K_t} \tag{7}$$

Substituting Equation (5) and (7) into (4) gives

$$G_s^* = \frac{G_m^*}{1-\frac{J_{tool}}{k_g}G_m^*} \tag{8}$$

Where G_s^* and G_m^* are the sample complex modulus and the measured complex modulus respectively.

For the parallel plate geometry, the sample complex shear modulus is

$$G_s^* = \frac{G_m^*}{1-J_{tool}G_m^*\frac{\pi R^4}{2h}} \tag{9}$$

The Equation (8) can be rewritten in the form of storage and loss moduli as

$$G_s^{'} + iG_s^{"} = \frac{G_m^{'}+iG_m^{"}}{1-\frac{J_{tool}}{k_g}(G_m^{'}+iG_m^{"})} \tag{10}$$

By rearranging Equation (10), the storage ($G_s^{'}$), loss ($G_s^{"}$) moduli and phase angle (δ_s) of the sample can be calculated as

$$G_s^{'} = \frac{G_m^{'}\left(1-\frac{J_{tool}}{k_g}G_m^{'}\right)-\frac{J_{tool}}{k_g}G_m^{"\,2}}{\left(1-\frac{J_{tool}}{k_g}G_m^{'}\right)^2+\left(\frac{J_{tool}}{k_g}G_m^{"}\right)^2} \tag{11}$$

$$G_s^{"} = \frac{G_m^{"}}{\left(1-\frac{J_{tool}}{k_g}G_m^{'}\right)^2+\left(\frac{J_{tool}}{k_g}G_m^{"}\right)^2} \tag{12}$$

$$tan(\delta) = \frac{G_m^{"}}{G_m^{'}\left(1-\frac{J_{tool}}{k_g}G_m^{'}\right)-\frac{J_{tool}}{k_g}G_m^{"\,2}} \tag{13}$$

The geometry constant or geometry conversion factor k_g for the commonly used rheometer fixture geometry is listed below:

For parallel plate, k_g was shown in Equation (6).

For cone and plate,

$$k_g = \frac{3}{2\pi R^4 \emptyset} \tag{14}$$

Where R is the plate radius and Ø is the cone angle.

For concentric cylinders or bob-cup geometry,

$$k_g = \frac{R_C^2 - R_B^2}{4\pi L R_B^3 R_C^2} \quad (15)$$

Where R_C , R_B is the radius of the cup and bob respectively and L is the bob length.

A2. INSTRUMENT COMPLIANCE MEASUREMENT AND CALCULATION

A2.1. Scope:

A2.1.1. This procedure is used to measure instrument compliance for DSR's.

A2.2. Procedure:

A2.2.1. Prepare the DSR in accordance with Section 8 of this standard using 4 mm parallel plates and allow approximately the plates to come to room temperature (approximately 20 minutes). Insure that any compliance correction values in the instrument software are set to zero.

A2.2.2. Apply a drop of SuperGlue™ (cyanoacrylate or any other type of super glue) to the center of the lower plate.

A2.2.3. Close the gap by moving the movable plate to form a thin layer (about 0.05 mm) of super glue between two plates. Ensure the thin layer of super glue film between plates is uniform.

A2.2.4. Clean up the extra super glue with a dry paper towel.

A2.2.5. Allow for sufficient time to fully cure the super glue (approximately 3 hours). Monitor the normal force as the cyanoacrylate will have a slight volume loss as it cures. Adjust the gap as necessary to maintain a normal force of 0 N.

A2.2.6. Perform a strain or stress sweep test at a frequency 1 rad/s.

Note 4—The strain/stress ramping range depends on the measuring system geometry (specifically the parallel plate radius) and the rheometer limits. Small strains and stresses are strongly suggested to avoid damaging the torque transducer. Start out at the lowest possible strain or stress achievable by the instrument and increase the strain in small increments.

A2.2.7. Plot angle displacement (angular rotation) versus torque obtained from the strain/stress test, and the instrument compliance is the slope of the linear fit (as shown in Figure 1).

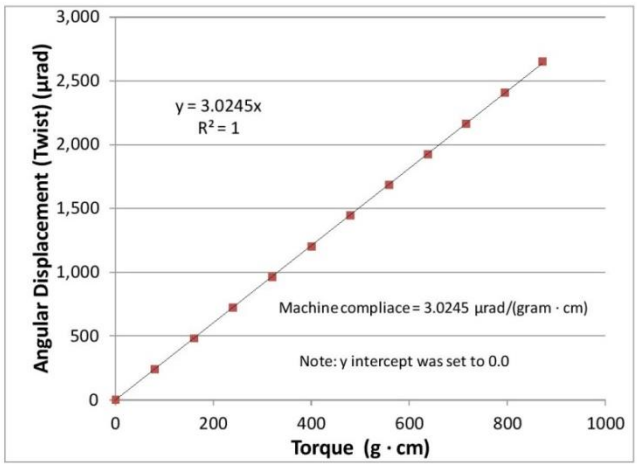

Figure 1—Example: Determination of Instrument Compliance from the Slope of the Linear Fit of the Angle Displacement and Torque Measurements

A3. DETERMINATION OF THERMAL EXPANSION OF THE MEASURING SYSTEM

A3.1. Scope:

A3.1.1. This procedure is used to measure the thermal expansion of the measuring system on DSR.

A3.2. Procedure:

A3.2.1. Mount the parallel plates onto DSR and leave the plates 1 mm apart.

A3.2.2. Heat the measuring system to 30°C and stabilize at this temperature for at least 30 min.

A3.2.3. Zero the gap using the normal force transducer and the instrument's "Zero Gap" function, and move the moveable plate so the plates are 1 mm apart. Lower the temperature to 20°C and condition for 20 minutes. Then move the moveable plate to the point where it just touches the fixed plate (indicated by a change in the normal force, note: the normal force should not exceed 10 g). The gap deviation from the zero position is the thermal expansion or change in length (ΔL) of the measuring system from the 10°C change in temperature (ΔT) The gap correction factor (g_α) of the system is

$$g_\alpha = (\Delta L) / (\Delta T) \quad (16)$$

where g_α = gap correction factor($\mu m°C^{-1}$)
ΔL = gap change in length (µm)

ΔT = change in temperature (°C)

Repeat this measurement several times and determine the average gap correction factor.

A3.2.4. Adjust the gap when changing temperature to adjust for the thermal contraction or expansion of the system, e.g., assuming $g_\alpha = 2\ \mu m\ °C^{-1}$) then when changing from 30°C to20°C the gap adjustment (Δh) is

(Δh) = g_α * (ΔT) = 2 µm/ °C * 10°C = 20 µm, i.e., the moveable plate is moved towards the stationary plate a distance of 20 µm.

A4. ANNEX – HOW TO DETERMINE m_r and G(t)

A4.1. Scope:

A4.1.1. This section provides an example of time temperature superposition (TTS) and master curve development of G'(ω) from the two frequency sweeps, interconversion from G'(ω) to G(t) and estimation of m_r and G(t) at 60 seconds from the G(t) master curve at the PG+10°C.

A4.2. Definition of terms:

A4.2.1. G'(ω) – Storage Modulus

A4.2.2. G(t) – Relaxation Modulus

A4.2.3. PG+10°C – Low Performance Grade temperature plus 10°C

A4.2.4. PG+20°C – Low Performance Grade temperature plus 20°C

A4.2.5. m_r(60 s) – slope of the relaxation modulus at a reference temperature of PG+10°C and 60 seconds

A4.2.6. G(60 s) – magnitude of the relaxation modulus at a reference temperature of PG+10°C and 60 seconds

A4.2.7. ω – Frequency (rad/s)

A4.2.8. a_T – Time-temperature superposition horizontal shift factor

A4.2.9. t – time (seconds)

A4.3. Example:

A4.3.1. A series of steps are involved when calculating the slope (m_r) and magnitude of the relaxation modulus G(t) from dynamic oscillatory shear data (frequency sweeps) at 60 seconds and a reference temperature of PG+10°C. The first step is to generate a G'(ω) master curve at a reference temperature of PG+10°C.

Plot the two frequency sweeps determined in Section 1. A typical representation of test data is shown in Figure 2. Fit the PG+10°C frequency sweep with a second order polynomial.

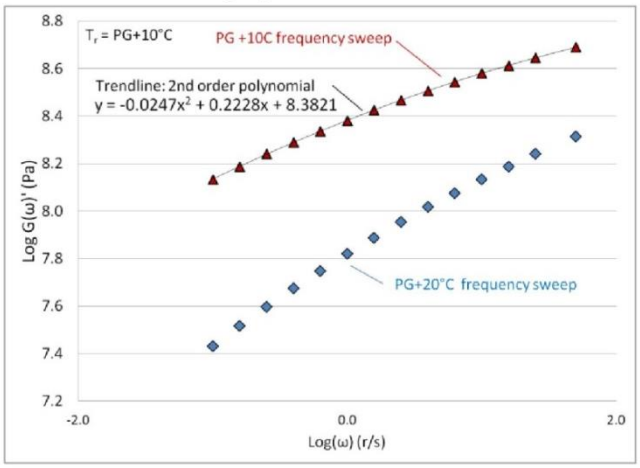

Figure 2—PG+10°C and PG+20°C Frequency Sweeps from Section 11, Procedure

A4.3.2. Use Excel™ solver to determine the horizontal shift factor (a_T) to translate the PG+20°C frequency sweep along the abscissa so that it overlaps the PG +10°C frequency sweep. The horizontal translation is accomplished by multiplying the PG+20°C frequencies by a_T and plotting the storage modulus as a function of the multiplied frequencies. The basis for the shift factor is known as time-temperature superposition (TTS). Table 2 demonstrates the calculation of the shift factor. To avoid error from extrapolation of the 2nd order polynomial, only G'(ω) data that approximately overlap are used to estimate a_T.

Table 2—Estimating the Horizontal Shift Factor a_T using Excel™ Solver

Solver—changing cell

Least squre difference (LSD) (log G' freq. sweep — calculated log G' based on 2nd order polynomial)^2

Solver target cell

ω (r/s)	log ω (r/s)	G' from PG+20°C ω sweep (Pa)	log G' (Pa)			a_T * ω (r/s)	log (a_T * ω) (r/s)	log G' (2nd order polynomial) from figure 1) (Pa)	LSD
				Shift factor =	0.0103				
3.98	0.60	1.04E+08	8.02	Sum LSD =	7.93E-06	4.08E-02	-1.39	8.02	3.26E-06
6.31	0.80	1.19E+08	8.08			6.47E-02	-1.19	8.08	1.72E-06
10.00	1.00	1.36E+08	8.13			1.03E-01	-0.99	8.13	3.60E-07
15.85	1.20	1.54E+08	8.19			1.63E-01	-0.79	8.19	1.91E-07
25.12	1.40	1.74E+08	8.24			2.58E-01	-0.59	8.24	1.58E-06
39.81	1.60	1.95E+08	8.29			4.08E-01	-0.39	8.29	2.19E-07
50.00	1.70	2.06E+08	8.31			5.13E-01	-0.29	8.31	6.03E-07

A4.3.3. Using the a_T determined in section 20.2.2 shift the PG+20°C frequency sweep so that it overlaps the PG+10C frequency sweep. The process is illustrated in Figure 3.

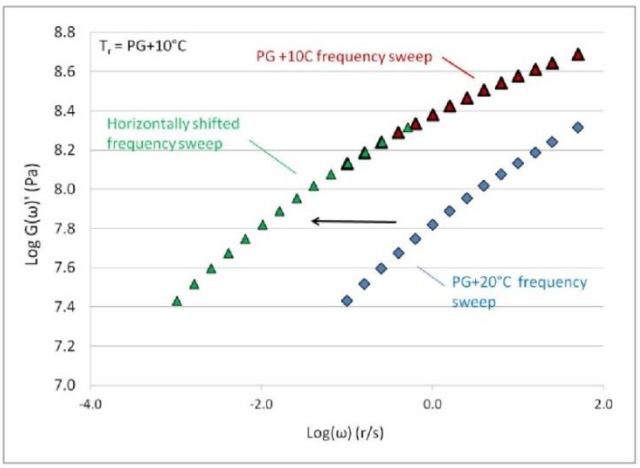

Figure 3—G' Master Curve at a Reference Temperature PG+10°C

A4.3.4. The relaxation modulus G(t) is then determined thru interconversion of the storage modulus *G'(ω)* by the approximate expression developed by Christensen (1982).

$$G(t) \approx G'(\omega)|_{\omega=2/\pi t} \quad (17)$$

Figure 4 shows the relaxation modulus determined using Equation 17. The relaxation modulus is fit with a 2nd order polynomial using the time points that bracket 60 seconds (0.78 to 2.78 in log scale) to generate the polynomial. The resulting 2nd order polynomial is

$$\log G(t) = -0.0366(\log t)^2 - 0.2195 \log t + 8.3311 \quad (18)$$

The slope of the relaxation modus at 60 seconds is determined by taking the first derivative of the 2nd order polynomial

$$\frac{d \log G(t)}{d \log t} = m_r = -0.0366 * 2 \log t - 0.2195 \quad (19)$$

Solve Equation 18 for G(60s) and Equation 19 for the slope, mr at 60 s.

G(60 s) = 66.85 MPa

m_r (60 s) = -0.35

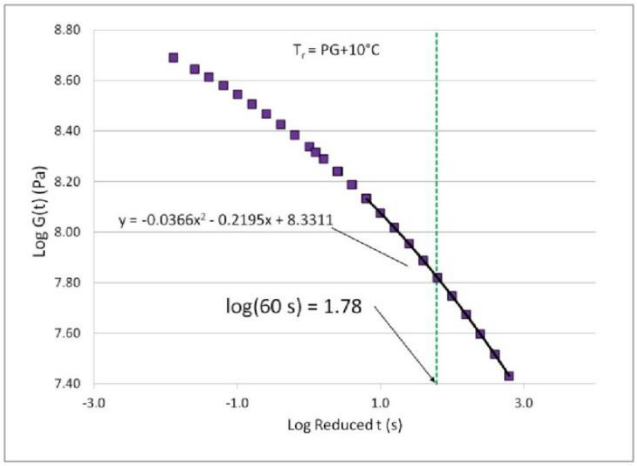

Figure 4—Relaxation Modulus Master Curve

References

[B1] Farrar MJ, Planche JP, Cookman AO, Salmans S. 4-mm DSR Ruggedness Testing. Asphalt Binder ETG Meeting; April 2014; San Antonio, TX.

Appendix C. Determination of the radial instrument compliance of the 4-mm parallel plate measurement system and its effect on the measured values of rheological parameters

The radial instrument compliance of the 4-mm parallel plate measurement system − consisting both of the radial compliances of the 4-mm parallel plate fixture (upper and lower plate) and of the shaft of the rheometer motor − was determined according to the Appendix A2 of the AASHTO standard draft "Standard Method of Test for Determining the Low Temperature Rheological Properties of Asphalt Binder Using a Dynamic Shear Rheometer (DSR)". Maximum Bond Krazy Glue® was used to adhere the upper and lower plate together, and it was allowed to cure at least 12 hours before stress sweeps were performed to determine the instrument compliance value. Instrument compliance measurement was repeated multiple times to ensure the accuracy of the measurement. In Figure C1 the results of four replicate measurements (performed on two different glue samples) are shown. The instrument compliance value was obtained as an average slope of these curves and equaled 0.00964 rad N^{-1} m^{-1}. This value is comparable to the compliance values obtained elsewhere for exactly the same rheometer set-up (Malvern Kinexus rheometer equipped with the commercially available KNX0057/KNX0058 4-mm parallel plate fixture) [C1].

It has been recently pointed out that the radial instrument compliance of single-head (stress-controlled) rheometers is frequency-dependent [C2]. However, the author wants to emphasize that the used Malvern Kinexus Pro rheometer is known to have relatively low motor inertia (13 μN m s^2 [C3]) and that no oscillation frequencies higher than 10 Hz were used in the rheological experiments of this study. For these reasons, the frequency dependence of the instrument compliance could be neglected in this study (see also Ref. [C2]).

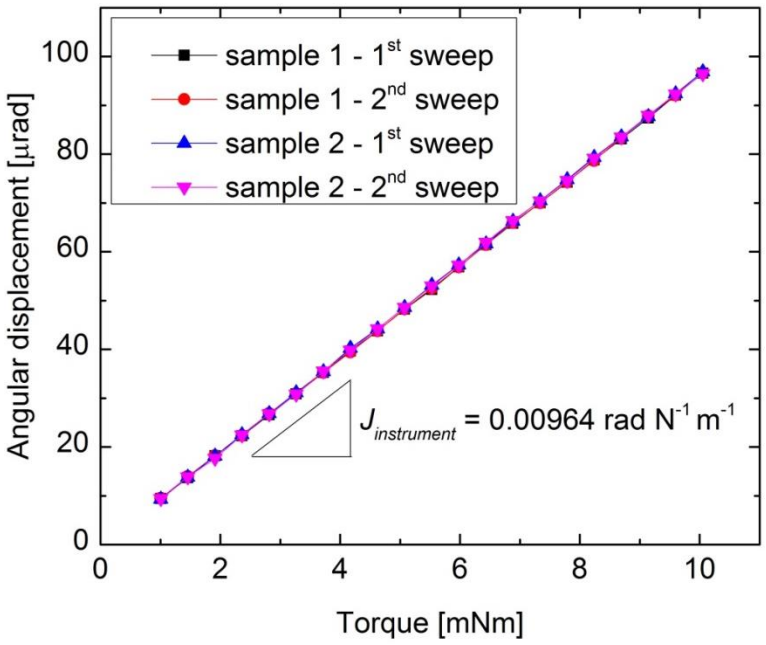

Figure C1. The determination of the radial instrument compliance from the stress sweep test results performed on two different super glue samples.

The instrument compliance effects have been traditionally considered to be significant when $G^* > 10$ MPa [C4]. Here the dependence of the error in G^* on the magnitude of G^* is studied. It appears that the absolute error in G^* value is quadratically dependent on the magnitude of G^* as can be seen from Figure C2a. Further, it follows that the relative error in G^* value is linearly dependent on the magnitude of G^*, see Figure C2b.

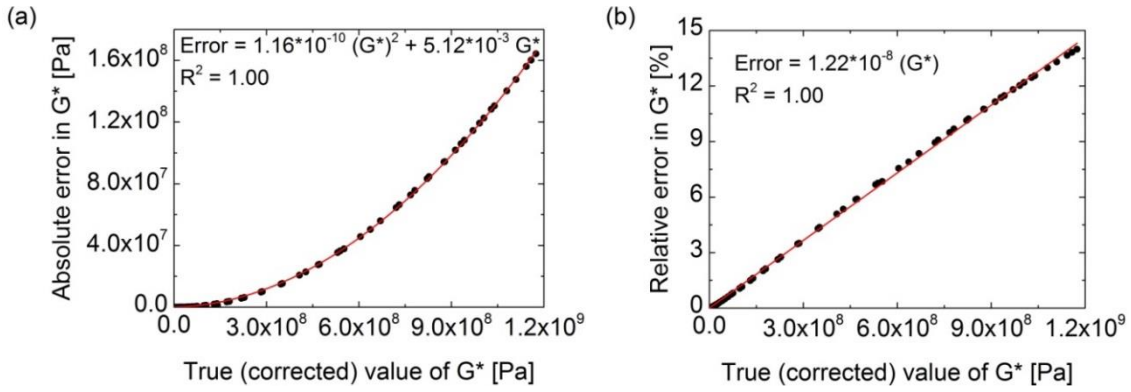

Figure C2. Dependence of (a) absolute and (b) relative error in G^* on the magnitude of G^*.

The influence of the instrument compliance correction on the rheological test results of bitumen B-18 at three selected temperatures (0 °C, -20 °C and -40 °C) is illustrated in Figure C3. It can be observed that the effect of compliance correction is most pronounced in the values of G''; this is because the compliance correction increases the value of this parameter by increasing both G^* and δ values (note that $G'' = G^* \sin \delta$). In addition, it is observed that the effects of the compliance correction are noticeable only when $G^* > 100$ MPa. However, it should be remembered that this threshold value is a function of the compliance of the rheometer system (in this case $J_{instrument} = 0.00964$ rad N^{-1} m^{-1}) so that it is the lower, the higher is the instrument compliance. Therefore, instrument compliance effects may be observable even when 100 MPa > G^* > 10 MPa if a more compliant rheometer system is used. Further, instrument compliance effects are evident in the vGP plot as can be seen from Figure C4. Importantly, the estimated value of G_g is significantly influenced by the instrument compliance: in this particular case G_g value changed from 1.07 GPa to 1.23 GPa when the measurement data were corrected for the instrument compliance.

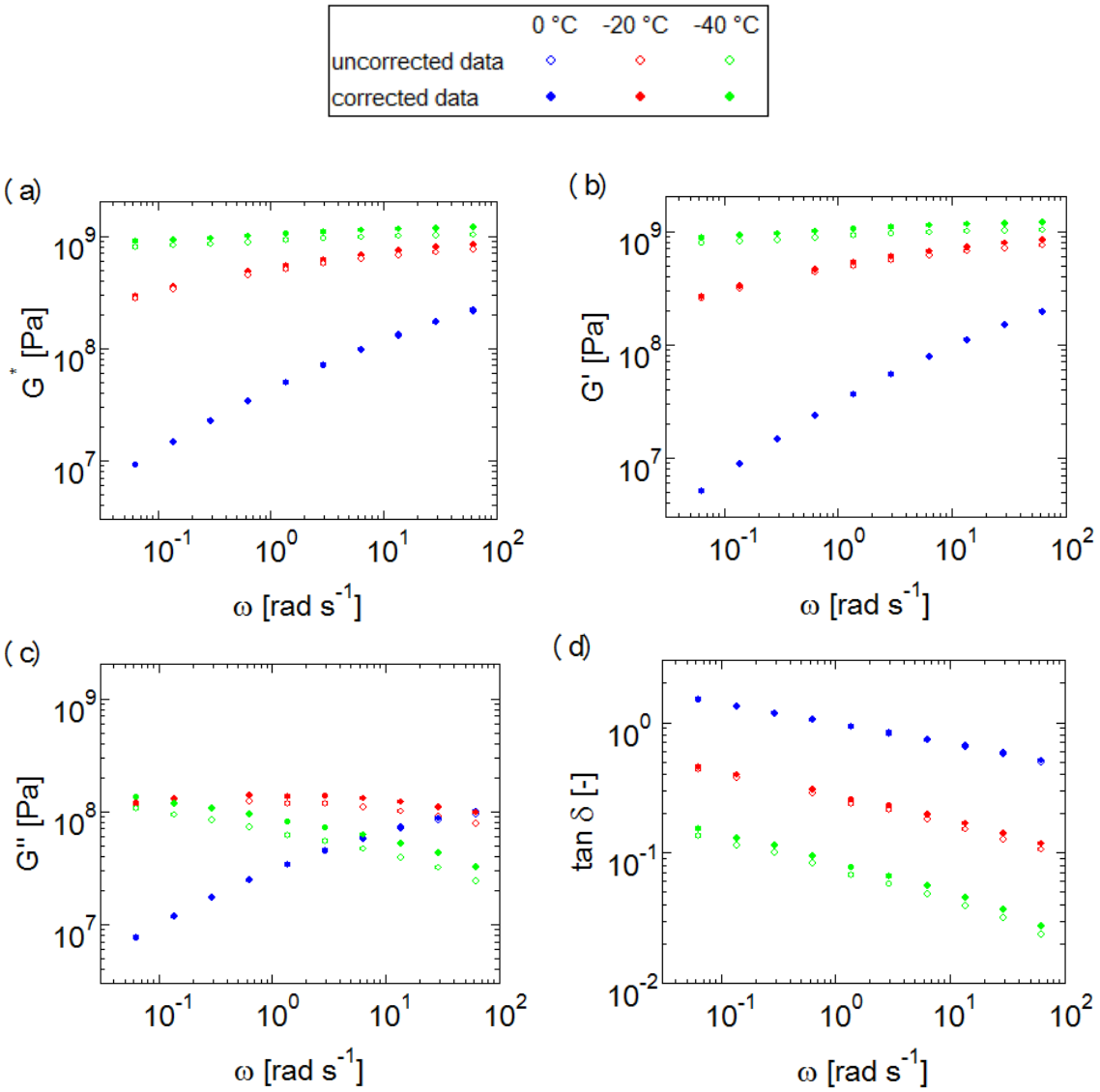

Figure C3. The effect of instrument compliance correction on (a) *G**, (b) *G'*, (c) *G''* and (d) tan δ at three selected temperatures. The open and solid symbols represent the data without and with compliance correction, respectively. Note that at 0 °C the uncorrected and corrected data completely overlap.

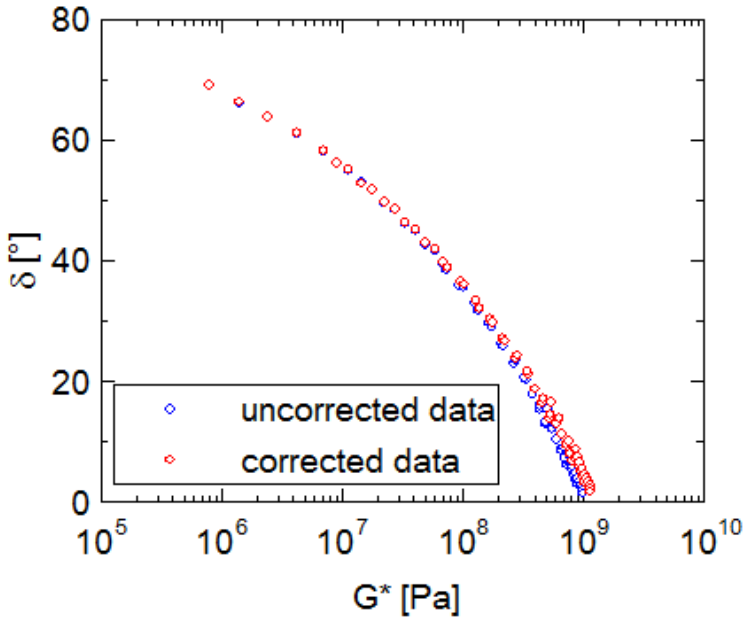

Figure C4. The effect of the instrument compliance correction on the data presented in the vGP plot.

Based on the repeatability of the instrument compliance measurement in this study and on the consistency between the instrument compliance values measured in this study and elsewhere for the commercially available 4-mm parallel plate fixture of Malvern Kinexus rheometers, the error in the measured instrument compliance value is expected to be not more than ±3 %. To illustrate the effect of this uncertainty on the calculated rheological test results, the compliance-corrected values of different rheological parameters were calculated using instrument compliance values that were 3 % higher and lower than the measured value. The uncorrected and corrected values of G^* measured at -40 °C are shown in Figure C5 with error bars corresponding to ±3 % error in the instrument compliance value. It can be seen that small errors in the measured instrument compliance value do not result in significant errors in the compliance-corrected G^* data; the relative errors in G^* are less than 0.5 % for the data set shown in Figure C5. This error is much smaller than the experimental error due to variations in the specimen preparation (see Appendix E).

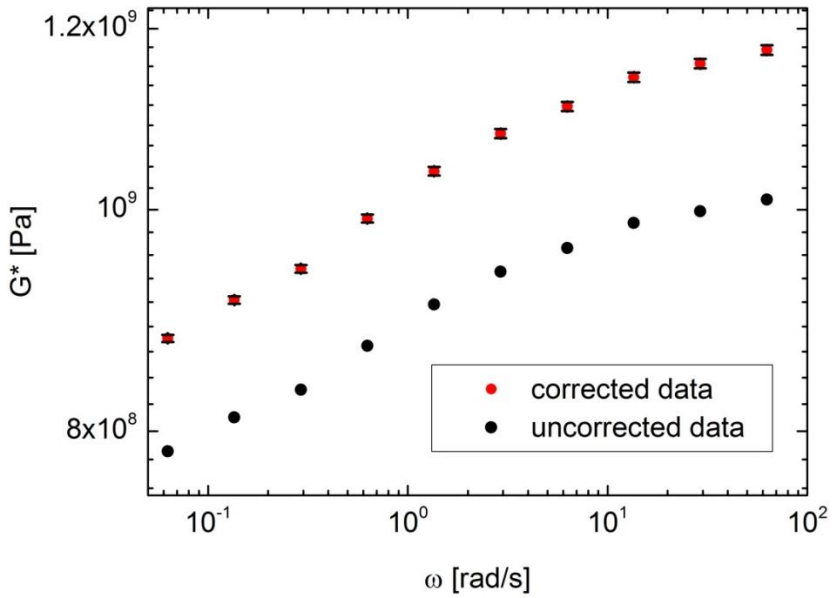

Figure C5. The uncorrected and corrected values of *G** measured at -40 °C with error bars corresponding to ±3 % error in the instrument compliance value.

References

[C1] Cookman AO. Personal communication. August 22, 2014.

[C2] Farrar M, Sui C, Salmans S, & Qin Q. 2014. Determining the Low Temperature Rheological Properties of Asphalt Binder Using a Dynamic Shear Rheometer (DSR). Topical report FP 08 prepared by Western Research Institute for the Federal Highway Administration, Contract DTFH61-07-D-00005, Fundamental Properties of Asphalts and Modified Asphalts, III.

[C3] Malvern Instruments Ltd. Kinexus range - Next generation rheometer redefines ease of us; http://www.malvern.com/en/products/product-range/kinexus-range/default.aspx; Accessed March 13, 2015.

[C4] Anderson DA, Christensen DW, Bahia HU, Dongre R, Sharma M, Antle CE et al. 1994. Binder characterization and evaluation, volume 3: Physical characterization. Report No.SHRP-A-369; National Research Council; Washington, DC.

Appendix D. Determination of the thermal expansion of the 4-mm parallel plate fixture

The thermal expansion of the 4-mm parallel plate fixture was determined according to the Appendix A3 of the AASHTO standard draft "Standard Method of Test for Determining the Low Temperature Rheological Properties of Asphalt Binder Using a Dynamic Shear Rheometer (DSR)". In this study, however, the thermal expansion was determined over a wider temperature range of 30 K (from 40 °C to 10 °C) to provide more accurate estimation of the gap correction factor. The measurement was performed multiple times, and an average gap change of 19.7 μm was obtained. This yields a gap correction factor of 0.66 μm K^{-1} that is really close to the default value determined by the rheometer manufacturer (0.64 μm K^{-1}).

Appendix E. Repeatability analysis of the 4-mm DSR testing technique

Prior to starting the actual experiments on the research samples, the repeatability of the 4-mm DSR test results was established. The main scope of this analysis was to ensure that consistent test results could be obtained by using the specimen preparation and measurement protocols described in Appendix B. A more extensive repeatability and reproducibility analysis for the 4-mm DSR measurement technique will be performed in the forthcoming round robin study organized by the Federal Highway Administration (FHWA) Asphalt Binder Expert Task Group (ETG).

Figure E1 shows results from three replicate frequency sweep measurements on bitumen B-18 in the temperature range of 10 °C to -40 °C. Different colors are used to indicate different replicates. It can be concluded that the test repeatability is relatively good regarding the very small diameter of the test geometry. Based on this limited analysis, the relative standard deviation of the repeatability of G^* values is expected to be not more than 5 %. This implies that the measured values of G^* are expected to be within ±7 % of the true values at a confidence level of 95 %, i.e. d2s value is estimated to be 14 %. In the case of tan δ values, the repeatability appears to be even better than this. This may be due to the fact that G^* values are influenced by errors in specimen dimensions (i.e. in specimen trimming in this case), while tan δ values are not affected by the dimensional errors [E1]. Finally, it should be noted that experimental errors appear to be largest at the highest measurement temperature of 10 °C. In general, however, the 4-mm parallel plate geometry is used only at temperatures at and below 0 °C, whereas the 8-mm parallel plate fixture is typically used at 10 °C and above.

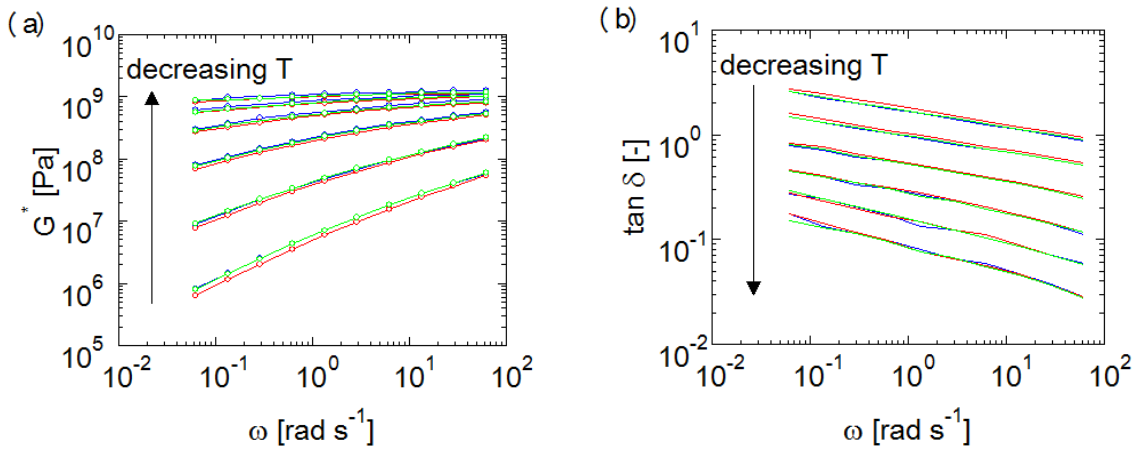

Figure E1. Repeatability of (a) G^* and (b) tan δ values measured with the 4-mm parallel plate geometry in the temperature range of 10 °C to -40 °C. Three replicate measurements are shown in different colors.

References

[E1] Rowe G, & Anderson D. 2013. Lecture 8: Sources of Error in Rheological Testing. Rheobit workshop organized by Asphalt Institute; 12.-14. June 2013; Stockholm, Sweden. pp. 37.

Appendix F. Consistency analysis of the interlaboratory rheological data measured with 4-mm and 8-mm parallel plate geometries

Two different rheometers located at two different laboratories were used to measure rheological properties of the investigated bitumens at different temperature ranges: a Malvern Kinexus Pro rheometer equipped with 4-mm parallel plate geometry was used to characterize low-temperature rheological properties, while intermediate- and high-temperature rheological data were obtained using a Paar Physica MCR 500 rheometer with 8-mm and 25-mm parallel plate geometries. In some of the analyses presented in this thesis the data measured with the two rheometers were combined to extend the experimental temperature range. For this reason, it was important to establish the consistency of the interlaboratory rheological data. Figure F1 shows a comparison between G^* data obtained with 4-mm and 8-mm parallel plate geometries was made at 0 °C and 1 Hz. This temperature-frequency combination was selected since the stiffness of all the investigated bitumens were expected to be in the measurable range of both 4-mm and 8-mm parallel plate geometries at these measurement conditions. It is observed that G^* values are systematically higher when measured with 4-mm parallel plates rather than with 8-mm parallel plates. However, the deviation is not great; in no case is the relative difference larger than 32 %. Considering the fact that the two data sets were collected by two different operators with two different rheometers at two different laboratories and using slightly different specimen preparation techniques, the consistency of the interlaboratory rheological data can be considered to be excellent. Consequently, the data measured with the two different rheometers can be combined and analyzed without any instrument corrections.

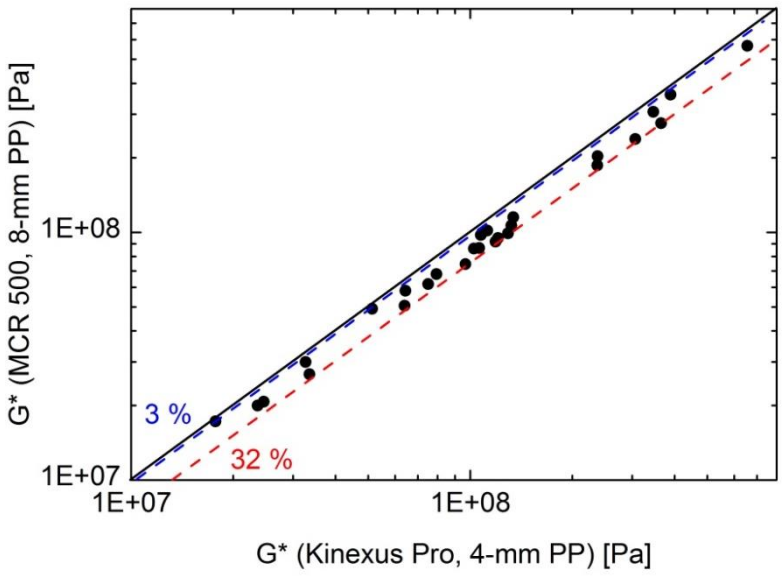

Figure F1. Consistency of G^* data measured at 0 °C and 1 Hz with 4-mm and 8-mm parallel plate geometries.

Appendix G. Processing of DSC data: Determination of $T_{g,onset}$, $T_{g,mid}$, $T_{g,end}$, ΔC_p and melting enthalpy

The glass transition related temperatures $T_{g,onset}$, $T_{g,mid}$ and $T_{g,end}$ were determined from the DSC heating scan using the so-called mid-point method (see the green box in Figure G1). First, baselines (tangents) of the heat flow curve above and below the glass transition region are drawn. Note that above T_g the baseline is taken above the melting range of bitumen wax, i.e. from the right side of the blue-shaded area in Figure G1. The shift in the baseline of the heat flow curve at the glass transition is determined. Further, when the shift in the heat flow baseline is normalized with respect to sample weight and heating rate, Equation G1, the heat capacity change ΔC_p at T_g is obtained.

$$\Delta C_p = \frac{\text{shift in heat flow baseline}}{\text{sample weight}} \frac{\mathrm{d}t}{\mathrm{d}T} \tag{G1}$$

where $\mathrm{d}t/\mathrm{d}T$ = the inverse of the heating rate [s/K]

The temperature at which the heat capacity change is half the total heat capacity change ΔC_p of the glass transition is the mid-point glass transition temperature $T_{g,mid}$. Finally, a tangent is drawn to the heat flow curve at $T_{g,mid}$. The onset temperature of the glass transition, $T_{g,onset}$, is defined as the temperature at which the baseline below the glass transition intersects the tangent drawn at $T_{g,mid}$. The endset temperature of the glass transition, $T_{g,end}$, is similarly defined using the tangent above the glass transition region. Note that in this study $T_{g,mid}$ is used as the definition of the glass transition temperature T_g.

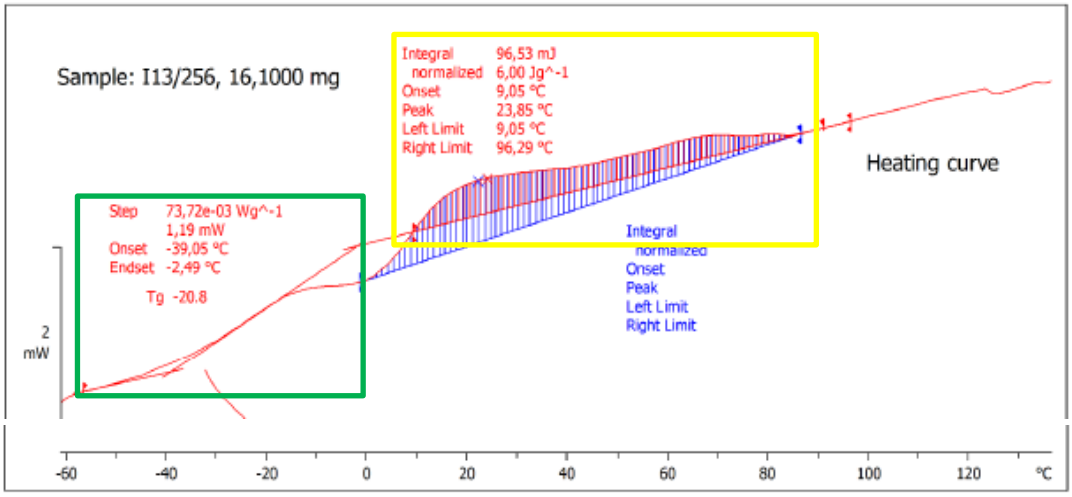

Figure G1. Total heat flow curves of bitumen B-12 illustrating the determination of the glass transition related parameters $T_{g,onset}$, $T_{g,mid}$, $T_{g,end}$ and ΔC_p (see the green box), and the melting enthalpy of the crystalline fraction of bitumen (see the yellow box).

Also the melting enthalpy of the crystalline fraction of bitumen (bitumen wax) is determined from the DSC heating scan, see the yellow box in Figure G1. Put simply, the melt baseline is extrapolated to lower temperatures until it intersects the heat flow curve, and the melting enthalpy is then defined as the area between the heat flow curve and extrapolated melt baseline.

Cold crystallization of bitumen waxes was observed in most of the investigated bitumens, see Table 4. The cold crystallization was detected as an exothermic event in the heating curve directly in or at the end of the glass transition. According to Masson et al. [G1], in this process the small and imperfect crystals that formed upon cooling melt and recrystallize to larger crystals with higher melting points.

References

[G1] Masson J, Polomark G, & Collins P. 2002. Time-dependent microstructure of bitumen and its fractions by modulated differential scanning calorimetry. Energy & Fuels; Vol. 16; pp. 470-476.

Appendix H. Calibration of GPC with narrow polystyrene standards

The GPC used in this study was calibrated with narrow polystyrene standards. The calibration curve is shown in Figure H1.

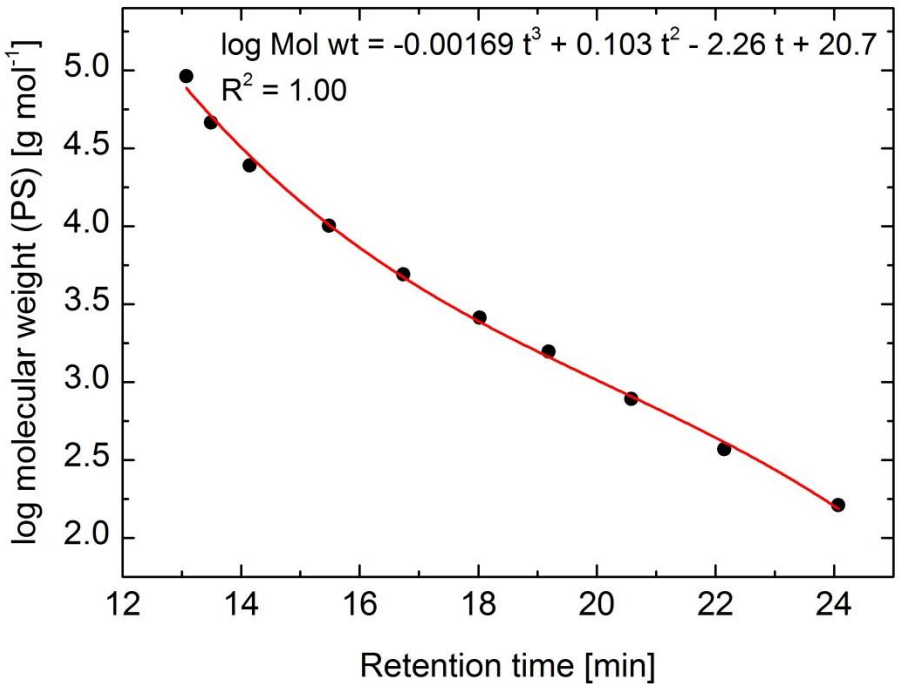

Figure H1. GPC calibration curve using narrow polystyrene standards.

Appendix I. Processing of GPC data: Calculation of M_w, M_n, M_z, M_{z+1} and M_w/M_n parameters, and division of GPC profiles into SMS, MMS and LMS fractions

The molecular weight characteristics of polymeric materials are often expressed in terms of different molecular weight parameters. The definitions of these molecular weight averages are given in the following:

Number-average molecular weight:

$$M_n = \frac{\sum N_i M_i}{\sum N_i} \tag{I1}$$

Weight-average molecular weight:

$$M_w = \frac{\sum N_i M_i^2}{\sum N_i M_i} \tag{I2}$$

Z-average molecular weight:

$$M_z = \frac{\sum N_i M_i^3}{\sum N_i M_i^2} \tag{I3}$$

Z+1-average molecular weight:

$$M_{z+1} = \frac{\sum N_i M_i^4}{\sum N_i M_i^3} \tag{I4}$$

where N_i is the number of molecules whose weight is M_i. It is easy to see that M_n, M_w, M_z and M_{z+1} are the first, second, third and fourth moments of average molar weight,

respectively. If the material is not perfectly monodisperse (that is typically the case), the following holds: $M_n < M_w < M_z < M_{z+1}$. Further, it is well known that M_n parameter is sensitive to low molecular weight molecules, while higher molecular weight components have a more pronounced effect on the values of M_w, and especially on those of M_z and M_{z+1}. The polydispersity, which is a measure of the breadth of the polymer molecular weight distribution, is defined as the ratio of the weight- and number-average molecular weights, M_w/M_n.

Moreover, the molecular weight distributions of the investigated bitumens were characterized by calculating the relative amounts of the small molecular size (SMS), medium molecular size (MMS) and large molecular size (LMS) species in bitumen. The division into these fractions was made by dividing the area below the chromatogram into three sections as shown in Figure I1. Consequently, SMS fraction represents the portion of species that have an apparent molecular weight of less than 5410 g mol^{-1} (elution time of more than 16.5 min), MMS fraction corresponds to apparent molecular weights between 5410 g mol^{-1} (elution time of 16.5 min) and 21200 g mol^{-1} (elution time of 14.5 min), and LMS fraction corresponds to apparent molecular weights greater than 21200 g mol^{-1} (elution time of less than 14.5 min).

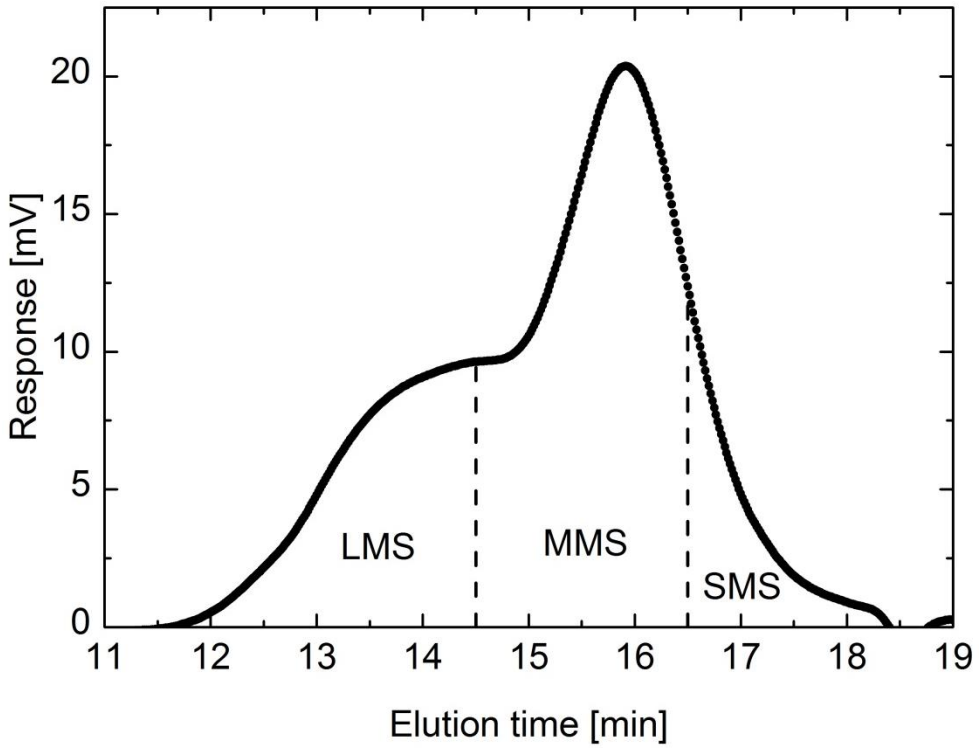

Figure I1. Illustration of the division of a GPC profile into SMS, MMS and LMS fractions.

Appendix J. Determination of the C=C peak area from the FT-IR data

The main parameter used in this paper was the absorption at 1600 cm^{-1}, which is related to the stretching vibration of C=C bonds. In bitumen, this region can be attributed to carbon-carbon stretching vibrations in the aromatic ring, since bitumen is known not to contain isolated double bonds [J1]. In this study, the area at 1600 cm^{-1} was integrated using a fixed wavenumber limit of 1637–1638 cm^{-1} up to the minimum after the signal. The fixed limit was used to reduce interference from C=O signals at 1700 cm^{-1}, which may become large after aging. An example of this integration is illustrated in Figure J1. A repeatability check using 6 repeats resulted in a standard deviation for area at 1600 cm^{-1} of 0.05.

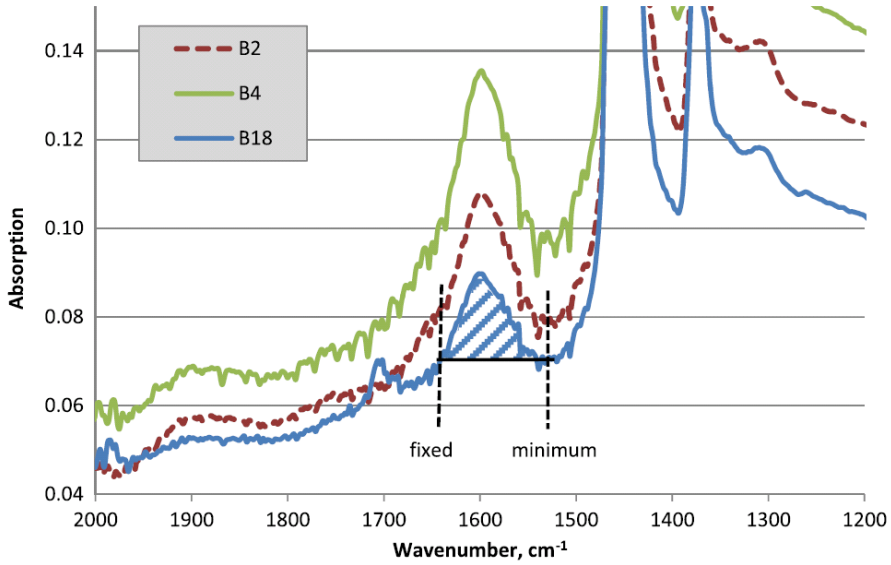

Figure J1. Example of the determination of the C=C peak area from the FT-IR spectrum [J2].

References

[J1] Lamontagne J, Dumas P, Mouillet V, & Kister J. 2001. Comparison by Fourier transform infrared (FTIR) spectroscopy of different ageing techniques: application to road bitumens. Fuel; Vol. 80; pp. 483-488.

[J2] Soenen H, & Redelius P. 2014. The effect of aromatic interactions on the elasticity of bituminous binders. Rheologica Acta; Vol. 53; pp. 741-754.

Appendix K. Analytical solutions of m and E_g with respect to the Kaelble-WLF parameters

The Kaelble-WLF equation is as follows:

$$\log a_T = -c_1\left(\frac{T - T_d}{c_2 + |T - T_d|} - \frac{T_r - T_d}{c_2 + |T_r - T_d|}\right) \tag{K1}$$

It is noted that the second term inside the parenthesis of Equation K1 does not contain T as a variable. Here it is also pointed out that the calculation of m is essentially a derivation of the shift factor function with respect to the function T_g/T. As T_g/T contains only T as a variable, the second term inside the parenthesis of Equation K1 equals zero when differentiated with respect to this function. Hence, this part of the Kaelble-WLF equation can be omitted when deriving the analytical solution of m with respect to the Kaelble-WLF parameters, and in this particular case Equation K1 reduces to:

$$\log a_T = \frac{-c_1(T - T_d)}{c_2 + |T - T_d|} \tag{K2}$$

When $T \leq T_d$, Equation K2 can be written in the following form:

$$\log a_T = \frac{-c_1(T - T_d)}{c_2 - T + T_d} = \frac{-c_1 T_g\left(\frac{T}{T_g}\right) + c_1 T_d}{c_2 - T_g\left(\frac{T}{T_g}\right) + T_d} \tag{K3}$$

By substituting

$$u = \frac{T_g}{T} \Leftrightarrow u^{-1} = \frac{T}{T_g} \tag{K4}$$

into Equation K3, Equation K5 is obtained:

$$\log a_T = \frac{-c_1 T_g u^{-1} + c_1 T_d}{c_2 - T_g u^{-1} + T_d} \tag{K5}$$

Now the definition of dynamic fragility

$$m = \left[\frac{d \log x}{d\left(\frac{T_g}{T}\right)}\right]_{T=T_g} \tag{K6}$$

where x is selected to be horizontal shift factor a_T, can be expressed in the following form:

$$m = \left[\frac{d \log a_T}{du}\right]_{T=T_g} = \left[\frac{d\left(\frac{-c_1 T_g u^{-1} + c_1 T_d}{c_2 - T_g u^{-1} + T_d}\right)}{du}\right]_{T=T_g}$$
$$= \left[\frac{\left(c_1 T_g u^{-2}\right)\left(c_2 - T_g u^{-1} + T_d\right) - \left(-c_1 T_g u^{-1} + c_1 T_d\right)\left(T_g u^{-2}\right)}{\left(c_2 - T_g u^{-1} + T_d\right)^2}\right]_{T=T_g} \tag{K7}$$

Further, after simplification, the equation for dynamic fragility acquires the following form:

$$m = \left[\frac{c_1 c_2 T_g u^{-2}}{\left(c_2 - T_g u^{-1} + T_d\right)^2}\right]_{T=T_g} \tag{K8}$$

After backsubstitution

$$u^{-1} = \frac{T}{T_g} \tag{K9}$$

is performed and the resulting equation simplified, dynamic fragility can be expressed as follows:

$$m = \left[\frac{c_1 c_2 \frac{T^2}{T_g}}{(c_2 - T + T_d)^2} \right]_{T=T_g} \tag{K10}$$

When considering that the dynamic fragility is determined at $T = T_g$, the final solution is obtained:

$$m = \frac{c_1^g c_2^g T_g}{(c_2^g - T_g + T_d)^2} \tag{K11}$$

In the above equation the superscript "g" denotes the fact that the equation is evaluated at $T = T_g$. It should be remembered that in the above solution $T_g \leq T_d$ is assumed.

Correspondingly, when $T \geq T_d$, Equation K2 can be written as follows:

$$\log a_T = \frac{-c_1(T - T_d)}{c_2 + T - T_d} \tag{K12}$$

In this case the derivation of m follows the same steps outlined in Equations K3-K10, only some sign changes are required. Finally, an equation equivalent to Equation K11 is obtained:

$$m = \frac{c_1^g c_2^g T_g}{(c_2^g + T_g - T_d)^2} \tag{K13}$$

Finally, considering the boundary conditions of the above analyses, it is noticed that Equations K11 and K13 can be combined as follows:

$$m = \frac{c_1^g c_2^g T_g}{\left(c_2^g + |T_d - T_g|\right)^2} \tag{K14}$$

Consequently, Equation K14 is valid in all conditions, i.e. both when $T_g \leq T_d$ and when $T_g > T_d$.

Also the apparent activation energy E_g at T_g could be solved analytically with respect to the Kaelble-WLF parameters by the derivation of shift factor equation. However, it is much more straightforward to derive the solution by making use of the well-known relationship between E_g and m:

$$E_g = ln\,10\,RT_g m \tag{K15}$$

By substituting Equation K14 into Equation K15, the analytical solution of the apparent activation energy at T_g with respect to the Kaelble-WLF parameters is obtained:

$$E_g = \frac{ln(10) c_1^g c_2^g R T_g^2}{\left(c_2^g + |T_d - T_g|\right)^2} \tag{K16}$$

Appendix L. Data of the 4-mm DSR measurements

This appendix presents the frequency sweep data collected at low temperatures using the 4-mm parallel plate fixture. The data both with (bolded text) and without (unbolded text) radial instrument compliance correction ($J_{instrument}$ = 0.00964 rad N^{-1} m^{-1}) is shown. The stiffest bitumen samples (Pen ≤ 15) were observed to slip on the rheometer plates during the frequency sweeps at the lowest measurement temperatures; this data is not shown. Note that bad data points have been cleaned from the compliance corrected data sets.

B-1								
T	*f*	*G**	*δ*		***T***	***f***	***G****	***δ***
[°C]	[Hz]	[Pa]	[°]		**[°C]**	**[Hz]**	**[Pa]**	**[°]**
10	10	2.546E+08	17.69		**10**	**10**	**2.635E+08**	**18.33**
10	4.641	2.185E+08	18.77		**10**	**4.641**	**2.250E+08**	**19.35**
10	2.154	1.852E+08	19.99		**10**	**2.154**	**1.897E+08**	**20.51**
10	1	1.550E+08	21.13		**10**	**1**	**1.582E+08**	**21.58**
10	0.4641	1.295E+08	22.27		**10**	**0.4641**	**1.316E+08**	**22.66**
10	0.2154	1.066E+08	23.35		**10**	**0.2154**	**1.080E+08**	**23.69**
10	0.1	8.708E+07	24.50		**10**	**0.1**	**8.805E+07**	**24.79**
10	0.04641	7.071E+07	25.74		**10**	**0.04641**	**7.134E+07**	**25.99**
10	0.02154	5.650E+07	27.10		**10**	**0.02154**	**5.690E+07**	**27.31**
10	0.01	4.466E+07	28.37		**10**	**0.01**	**4.491E+07**	**28.54**
0	10	4.639E+08	11.67		**0**	**10**	**4.950E+08**	**12.47**
0	4.641	4.199E+08	12.79		**0**	**4.641**	**4.451E+08**	**13.57**
0	2.154	3.754E+08	14.04		**0**	**2.154**	**3.953E+08**	**14.80**
0	1	3.311E+08	15.24		**0**	**1**	**3.464E+08**	**15.96**
0	0.4641	2.901E+08	16.46		**0**	**0.4641**	**3.017E+08**	**17.14**
0	0.2154	2.510E+08	17.63		**0**	**0.2154**	**2.596E+08**	**18.26**
0	0.1	2.145E+08	18.87		**0**	**0.1**	**2.207E+08**	**19.44**
0	0.04641	1.830E+08	20.00		**0**	**0.04641**	**1.875E+08**	**20.50**
0	0.02154	1.534E+08	21.19		**0**	**0.02154**	**1.565E+08**	**21.64**
0	0.01	1.272E+08	22.64		**0**	**0.01**	**1.293E+08**	**23.04**
-10	10	7.287E+08	5.98		**-10**	**10**	**8.099E+08**	**6.65**
-10	4.641	6.915E+08	6.98		**-10**	**4.641**	**7.641E+08**	**7.72**
-10	2.154	6.493E+08	7.98		**-10**	**2.154**	**7.127E+08**	**8.77**
-10	1	5.998E+08	9.00		**-10**	**1**	**6.533E+08**	**9.81**
-10	0.4641	5.612E+08	10.09		**-10**	**0.4641**	**6.076E+08**	**10.94**
-10	0.2154	5.080E+08	11.35		**-10**	**0.2154**	**5.456E+08**	**12.20**
-10	0.1	4.594E+08	12.14		**-10**	**0.1**	**4.898E+08**	**12.96**
-10	0.04641	4.148E+08	13.49		**-10**	**0.04641**	**4.393E+08**	**14.31**
-10	0.02154	3.631E+08	16.20		**-10**	**0.01**	**3.389E+08**	**16.96**
-10	0.01	3.243E+08	16.21		**-20**	**10**	**1.035E+09**	**3.53**
-20	10	9.054E+08	3.09		**-20**	**4.641**	**1.005E+09**	**4.21**
-20	4.641	8.822E+08	3.70		**-20**	**2.154**	**9.593E+08**	**4.85**
-20	2.154	8.472E+08	4.28		**-20**	**1**	**9.234E+08**	**5.67**
-20	1	8.192E+08	5.03		**-20**	**0.4641**	**8.804E+08**	**6.54**
-20	0.4641	7.853E+08	5.83		**-20**	**0.2155**	**8.330E+08**	**6.98**
-20	0.2155	7.474E+08	6.26		**-20**	**0.1**	**7.792E+08**	**8.29**
-20	0.1	7.040E+08	7.48		**-20**	**0.04642**	**7.171E+08**	**9.53**
-20	0.04642	6.531E+08	8.67		**-20**	**0.02154**	**6.762E+08**	**10.07**
-20	0.02154	6.191E+08	9.21		**-20**	**0.01**	**6.142E+08**	**11.87**
-20	0.01	5.669E+08	10.94		**-30**	**10**	**1.185E+09**	**1.75**
-30	10	1.018E+09	1.51		**-30**	**4.641**	**1.164E+09**	**2.36**
-30	4.641	1.003E+09	2.03		**-30**	**2.154**	**1.128E+09**	**2.82**
-30	2.154	9.758E+08	2.44		**-30**	**1**	**1.106E+09**	**3.33**
-30	1	9.596E+08	2.88		**-30**	**0.4641**	**1.080E+09**	**3.91**
-30	0.4641	9.399E+08	3.40		**-30**	**0.1**	**1.002E+09**	**5.20**
-30	0.2155	9.012E+08	2.46		**-30**	**0.02154**	**9.347E+08**	**7.10**
-30	0.1	8.802E+08	4.57		**-30**	**0.01**	**8.560E+08**	**7.74**
-30	0.04642	8.482E+08	7.06					
-30	0.02154	8.283E+08	6.29					
-30	0.01	7.660E+08	6.92					

B-2								
T	*f*	*G**	*δ*		***T***	***f***	***G****	***δ***
[°C]	[Hz]	[Pa]	[°]		**[°C]**	**[Hz]**	**[Pa]**	**[°]**
10	10	4.779E+08	10.37		**10**	**10**	**5.111E+08**	**11.10**
10	4.641	4.341E+08	11.81		**10**	**4.641**	**4.612E+08**	**12.56**
10	2.154	3.912E+08	13.50		**10**	**2.154**	**4.129E+08**	**14.26**
10	1	3.477E+08	15.29		**10**	**1**	**3.646E+08**	**16.05**
10	0.4641	3.035E+08	17.36		**10**	**0.4641**	**3.162E+08**	**18.11**
10	0.2154	2.608E+08	19.54		**10**	**0.2154**	**2.700E+08**	**20.26**
10	0.1	2.192E+08	22.10		**10**	**0.1**	**2.255E+08**	**22.77**
10	0.04641	1.816E+08	24.90		**10**	**0.04641**	**1.858E+08**	**25.52**
10	0.02154	1.465E+08	27.80		**10**	**0.02154**	**1.492E+08**	**28.36**
10	0.01	1.134E+08	31.43		**10**	**0.01**	**1.149E+08**	**31.91**
0	10	6.952E+08	4.71		**0**	**10**	**7.690E+08**	**5.21**
0	4.641	6.660E+08	5.61		**0**	**4.641**	**7.332E+08**	**6.18**
0	2.154	6.343E+08	6.54		**0**	**2.154**	**6.949E+08**	**7.16**
0	1	6.024E+08	7.52		**0**	**1**	**6.566E+08**	**8.20**
0	0.4641	5.616E+08	8.64		**0**	**0.4641**	**6.083E+08**	**9.37**
0	0.2154	5.223E+08	8.44		**0**	**0.1**	**5.089E+08**	**12.02**
0	0.1	4.760E+08	11.23		**0**	**0.04641**	**4.579E+08**	**13.25**
0	0.04641	4.313E+08	12.46		**0**	**0.01**	**3.545E+08**	**17.94**
0	0.02154	3.788E+08	16.00		**-10**	**4.641**	**1.000E+09**	**2.73**
0	0.01	3.387E+08	17.11		**-10**	**2.154**	**9.566E+08**	**3.20**
-10	10	8.922E+08	1.73		**-10**	**1**	**9.310E+08**	**3.73**
-10	4.641	8.785E+08	2.39		**-10**	**0.4641**	**9.213E+08**	**4.32**
-10	2.154	8.448E+08	2.83		**-10**	**0.2154**	**8.796E+08**	**5.11**
-10	1	8.249E+08	3.30		**-10**	**0.1**	**8.380E+08**	**5.76**
-10	0.4641	8.173E+08	3.83		**-10**	**0.04641**	**8.063E+08**	**7.23**
-10	0.2154	7.844E+08	4.56		**-10**	**0.01**	**6.972E+08**	**8.93**
-10	0.1	7.512E+08	5.16		**-20**	**4.641**	**1.127E+09**	**1.50**
-10	0.04641	7.259E+08	6.51		**-20**	**2.154**	**1.105E+09**	**1.72**
-10	0.02154	6.393E+08	11.77		**-20**	**1**	**1.083E+09**	**2.03**
-10	0.01	6.364E+08	8.14		**-20**	**0.4641**	**1.077E+09**	**2.39**
-20	10	9.802E+08	0.81		**-20**	**0.2155**	**1.054E+09**	**3.06**
-20	4.641	9.747E+08	1.30		**-20**	**0.1**	**1.034E+09**	**3.48**
-20	2.154	9.586E+08	1.49		**-20**	**0.02154**	**9.859E+08**	**4.12**
-20	1	9.420E+08	1.77		**-20**	**0.01**	**9.335E+08**	**4.79**
-20	0.4641	9.371E+08	2.08					
-20	0.2155	9.199E+08	2.67					
-20	0.1	9.044E+08	3.05					
-20	0.04642	8.843E+08	4.19					
-20	0.02154	8.677E+08	3.62					
-20	0.01	8.270E+08	4.24					

B-3								
T	*f*	*G**	*δ*		***T***	***f***	***G****	***δ***
[°C]	[Hz]	[Pa]	[°]		**[°C]**	**[Hz]**	**[Pa]**	**[°]**
10	10	2.662E+08	18.25		**10**	**10**	**2.758E+08**	**18.93**
10	4.641	2.264E+08	20.64		**10**	**4.641**	**2.333E+08**	**21.29**
10	2.154	1.889E+08	23.35		**10**	**2.154**	**1.935E+08**	**23.95**
10	1	1.538E+08	26.18		**10**	**1**	**1.568E+08**	**26.73**
10	0.4641	1.212E+08	29.33		**10**	**0.4641**	**1.230E+08**	**29.80**
10	0.2154	9.373E+07	32.62		**10**	**0.2154**	**9.476E+07**	**33.03**
10	0.1	7.047E+07	36.15		**10**	**0.1**	**7.103E+07**	**36.48**
10	0.04641	5.151E+07	39.96		**10**	**0.04641**	**5.179E+07**	**40.22**
10	0.02154	3.601E+07	44.17		**10**	**0.02154**	**3.614E+07**	**44.37**
10	0.01	2.433E+07	48.43		**10**	**0.01**	**2.438E+07**	**48.58**
0	10	4.877E+08	9.05		**0**	**10**	**5.225E+08**	**9.70**
0	4.641	4.500E+08	10.40		**0**	**4.641**	**4.793E+08**	**11.09**
0	2.154	4.114E+08	12.05		**0**	**2.154**	**4.356E+08**	**12.77**
0	1	3.704E+08	13.87		**0**	**1**	**3.898E+08**	**14.61**
0	0.4641	3.264E+08	15.80		**0**	**0.4641**	**3.412E+08**	**16.53**
0	0.2154	2.843E+08	17.85		**0**	**0.2154**	**2.953E+08**	**18.57**
0	0.1	2.425E+08	20.32		**0**	**0.1**	**2.503E+08**	**21.01**
0	0.04641	2.033E+08	23.01		**0**	**0.04641**	**2.087E+08**	**23.66**
0	0.02154	1.658E+08	25.54		**0**	**0.02154**	**1.693E+08**	**26.12**
0	0.01	1.316E+08	29.30		**0**	**0.01**	**1.338E+08**	**29.82**
-10	10	7.297E+08	3.77		**-10**	**10**	**8.115E+08**	**4.19**
-10	4.641	7.103E+08	4.27		**-10**	**4.641**	**7.875E+08**	**4.73**
-10	2.154	6.692E+08	5.11		**-10**	**2.154**	**7.372E+08**	**5.63**
-10	1	6.408E+08	6.23		**-10**	**1**	**7.027E+08**	**6.83**
-10	0.4641	6.173E+08	6.93		**-10**	**0.4641**	**6.745E+08**	**7.57**
-10	0.2154	5.824E+08	7.99		**-10**	**0.2154**	**6.328E+08**	**8.69**
-10	0.1	5.417E+08	9.51		**-10**	**0.1**	**5.850E+08**	**10.27**
-10	0.04641	4.996E+08	11.37		**-10**	**0.04641**	**5.359E+08**	**12.21**
-10	0.02154	4.553E+08	16.13		**-10**	**0.01**	**4.320E+08**	**15.44**
-10	0.01	4.084E+08	14.58		**-20**	**10**	**9.672E+08**	**1.99**
-20	10	8.530E+08	1.75		**-20**	**4.641**	**9.524E+08**	**2.35**
-20	4.641	8.416E+08	2.07		**-20**	**2.154**	**9.233E+08**	**2.77**
-20	2.154	8.188E+08	2.46		**-20**	**1**	**9.036E+08**	**3.30**
-20	1	8.033E+08	2.93		**-20**	**0.4641**	**8.869E+08**	**3.78**
-20	0.4641	7.901E+08	3.37		**-20**	**0.2155**	**8.548E+08**	**4.61**
-20	0.2155	7.646E+08	4.12		**-20**	**0.1**	**8.266E+08**	**5.15**
-20	0.1	7.420E+08	4.62		**-20**	**0.04642**	**7.970E+08**	**6.03**
-20	0.04642	7.181E+08	5.43		**-20**	**0.01**	**7.014E+08**	**8.80**
-20	0.02154	6.915E+08	5.87		**-30**	**10**	**1.058E+09**	**1.06**
-20	0.01	6.400E+08	8.02		**-30**	**4.641**	**1.049E+09**	**1.34**
-30	10	9.230E+08	0.93		**-30**	**2.154**	**1.028E+09**	**1.59**
-30	4.641	9.163E+08	1.17		**-30**	**1**	**1.009E+09**	**1.91**
-30	2.154	9.001E+08	1.39		**-30**	**0.4641**	**1.005E+09**	**2.25**
-30	1	8.856E+08	1.67		**-30**	**0.2155**	**9.882E+08**	**2.77**
-30	0.4641	8.825E+08	1.97		**-30**	**0.02154**	**9.340E+08**	**4.27**
-30	0.2155	8.694E+08	2.43		**-30**	**0.01**	**8.844E+08**	**4.69**
-30	0.1	8.495E+08	2.56					
-30	0.04642	8.338E+08	2.31					
-30	0.02154	8.273E+08	3.78					
-30	0.01	7.882E+08	4.18					

B-4								
T	*f*	*G**	*δ*		***T***	***f***	***G****	***δ***
[°C]	[Hz]	[Pa]	[°]		**[°C]**	**[Hz]**	**[Pa]**	**[°]**
10	10	1.541E+08	21.94		**10**	**10**	**1.572E+08**	**22.41**
10	4.641	1.273E+08	24.06		**10**	**4.641**	**1.293E+08**	**24.48**
10	2.154	1.035E+08	25.95		**10**	**2.154**	**1.048E+08**	**26.32**
10	1	8.291E+07	27.91		**10**	**1**	**8.376E+07**	**28.22**
10	0.4641	6.528E+07	30.02		**10**	**0.4641**	**6.579E+07**	**30.28**
10	0.2154	5.072E+07	32.27		**10**	**0.2154**	**5.103E+07**	**32.48**
10	0.1	3.894E+07	34.63		**10**	**0.1**	**3.911E+07**	**34.81**
10	0.04641	2.922E+07	37.16		**10**	**0.04641**	**2.932E+07**	**37.30**
10	0.02154	2.146E+07	40.01		**10**	**0.02154**	**2.151E+07**	**40.12**
10	0.01	1.549E+07	43.06		**10**	**0.01**	**1.552E+07**	**43.15**
0	10	3.423E+08	13.68		**0**	**10**	**3.588E+08**	**14.35**
0	4.641	3.040E+08	15.30		**0**	**4.641**	**3.168E+08**	**15.96**
0	2.154	2.662E+08	16.80		**0**	**2.154**	**2.759E+08**	**17.44**
0	1	2.301E+08	18.46		**0**	**1**	**2.373E+08**	**19.06**
0	0.4641	1.954E+08	19.96		**0**	**0.4641**	**2.005E+08**	**20.50**
0	0.2154	1.643E+08	21.67		**0**	**0.2154**	**1.679E+08**	**22.16**
0	0.1	1.365E+08	23.47		**0**	**0.1**	**1.389E+08**	**23.91**
0	0.04641	1.118E+08	25.32		**0**	**0.04641**	**1.134E+08**	**25.70**
0	0.02154	8.951E+07	27.82		**0**	**0.02154**	**9.050E+07**	**28.15**
0	0.01	7.093E+07	30.14		**0**	**0.01**	**7.154E+07**	**30.43**
-10	10	6.168E+08	7.28		**-10**	**10**	**6.738E+08**	**7.96**
-10	4.641	5.785E+08	8.42		**-10**	**4.641**	**6.283E+08**	**9.15**
-10	2.154	5.386E+08	9.51		**-10**	**2.154**	**5.813E+08**	**10.27**
-10	1	4.836E+08	10.58		**-10**	**1**	**5.177E+08**	**11.34**
-10	0.4641	4.478E+08	11.80		**-10**	**0.4641**	**4.767E+08**	**12.58**
-10	0.2154	3.979E+08	11.94		**-10**	**0.1**	**3.776E+08**	**15.03**
-10	0.1	3.594E+08	14.29		**-10**	**0.02154**	**2.910E+08**	**18.66**
-10	0.04641	3.140E+08	15.05		**-10**	**0.01**	**2.468E+08**	**19.95**
-10	0.02154	2.802E+08	17.95		**-20**	**10**	**9.138E+08**	**4.40**
-10	0.01	2.391E+08	19.31		**-20**	**4.641**	**8.846E+08**	**5.14**
-20	10	8.114E+08	3.90		**-20**	**2.154**	**8.331E+08**	**5.95**
-20	4.641	7.884E+08	4.58		**-20**	**1**	**7.930E+08**	**6.98**
-20	2.154	7.473E+08	5.34		**-20**	**0.4641**	**7.535E+08**	**7.63**
-20	1	7.150E+08	6.29		**-20**	**0.2155**	**7.070E+08**	**8.58**
-20	0.4641	6.829E+08	6.91		**-20**	**0.1**	**6.556E+08**	**9.20**
-20	0.2155	6.446E+08	7.82		**-20**	**0.02154**	**5.637E+08**	**11.54**
-20	0.1	6.016E+08	8.44		**-20**	**0.01**	**5.059E+08**	**13.14**
-20	0.04642	5.548E+08	8.42		**-30**	**10**	**1.078E+09**	**2.42**
-20	0.02154	5.236E+08	10.71		**-30**	**4.641**	**1.062E+09**	**2.97**
-20	0.01	4.736E+08	12.29		**-30**	**2.154**	**1.033E+09**	**3.55**
-30	10	9.382E+08	2.11		**-30**	**1**	**9.861E+08**	**4.31**
-30	4.641	9.257E+08	2.59		**-30**	**0.4641**	**9.629E+08**	**4.61**
-30	2.154	9.041E+08	3.11		**-30**	**0.1**	**8.851E+08**	**5.86**
-30	1	8.679E+08	3.80		**-30**	**0.01**	**7.463E+08**	**8.58**
-30	0.4641	8.499E+08	4.07					
-30	0.2155	8.132E+08	4.00					
-30	0.1	7.889E+08	5.22					
-30	0.04642	7.589E+08	7.34					
-30	0.02154	7.185E+08	6.04					
-30	0.01	6.770E+08	7.78					

B-5								
T	*f*	*G**	*δ*		***T***	***f***	***G****	***δ***
[°C]	[Hz]	[Pa]	[°]		**[°C]**	**[Hz]**	**[Pa]**	**[°]**
10	10	2.485E+08	19.24		**10**	**10**	**2.568E+08**	**19.91**
10	4.641	2.091E+08	22.05		**10**	**4.641**	**2.148E+08**	**22.69**
10	2.154	1.713E+08	24.78		**10**	**2.154**	**1.750E+08**	**25.37**
10	1	1.352E+08	27.60		**10**	**1**	**1.375E+08**	**28.11**
10	0.4641	1.077E+08	30.80		**10**	**0.4641**	**1.091E+08**	**31.25**
10	0.2154	8.218E+07	34.07		**10**	**0.2154**	**8.296E+07**	**34.44**
10	0.1	6.124E+07	37.66		**10**	**0.1**	**6.165E+07**	**37.96**
10	0.04641	4.420E+07	41.38		**10**	**0.04641**	**4.441E+07**	**41.61**
10	0.02154	3.061E+07	45.57		**10**	**0.02154**	**3.070E+07**	**45.74**
10	0.01	2.051E+07	49.90		**10**	**0.01**	**2.055E+07**	**50.03**
0	10	4.752E+08	9.63		**0**	**10**	**5.081E+08**	**10.31**
0	4.641	4.361E+08	11.49		**0**	**4.641**	**4.635E+08**	**12.23**
0	2.154	3.942E+08	13.19		**0**	**2.154**	**4.163E+08**	**13.95**
0	1	3.482E+08	15.08		**0**	**1**	**3.652E+08**	**15.83**
0	0.4641	3.072E+08	17.09		**0**	**0.4641**	**3.201E+08**	**17.83**
0	0.2154	2.641E+08	19.14		**0**	**0.2154**	**2.735E+08**	**19.85**
0	0.1	2.233E+08	21.73		**0**	**0.1**	**2.299E+08**	**22.41**
0	0.04641	1.833E+08	24.47		**0**	**0.04641**	**1.876E+08**	**25.09**
0	0.02154	1.483E+08	27.37		**0**	**0.02154**	**1.510E+08**	**27.92**
0	0.01	1.162E+08	30.78		**0**	**0.01**	**1.178E+08**	**31.26**
-10	10	6.626E+08	3.99		**-10**	**10**	**7.293E+08**	**4.39**
-10	4.641	6.403E+08	4.93		**-10**	**4.641**	**7.023E+08**	**5.41**
-10	2.154	6.246E+08	5.78		**-10**	**2.154**	**6.833E+08**	**6.33**
-10	1	5.894E+08	6.74		**-10**	**1**	**6.413E+08**	**7.34**
-10	0.4641	5.497E+08	7.82		**-10**	**0.4641**	**5.945E+08**	**8.46**
-10	0.2154	5.133E+08	8.22		**-10**	**0.1**	**5.073E+08**	**11.52**
-10	0.1	4.746E+08	10.77		**-10**	**0.02154**	**4.007E+08**	**16.40**
-10	0.04641	4.364E+08	11.04		**-10**	**0.01**	**3.606E+08**	**16.60**
-10	0.02154	3.804E+08	15.55		**-20**	**10**	**8.720E+08**	**2.13**
-10	0.01	3.441E+08	15.82		**-20**	**4.641**	**8.613E+08**	**2.64**
-20	10	7.781E+08	1.90		**-20**	**2.154**	**8.423E+08**	**3.15**
-20	4.641	7.697E+08	2.36		**-20**	**1**	**8.310E+08**	**3.56**
-20	2.154	7.544E+08	2.82		**-20**	**0.4641**	**7.913E+08**	**4.21**
-20	1	7.454E+08	3.19		**-20**	**0.1**	**7.294E+08**	**5.87**
-20	0.4641	7.134E+08	3.79		**-20**	**0.02154**	**6.731E+08**	**7.53**
-20	0.2155	6.856E+08	3.32		**-20**	**0.01**	**6.247E+08**	**8.37**
-20	0.1	6.628E+08	5.33		**-30**	**10**	**9.666E+08**	**1.10**
-20	0.04642	6.636E+08	7.07		**-30**	**4.641**	**9.546E+08**	**1.51**
-20	0.02154	6.161E+08	6.89		**-30**	**2.154**	**9.466E+08**	**1.81**
-20	0.01	5.754E+08	7.71		**-30**	**1**	**9.309E+08**	**2.23**
-30	10	8.525E+08	0.97		**-30**	**0.4641**	**9.093E+08**	**2.51**
-30	4.641	8.432E+08	1.33		**-30**	**0.1**	**8.699E+08**	**3.32**
-30	2.154	8.369E+08	1.60		**-30**	**0.04642**	**8.458E+08**	**3.94**
-30	1	8.247E+08	1.97		**-30**	**0.01**	**7.657E+08**	**5.94**
-30	0.4641	8.077E+08	2.23					
-30	0.2155	7.864E+08	1.46					
-30	0.1	7.765E+08	2.96					
-30	0.04642	7.573E+08	3.53					
-30	0.02154	7.358E+08	3.74					
-30	0.01	6.926E+08	5.37					

B-6								
T	*f*	*G**	*δ*		***T***	***f***	***G****	***δ***
[°C]	[Hz]	[Pa]	[°]		**[°C]**	**[Hz]**	**[Pa]**	**[°]**
10	10	2.038E+08	24.22		**10**	**10**	**2.092E+08**	**24.90**
10	4.641	1.643E+08	26.83		**10**	**4.641**	**1.677E+08**	**27.43**
10	2.154	1.297E+08	29.45		**10**	**2.154**	**1.317E+08**	**29.97**
10	1	9.990E+07	32.04		**10**	**1**	**1.011E+08**	**32.47**
10	0.4641	7.535E+07	34.82		**10**	**0.4641**	**7.600E+07**	**35.17**
10	0.2154	5.575E+07	37.60		**10**	**0.2154**	**5.609E+07**	**37.87**
10	0.1	4.024E+07	40.47		**10**	**0.1**	**4.041E+07**	**40.68**
10	0.04641	2.807E+07	43.50		**10**	**0.04641**	**2.815E+07**	**43.65**
10	0.02154	1.906E+07	46.70		**10**	**0.02154**	**1.909E+07**	**46.81**
10	0.01	1.272E+07	49.89		**10**	**0.01**	**1.273E+07**	**49.96**
0	10	4.501E+08	13.32		**0**	**10**	**4.791E+08**	**14.20**
0	4.641	3.996E+08	15.50		**0**	**4.641**	**4.221E+08**	**16.40**
0	2.154	3.498E+08	17.55		**0**	**2.154**	**3.667E+08**	**18.43**
0	1	2.949E+08	19.77		**0**	**1**	**3.066E+08**	**20.59**
0	0.4641	2.494E+08	21.92		**0**	**0.4641**	**2.577E+08**	**22.68**
0	0.2154	2.053E+08	24.13		**0**	**0.2154**	**2.108E+08**	**24.81**
0	0.1	1.660E+08	26.67		**0**	**0.1**	**1.694E+08**	**27.27**
0	0.04641	1.306E+08	29.41		**0**	**0.04641**	**1.327E+08**	**29.93**
0	0.02154	1.009E+08	32.46		**0**	**0.02154**	**1.021E+08**	**32.89**
0	0.01	7.600E+07	34.98		**0**	**0.01**	**7.666E+07**	**35.33**
-10	10	7.406E+08	5.67		**-10**	**10**	**8.247E+08**	**6.32**
-10	4.641	7.032E+08	6.93		**-10**	**4.641**	**7.784E+08**	**7.67**
-10	2.154	6.620E+08	8.14		**-10**	**2.154**	**7.279E+08**	**8.96**
-10	1	6.205E+08	9.51		**-10**	**1**	**6.779E+08**	**10.40**
-10	0.4641	5.661E+08	10.91		**-10**	**0.4641**	**6.132E+08**	**11.83**
-10	0.2154	5.190E+08	12.52		**-10**	**0.2154**	**5.581E+08**	**13.48**
-10	0.1	4.632E+08	14.43		**-10**	**0.1**	**4.938E+08**	**15.40**
-10	0.04641	4.058E+08	16.89		**-10**	**0.04641**	**4.288E+08**	**17.88**
-10	0.02154	3.512E+08	18.65		**-10**	**0.02154**	**3.682E+08**	**19.58**
-10	0.01	3.048E+08	20.63		**-10**	**0.01**	**3.173E+08**	**21.52**
-20	10	9.324E+08	2.67		**-20**	**10**	**1.070E+09**	**3.07**
-20	4.641	9.152E+08	3.19		**-20**	**4.641**	**1.048E+09**	**3.65**
-20	2.154	8.803E+08	3.72		**-20**	**2.154**	**1.002E+09**	**4.24**
-20	1	8.583E+08	4.52		**-20**	**1**	**9.735E+08**	**5.13**
-20	0.4641	8.236E+08	5.38		**-20**	**0.4641**	**9.290E+08**	**6.07**
-20	0.2155	7.847E+08	5.89		**-20**	**0.2155**	**8.798E+08**	**6.61**
-20	0.1	7.413E+08	7.43		**-20**	**0.1**	**8.252E+08**	**8.27**
-20	0.04642	7.105E+08	12.41		**-20**	**0.02154**	**7.205E+08**	**10.33**
-20	0.02154	6.560E+08	9.40		**-20**	**0.01**	**6.427E+08**	**12.71**
-20	0.01	5.912E+08	11.68		**-30**	**10**	**1.199E+09**	**1.46**
-30	10	1.028E+09	1.25		**-30**	**4.641**	**1.196E+09**	**1.90**
-30	4.641	1.026E+09	1.63		**-30**	**2.154**	**1.161E+09**	**2.32**
-30	2.154	1.001E+09	2.00		**-30**	**1**	**1.133E+09**	**2.62**
-30	1	9.799E+08	2.27		**-30**	**0.4641**	**1.115E+09**	**3.26**
-30	0.4641	9.658E+08	2.82		**-30**	**0.1**	**1.049E+09**	**4.12**
-30	0.2155	9.290E+08	2.35		**-40**	**10**	**1.292E+09**	**0.81**
-30	0.1	9.164E+08	3.60		**-40**	**4.641**	**1.291E+09**	**1.12**
-30	0.04642	8.959E+08	5.04		**-40**	**2.154**	**1.272E+09**	**1.37**
-30	0.02154	8.394E+08	6.91		**-40**	**1**	**1.256E+09**	**1.48**
-30	0.01	8.404E+08	5.81		**-40**	**0.4641**	**1.241E+09**	**1.90**
-40	10	1.096E+09	0.68		**-40**	**0.2155**	**1.224E+09**	**2.17**
-40	4.641	1.095E+09	0.95		**-40**	**0.1**	**1.194E+09**	**2.62**
-40	2.154	1.081E+09	1.17		**-40**	**0.04642**	**1.173E+09**	**3.23**
-40	1	1.070E+09	1.26		**-40**	**0.02154**	**1.161E+09**	**3.70**
-40	0.4641	1.059E+09	1.62		**-40**	**0.01**	**1.119E+09**	**4.69**
-40	0.2155	1.047E+09	1.86					
-40	0.1	1.025E+09	2.25					
-40	0.04642	1.009E+09	2.78					
-40	0.02154	1.001E+09	3.18					
-40	0.01	9.690E+08	4.06					

B-7								
T	*f*	*G**	*δ*		***T***	***f***	***G****	***δ***
[°C]	[Hz]	[Pa]	[°]		**[°C]**	**[Hz]**	**[Pa]**	**[°]**
10	10	8.921E+07	31.64		**10**	**10**	**9.016E+07**	**32.02**
10	4.641	6.768E+07	33.67		**10**	**4.641**	**6.821E+07**	**33.97**
10	2.154	5.012E+07	35.83		**10**	**2.154**	**5.040E+07**	**36.07**
10	1	3.670E+07	37.98		**10**	**1**	**3.685E+07**	**38.16**
10	0.4641	2.629E+07	40.11		**10**	**0.4641**	**2.637E+07**	**40.24**
10	0.2154	1.848E+07	42.26		**10**	**0.2154**	**1.852E+07**	**42.36**
10	0.1	1.275E+07	44.43		**10**	**0.1**	**1.277E+07**	**44.50**
10	0.04641	8.629E+06	46.58		**10**	**0.04641**	**8.636E+06**	**46.63**
10	0.02154	5.731E+06	48.78		**10**	**0.02154**	**5.734E+06**	**48.82**
10	0.01	3.750E+06	50.89		**10**	**0.01**	**3.752E+06**	**50.91**
0	10	2.393E+08	21.49		**0**	**10**	**2.469E+08**	**22.21**
0	4.641	1.988E+08	23.52		**0**	**4.641**	**2.039E+08**	**24.16**
0	2.154	1.595E+08	25.49		**0**	**2.154**	**1.628E+08**	**26.04**
0	1	1.273E+08	27.64		**0**	**1**	**1.294E+08**	**28.12**
0	0.4641	1.006E+08	29.82		**0**	**0.4641**	**1.018E+08**	**30.22**
0	0.2154	7.734E+07	31.90		**0**	**0.2154**	**7.805E+07**	**32.23**
0	0.1	5.832E+07	34.01		**0**	**0.1**	**5.871E+07**	**34.27**
0	0.04641	4.333E+07	36.12		**0**	**0.04641**	**4.354E+07**	**36.32**
0	0.02154	3.163E+07	38.48		**0**	**0.02154**	**3.174E+07**	**38.64**
0	0.01	2.258E+07	40.76		**0**	**0.01**	**2.263E+07**	**40.88**
-10	10	4.769E+08	11.49		**-10**	**10**	**5.098E+08**	**12.29**
-10	4.641	4.316E+08	13.22		**-10**	**4.641**	**4.583E+08**	**14.06**
-10	2.154	3.925E+08	15.06		**-10**	**2.154**	**4.142E+08**	**15.92**
-10	1	3.380E+08	17.06		**-10**	**1**	**3.538E+08**	**17.88**
-10	0.4641	2.891E+08	18.85		**-10**	**0.4641**	**3.005E+08**	**19.62**
-10	0.2154	2.439E+08	20.60		**-10**	**0.2154**	**2.518E+08**	**21.30**
-10	0.1	2.032E+08	23.01		**-10**	**0.1**	**2.086E+08**	**23.66**
-10	0.04641	1.662E+08	24.51		**-10**	**0.04641**	**1.697E+08**	**25.07**
-10	0.02154	1.338E+08	27.17		**-10**	**0.02154**	**1.360E+08**	**27.67**
-10	0.01	1.057E+08	29.35		**-10**	**0.01**	**1.071E+08**	**29.77**
-20	10	6.884E+08	5.93		**-20**	**10**	**7.604E+08**	**6.55**
-20	4.641	6.552E+08	6.91		**-20**	**4.641**	**7.199E+08**	**7.60**
-20	2.154	6.166E+08	8.17		**-20**	**2.154**	**6.734E+08**	**8.93**
-20	1	5.757E+08	9.48		**-20**	**1**	**6.247E+08**	**10.30**
-20	0.4641	5.259E+08	10.98		**-20**	**0.4641**	**5.664E+08**	**11.84**
-20	0.2155	4.793E+08	10.96		**-20**	**0.1**	**4.546E+08**	**15.20**
-20	0.1	4.285E+08	14.31		**-20**	**0.04642**	**3.990E+08**	**17.00**
-20	0.04642	3.789E+08	16.12		**-20**	**0.02154**	**3.459E+08**	**18.78**
-20	0.02154	3.309E+08	17.94		**-20**	**0.01**	**2.866E+08**	**20.75**
-20	0.01	2.763E+08	19.97		**-30**	**10**	**9.423E+08**	**3.28**
-30	10	8.337E+08	2.90		**-30**	**4.641**	**9.157E+08**	**4.04**
-30	4.641	8.129E+08	3.59		**-30**	**2.154**	**8.865E+08**	**4.85**
-30	2.154	7.898E+08	4.32		**-30**	**1**	**8.542E+08**	**5.77**
-30	1	7.642E+08	5.16		**-30**	**0.4641**	**8.044E+08**	**6.76**
-30	0.4641	7.243E+08	6.08		**-30**	**0.2155**	**7.538E+08**	**7.82**
-30	0.2155	6.831E+08	7.09		**-30**	**0.1**	**6.997E+08**	**9.14**
-30	0.1	6.386E+08	8.34		**-30**	**0.04642**	**6.517E+08**	**10.63**
-30	0.04642	5.986E+08	9.75		**-30**	**0.02154**	**5.909E+08**	**12.69**
-30	0.02154	5.471E+08	11.74		**-40**	**10**	**1.064E+09**	**1.61**
-30	0.01	4.909E+08	12.69		**-40**	**4.641**	**1.046E+09**	**2.17**
-40	10	9.273E+08	1.41		**-40**	**2.154**	**1.032E+09**	**2.62**
-40	4.641	9.136E+08	1.90		**-40**	**1**	**1.013E+09**	**3.22**
-40	2.154	9.032E+08	2.30		**-40**	**0.4641**	**9.741E+08**	**3.88**
-40	1	8.882E+08	2.82		**-40**	**0.1**	**9.015E+08**	**5.38**
-40	0.4641	8.585E+08	3.42		**-40**	**0.02154**	**8.428E+08**	**7.80**
-40	0.2155	8.359E+08	3.46		**-40**	**0.01**	**7.739E+08**	**8.37**
-40	0.1	8.018E+08	4.78					
-40	0.04642	7.613E+08	3.92					
-40	0.02154	7.554E+08	6.99					
-40	0.01	6.997E+08	7.56					

B-8								
T	*f*	*G**	*δ*		***T***	***f***	***G****	***δ***
[°C]	[Hz]	[Pa]	[°]		**[°C]**	**[Hz]**	**[Pa]**	**[°]**
10	10	1.514E+08	25.87		**10**	**10**	**1.543E+08**	**26.40**
10	4.641	1.204E+08	29.21		**10**	**4.641**	**1.222E+08**	**29.69**
10	2.154	9.306E+07	32.35		**10**	**2.154**	**9.408E+07**	**32.75**
10	1	7.006E+07	35.65		**10**	**1**	**7.062E+07**	**35.98**
10	0.4641	5.112E+07	39.21		**10**	**0.4641**	**5.140E+07**	**39.47**
10	0.2154	3.637E+07	42.93		**10**	**0.2154**	**3.650E+07**	**43.12**
10	0.1	2.521E+07	46.77		**10**	**0.1**	**2.527E+07**	**46.91**
10	0.04641	1.692E+07	50.85		**10**	**0.04641**	**1.694E+07**	**50.96**
10	0.02154	1.084E+07	55.08		**10**	**0.02154**	**1.085E+07**	**55.15**
10	0.01	6.713E+06	59.35		**10**	**0.01**	**6.716E+06**	**59.40**
0	10	3.565E+08	14.11		**0**	**10**	**3.744E+08**	**14.84**
0	4.641	3.137E+08	16.38		**0**	**4.641**	**3.274E+08**	**17.12**
0	2.154	2.699E+08	18.25		**0**	**2.154**	**2.798E+08**	**18.95**
0	1	2.301E+08	20.68		**0**	**1**	**2.372E+08**	**21.34**
0	0.4641	1.916E+08	23.31		**0**	**0.4641**	**1.964E+08**	**23.93**
0	0.2154	1.561E+08	25.99		**0**	**0.2154**	**1.592E+08**	**26.54**
0	0.1	1.242E+08	28.87		**0**	**0.1**	**1.261E+08**	**29.35**
0	0.04641	9.661E+07	31.97		**0**	**0.04641**	**9.772E+07**	**32.38**
0	0.02154	7.237E+07	35.58		**0**	**0.02154**	**7.297E+07**	**35.92**
0	0.01	5.352E+07	39.41		**0**	**0.01**	**5.383E+07**	**39.68**
-10	10	6.323E+08	6.43		**-10**	**10**	**6.925E+08**	**7.04**
-10	4.641	5.976E+08	7.62		**-10**	**4.641**	**6.509E+08**	**8.31**
-10	2.154	5.585E+08	8.85		**-10**	**2.154**	**6.046E+08**	**9.59**
-10	1	5.156E+08	10.16		**-10**	**1**	**5.545E+08**	**10.94**
-10	0.4641	4.751E+08	11.65		**-10**	**0.4641**	**5.077E+08**	**12.46**
-10	0.2154	4.231E+08	12.18		**-10**	**0.1**	**4.029E+08**	**16.04**
-10	0.1	3.824E+08	15.21		**-10**	**0.04641**	**3.532E+08**	**17.79**
-10	0.04641	3.375E+08	16.97		**-10**	**0.02154**	**2.987E+08**	**20.01**
-10	0.02154	2.875E+08	19.23		**-10**	**0.01**	**2.506E+08**	**22.71**
-10	0.01	2.428E+08	21.97		**-20**	**10**	**9.183E+08**	**3.60**
-20	10	8.149E+08	3.20		**-20**	**4.641**	**8.905E+08**	**4.22**
-20	4.641	7.930E+08	3.76		**-20**	**2.154**	**8.501E+08**	**4.95**
-20	2.154	7.609E+08	4.43		**-20**	**1**	**8.113E+08**	**5.79**
-20	1	7.297E+08	5.21		**-20**	**0.4641**	**7.812E+08**	**6.68**
-20	0.4641	7.054E+08	6.03		**-20**	**0.2155**	**7.299E+08**	**7.76**
-20	0.2155	6.634E+08	7.05		**-20**	**0.1**	**6.818E+08**	**8.83**
-20	0.1	6.236E+08	8.07		**-20**	**0.04642**	**6.409E+08**	**10.35**
-20	0.04642	5.894E+08	9.51		**-20**	**0.01**	**5.251E+08**	**13.13**
-20	0.02154	5.443E+08	10.09		**-30**	**10**	**1.039E+09**	**1.82**
-20	0.01	4.904E+08	12.24		**-30**	**4.641**	**1.028E+09**	**2.34**
-30	10	9.087E+08	1.59		**-30**	**2.154**	**9.942E+08**	**2.80**
-30	4.641	9.003E+08	2.05		**-30**	**1**	**9.722E+08**	**3.26**
-30	2.154	8.740E+08	2.46		**-30**	**0.4641**	**9.516E+08**	**3.78**
-30	1	8.570E+08	2.88		**-30**	**0.1**	**8.844E+08**	**4.95**
-30	0.4641	8.410E+08	3.34		**-30**	**0.04642**	**8.601E+08**	**5.73**
-30	0.2155	8.012E+08	2.81		**-30**	**0.01**	**7.535E+08**	**8.38**
-30	0.1	7.882E+08	4.41		**-40**	**10**	**1.131E+09**	**1.11**
-30	0.04642	7.690E+08	5.12		**-40**	**4.641**	**1.124E+09**	**1.43**
-30	0.02154	7.368E+08	5.49		**-40**	**2.154**	**1.107E+09**	**1.61**
-30	0.01	6.830E+08	7.59		**-40**	**1**	**1.085E+09**	**1.96**
-40	10	9.776E+08	0.96		**-40**	**0.4641**	**1.079E+09**	**2.35**
-40	4.641	9.729E+08	1.24		**-40**	**0.2155**	**1.049E+09**	**2.87**
-40	2.154	9.599E+08	1.40		**-40**	**0.02154**	**9.653E+08**	**4.51**
-40	1	9.434E+08	1.70		**-40**	**0.01**	**9.515E+08**	**4.87**
-40	0.4641	9.386E+08	2.04					
-40	0.2155	9.164E+08	2.51					
-40	0.1	8.986E+08	2.54					
-40	0.04642	8.866E+08	4.82					
-40	0.02154	8.518E+08	3.98					
-40	0.01	8.411E+08	4.31					

B-9								
T	*f*	*G**	*δ*		***T***	***f***	***G****	***δ***
[°C]	[Hz]	[Pa]	[°]		**[°C]**	**[Hz]**	**[Pa]**	**[°]**
10	10	7.094E+07	29.03		**10**	**10**	**7.155E+07**	**29.30**
10	4.641	5.510E+07	30.78		**10**	**4.641**	**5.547E+07**	**31.01**
10	2.154	4.229E+07	32.45		**10**	**2.154**	**4.250E+07**	**32.63**
10	1	3.195E+07	34.14		**10**	**1**	**3.206E+07**	**34.29**
10	0.4641	2.376E+07	35.89		**10**	**0.4641**	**2.382E+07**	**36.00**
10	0.2154	1.747E+07	37.72		**10**	**0.2154**	**1.751E+07**	**37.81**
10	0.1	1.267E+07	39.65		**10**	**0.1**	**1.269E+07**	**39.71**
10	0.04641	9.119E+06	41.67		**10**	**0.04641**	**9.128E+06**	**41.72**
10	0.02154	6.451E+06	43.75		**10**	**0.02154**	**6.455E+06**	**43.79**
10	0.01	4.448E+06	46.04		**10**	**0.01**	**4.450E+06**	**46.06**
0	10	1.886E+08	20.72		**0**	**10**	**1.933E+08**	**21.27**
0	4.641	1.570E+08	22.48		**0**	**4.641**	**1.602E+08**	**22.97**
0	2.154	1.293E+08	23.99		**0**	**2.154**	**1.314E+08**	**24.42**
0	1	1.049E+08	25.58		**0**	**1**	**1.063E+08**	**25.95**
0	0.4641	8.405E+07	27.07		**0**	**0.4641**	**8.493E+07**	**27.38**
0	0.2154	6.634E+07	28.67		**0**	**0.2154**	**6.687E+07**	**28.93**
0	0.1	5.190E+07	30.22		**0**	**0.1**	**5.223E+07**	**30.42**
0	0.04641	3.997E+07	31.93		**0**	**0.04641**	**4.016E+07**	**32.10**
0	0.02154	3.043E+07	33.69		**0**	**0.02154**	**3.054E+07**	**33.82**
0	0.01	2.283E+07	35.63		**0**	**0.01**	**2.289E+07**	**35.73**
-10	10	4.153E+08	12.96		**-10**	**10**	**4.399E+08**	**13.74**
-10	4.641	3.703E+08	14.46		**-10**	**4.641**	**3.896E+08**	**15.23**
-10	2.154	3.265E+08	15.91		**-10**	**2.154**	**3.413E+08**	**16.65**
-10	1	2.777E+08	17.36		**-10**	**1**	**2.883E+08**	**18.04**
-10	0.4641	2.426E+08	18.82		**-10**	**0.4641**	**2.505E+08**	**19.46**
-10	0.2154	2.060E+08	20.28		**-10**	**0.2154**	**2.116E+08**	**20.86**
-10	0.1	1.728E+08	21.54		**-10**	**0.1**	**1.767E+08**	**22.05**
-10	0.04641	1.404E+08	23.45		**-10**	**0.04641**	**1.429E+08**	**23.90**
-10	0.02154	1.166E+08	25.08		**-10**	**0.02154**	**1.183E+08**	**25.48**
-10	0.01	9.407E+07	26.68		**-10**	**0.01**	**9.517E+07**	**27.02**
-20	10	6.157E+08	8.22		**-20**	**10**	**6.724E+08**	**8.98**
-20	4.641	5.709E+08	9.44		**-20**	**4.641**	**6.192E+08**	**10.25**
-20	2.154	5.251E+08	10.70		**-20**	**2.154**	**5.655E+08**	**11.54**
-20	1	4.740E+08	12.10		**-20**	**1**	**5.065E+08**	**12.94**
-20	0.4641	4.290E+08	13.23		**-20**	**0.4641**	**4.553E+08**	**14.06**
-20	0.2155	3.832E+08	14.66		**-20**	**0.2155**	**4.039E+08**	**15.47**
-20	0.1	3.373E+08	15.87		**-20**	**0.1**	**3.531E+08**	**16.64**
-20	0.04642	3.005E+08	18.02		**-20**	**0.02154**	**2.645E+08**	**19.46**
-20	0.02154	2.556E+08	18.78		**-20**	**0.01**	**2.249E+08**	**20.94**
-20	0.01	2.185E+08	20.32		**-30**	**10**	**8.908E+08**	**5.31**
-30	10	7.933E+08	4.73		**-30**	**4.641**	**8.494E+08**	**6.39**
-30	4.641	7.605E+08	5.72		**-30**	**2.154**	**8.020E+08**	**7.39**
-30	2.154	7.224E+08	6.65		**-30**	**1**	**7.430E+08**	**8.42**
-30	1	6.743E+08	7.64		**-30**	**0.4641**	**6.949E+08**	**9.53**
-30	0.4641	6.346E+08	8.70		**-30**	**0.1**	**5.847E+08**	**11.99**
-30	0.2155	5.806E+08	8.08		**-30**	**0.02154**	**4.722E+08**	**14.82**
-30	0.1	5.417E+08	11.10		**-30**	**0.01**	**4.080E+08**	**17.04**
-30	0.04642	4.910E+08	11.30		**-40**	**10**	**1.064E+09**	**3.27**
-30	0.02154	4.440E+08	13.92		**-40**	**4.641**	**1.035E+09**	**3.84**
-30	0.01	3.871E+08	16.14		**-40**	**2.154**	**9.918E+08**	**4.46**
-40	10	9.277E+08	2.85		**-40**	**1**	**9.551E+08**	**5.24**
-40	4.641	9.056E+08	3.36		**-40**	**0.4641**	**9.205E+08**	**6.11**
-40	2.154	8.723E+08	3.92		**-40**	**0.2155**	**8.716E+08**	**7.08**
-40	1	8.440E+08	4.63		**-40**	**0.04642**	**7.778E+08**	**9.19**
-40	0.4641	8.169E+08	5.42		**-40**	**0.01**	**6.475E+08**	**11.40**
-40	0.2155	7.783E+08	6.32					
-40	0.1	7.367E+08	6.89					
-40	0.04642	7.030E+08	8.30					
-40	0.02154	6.543E+08	10.36					
-40	0.01	5.951E+08	10.47					

B-10								
T	*f*	*G**	*δ*		***T***	***f***	***G****	***δ***
[°C]	[Hz]	[Pa]	[°]		**[°C]**	**[Hz]**	**[Pa]**	**[°]**
10	10	7.713E+07	32.25		**10**	**10**	**7.783E+07**	**32.57**
10	4.641	5.848E+07	34.16		**10**	**4.641**	**5.888E+07**	**34.43**
10	2.154	4.347E+07	36.03		**10**	**2.154**	**4.368E+07**	**36.24**
10	1	3.189E+07	38.02		**10**	**1**	**3.200E+07**	**38.18**
10	0.4641	2.301E+07	40.15		**10**	**0.4641**	**2.307E+07**	**40.27**
10	0.2154	1.630E+07	42.39		**10**	**0.2154**	**1.633E+07**	**42.48**
10	0.1	1.136E+07	44.78		**10**	**0.1**	**1.137E+07**	**44.84**
10	0.04641	7.762E+06	47.22		**10**	**0.04641**	**7.768E+06**	**47.26**
10	0.02154	5.193E+06	49.76		**10**	**0.02154**	**5.196E+06**	**49.79**
10	0.01	3.429E+06	52.24		**10**	**0.01**	**3.430E+06**	**52.26**
0	10	2.093E+08	22.81		**0**	**10**	**2.150E+08**	**23.47**
0	4.641	1.721E+08	24.09		**0**	**4.641**	**1.759E+08**	**24.66**
0	2.154	1.400E+08	25.67		**0**	**2.154**	**1.425E+08**	**26.16**
0	1	1.108E+08	27.24		**0**	**1**	**1.123E+08**	**27.65**
0	0.4641	8.823E+07	29.11		**0**	**0.4641**	**8.918E+07**	**29.45**
0	0.2154	6.876E+07	31.06		**0**	**0.2154**	**6.932E+07**	**31.34**
0	0.1	5.268E+07	33.05		**0**	**0.1**	**5.301E+07**	**33.28**
0	0.04641	3.971E+07	35.45		**0**	**0.04641**	**3.989E+07**	**35.63**
0	0.02154	2.931E+07	37.72		**0**	**0.02154**	**2.940E+07**	**37.87**
0	0.01	2.132E+07	40.34		**0**	**0.01**	**2.137E+07**	**40.45**
-10	10	4.320E+08	13.93		**-10**	**10**	**4.586E+08**	**14.81**
-10	4.641	3.818E+08	15.31		**-10**	**4.641**	**4.023E+08**	**16.15**
-10	2.154	3.355E+08	16.57		**-10**	**2.154**	**3.511E+08**	**17.36**
-10	1	2.948E+08	17.76		**-10**	**1**	**3.066E+08**	**18.50**
-10	0.4641	2.476E+08	19.31		**-10**	**0.4641**	**2.559E+08**	**19.98**
-10	0.2154	2.092E+08	20.85		**-10**	**0.2154**	**2.150E+08**	**21.45**
-10	0.1	1.742E+08	22.15		**-10**	**0.1**	**1.781E+08**	**22.68**
-10	0.04641	1.432E+08	24.74		**-10**	**0.04641**	**1.459E+08**	**25.22**
-10	0.02154	1.158E+08	26.51		**-10**	**0.02154**	**1.175E+08**	**26.93**
-10	0.01	9.335E+07	28.42		**-10**	**0.01**	**9.442E+07**	**28.78**
-20	10	6.306E+08	9.15		**-20**	**10**	**6.900E+08**	**10.02**
-20	4.641	5.852E+08	9.93		**-20**	**4.641**	**6.358E+08**	**10.80**
-20	2.154	5.409E+08	10.85		**-20**	**2.154**	**5.837E+08**	**11.72**
-20	1	4.900E+08	11.89		**-20**	**1**	**5.248E+08**	**12.75**
-20	0.4641	4.405E+08	12.89		**-20**	**0.4641**	**4.683E+08**	**13.72**
-20	0.2155	3.920E+08	13.52		**-20**	**0.1**	**3.658E+08**	**16.34**
-20	0.1	3.488E+08	15.56		**-20**	**0.02154**	**2.750E+08**	**19.42**
-20	0.04642	3.019E+08	17.92		**-20**	**0.01**	**2.379E+08**	**20.93**
-20	0.02154	2.654E+08	18.72		**-30**	**10**	**9.041E+08**	**6.36**
-20	0.01	2.308E+08	20.28		**-30**	**4.641**	**8.549E+08**	**7.15**
-30	10	8.040E+08	5.65		**-30**	**2.154**	**8.115E+08**	**7.74**
-30	4.641	7.650E+08	6.39		**-30**	**1**	**7.564E+08**	**8.42**
-30	2.154	7.302E+08	6.96		**-30**	**0.4641**	**7.033E+08**	**9.15**
-30	1	6.854E+08	7.63		**-30**	**0.2155**	**6.465E+08**	**10.13**
-30	0.4641	6.416E+08	8.34		**-30**	**0.1**	**5.941E+08**	**11.09**
-30	0.2155	5.941E+08	9.30		**-30**	**0.01**	**4.363E+08**	**14.74**
-30	0.1	5.497E+08	10.25		**-40**	**10**	**1.077E+09**	**4.44**
-30	0.04642	5.408E+08	9.34		**-40**	**4.641**	**1.040E+09**	**4.83**
-30	0.02154	4.633E+08	11.81		**-40**	**2.154**	**9.966E+08**	**5.16**
-30	0.01	4.122E+08	13.91		**-40**	**1**	**9.622E+08**	**5.42**
-40	10	9.372E+08	3.87		**-40**	**0.4641**	**9.038E+08**	**5.98**
-40	4.641	9.094E+08	4.23		**-40**	**0.04642**	**7.729E+08**	**7.84**
-40	2.154	8.761E+08	4.53		**-40**	**0.02154**	**7.356E+08**	**8.82**
-40	1	8.495E+08	4.79					
-40	0.4641	8.038E+08	5.31					
-40	0.2155	7.686E+08	5.25					
-40	0.1	7.339E+08	6.09					
-40	0.04642	6.987E+08	7.08					
-40	0.02154	6.683E+08	8.01					
-40	0.01	5.965E+08	10.58					

B-11								
T	*f*	*G**	*δ*		***T***	***f***	***G****	***δ***
[°C]	[Hz]	[Pa]	[°]		**[°C]**	**[Hz]**	**[Pa]**	**[°]**
10	10	8.441E+07	33.14		**10**	**10**	**8.524E+07**	**33.51**
10	4.641	6.292E+07	36.51		**10**	**4.641**	**6.336E+07**	**36.81**
10	2.154	4.571E+07	39.87		**10**	**2.154**	**4.593E+07**	**40.10**
10	1	3.228E+07	43.38		**10**	**1**	**3.238E+07**	**43.56**
10	0.4641	2.207E+07	46.98		**10**	**0.4641**	**2.212E+07**	**47.11**
10	0.2154	1.469E+07	50.63		**10**	**0.2154**	**1.471E+07**	**50.72**
10	0.1	9.554E+06	54.30		**10**	**0.1**	**9.562E+06**	**54.36**
10	0.04641	5.975E+06	57.95		**10**	**0.04641**	**5.978E+06**	**57.99**
10	0.02154	3.603E+06	61.46		**10**	**0.02154**	**3.604E+06**	**61.49**
10	0.01	2.133E+06	64.82		**10**	**0.01**	**2.133E+06**	**64.84**
0	10	2.421E+08	19.60		**0**	**10**	**2.500E+08**	**20.26**
0	4.641	2.030E+08	22.34		**0**	**4.641**	**2.084E+08**	**22.97**
0	2.154	1.664E+08	24.90		**0**	**2.154**	**1.699E+08**	**25.47**
0	1	1.318E+08	27.70		**0**	**1**	**1.340E+08**	**28.20**
0	0.4641	1.048E+08	30.45		**0**	**0.4641**	**1.061E+08**	**30.88**
0	0.2154	8.016E+07	33.43		**0**	**0.2154**	**8.091E+07**	**33.78**
0	0.1	5.989E+07	36.68		**0**	**0.1**	**6.029E+07**	**36.97**
0	0.04641	4.355E+07	40.06		**0**	**0.04641**	**4.375E+07**	**40.29**
0	0.02154	3.055E+07	43.89		**0**	**0.02154**	**3.065E+07**	**44.05**
0	0.01	2.095E+07	47.67		**0**	**0.01**	**2.099E+07**	**47.79**
-10	10	4.612E+08	9.67		**-10**	**10**	**4.921E+08**	**10.33**
-10	4.641	4.233E+08	11.45		**-10**	**4.641**	**4.491E+08**	**12.16**
-10	2.154	3.894E+08	13.12		**-10**	**2.154**	**4.109E+08**	**13.86**
-10	1	3.436E+08	14.91		**-10**	**1**	**3.601E+08**	**15.64**
-10	0.4641	2.973E+08	16.86		**-10**	**0.4641**	**3.094E+08**	**17.57**
-10	0.2154	2.557E+08	18.84		**-10**	**0.2154**	**2.646E+08**	**19.52**
-10	0.1	2.162E+08	21.37		**-10**	**0.1**	**2.223E+08**	**22.01**
-10	0.04641	1.816E+08	23.76		**-10**	**0.04641**	**1.859E+08**	**24.35**
-10	0.02154	1.463E+08	27.19		**-10**	**0.02154**	**1.489E+08**	**27.73**
-10	0.01	1.154E+08	29.54		**-10**	**0.01**	**1.170E+08**	**30.00**
-20	10	6.426E+08	4.74		**-20**	**10**	**7.051E+08**	**5.20**
-20	4.641	6.169E+08	5.79		**-20**	**4.641**	**6.742E+08**	**6.33**
-20	2.154	5.904E+08	6.79		**-20**	**2.154**	**6.426E+08**	**7.40**
-20	1	5.527E+08	7.92		**-20**	**1**	**5.979E+08**	**8.57**
-20	0.4641	5.148E+08	9.05		**-20**	**0.4641**	**5.537E+08**	**9.74**
-20	0.2155	4.749E+08	10.32		**-20**	**0.2155**	**5.077E+08**	**11.04**
-20	0.1	4.333E+08	11.80		**-20**	**0.1**	**4.602E+08**	**12.55**
-20	0.04642	3.975E+08	12.76		**-20**	**0.02154**	**3.659E+08**	**15.85**
-20	0.02154	3.488E+08	15.09		**-20**	**0.01**	**3.218E+08**	**18.16**
-20	0.01	3.087E+08	17.39		**-30**	**10**	**8.557E+08**	**2.82**
-30	10	7.651E+08	2.52		**-30**	**4.641**	**8.320E+08**	**3.47**
-30	4.641	7.462E+08	3.11		**-30**	**2.154**	**8.116E+08**	**4.11**
-30	2.154	7.298E+08	3.70		**-30**	**1**	**7.919E+08**	**4.74**
-30	1	7.139E+08	4.27		**-30**	**0.4641**	**7.477E+08**	**5.56**
-30	0.4641	6.778E+08	5.04		**-30**	**0.2155**	**7.123E+08**	**6.65**
-30	0.2155	6.487E+08	6.05		**-30**	**0.1**	**6.733E+08**	**7.79**
-30	0.1	6.164E+08	7.13		**-30**	**0.01**	**5.344E+08**	**11.75**
-30	0.04642	6.096E+08	5.89		**-40**	**10**	**9.552E+08**	**1.39**
-30	0.02154	5.503E+08	8.57		**-40**	**4.641**	**9.492E+08**	**1.96**
-30	0.01	4.983E+08	10.94		**-40**	**2.154**	**9.321E+08**	**2.40**
-40	10	8.437E+08	1.23		**-40**	**1**	**9.251E+08**	**2.72**
-40	4.641	8.390E+08	1.74		**-40**	**0.4641**	**8.895E+08**	**3.27**
-40	2.154	8.257E+08	2.13		**-40**	**0.1**	**8.341E+08**	**4.38**
-40	1	8.201E+08	2.41		**-40**	**0.02154**	**7.925E+08**	**5.68**
-40	0.4641	7.921E+08	2.91		**-40**	**0.01**	**7.623E+08**	**6.85**
-40	0.2155	7.658E+08	2.78					
-40	0.1	7.480E+08	3.93					
-40	0.04642	7.440E+08	5.52					
-40	0.02154	7.145E+08	5.12					
-40	0.01	6.899E+08	6.20					

B-12								
T	*f*	*G**	*δ*		***T***	***f***	***G****	***δ***
[°C]	[Hz]	[Pa]	[°]		**[°C]**	**[Hz]**	**[Pa]**	**[°]**
10	10	8.065E+07	31.50		**10**	**10**	**8.142E+07**	**31.84**
10	4.641	6.157E+07	34.04		**10**	**4.641**	**6.201E+07**	**34.32**
10	2.154	4.586E+07	36.86		**10**	**2.154**	**4.609E+07**	**37.08**
10	1	3.334E+07	39.79		**10**	**1**	**3.346E+07**	**39.96**
10	0.4641	2.365E+07	42.91		**10**	**0.4641**	**2.370E+07**	**43.04**
10	0.2154	1.641E+07	46.19		**10**	**0.2154**	**1.643E+07**	**46.28**
10	0.1	1.114E+07	49.57		**10**	**0.1**	**1.115E+07**	**49.63**
10	0.04641	7.260E+06	53.15		**10**	**0.04641**	**7.264E+06**	**53.19**
10	0.02154	4.602E+06	56.80		**10**	**0.02154**	**4.604E+06**	**56.83**
10	0.01	2.862E+06	60.28		**10**	**0.01**	**2.863E+06**	**60.30**
0	10	2.300E+08	19.82		**0**	**10**	**2.371E+08**	**20.46**
0	4.641	1.937E+08	21.70		**0**	**4.641**	**1.987E+08**	**22.28**
0	2.154	1.599E+08	23.84		**0**	**2.154**	**1.632E+08**	**24.36**
0	1	1.300E+08	26.05		**0**	**1**	**1.321E+08**	**26.51**
0	0.4641	1.033E+08	28.46		**0**	**0.4641**	**1.046E+08**	**28.85**
0	0.2154	8.062E+07	30.89		**0**	**0.2154**	**8.140E+07**	**31.22**
0	0.1	6.181E+07	33.66		**0**	**0.1**	**6.226E+07**	**33.93**
0	0.04641	4.630E+07	36.43		**0**	**0.04641**	**4.654E+07**	**36.65**
0	0.02154	3.366E+07	39.81		**0**	**0.02154**	**3.378E+07**	**39.98**
0	0.01	2.409E+07	43.20		**0**	**0.01**	**2.415E+07**	**43.33**
-10	10	4.781E+08	10.76		**-10**	**10**	**5.113E+08**	**11.51**
-10	4.641	4.358E+08	12.15		**-10**	**4.641**	**4.630E+08**	**12.92**
-10	2.154	3.914E+08	13.67		**-10**	**2.154**	**4.131E+08**	**14.44**
-10	1	3.381E+08	15.37		**-10**	**1**	**3.540E+08**	**16.11**
-10	0.4641	3.031E+08	16.99		**-10**	**0.4641**	**3.158E+08**	**17.72**
-10	0.2154	2.612E+08	18.54		**-10**	**0.2154**	**2.704E+08**	**19.22**
-10	0.1	2.206E+08	20.44		**-10**	**0.1**	**2.271E+08**	**21.07**
-10	0.04641	1.879E+08	23.38		**-10**	**0.04641**	**1.925E+08**	**23.98**
-10	0.02154	1.515E+08	24.98		**-10**	**0.02154**	**1.544E+08**	**25.50**
-10	0.01	1.223E+08	27.75		**-10**	**0.01**	**1.241E+08**	**28.21**
-20	10	6.977E+08	5.57		**-20**	**10**	**7.719E+08**	**6.17**
-20	4.641	6.636E+08	6.70		**-20**	**4.641**	**7.302E+08**	**7.38**
-20	2.154	6.251E+08	7.72		**-20**	**2.154**	**6.836E+08**	**8.45**
-20	1	5.763E+08	8.82		**-20**	**1**	**6.256E+08**	**9.58**
-20	0.4641	5.370E+08	9.96		**-20**	**0.4641**	**5.794E+08**	**10.75**
-20	0.2155	4.932E+08	11.31		**-20**	**0.2155**	**5.285E+08**	**12.14**
-20	0.1	4.461E+08	12.65		**-20**	**0.1**	**4.747E+08**	**13.48**
-20	0.04642	4.075E+08	12.97		**-20**	**0.02154**	**3.758E+08**	**16.81**
-20	0.02154	3.579E+08	15.98		**-20**	**0.01**	**3.311E+08**	**18.02**
-20	0.01	3.173E+08	17.24		**-30**	**10**	**9.543E+08**	**3.47**
-30	10	8.431E+08	3.07		**-30**	**4.641**	**9.277E+08**	**4.24**
-30	4.641	8.224E+08	3.76		**-30**	**2.154**	**8.911E+08**	**5.03**
-30	2.154	7.935E+08	4.48		**-30**	**1**	**8.458E+08**	**6.13**
-30	1	7.576E+08	5.49		**-30**	**0.4641**	**8.148E+08**	**6.50**
-30	0.4641	7.326E+08	5.85		**-30**	**0.2155**	**7.674E+08**	**7.86**
-30	0.2155	6.942E+08	7.11		**-30**	**0.1**	**7.176E+08**	**8.94**
-30	0.1	6.534E+08	8.14		**-30**	**0.01**	**5.472E+08**	**13.27**
-30	0.04642	6.250E+08	8.13		**-40**	**10**	**1.093E+09**	**2.02**
-30	0.02154	5.712E+08	9.01		**-40**	**4.641**	**1.074E+09**	**2.51**
-30	0.01	5.096E+08	12.34		**-40**	**2.154**	**1.048E+09**	**2.97**
-40	10	9.495E+08	1.75		**-40**	**1**	**1.011E+09**	**3.47**
-40	4.641	9.353E+08	2.18		**-40**	**0.4641**	**9.887E+08**	**4.06**
-40	2.154	9.150E+08	2.60		**-40**	**0.1**	**9.193E+08**	**5.65**
-40	1	8.871E+08	3.05		**-40**	**0.01**	**7.983E+08**	**8.89**
-40	0.4641	8.699E+08	3.57					
-40	0.2155	8.382E+08	2.44					
-40	0.1	8.159E+08	5.01					
-40	0.04642	7.849E+08	5.02					
-40	0.02154	7.583E+08	5.41					
-40	0.01	7.196E+08	8.01					

B-13								
T	*f*	*G**	*δ*		***T***	***f***	***G****	***δ***
[°C]	[Hz]	[Pa]	[°]		**[°C]**	**[Hz]**	**[Pa]**	**[°]**
10	10	6.709E+07	33.08		**10**	**10**	**6.762E+07**	**33.37**
10	4.641	5.022E+07	35.89		**10**	**4.641**	**5.050E+07**	**36.13**
10	2.154	3.683E+07	38.58		**10**	**2.154**	**3.698E+07**	**38.77**
10	1	2.636E+07	41.39		**10**	**1**	**2.644E+07**	**41.52**
10	0.4641	1.845E+07	44.32		**10**	**0.4641**	**1.848E+07**	**44.42**
10	0.2154	1.264E+07	47.29		**10**	**0.2154**	**1.266E+07**	**47.37**
10	0.1	8.486E+06	50.37		**10**	**0.1**	**8.493E+06**	**50.42**
10	0.04641	5.489E+06	53.59		**10**	**0.04641**	**5.492E+06**	**53.63**
10	0.02154	3.482E+06	56.87		**10**	**0.02154**	**3.483E+06**	**56.89**
10	0.01	2.167E+06	60.04		**10**	**0.01**	**2.167E+06**	**60.05**
0	10	1.997E+08	21.73		**0**	**10**	**2.049E+08**	**22.33**
0	4.641	1.646E+08	24.08		**0**	**4.641**	**1.681E+08**	**24.62**
0	2.154	1.334E+08	26.26		**0**	**2.154**	**1.356E+08**	**26.74**
0	1	1.061E+08	28.46		**0**	**1**	**1.074E+08**	**28.87**
0	0.4641	8.243E+07	30.87		**0**	**0.4641**	**8.324E+07**	**31.21**
0	0.2154	6.299E+07	33.41		**0**	**0.2154**	**6.345E+07**	**33.68**
0	0.1	4.733E+07	35.97		**0**	**0.1**	**4.759E+07**	**36.19**
0	0.04641	3.471E+07	38.98		**0**	**0.04641**	**3.484E+07**	**39.15**
0	0.02154	2.496E+07	41.83		**0**	**0.02154**	**2.503E+07**	**41.97**
0	0.01	1.744E+07	44.95		**0**	**0.01**	**1.747E+07**	**45.05**
-10	10	4.465E+08	12.54		**-10**	**10**	**4.751E+08**	**13.36**
-10	4.641	3.995E+08	14.22		**-10**	**4.641**	**4.221E+08**	**15.04**
-10	2.154	3.522E+08	15.88		**-10**	**2.154**	**3.695E+08**	**16.68**
-10	1	3.029E+08	17.49		**-10**	**1**	**3.155E+08**	**18.25**
-10	0.4641	2.612E+08	19.38		**-10**	**0.4641**	**2.704E+08**	**20.09**
-10	0.2154	2.207E+08	21.20		**-10**	**0.2154**	**2.272E+08**	**21.85**
-10	0.1	1.839E+08	23.01		**-10**	**0.1**	**1.883E+08**	**23.60**
-10	0.04641	1.488E+08	24.22		**-10**	**0.04641**	**1.516E+08**	**24.72**
-10	0.02154	1.195E+08	27.98		**-10**	**0.02154**	**1.212E+08**	**28.43**
-10	0.01	9.513E+07	30.55		**-10**	**0.01**	**9.622E+07**	**30.94**
-20	10	6.855E+08	7.03		**-20**	**10**	**7.567E+08**	**7.77**
-20	4.641	6.458E+08	8.22		**-20**	**4.641**	**7.085E+08**	**9.02**
-20	2.154	6.007E+08	9.42		**-20**	**2.154**	**6.543E+08**	**10.27**
-20	1	5.485E+08	10.79		**-20**	**1**	**5.926E+08**	**11.67**
-20	0.4641	5.029E+08	11.96		**-20**	**0.4641**	**5.396E+08**	**12.84**
-20	0.2155	4.454E+08	12.84		**-20**	**0.2155**	**4.739E+08**	**13.68**
-20	0.1	4.021E+08	14.84		**-20**	**0.1**	**4.249E+08**	**15.70**
-20	0.04642	3.566E+08	15.28		**-20**	**0.02154**	**3.257E+08**	**19.45**
-20	0.02154	3.124E+08	18.63		**-20**	**0.01**	**2.742E+08**	**21.87**
-20	0.01	2.648E+08	21.09		**-30**	**10**	**9.808E+08**	**4.46**
-30	10	8.638E+08	3.93		**-30**	**4.641**	**9.497E+08**	**5.32**
-30	4.641	8.397E+08	4.70		**-30**	**2.154**	**8.954E+08**	**6.20**
-30	2.154	7.971E+08	5.51		**-30**	**1**	**8.489E+08**	**7.17**
-30	1	7.602E+08	6.42		**-30**	**0.4641**	**8.076E+08**	**8.09**
-30	0.4641	7.271E+08	7.27		**-30**	**0.1**	**6.893E+08**	**10.50**
-30	0.2155	6.626E+08	7.39		**-30**	**0.04642**	**6.402E+08**	**11.44**
-30	0.1	6.301E+08	9.59		**-30**	**0.02154**	**5.895E+08**	**12.44**
-30	0.04642	5.890E+08	10.52		**-30**	**0.01**	**5.228E+08**	**14.71**
-30	0.02154	5.459E+08	11.51		**-40**	**10**	**1.149E+09**	**2.35**
-30	0.01	4.885E+08	13.72		**-40**	**4.641**	**1.126E+09**	**3.08**
-40	10	9.911E+08	2.03		**-40**	**2.154**	**1.087E+09**	**3.68**
-40	4.641	9.745E+08	2.66		**-40**	**1**	**1.061E+09**	**4.41**
-40	2.154	9.450E+08	3.20		**-40**	**0.4641**	**1.027E+09**	**4.96**
-40	1	9.257E+08	3.84		**-40**	**0.2155**	**9.511E+08**	**5.53**
-40	0.4641	8.999E+08	4.34		**-40**	**0.1**	**9.336E+08**	**6.31**
-40	0.2155	8.409E+08	4.89		**-40**	**0.04642**	**8.824E+08**	**7.56**
-40	0.1	8.272E+08	5.59		**-40**	**0.01**	**7.345E+08**	**10.64**
-40	0.04642	7.870E+08	6.74					
-40	0.02154	7.642E+08	7.21					
-40	0.01	6.677E+08	9.67					

B-14								
T	*f*	*G**	*δ*		***T***	***f***	***G****	***δ***
[°C]	[Hz]	[Pa]	[°]		**[°C]**	**[Hz]**	**[Pa]**	**[°]**
10	10	5.005E+07	35.07		**10**	**10**	**5.033E+07**	**35.30**
10	4.641	3.693E+07	37.45		**10**	**4.641**	**3.708E+07**	**37.63**
10	2.154	2.671E+07	39.84		**10**	**2.154**	**2.679E+07**	**39.97**
10	1	1.894E+07	42.30		**10**	**1**	**1.898E+07**	**42.41**
10	0.4641	1.318E+07	44.83		**10**	**0.4641**	**1.319E+07**	**44.91**
10	0.2154	8.997E+06	47.44		**10**	**0.2154**	**9.004E+06**	**47.49**
10	0.1	6.050E+06	50.08		**10**	**0.1**	**6.054E+06**	**50.11**
10	0.04641	3.941E+06	52.83		**10**	**0.04641**	**3.942E+06**	**52.85**
10	0.02154	2.509E+06	55.78		**10**	**0.02154**	**2.510E+06**	**55.80**
10	0.01	1.576E+06	58.61		**10**	**0.01**	**1.576E+06**	**58.62**
0	10	1.571E+08	24.13		**0**	**10**	**1.603E+08**	**24.65**
0	4.641	1.275E+08	26.36		**0**	**4.641**	**1.295E+08**	**26.82**
0	2.154	1.009E+08	28.43		**0**	**2.154**	**1.022E+08**	**28.81**
0	1	7.872E+07	30.52		**0**	**1**	**7.946E+07**	**30.84**
0	0.4641	6.042E+07	32.67		**0**	**0.4641**	**6.085E+07**	**32.94**
0	0.2154	4.553E+07	34.87		**0**	**0.2154**	**4.577E+07**	**35.07**
0	0.1	3.362E+07	37.17		**0**	**0.1**	**3.374E+07**	**37.33**
0	0.04641	2.446E+07	39.63		**0**	**0.04641**	**2.452E+07**	**39.75**
0	0.02154	1.740E+07	42.21		**0**	**0.02154**	**1.743E+07**	**42.30**
0	0.01	1.217E+07	45.08		**0**	**0.01**	**1.218E+07**	**45.15**
-10	10	3.967E+08	14.26		**-10**	**10**	**4.190E+08**	**15.08**
-10	4.641	3.498E+08	16.24		**-10**	**4.641**	**3.668E+08**	**17.05**
-10	2.154	3.016E+08	17.98		**-10**	**2.154**	**3.141E+08**	**18.75**
-10	1	2.525E+08	19.60		**-10**	**1**	**2.611E+08**	**20.30**
-10	0.4641	2.169E+08	21.59		**-10**	**0.4641**	**2.231E+08**	**22.24**
-10	0.2154	1.790E+08	23.55		**-10**	**0.2154**	**1.832E+08**	**24.13**
-10	0.1	1.464E+08	25.42		**-10**	**0.1**	**1.491E+08**	**25.93**
-10	0.04641	1.176E+08	26.90		**-10**	**0.04641**	**1.194E+08**	**27.33**
-10	0.02154	9.166E+07	29.78		**-10**	**0.02154**	**9.268E+07**	**30.15**
-10	0.01	7.129E+07	32.30		**-10**	**0.01**	**7.189E+07**	**32.60**
-20	10	6.395E+08	8.34		**-20**	**10**	**7.008E+08**	**9.15**
-20	4.641	5.944E+08	9.70		**-20**	**4.641**	**6.468E+08**	**10.56**
-20	2.154	5.459E+08	11.05		**-20**	**2.154**	**5.896E+08**	**11.94**
-20	1	4.937E+08	12.41		**-20**	**1**	**5.290E+08**	**13.31**
-20	0.4641	4.419E+08	13.90		**-20**	**0.4641**	**4.698E+08**	**14.80**
-20	0.2155	3.902E+08	14.94		**-20**	**0.2155**	**4.116E+08**	**15.78**
-20	0.1	3.415E+08	16.92		**-20**	**0.1**	**3.576E+08**	**17.74**
-20	0.04642	2.950E+08	18.86		**-20**	**0.04642**	**3.069E+08**	**19.65**
-20	0.02154	2.506E+08	21.07		**-20**	**0.02154**	**2.589E+08**	**21.81**
-20	0.01	2.098E+08	22.70		**-20**	**0.01**	**2.155E+08**	**23.36**
-30	10	8.295E+08	4.80		**-30**	**10**	**9.366E+08**	**5.42**
-30	4.641	7.984E+08	5.65		**-30**	**4.641**	**8.970E+08**	**6.36**
-30	2.154	7.595E+08	6.61		**-30**	**2.154**	**8.481E+08**	**7.38**
-30	1	7.058E+08	7.62		**-30**	**1**	**7.814E+08**	**8.44**
-30	0.4641	6.689E+08	8.71		**-30**	**0.4641**	**7.362E+08**	**9.59**
-30	0.2155	6.184E+08	9.89		**-30**	**0.2155**	**6.753E+08**	**10.81**
-30	0.1	5.638E+08	11.35		**-30**	**0.1**	**6.105E+08**	**12.31**
-30	0.04642	5.235E+08	9.68		**-30**	**0.02154**	**4.945E+08**	**15.15**
-30	0.02154	4.638E+08	14.19		**-30**	**0.01**	**4.316E+08**	**16.72**
-30	0.01	4.082E+08	15.79		**-40**	**10**	**1.118E+09**	**2.93**
-40	10	9.687E+08	2.54		**-40**	**4.641**	**1.093E+09**	**3.74**
-40	4.641	9.494E+08	3.25		**-40**	**2.154**	**1.042E+09**	**4.38**
-40	2.154	9.107E+08	3.83		**-40**	**1**	**1.001E+09**	**5.17**
-40	1	8.795E+08	4.54		**-40**	**0.4641**	**9.699E+08**	**6.01**
-40	0.4641	8.556E+08	5.30		**-40**	**0.1**	**8.676E+08**	**7.88**
-40	0.2155	8.058E+08	4.50		**-40**	**0.04642**	**8.054E+08**	**8.42**
-40	0.1	7.752E+08	7.04		**-40**	**0.02154**	**7.651E+08**	**9.93**
-40	0.04642	7.253E+08	7.58		**-40**	**0.01**	**6.968E+08**	**12.11**
-40	0.02154	6.927E+08	8.99					
-40	0.01	6.366E+08	11.05					

B-15								
T	*f*	*G**	*δ*		***T***	***f***	***G****	***δ***
[°C]	[Hz]	[Pa]	[°]		**[°C]**	**[Hz]**	**[Pa]**	**[°]**
10	10	7.278E+07	34.31		**10**	**10**	**7.339E+07**	**34.63**
10	4.641	5.388E+07	37.27		**10**	**4.641**	**5.420E+07**	**37.53**
10	2.154	3.892E+07	40.16		**10**	**2.154**	**3.908E+07**	**40.36**
10	1	2.745E+07	43.14		**10**	**1**	**2.753E+07**	**43.29**
10	0.4641	1.890E+07	46.20		**10**	**0.4641**	**1.893E+07**	**46.31**
10	0.2154	1.266E+07	49.36		**10**	**0.2154**	**1.268E+07**	**49.44**
10	0.1	8.269E+06	52.62		**10**	**0.1**	**8.275E+06**	**52.67**
10	0.04641	5.277E+06	55.88		**10**	**0.04641**	**5.279E+06**	**55.92**
10	0.02154	3.289E+06	59.12		**10**	**0.02154**	**3.290E+06**	**59.15**
10	0.01	1.996E+06	62.34		**10**	**0.01**	**1.996E+06**	**62.35**
0	10	2.220E+08	22.07		**0**	**10**	**2.285E+08**	**22.75**
0	4.641	1.822E+08	24.21		**0**	**4.641**	**1.865E+08**	**24.82**
0	2.154	1.469E+08	26.61		**0**	**2.154**	**1.496E+08**	**27.14**
0	1	1.171E+08	29.05		**0**	**1**	**1.188E+08**	**29.51**
0	0.4641	9.035E+07	31.63		**0**	**0.4641**	**9.132E+07**	**32.01**
0	0.2154	6.846E+07	34.30		**0**	**0.2154**	**6.900E+07**	**34.61**
0	0.1	5.089E+07	37.01		**0**	**0.1**	**5.118E+07**	**37.25**
0	0.04641	3.707E+07	40.01		**0**	**0.04641**	**3.721E+07**	**40.20**
0	0.02154	2.623E+07	43.08		**0**	**0.02154**	**2.630E+07**	**43.23**
0	0.01	1.817E+07	46.36		**0**	**0.01**	**1.820E+07**	**46.46**
-10	10	4.985E+08	11.39		**-10**	**10**	**5.346E+08**	**12.22**
-10	4.641	4.488E+08	13.22		**-10**	**4.641**	**4.776E+08**	**14.08**
-10	2.154	3.991E+08	14.96		**-10**	**2.154**	**4.216E+08**	**15.82**
-10	1	3.409E+08	16.83		**-10**	**1**	**3.570E+08**	**17.65**
-10	0.4641	3.017E+08	18.71		**-10**	**0.4641**	**3.141E+08**	**19.51**
-10	0.2154	2.556E+08	20.69		**-10**	**0.2154**	**2.643E+08**	**21.43**
-10	0.1	2.140E+08	23.27		**-10**	**0.1**	**2.200E+08**	**23.96**
-10	0.04641	1.731E+08	24.30		**-10**	**0.04641**	**1.770E+08**	**24.88**
-10	0.02154	1.391E+08	28.08		**-10**	**0.02154**	**1.415E+08**	**28.61**
-10	0.01	1.081E+08	30.72		**-10**	**0.01**	**1.095E+08**	**31.16**
-20	10	7.338E+08	6.18		**-20**	**10**	**8.161E+08**	**6.88**
-20	4.641	6.958E+08	7.16		**-20**	**4.641**	**7.693E+08**	**7.92**
-20	2.154	6.495E+08	8.29		**-20**	**2.154**	**7.128E+08**	**9.10**
-20	1	6.020E+08	9.54		**-20**	**1**	**6.559E+08**	**10.40**
-20	0.4641	5.566E+08	10.91		**-20**	**0.4641**	**6.020E+08**	**11.81**
-20	0.2155	4.965E+08	10.93		**-20**	**0.1**	**4.820E+08**	**14.84**
-20	0.1	4.527E+08	13.92		**-20**	**0.04642**	**4.363E+08**	**16.23**
-20	0.04642	4.123E+08	15.31		**-20**	**0.02154**	**3.696E+08**	**18.74**
-20	0.02154	3.525E+08	17.84		**-20**	**0.01**	**3.131E+08**	**20.34**
-20	0.01	3.009E+08	19.51		**-30**	**10**	**1.022E+09**	**3.57**
-30	10	8.957E+08	3.12		**-30**	**4.641**	**9.935E+08**	**4.50**
-30	4.641	8.737E+08	3.95		**-30**	**2.154**	**9.391E+08**	**5.30**
-30	2.154	8.314E+08	4.69		**-30**	**1**	**9.027E+08**	**6.29**
-30	1	8.029E+08	5.59		**-30**	**0.4641**	**8.593E+08**	**7.09**
-30	0.4641	7.685E+08	6.33		**-30**	**0.2155**	**8.098E+08**	**8.38**
-30	0.2155	7.289E+08	7.54		**-30**	**0.1**	**7.525E+08**	**9.35**
-30	0.1	6.822E+08	8.47		**-30**	**0.02154**	**6.463E+08**	**12.01**
-30	0.04642	6.676E+08	10.76		**-30**	**0.01**	**5.725E+08**	**14.24**
-30	0.02154	5.942E+08	11.03		**-40**	**10**	**1.173E+09**	**2.17**
-30	0.01	5.315E+08	13.20		**-40**	**4.641**	**1.151E+09**	**2.60**
-40	10	1.010E+09	1.87		**-40**	**2.154**	**1.108E+09**	**3.08**
-40	4.641	9.927E+08	2.24		**-40**	**1**	**1.090E+09**	**3.62**
-40	2.154	9.611E+08	2.67		**-40**	**0.4641**	**1.062E+09**	**4.29**
-40	1	9.469E+08	3.14		**-40**	**0.1**	**9.784E+08**	**5.88**
-40	0.4641	9.264E+08	3.74		**-40**	**0.01**	**8.526E+08**	**9.40**
-40	0.2155	8.914E+08	3.69					
-40	0.1	8.621E+08	5.18					
-40	0.04642	8.120E+08	5.49					
-40	0.02154	7.874E+08	5.86					
-40	0.01	7.635E+08	8.41					

B-16								
T	*f*	*G**	*δ*		***T***	***f***	***G****	***δ***
[°C]	[Hz]	[Pa]	[°]		**[°C]**	**[Hz]**	**[Pa]**	**[°]**
10	10	7.321E+07	35.78		**10**	**10**	**7.381E+07**	**36.12**
10	4.641	5.359E+07	38.98		**10**	**4.641**	**5.390E+07**	**39.25**
10	2.154	3.806E+07	42.23		**10**	**2.154**	**3.821E+07**	**42.43**
10	1	2.631E+07	45.59		**10**	**1**	**2.637E+07**	**45.73**
10	0.4641	1.767E+07	49.02		**10**	**0.4641**	**1.770E+07**	**49.12**
10	0.2154	1.156E+07	52.52		**10**	**0.2154**	**1.157E+07**	**52.60**
10	0.1	7.358E+06	56.05		**10**	**0.1**	**7.362E+06**	**56.10**
10	0.04641	4.548E+06	59.58		**10**	**0.04641**	**4.550E+06**	**59.61**
10	0.02154	2.725E+06	62.96		**10**	**0.02154**	**2.725E+06**	**62.97**
10	0.01	1.589E+06	66.19		**10**	**0.01**	**1.589E+06**	**66.20**
0	10	2.295E+08	21.92		**0**	**10**	**2.364E+08**	**22.62**
0	4.641	1.885E+08	24.58		**0**	**4.641**	**1.931E+08**	**25.22**
0	2.154	1.518E+08	27.23		**0**	**2.154**	**1.547E+08**	**27.79**
0	1	1.192E+08	29.91		**0**	**1**	**1.209E+08**	**30.39**
0	0.4641	9.176E+07	32.77		**0**	**0.4641**	**9.274E+07**	**33.17**
0	0.2154	6.879E+07	35.76		**0**	**0.2154**	**6.932E+07**	**36.08**
0	0.1	5.046E+07	38.80		**0**	**0.1**	**5.074E+07**	**39.05**
0	0.04641	3.600E+07	42.22		**0**	**0.04641**	**3.613E+07**	**42.41**
0	0.02154	2.500E+07	45.57		**0**	**0.02154**	**2.506E+07**	**45.71**
0	0.01	1.689E+07	49.18		**0**	**0.01**	**1.691E+07**	**49.28**
-10	10	5.069E+08	10.93		**-10**	**10**	**5.444E+08**	**11.75**
-10	4.641	4.592E+08	12.87		**-10**	**4.641**	**4.895E+08**	**13.74**
-10	2.154	4.100E+08	14.69		**-10**	**2.154**	**4.338E+08**	**15.57**
-10	1	3.521E+08	16.71		**-10**	**1**	**3.693E+08**	**17.55**
-10	0.4641	3.107E+08	18.65		**-10**	**0.4641**	**3.239E+08**	**19.47**
-10	0.2154	2.607E+08	20.46		**-10**	**0.2154**	**2.698E+08**	**21.20**
-10	0.1	2.188E+08	23.38		**-10**	**0.1**	**2.250E+08**	**24.08**
-10	0.04641	1.755E+08	26.31		**-10**	**0.04641**	**1.794E+08**	**26.94**
-10	0.02154	1.411E+08	27.83		**-10**	**0.02154**	**1.436E+08**	**28.36**
-10	0.01	1.111E+08	31.45		**-10**	**0.01**	**1.126E+08**	**31.92**
-20	10	7.358E+08	5.63		**-20**	**10**	**8.188E+08**	**6.27**
-20	4.641	6.992E+08	6.76		**-20**	**4.641**	**7.735E+08**	**7.49**
-20	2.154	6.577E+08	7.92		**-20**	**2.154**	**7.228E+08**	**8.71**
-20	1	6.083E+08	9.21		**-20**	**1**	**6.634E+08**	**10.05**
-20	0.4641	5.658E+08	10.54		**-20**	**0.4641**	**6.130E+08**	**11.43**
-20	0.2155	5.104E+08	10.82		**-20**	**0.1**	**4.955E+08**	**14.87**
-20	0.1	4.647E+08	13.92		**-20**	**0.04642**	**4.447E+08**	**16.82**
-20	0.04642	4.199E+08	15.85		**-20**	**0.02154**	**3.822E+08**	**18.43**
-20	0.02154	3.639E+08	17.51		**-20**	**0.01**	**3.277E+08**	**20.69**
-20	0.01	3.143E+08	19.81		**-30**	**10**	**1.015E+09**	**3.37**
-30	10	8.902E+08	2.95		**-30**	**4.641**	**9.827E+08**	**4.13**
-30	4.641	8.652E+08	3.64		**-30**	**2.154**	**9.502E+08**	**4.94**
-30	2.154	8.400E+08	4.37		**-30**	**1**	**8.969E+08**	**5.86**
-30	1	7.982E+08	5.21		**-30**	**0.4641**	**8.625E+08**	**6.70**
-30	0.4641	7.710E+08	5.98		**-30**	**0.2155**	**8.164E+08**	**7.77**
-30	0.2155	7.342E+08	6.99		**-30**	**0.1**	**7.602E+08**	**8.93**
-30	0.1	6.885E+08	8.09		**-30**	**0.02154**	**6.558E+08**	**11.67**
-30	0.04642	6.263E+08	10.98		**-30**	**0.01**	**5.777E+08**	**13.56**
-30	0.02154	6.022E+08	10.70		**-40**	**10**	**1.155E+09**	**1.96**
-30	0.01	5.359E+08	12.57		**-40**	**4.641**	**1.138E+09**	**2.36**
-40	10	9.959E+08	1.69		**-40**	**2.154**	**1.107E+09**	**2.88**
-40	4.641	9.832E+08	2.04		**-40**	**1**	**1.065E+09**	**3.54**
-40	2.154	9.600E+08	2.49		**-40**	**0.4641**	**1.052E+09**	**3.90**
-40	1	9.282E+08	3.09		**-40**	**0.1**	**9.703E+08**	**5.65**
-40	0.4641	9.186E+08	3.40		**-40**	**0.04642**	**9.342E+08**	**6.68**
-40	0.2155	8.889E+08	3.72		**-40**	**0.02154**	**8.838E+08**	**7.91**
-40	0.1	8.558E+08	4.98					
-40	0.04642	8.278E+08	5.92					
-40	0.02154	7.882E+08	7.05					
-40	0.01	7.787E+08	7.45					

B-17								
T	*f*	*G**	*δ*		***T***	***f***	***G****	***δ***
[°C]	[Hz]	[Pa]	[°]		**[°C]**	**[Hz]**	**[Pa]**	**[°]**
10	10	4.105E+07	36.98		**10**	**10**	**4.123E+07**	**37.18**
10	4.641	2.969E+07	39.63		**10**	**4.641**	**2.979E+07**	**39.78**
10	2.154	2.101E+07	42.13		**10**	**2.154**	**2.105E+07**	**42.24**
10	1	1.455E+07	44.67		**10**	**1**	**1.457E+07**	**44.75**
10	0.4641	9.876E+06	47.27		**10**	**0.4641**	**9.885E+06**	**47.32**
10	0.2154	6.563E+06	49.90		**10**	**0.2154**	**6.566E+06**	**49.94**
10	0.1	4.295E+06	52.53		**10**	**0.1**	**4.297E+06**	**52.56**
10	0.04641	2.722E+06	55.14		**10**	**0.04641**	**2.723E+06**	**55.16**
10	0.02154	1.683E+06	57.66		**10**	**0.02154**	**1.683E+06**	**57.67**
10	0.01	1.027E+06	60.13		**10**	**0.01**	**1.027E+06**	**60.13**
0	10	1.343E+08	25.83		**0**	**10**	**1.366E+08**	**26.30**
0	4.641	1.071E+08	28.25		**0**	**4.641**	**1.085E+08**	**28.66**
0	2.154	8.351E+07	30.47		**0**	**2.154**	**8.434E+07**	**30.81**
0	1	6.392E+07	32.71		**0**	**1**	**6.440E+07**	**32.99**
0	0.4641	4.801E+07	35.02		**0**	**0.4641**	**4.827E+07**	**35.24**
0	0.2154	3.541E+07	37.38		**0**	**0.2154**	**3.555E+07**	**37.55**
0	0.1	2.567E+07	39.82		**0**	**0.1**	**2.574E+07**	**39.95**
0	0.04641	1.826E+07	42.29		**0**	**0.04641**	**1.830E+07**	**42.39**
0	0.02154	1.266E+07	45.23		**0**	**0.02154**	**1.268E+07**	**45.30**
0	0.01	8.611E+06	47.85		**0**	**0.01**	**8.618E+06**	**47.90**
-10	10	3.428E+08	15.72		**-10**	**10**	**3.592E+08**	**16.49**
-10	4.641	3.003E+08	17.66		**-10**	**4.641**	**3.126E+08**	**18.41**
-10	2.154	2.566E+08	19.55		**-10**	**2.154**	**2.655E+08**	**20.26**
-10	1	2.083E+08	21.36		**-10**	**1**	**2.141E+08**	**21.98**
-10	0.4641	1.771E+08	23.43		**-10**	**0.4641**	**1.812E+08**	**24.00**
-10	0.2154	1.438E+08	25.51		**-10**	**0.2154**	**1.464E+08**	**26.01**
-10	0.1	1.155E+08	27.75		**-10**	**0.1**	**1.171E+08**	**28.18**
-10	0.04641	9.205E+07	29.65		**-10**	**0.04641**	**9.308E+07**	**30.02**
-10	0.02154	6.973E+07	32.25		**-10**	**0.02154**	**7.030E+07**	**32.55**
-10	0.01	5.280E+07	34.68		**-10**	**0.01**	**5.312E+07**	**34.92**
-20	10	5.668E+08	9.09		**-20**	**10**	**6.144E+08**	**9.86**
-20	4.641	5.239E+08	10.55		**-20**	**4.641**	**5.640E+08**	**11.37**
-20	2.154	4.772E+08	12.01		**-20**	**2.154**	**5.102E+08**	**12.85**
-20	1	4.301E+08	13.50		**-20**	**1**	**4.565E+08**	**14.35**
-20	0.4641	3.791E+08	15.18		**-20**	**0.4641**	**3.993E+08**	**16.01**
-20	0.2155	3.316E+08	15.89		**-20**	**0.1**	**2.990E+08**	**19.62**
-20	0.1	2.877E+08	18.85		**-20**	**0.04642**	**2.525E+08**	**21.36**
-20	0.04642	2.445E+08	20.65		**-20**	**0.02154**	**2.113E+08**	**23.05**
-20	0.02154	2.057E+08	22.41		**-20**	**0.01**	**1.707E+08**	**24.75**
-20	0.01	1.671E+08	24.20		**-30**	**10**	**8.318E+08**	**5.61**
-30	10	7.463E+08	5.03		**-30**	**4.641**	**7.922E+08**	**6.95**
-30	4.641	7.144E+08	6.27		**-30**	**2.154**	**7.415E+08**	**8.12**
-30	2.154	6.730E+08	7.36		**-30**	**1**	**6.823E+08**	**9.52**
-30	1	6.241E+08	8.70		**-30**	**0.4641**	**6.351E+08**	**10.53**
-30	0.4641	5.845E+08	9.68		**-30**	**0.2155**	**5.779E+08**	**11.95**
-30	0.2155	5.359E+08	11.07		**-30**	**0.1**	**5.206E+08**	**13.36**
-30	0.1	4.865E+08	12.46		**-30**	**0.02154**	**4.090E+08**	**16.44**
-30	0.04642	4.425E+08	15.63		**-30**	**0.01**	**3.550E+08**	**18.59**
-30	0.02154	3.879E+08	15.57		**-40**	**10**	**1.006E+09**	**3.31**
-30	0.01	3.391E+08	17.74		**-40**	**4.641**	**9.819E+08**	**4.10**
-40	10	8.830E+08	2.91		**-40**	**2.154**	**9.432E+08**	**4.87**
-40	4.641	8.646E+08	3.61		**-40**	**1**	**8.918E+08**	**5.70**
-40	2.154	8.346E+08	4.31		**-40**	**0.4641**	**8.617E+08**	**6.56**
-40	1	7.942E+08	5.07		**-40**	**0.2155**	**8.171E+08**	**7.54**
-40	0.4641	7.703E+08	5.86		**-40**	**0.1**	**7.632E+08**	**8.66**
-40	0.2155	7.346E+08	6.77		**-40**	**0.02154**	**6.736E+08**	**11.10**
-40	0.1	6.909E+08	7.83		**-40**	**0.01**	**5.906E+08**	**13.26**
-40	0.04642	6.709E+08	7.41					
-40	0.02154	6.171E+08	10.16					
-40	0.01	5.470E+08	12.27					

B-18								
T	*f*	*G**	*δ*		***T***	***f***	***G****	***δ***
[°C]	[Hz]	[Pa]	[°]		**[°C]**	**[Hz]**	**[Pa]**	**[°]**
10	10	5.938E+07	41.59		**10**	**10**	**5.975E+07**	**41.91**
10	4.641	4.124E+07	44.96		**10**	**4.641**	**4.141E+07**	**45.19**
10	2.154	2.772E+07	48.39		**10**	**2.154**	**2.780E+07**	**48.56**
10	1	1.809E+07	51.76		**10**	**1**	**1.812E+07**	**51.87**
10	0.4641	1.148E+07	55.01		**10**	**0.4641**	**1.149E+07**	**55.09**
10	0.2154	7.078E+06	58.13		**10**	**0.2154**	**7.082E+06**	**58.18**
10	0.1	4.253E+06	61.09		**10**	**0.1**	**4.254E+06**	**61.12**
10	0.04641	2.470E+06	63.81		**10**	**0.04641**	**2.470E+06**	**63.83**
10	0.02154	1.412E+06	66.32		**10**	**0.02154**	**1.412E+06**	**66.33**
10	0.01	7.939E+05	69.02		**10**	**0.01**	**7.940E+05**	**69.02**
0	10	2.125E+08	26.26		**0**	**10**	**2.183E+08**	**27.03**
0	4.641	1.675E+08	29.69		**0**	**4.641**	**1.709E+08**	**30.36**
0	2.154	1.288E+08	32.87		**0**	**2.154**	**1.308E+08**	**33.44**
0	1	9.573E+07	35.96		**0**	**1**	**9.676E+07**	**36.42**
0	0.4641	6.964E+07	39.39		**0**	**0.4641**	**7.016E+07**	**39.74**
0	0.2154	4.923E+07	42.72		**0**	**0.2154**	**4.948E+07**	**42.99**
0	0.1	3.366E+07	46.13		**0**	**0.1**	**3.377E+07**	**46.32**
0	0.04641	2.247E+07	49.55		**0**	**0.04641**	**2.252E+07**	**49.68**
0	0.02154	1.452E+07	52.69		**0**	**0.02154**	**1.454E+07**	**52.78**
0	0.01	9.100E+06	56.16		**0**	**0.01**	**9.107E+06**	**56.22**
-10	10	4.949E+08	12.83		**-10**	**10**	**5.302E+08**	**13.77**
-10	4.641	4.408E+08	15.31		**-10**	**4.641**	**4.684E+08**	**16.29**
-10	2.154	3.861E+08	17.72		**-10**	**2.154**	**4.068E+08**	**18.70**
-10	1	3.360E+08	20.12		**-10**	**1**	**3.513E+08**	**21.08**
-10	0.4641	2.726E+08	22.93		**-10**	**0.4641**	**2.824E+08**	**23.80**
-10	0.2154	2.217E+08	25.78		**-10**	**0.2154**	**2.279E+08**	**26.57**
-10	0.1	1.755E+08	29.00		**-10**	**0.1**	**1.793E+08**	**29.68**
-10	0.04641	1.377E+08	31.48		**-10**	**0.04641**	**1.399E+08**	**32.06**
-10	0.02154	1.029E+08	35.49		**-10**	**0.02154**	**1.041E+08**	**35.97**
-10	0.01	7.500E+07	38.44		**-10**	**0.01**	**7.561E+07**	**38.82**
-20	10	7.426E+08	6.03		**-20**	**10**	**8.271E+08**	**6.72**
-20	4.641	7.052E+08	7.21		**-20**	**4.641**	**7.807E+08**	**7.99**
-20	2.154	6.641E+08	8.62		**-20**	**2.154**	**7.304E+08**	**9.49**
-20	1	6.135E+08	10.21		**-20**	**1**	**6.694E+08**	**11.15**
-20	0.4641	5.591E+08	11.95		**-20**	**0.4641**	**6.048E+08**	**12.95**
-20	0.2155	5.023E+08	13.34		**-20**	**0.2155**	**5.386E+08**	**14.33**
-20	0.1	4.443E+08	15.95		**-20**	**0.1**	**4.722E+08**	**16.98**
-20	0.04642	4.048E+08	17.08		**-20**	**0.02154**	**3.473E+08**	**21.56**
-20	0.02154	3.324E+08	20.59		**-20**	**0.01**	**2.867E+08**	**24.29**
-20	0.01	2.766E+08	23.39		**-30**	**10**	**1.030E+09**	**3.29**
-30	10	9.015E+08	2.88		**-30**	**4.641**	**1.005E+09**	**4.05**
-30	4.641	8.823E+08	3.56		**-30**	**2.154**	**9.705E+08**	**4.93**
-30	2.154	8.559E+08	4.34		**-30**	**1**	**9.310E+08**	**5.93**
-30	1	8.252E+08	5.25		**-30**	**0.4641**	**8.755E+08**	**7.10**
-30	0.4641	7.815E+08	6.33		**-30**	**0.1**	**7.676E+08**	**9.98**
-30	0.2155	7.385E+08	6.79		**-30**	**0.02154**	**6.364E+08**	**13.95**
-30	0.1	6.948E+08	9.03		**-30**	**0.01**	**5.526E+08**	**16.48**
-30	0.04642	6.567E+08	9.73		**-40**	**10**	**1.169E+09**	**1.58**
-30	0.02154	5.861E+08	12.82		**-40**	**4.641**	**1.159E+09**	**2.11**
-30	0.01	5.147E+08	15.32		**-40**	**2.154**	**1.142E+09**	**2.60**
-40	10	1.006E+09	1.36		**-40**	**1**	**1.110E+09**	**3.18**
-40	4.641	9.987E+08	1.82		**-40**	**0.4641**	**1.079E+09**	**3.80**
-40	2.154	9.864E+08	2.24		**-40**	**0.2155**	**1.040E+09**	**4.42**
-40	1	9.625E+08	2.76		**-40**	**0.1**	**9.906E+08**	**5.41**
-40	0.4641	9.391E+08	3.30		**-40**	**0.04642**	**9.417E+08**	**6.47**
-40	0.2155	9.091E+08	3.86		**-40**	**0.02154**	**9.129E+08**	**7.35**
-40	0.1	8.715E+08	4.76		**-40**	**0.01**	**8.790E+08**	**8.65**
-40	0.04642	8.337E+08	5.72					
-40	0.02154	8.112E+08	6.52					
-40	0.01	7.845E+08	7.71					

B-19								
T	*f*	*G**	*δ*		***T***	***f***	***G****	***δ***
[°C]	[Hz]	[Pa]	[°]		**[°C]**	**[Hz]**	**[Pa]**	**[°]**
10	10	4.698E+07	33.42		**10**	**10**	**4.723E+07**	**33.62**
10	4.641	3.511E+07	35.88		**10**	**4.641**	**3.525E+07**	**36.04**
10	2.154	2.580E+07	38.22		**10**	**2.154**	**2.587E+07**	**38.34**
10	1	1.855E+07	40.63		**10**	**1**	**1.859E+07**	**40.72**
10	0.4641	1.309E+07	43.18		**10**	**0.4641**	**1.311E+07**	**43.25**
10	0.2154	9.075E+06	45.82		**10**	**0.2154**	**9.083E+06**	**45.87**
10	0.1	6.150E+06	48.59		**10**	**0.1**	**6.153E+06**	**48.62**
10	0.04641	4.060E+06	51.47		**10**	**0.04641**	**4.061E+06**	**51.50**
10	0.02154	2.627E+06	54.48		**10**	**0.02154**	**2.627E+06**	**54.50**
10	0.01	1.674E+06	56.87		**10**	**0.01**	**1.674E+06**	**56.88**
0	10	1.443E+08	23.46		**0**	**10**	**1.470E+08**	**23.93**
0	4.641	1.175E+08	25.25		**0**	**4.641**	**1.193E+08**	**25.65**
0	2.154	9.415E+07	27.18		**0**	**2.154**	**9.525E+07**	**27.53**
0	1	7.442E+07	29.16		**0**	**1**	**7.510E+07**	**29.45**
0	0.4641	5.769E+07	31.23		**0**	**0.4641**	**5.809E+07**	**31.47**
0	0.2154	4.401E+07	33.39		**0**	**0.2154**	**4.424E+07**	**33.58**
0	0.1	3.313E+07	35.69		**0**	**0.1**	**3.326E+07**	**35.84**
0	0.04641	2.446E+07	38.01		**0**	**0.04641**	**2.452E+07**	**38.13**
0	0.02154	1.766E+07	40.68		**0**	**0.02154**	**1.769E+07**	**40.77**
0	0.01	1.247E+07	43.54		**0**	**0.01**	**1.248E+07**	**43.61**
-10	10	3.326E+08	14.63		**-10**	**10**	**3.481E+08**	**15.33**
-10	4.641	2.917E+08	16.11		**-10**	**4.641**	**3.034E+08**	**16.78**
-10	2.154	2.535E+08	17.70		**-10**	**2.154**	**2.623E+08**	**18.33**
-10	1	2.148E+08	19.32		**-10**	**1**	**2.210E+08**	**19.90**
-10	0.4641	1.824E+08	20.95		**-10**	**0.4641**	**1.867E+08**	**21.48**
-10	0.2154	1.521E+08	22.75		**-10**	**0.2154**	**1.551E+08**	**23.22**
-10	0.1	1.254E+08	24.58		**-10**	**0.1**	**1.274E+08**	**25.00**
-10	0.04641	1.000E+08	25.93		**-10**	**0.04641**	**1.013E+08**	**26.29**
-10	0.02154	8.118E+07	28.76		**-10**	**0.02154**	**8.198E+07**	**29.08**
-10	0.01	6.355E+07	30.99		**-10**	**0.01**	**6.403E+07**	**31.25**
-20	10	5.357E+08	8.95		**-20**	**10**	**5.780E+08**	**9.67**
-20	4.641	4.977E+08	10.06		**-20**	**4.641**	**5.338E+08**	**10.80**
-20	2.154	4.525E+08	11.33		**-20**	**2.154**	**4.821E+08**	**12.08**
-20	1	4.088E+08	12.63		**-20**	**1**	**4.327E+08**	**13.39**
-20	0.4641	3.672E+08	13.99		**-20**	**0.4641**	**3.862E+08**	**14.73**
-20	0.2155	3.246E+08	15.50		**-20**	**0.2155**	**3.393E+08**	**16.22**
-20	0.1	2.835E+08	16.74		**-20**	**0.1**	**2.946E+08**	**17.41**
-20	0.04642	2.505E+08	16.73		**-20**	**0.02154**	**2.198E+08**	**20.92**
-20	0.02154	2.137E+08	20.31		**-20**	**0.01**	**1.835E+08**	**22.43**
-20	0.01	1.793E+08	21.89		**-30**	**10**	**7.856E+08**	**5.99**
-30	10	7.089E+08	5.40		**-30**	**4.641**	**7.511E+08**	**6.74**
-30	4.641	6.808E+08	6.11		**-30**	**2.154**	**6.993E+08**	**7.75**
-30	2.154	6.381E+08	7.07		**-30**	**1**	**6.508E+08**	**8.87**
-30	1	5.975E+08	8.14		**-30**	**0.4641**	**6.071E+08**	**9.88**
-30	0.4641	5.606E+08	9.12		**-30**	**0.2155**	**5.573E+08**	**11.06**
-30	0.2155	5.180E+08	10.27		**-30**	**0.1**	**5.090E+08**	**11.98**
-30	0.1	4.762E+08	11.19		**-30**	**0.02154**	**4.140E+08**	**14.51**
-30	0.04642	4.280E+08	11.88		**-30**	**0.01**	**3.603E+08**	**16.46**
-30	0.02154	3.922E+08	13.73		**-40**	**10**	**9.526E+08**	**3.24**
-30	0.01	3.438E+08	15.69		**-40**	**4.641**	**9.337E+08**	**4.04**
-40	10	8.418E+08	2.86		**-40**	**2.154**	**8.909E+08**	**4.70**
-40	4.641	8.270E+08	3.58		**-40**	**1**	**8.590E+08**	**5.48**
-40	2.154	7.933E+08	4.19		**-40**	**0.4641**	**8.155E+08**	**6.30**
-40	1	7.680E+08	4.90		**-40**	**0.2155**	**7.698E+08**	**7.26**
-40	0.4641	7.332E+08	5.66		**-40**	**0.1**	**7.273E+08**	**7.90**
-40	0.2155	6.962E+08	6.56		**-40**	**0.04642**	**6.863E+08**	**9.08**
-40	0.1	6.613E+08	7.17		**-40**	**0.01**	**5.840E+08**	**11.46**
-40	0.04642	6.274E+08	8.30					
-40	0.02154	5.798E+08	8.78					
-40	0.01	5.410E+08	10.60					

B-20								
T	*f*	*G**	*δ*		***T***	***f***	***G****	***δ***
[°C]	[Hz]	[Pa]	[°]		**[°C]**	**[Hz]**	**[Pa]**	**[°]**
10	10	5.835E+07	39.19		**10**	**10**	**5.871E+07**	**39.49**
10	4.641	4.167E+07	42.72		**10**	**4.641**	**4.184E+07**	**42.95**
10	2.154	2.867E+07	46.48		**10**	**2.154**	**2.875E+07**	**46.65**
10	1	1.920E+07	50.35		**10**	**1**	**1.923E+07**	**50.46**
10	0.4641	1.242E+07	54.27		**10**	**0.4641**	**1.243E+07**	**54.35**
10	0.2154	7.823E+06	58.21		**10**	**0.2154**	**7.828E+06**	**58.27**
10	0.1	4.773E+06	62.16		**10**	**0.1**	**4.775E+06**	**62.20**
10	0.04641	2.821E+06	65.76		**10**	**0.04641**	**2.821E+06**	**65.78**
10	0.02154	1.631E+06	69.40		**10**	**0.02154**	**1.631E+06**	**69.41**
10	0.01	9.419E+05	72.23		**10**	**0.01**	**9.420E+05**	**72.24**
0	10	2.036E+08	23.63		**0**	**10**	**2.089E+08**	**24.29**
0	4.641	1.659E+08	26.21		**0**	**4.641**	**1.693E+08**	**26.81**
0	2.154	1.317E+08	29.18		**0**	**2.154**	**1.338E+08**	**29.69**
0	1	1.013E+08	32.15		**0**	**1**	**1.025E+08**	**32.58**
0	0.4641	7.646E+07	35.47		**0**	**0.4641**	**7.712E+07**	**35.83**
0	0.2154	5.606E+07	38.86		**0**	**0.2154**	**5.640E+07**	**39.14**
0	0.1	3.995E+07	42.44		**0**	**0.1**	**4.011E+07**	**42.66**
0	0.04641	2.756E+07	46.44		**0**	**0.04641**	**2.763E+07**	**46.60**
0	0.02154	1.847E+07	50.25		**0**	**0.02154**	**1.850E+07**	**50.36**
0	0.01	1.198E+07	54.39		**0**	**0.01**	**1.199E+07**	**54.46**
-10	10	4.939E+08	11.79		**-10**	**10**	**5.293E+08**	**12.65**
-10	4.641	4.484E+08	13.44		**-10**	**4.641**	**4.771E+08**	**14.32**
-10	2.154	3.964E+08	15.40		**-10**	**2.154**	**4.185E+08**	**16.29**
-10	1	3.452E+08	17.43		**-10**	**1**	**3.616E+08**	**18.29**
-10	0.4641	2.953E+08	19.74		**-10**	**0.4641**	**3.070E+08**	**20.56**
-10	0.2154	2.481E+08	21.89		**-10**	**0.2154**	**2.562E+08**	**22.65**
-10	0.1	2.038E+08	24.56		**-10**	**0.1**	**2.092E+08**	**25.25**
-10	0.04641	1.645E+08	27.44		**-10**	**0.04641**	**1.679E+08**	**28.05**
-10	0.02154	1.276E+08	31.10		**-10**	**0.02154**	**1.296E+08**	**31.63**
-10	0.01	9.889E+07	34.08		**-10**	**0.01**	**1.000E+08**	**34.52**
-20	10	7.331E+08	5.62		**-20**	**10**	**8.155E+08**	**6.26**
-20	4.641	6.983E+08	6.81		**-20**	**4.641**	**7.724E+08**	**7.54**
-20	2.154	6.561E+08	8.00		**-20**	**2.154**	**7.209E+08**	**8.79**
-20	1	6.040E+08	9.29		**-20**	**1**	**6.583E+08**	**10.13**
-20	0.4641	5.639E+08	10.71		**-20**	**0.4641**	**6.107E+08**	**11.61**
-20	0.2155	5.125E+08	12.28		**-20**	**0.2155**	**5.506E+08**	**13.21**
-20	0.1	4.608E+08	14.09		**-20**	**0.1**	**4.911E+08**	**15.04**
-20	0.04642	4.084E+08	15.39		**-20**	**0.02154**	**3.757E+08**	**19.00**
-20	0.02154	3.581E+08	18.08		**-20**	**0.01**	**3.204E+08**	**21.55**
-20	0.01	3.077E+08	20.65		**-30**	**10**	**1.014E+09**	**3.34**
-30	10	8.897E+08	2.93		**-30**	**4.641**	**9.838E+08**	**4.09**
-30	4.641	8.661E+08	3.60		**-30**	**2.154**	**9.396E+08**	**4.77**
-30	2.154	8.318E+08	4.22		**-30**	**1**	**9.061E+08**	**5.64**
-30	1	8.055E+08	5.02		**-30**	**0.4641**	**8.676E+08**	**6.64**
-30	0.4641	7.750E+08	5.93		**-30**	**0.1**	**7.679E+08**	**8.88**
-30	0.2155	7.370E+08	6.39		**-30**	**0.02154**	**6.540E+08**	**11.72**
-30	0.1	6.948E+08	8.03		**-30**	**0.01**	**5.941E+08**	**13.12**
-30	0.04642	6.713E+08	8.56		**-40**	**10**	**1.164E+09**	**1.84**
-30	0.02154	6.007E+08	10.76		**-40**	**4.641**	**1.145E+09**	**2.28**
-30	0.01	5.500E+08	12.13		**-40**	**2.154**	**1.101E+09**	**2.71**
-40	10	1.002E+09	1.58		**-40**	**1**	**1.089E+09**	**3.24**
-40	4.641	9.881E+08	1.97		**-40**	**0.4641**	**1.071E+09**	**3.81**
-40	2.154	9.556E+08	2.35		**-40**	**0.2155**	**1.027E+09**	**4.51**
-40	1	9.465E+08	2.81		**-40**	**0.1**	**9.857E+08**	**5.43**
-40	0.4641	9.326E+08	3.32		**-40**	**0.02154**	**9.495E+08**	**7.12**
-40	0.2155	8.993E+08	3.95		**-40**	**0.01**	**8.790E+08**	**8.02**
-40	0.1	8.677E+08	4.78					
-40	0.04642	8.357E+08	4.62					
-40	0.02154	8.399E+08	6.30					
-40	0.01	7.844E+08	7.15					

B-21								
T	*f*	*G**	*δ*		***T***	***f***	***G****	***δ***
[°C]	[Hz]	[Pa]	[°]		**[°C]**	**[Hz]**	**[Pa]**	**[°]**
10	10	3.190E+07	36.22		**10**	**10**	**3.202E+07**	**36.37**
10	4.641	2.331E+07	38.50		**10**	**4.641**	**2.337E+07**	**38.62**
10	2.154	1.675E+07	40.84		**10**	**2.154**	**1.678E+07**	**40.92**
10	1	1.173E+07	43.23		**10**	**1**	**1.174E+07**	**43.29**
10	0.4641	8.083E+06	45.67		**10**	**0.4641**	**8.089E+06**	**45.72**
10	0.2154	5.467E+06	48.17		**10**	**0.2154**	**5.469E+06**	**48.20**
10	0.1	3.618E+06	50.66		**10**	**0.1**	**3.619E+06**	**50.69**
10	0.04641	2.336E+06	53.18		**10**	**0.04641**	**2.336E+06**	**53.19**
10	0.02154	1.482E+06	55.66		**10**	**0.02154**	**1.483E+06**	**55.67**
10	0.01	9.311E+05	57.88		**10**	**0.01**	**9.311E+05**	**57.89**
0	10	1.054E+08	25.62		**0**	**10**	**1.068E+08**	**25.99**
0	4.641	8.408E+07	27.86		**0**	**4.641**	**8.495E+07**	**28.18**
0	2.154	6.641E+07	29.87		**0**	**2.154**	**6.694E+07**	**30.13**
0	1	5.104E+07	31.87		**0**	**1**	**5.134E+07**	**32.09**
0	0.4641	3.868E+07	34.00		**0**	**0.4641**	**3.885E+07**	**34.17**
0	0.2154	2.894E+07	36.20		**0**	**0.2154**	**2.903E+07**	**36.34**
0	0.1	2.123E+07	38.52		**0**	**0.1**	**2.128E+07**	**38.62**
0	0.04641	1.529E+07	40.89		**0**	**0.04641**	**1.532E+07**	**40.97**
0	0.02154	1.079E+07	43.56		**0**	**0.02154**	**1.080E+07**	**43.62**
0	0.01	7.475E+06	46.30		**0**	**0.01**	**7.481E+06**	**46.34**
-10	10	2.742E+08	16.52		**-10**	**10**	**2.846E+08**	**17.16**
-10	4.641	2.361E+08	18.43		**-10**	**4.641**	**2.437E+08**	**19.04**
-10	2.154	2.010E+08	20.07		**-10**	**2.154**	**2.064E+08**	**20.63**
-10	1	1.657E+08	21.80		**-10**	**1**	**1.692E+08**	**22.30**
-10	0.4641	1.392E+08	23.52		**-10**	**0.4641**	**1.417E+08**	**23.97**
-10	0.2154	1.137E+08	25.26		**-10**	**0.2154**	**1.153E+08**	**25.65**
-10	0.1	9.174E+07	27.12		**-10**	**0.1**	**9.278E+07**	**27.46**
-10	0.04641	7.261E+07	28.87		**-10**	**0.04641**	**7.325E+07**	**29.15**
-10	0.02154	5.569E+07	31.76		**-10**	**0.02154**	**5.605E+07**	**31.99**
-10	0.01	4.303E+07	34.01		**-10**	**0.01**	**4.324E+07**	**34.20**
-20	10	4.806E+08	10.22		**-20**	**10**	**5.143E+08**	**10.95**
-20	4.641	4.393E+08	11.71		**-20**	**4.641**	**4.671E+08**	**12.47**
-20	2.154	3.951E+08	13.08		**-20**	**2.154**	**4.174E+08**	**13.83**
-20	1	3.498E+08	14.63		**-20**	**1**	**3.670E+08**	**15.37**
-20	0.4641	3.102E+08	15.96		**-20**	**0.4641**	**3.235E+08**	**16.67**
-20	0.2155	2.692E+08	17.26		**-20**	**0.2155**	**2.791E+08**	**17.92**
-20	0.1	2.330E+08	19.02		**-20**	**0.1**	**2.403E+08**	**19.65**
-20	0.04642	2.011E+08	19.63		**-20**	**0.02154**	**1.732E+08**	**22.88**
-20	0.02154	1.694E+08	22.36		**-20**	**0.01**	**1.401E+08**	**25.16**
-20	0.01	1.377E+08	24.70		**-30**	**10**	**7.322E+08**	**6.97**
-30	10	6.653E+08	6.33		**-30**	**4.641**	**6.898E+08**	**7.98**
-30	4.641	6.302E+08	7.29		**-30**	**2.154**	**6.426E+08**	**9.08**
-30	2.154	5.906E+08	8.34		**-30**	**1**	**5.872E+08**	**10.17**
-30	1	5.436E+08	9.41		**-30**	**0.4641**	**5.405E+08**	**11.41**
-30	0.4641	5.035E+08	10.62		**-30**	**0.1**	**4.403E+08**	**14.12**
-30	0.2155	4.586E+08	10.87		**-30**	**0.02154**	**3.475E+08**	**16.14**
-30	0.1	4.157E+08	13.32		**-30**	**0.01**	**3.020E+08**	**18.28**
-30	0.04642	3.810E+08	13.31		**-40**	**10**	**9.203E+08**	**3.91**
-30	0.02154	3.321E+08	15.41		**-40**	**4.641**	**8.924E+08**	**4.80**
-30	0.01	2.904E+08	17.56		**-40**	**2.154**	**8.509E+08**	**5.62**
-40	10	8.165E+08	3.46		**-40**	**1**	**8.031E+08**	**6.47**
-40	4.641	7.945E+08	4.27		**-40**	**0.4641**	**7.637E+08**	**7.39**
-40	2.154	7.615E+08	5.03		**-40**	**0.1**	**6.675E+08**	**9.15**
-40	1	7.231E+08	5.82		**-40**	**0.01**	**5.172E+08**	**12.89**
-40	0.4641	6.912E+08	6.69					
-40	0.2155	6.420E+08	6.30					
-40	0.1	6.116E+08	8.37					
-40	0.04642	5.786E+08	10.19					
-40	0.02154	5.279E+08	11.85					
-40	0.01	4.834E+08	12.04					

B-22								
T	*f*	*G**	*δ*		***T***	***f***	***G****	***δ***
[°C]	[Hz]	[Pa]	[°]		**[°C]**	**[Hz]**	**[Pa]**	**[°]**
10	10	3.942E+07	41.68		**10**	**10**	**3.958E+07**	**41.89**
10	4.641	2.726E+07	45.04		**10**	**4.641**	**2.733E+07**	**45.20**
10	2.154	1.834E+07	48.25		**10**	**2.154**	**1.837E+07**	**48.36**
10	1	1.199E+07	51.41		**10**	**1**	**1.201E+07**	**51.49**
10	0.4641	7.633E+06	54.56		**10**	**0.4641**	**7.638E+06**	**54.61**
10	0.2154	4.735E+06	57.62		**10**	**0.2154**	**4.737E+06**	**57.65**
10	0.1	2.862E+06	60.53		**10**	**0.1**	**2.863E+06**	**60.55**
10	0.04641	1.692E+06	63.35		**10**	**0.04641**	**1.692E+06**	**63.36**
10	0.02154	9.814E+05	65.81		**10**	**0.02154**	**9.815E+05**	**65.81**
10	0.01	5.631E+05	68.10		**10**	**0.01**	**5.631E+05**	**68.11**
0	10	1.443E+08	27.84		**0**	**10**	**1.469E+08**	**28.38**
0	4.641	1.125E+08	30.96		**0**	**4.641**	**1.140E+08**	**31.42**
0	2.154	8.560E+07	33.79		**0**	**2.154**	**8.645E+07**	**34.17**
0	1	6.356E+07	36.66		**0**	**1**	**6.401E+07**	**36.96**
0	0.4641	4.607E+07	39.61		**0**	**0.4641**	**4.629E+07**	**39.84**
0	0.2154	3.255E+07	42.65		**0**	**0.2154**	**3.266E+07**	**42.82**
0	0.1	2.242E+07	45.70		**0**	**0.1**	**2.247E+07**	**45.83**
0	0.04641	1.505E+07	48.94		**0**	**0.04641**	**1.507E+07**	**49.03**
0	0.02154	9.802E+06	52.38		**0**	**0.02154**	**9.811E+06**	**52.44**
0	0.01	6.232E+06	55.51		**0**	**0.01**	**6.235E+06**	**55.55**
-10	10	3.723E+08	15.43		**-10**	**10**	**3.918E+08**	**16.26**
-10	4.641	3.242E+08	17.80		**-10**	**4.641**	**3.387E+08**	**18.62**
-10	2.154	2.760E+08	20.09		**-10**	**2.154**	**2.862E+08**	**20.87**
-10	1	2.311E+08	22.37		**-10**	**1**	**2.381E+08**	**23.09**
-10	0.4641	1.885E+08	24.90		**-10**	**0.4641**	**1.931E+08**	**25.55**
-10	0.2154	1.510E+08	27.54		**-10**	**0.2154**	**1.539E+08**	**28.10**
-10	0.1	1.181E+08	29.92		**-10**	**0.1**	**1.198E+08**	**30.39**
-10	0.04641	9.087E+07	33.35		**-10**	**0.04641**	**9.183E+07**	**33.75**
-10	0.02154	6.761E+07	36.21		**-10**	**0.02154**	**6.812E+07**	**36.53**
-10	0.01	4.983E+07	39.02		**-10**	**0.01**	**5.009E+07**	**39.27**
-20	10	5.974E+08	8.32		**-20**	**10**	**6.506E+08**	**9.07**
-20	4.641	5.572E+08	9.85		**-20**	**4.641**	**6.030E+08**	**10.66**
-20	2.154	5.102E+08	11.45		**-20**	**2.154**	**5.480E+08**	**12.32**
-20	1	4.601E+08	13.12		**-20**	**1**	**4.905E+08**	**14.00**
-20	0.4641	4.088E+08	15.03		**-20**	**0.4641**	**4.324E+08**	**15.92**
-20	0.2155	3.568E+08	16.23		**-20**	**0.1**	**3.215E+08**	**19.92**
-20	0.1	3.086E+08	19.09		**-20**	**0.04642**	**2.695E+08**	**22.23**
-20	0.04642	2.604E+08	21.45		**-20**	**0.02154**	**2.220E+08**	**24.76**
-20	0.02154	2.159E+08	24.05		**-20**	**0.01**	**1.806E+08**	**26.66**
-20	0.01	1.766E+08	26.03		**-30**	**10**	**8.673E+08**	**4.99**
-30	10	7.746E+08	4.46		**-30**	**4.641**	**8.304E+08**	**5.99**
-30	4.641	7.452E+08	5.37		**-30**	**2.154**	**7.858E+08**	**7.11**
-30	2.154	7.091E+08	6.42		**-30**	**1**	**7.312E+08**	**8.29**
-30	1	6.645E+08	7.53		**-30**	**0.4641**	**6.866E+08**	**9.65**
-30	0.4641	6.277E+08	8.82		**-30**	**0.2155**	**6.280E+08**	**11.17**
-30	0.2155	5.786E+08	10.28		**-30**	**0.1**	**5.686E+08**	**12.74**
-30	0.1	5.280E+08	11.81		**-30**	**0.02154**	**4.474E+08**	**16.52**
-30	0.04642	4.567E+08	15.78		**-30**	**0.01**	**3.801E+08**	**19.16**
-30	0.02154	4.223E+08	15.56		**-40**	**10**	**1.021E+09**	**2.54**
-30	0.01	3.621E+08	18.22		**-40**	**4.641**	**1.002E+09**	**3.29**
-40	10	8.948E+08	2.23		**-40**	**2.154**	**9.739E+08**	**4.00**
-40	4.641	8.803E+08	2.89		**-40**	**1**	**9.368E+08**	**4.75**
-40	2.154	8.584E+08	3.52		**-40**	**0.4641**	**9.025E+08**	**5.58**
-40	1	8.295E+08	4.20		**-40**	**0.2155**	**8.704E+08**	**6.13**
-40	0.4641	8.026E+08	4.96		**-40**	**0.1**	**8.203E+08**	**7.59**
-40	0.2155	7.772E+08	5.48		**-40**	**0.02154**	**7.233E+08**	**10.33**
-40	0.1	7.372E+08	6.82					
-40	0.04642	6.937E+08	9.39					
-40	0.02154	6.583E+08	9.40					
-40	0.01	5.898E+08	12.29					

B-23								
T	*f*	*G**	*δ*		***T***	***f***	***G****	***δ***
[°C]	[Hz]	[Pa]	[°]		**[°C]**	**[Hz]**	**[Pa]**	**[°]**
10	10	2.200E+07	42.97		**10**	**10**	**2.205E+07**	**43.09**
10	4.641	1.515E+07	45.91		**10**	**4.641**	**1.517E+07**	**46.00**
10	2.154	1.015E+07	48.65		**10**	**2.154**	**1.016E+07**	**48.71**
10	1	6.633E+06	51.37		**10**	**1**	**6.637E+06**	**51.41**
10	0.4641	4.249E+06	54.06		**10**	**0.4641**	**4.250E+06**	**54.09**
10	0.2154	2.663E+06	56.67		**10**	**0.2154**	**2.663E+06**	**56.69**
10	0.1	1.636E+06	59.14		**10**	**0.1**	**1.636E+06**	**59.15**
10	0.04641	9.867E+05	61.40		**10**	**0.04641**	**9.868E+05**	**61.40**
10	0.02154	5.903E+05	63.70		**10**	**0.02154**	**5.903E+05**	**63.71**
10	0.01	3.580E+05	65.56		**10**	**0.01**	**3.580E+05**	**65.56**
0	10	7.932E+07	31.61		**0**	**10**	**8.006E+07**	**31.94**
0	4.641	6.040E+07	33.86		**0**	**4.641**	**6.082E+07**	**34.12**
0	2.154	4.479E+07	36.27		**0**	**2.154**	**4.502E+07**	**36.49**
0	1	3.260E+07	38.79		**0**	**1**	**3.271E+07**	**38.95**
0	0.4641	2.325E+07	41.32		**0**	**0.4641**	**2.330E+07**	**41.44**
0	0.2154	1.625E+07	43.88		**0**	**0.2154**	**1.627E+07**	**43.97**
0	0.1	1.115E+07	46.51		**0**	**0.1**	**1.116E+07**	**46.58**
0	0.04641	7.489E+06	49.22		**0**	**0.04641**	**7.494E+06**	**49.27**
0	0.02154	4.905E+06	51.94		**0**	**0.02154**	**4.907E+06**	**51.97**
0	0.01	3.148E+06	54.62		**0**	**0.01**	**3.149E+06**	**54.64**
-10	10	2.414E+08	19.80		**-10**	**10**	**2.492E+08**	**20.47**
-10	4.641	2.024E+08	22.19		**-10**	**4.641**	**2.078E+08**	**22.81**
-10	2.154	1.665E+08	24.34		**-10**	**2.154**	**1.701E+08**	**24.89**
-10	1	1.324E+08	26.61		**-10**	**1**	**1.346E+08**	**27.09**
-10	0.4641	1.060E+08	28.69		**-10**	**0.4641**	**1.074E+08**	**29.10**
-10	0.2154	8.241E+07	30.92		**-10**	**0.2154**	**8.322E+07**	**31.26**
-10	0.1	6.314E+07	33.23		**-10**	**0.1**	**6.360E+07**	**33.51**
-10	0.04641	4.675E+07	35.20		**-10**	**0.04641**	**4.700E+07**	**35.42**
-10	0.02154	3.467E+07	38.61		**-10**	**0.02154**	**3.480E+07**	**38.78**
-10	0.01	2.487E+07	40.71		**-10**	**0.01**	**2.493E+07**	**40.84**
-20	10	4.467E+08	12.06		**-20**	**10**	**4.754E+08**	**12.85**
-20	4.641	4.010E+08	13.96		**-20**	**4.641**	**4.238E+08**	**14.77**
-20	2.154	3.544E+08	15.75		**-20**	**2.154**	**3.719E+08**	**16.55**
-20	1	3.022E+08	17.57		**-20**	**1**	**3.147E+08**	**18.33**
-20	0.4641	2.641E+08	19.42		**-20**	**0.4641**	**2.735E+08**	**20.14**
-20	0.2155	2.219E+08	21.38		**-20**	**0.2155**	**2.284E+08**	**22.04**
-20	0.1	1.845E+08	23.41		**-20**	**0.1**	**1.889E+08**	**24.00**
-20	0.04642	1.545E+08	25.53		**-20**	**0.04642**	**1.575E+08**	**26.07**
-20	0.02154	1.211E+08	28.03		**-20**	**0.02154**	**1.229E+08**	**28.48**
-20	0.01	9.520E+07	30.32		**-20**	**0.01**	**9.629E+07**	**30.71**
-30	10	6.329E+08	7.22		**-30**	**10**	**6.931E+08**	**7.91**
-30	4.641	5.927E+08	8.63		**-30**	**4.641**	**6.450E+08**	**9.40**
-30	2.154	5.509E+08	10.02		**-30**	**2.154**	**5.956E+08**	**10.84**
-30	1	4.995E+08	11.62		**-30**	**1**	**5.358E+08**	**12.47**
-30	0.4641	4.524E+08	13.11		**-30**	**0.4641**	**4.817E+08**	**13.98**
-30	0.2155	4.039E+08	14.82		**-30**	**0.2155**	**4.270E+08**	**15.68**
-30	0.1	3.555E+08	16.42		**-30**	**0.1**	**3.731E+08**	**17.26**
-30	0.04642	3.022E+08	21.81		**-30**	**0.02154**	**2.746E+08**	**20.28**
-30	0.02154	2.651E+08	19.56		**-30**	**0.01**	**2.258E+08**	**23.50**
-30	0.01	2.195E+08	22.81		**-40**	**10**	**8.884E+08**	**4.81**
-40	10	7.914E+08	4.28		**-40**	**4.641**	**8.498E+08**	**5.68**
-40	4.641	7.607E+08	5.08		**-40**	**2.154**	**7.986E+08**	**6.69**
-40	2.154	7.196E+08	6.02		**-40**	**1**	**7.540E+08**	**7.85**
-40	1	6.833E+08	7.11		**-40**	**0.4641**	**7.112E+08**	**9.01**
-40	0.4641	6.481E+08	8.20		**-40**	**0.2155**	**6.577E+08**	**10.34**
-40	0.2155	6.035E+08	9.48		**-40**	**0.1**	**5.986E+08**	**11.56**
-40	0.1	5.536E+08	10.68		**-40**	**0.04642**	**5.486E+08**	**12.99**
-40	0.04642	5.107E+08	12.08		**-40**	**0.01**	**4.342E+08**	**16.73**
-40	0.02154	4.603E+08	14.71					
-40	0.01	4.105E+08	15.79					

B-24								
T	*f*	*G**	*δ*		***T***	***f***	***G****	***δ***
[°C]	[Hz]	[Pa]	[°]		**[°C]**	**[Hz]**	**[Pa]**	**[°]**
10	10	1.985E+07	47.04		**10**	**10**	**1.989E+07**	**47.16**
10	4.641	1.317E+07	50.15		**10**	**4.641**	**1.318E+07**	**50.23**
10	2.154	8.508E+06	53.41		**10**	**2.154**	**8.514E+06**	**53.46**
10	1	5.361E+06	56.64		**10**	**1**	**5.363E+06**	**56.68**
10	0.4641	3.294E+06	59.82		**10**	**0.4641**	**3.295E+06**	**59.85**
10	0.2154	1.975E+06	62.77		**10**	**0.2154**	**1.975E+06**	**62.79**
10	0.1	1.149E+06	65.52		**10**	**0.1**	**1.149E+06**	**65.53**
10	0.04641	6.590E+05	68.18		**10**	**0.04641**	**6.591E+05**	**68.18**
10	0.02154	3.769E+05	70.69		**10**	**0.02154**	**3.769E+05**	**70.70**
10	0.01	2.200E+05	73.14		**10**	**0.01**	**2.200E+05**	**73.14**
0	10	8.510E+07	32.92		**0**	**10**	**8.595E+07**	**33.29**
0	4.641	6.391E+07	35.52		**0**	**4.641**	**6.437E+07**	**35.81**
0	2.154	4.692E+07	38.36		**0**	**2.154**	**4.716E+07**	**38.59**
0	1	3.348E+07	41.25		**0**	**1**	**3.359E+07**	**41.42**
0	0.4641	2.334E+07	44.24		**0**	**0.4641**	**2.339E+07**	**44.37**
0	0.2154	1.590E+07	47.32		**0**	**0.2154**	**1.593E+07**	**47.41**
0	0.1	1.061E+07	50.48		**0**	**0.1**	**1.062E+07**	**50.54**
0	0.04641	6.896E+06	53.61		**0**	**0.04641**	**6.900E+06**	**53.65**
0	0.02154	4.348E+06	56.97		**0**	**0.02154**	**4.349E+06**	**57.00**
0	0.01	2.689E+06	60.04		**0**	**0.01**	**2.690E+06**	**60.06**
-10	10	2.649E+08	19.77		**-10**	**10**	**2.744E+08**	**20.51**
-10	4.641	2.215E+08	22.30		**-10**	**4.641**	**2.279E+08**	**22.98**
-10	2.154	1.820E+08	24.61		**-10**	**2.154**	**1.863E+08**	**25.23**
-10	1	1.447E+08	27.00		**-10**	**1**	**1.473E+08**	**27.53**
-10	0.4641	1.148E+08	29.44		**-10**	**0.4641**	**1.164E+08**	**29.90**
-10	0.2154	8.899E+07	32.04		**-10**	**0.2154**	**8.993E+07**	**32.42**
-10	0.1	6.747E+07	34.78		**-10**	**0.1**	**6.800E+07**	**35.09**
-10	0.04641	4.899E+07	37.65		**-10**	**0.04641**	**4.926E+07**	**37.89**
-10	0.02154	3.606E+07	40.86		**-10**	**0.02154**	**3.619E+07**	**41.05**
-10	0.01	2.537E+07	43.99		**-10**	**0.01**	**2.543E+07**	**44.13**
-20	10	4.896E+08	11.45		**-20**	**10**	**5.244E+08**	**12.27**
-20	4.641	4.429E+08	13.42		**-20**	**4.641**	**4.709E+08**	**14.29**
-20	2.154	3.925E+08	15.23		**-20**	**2.154**	**4.142E+08**	**16.09**
-20	1	3.409E+08	17.11		**-20**	**1**	**3.570E+08**	**17.94**
-20	0.4641	2.948E+08	19.10		**-20**	**0.4641**	**3.066E+08**	**19.89**
-20	0.2155	2.485E+08	21.27		**-20**	**0.2155**	**2.567E+08**	**22.01**
-20	0.1	2.060E+08	23.45		**-20**	**0.1**	**2.115E+08**	**24.12**
-20	0.04642	1.677E+08	25.86		**-20**	**0.04642**	**1.713E+08**	**26.45**
-20	0.02154	1.347E+08	28.33		**-20**	**0.02154**	**1.370E+08**	**28.85**
-20	0.01	1.044E+08	30.75		**-20**	**0.01**	**1.058E+08**	**31.18**
-30	10	6.896E+08	6.82		**-30**	**10**	**7.617E+08**	**7.53**
-30	4.641	6.487E+08	8.00		**-30**	**4.641**	**7.120E+08**	**8.78**
-30	2.154	6.027E+08	9.31		**-30**	**2.154**	**6.567E+08**	**10.15**
-30	1	5.535E+08	10.77		**-30**	**1**	**5.985E+08**	**11.65**
-30	0.4641	5.038E+08	12.32		**-30**	**0.4641**	**5.406E+08**	**13.24**
-30	0.2155	4.482E+08	12.54		**-30**	**0.1**	**4.213E+08**	**16.46**
-30	0.1	3.989E+08	15.56		**-30**	**0.02154**	**3.147E+08**	**20.68**
-30	0.04642	3.698E+08	14.22		**-30**	**0.01**	**2.630E+08**	**22.29**
-30	0.02154	3.023E+08	19.84		**-40**	**10**	**9.570E+08**	**4.36**
-30	0.01	2.544E+08	21.52		**-40**	**4.641**	**9.252E+08**	**5.14**
-40	10	8.453E+08	3.85		**-40**	**2.154**	**8.857E+08**	**6.13**
-40	4.641	8.205E+08	4.56		**-40**	**1**	**8.303E+08**	**7.21**
-40	2.154	7.894E+08	5.46		**-40**	**0.4641**	**7.944E+08**	**8.26**
-40	1	7.452E+08	6.47		**-40**	**0.1**	**6.733E+08**	**10.99**
-40	0.4641	7.163E+08	7.45		**-40**	**0.01**	**4.947E+08**	**16.65**
-40	0.2155	6.624E+08	7.71					
-40	0.1	6.168E+08	10.06					
-40	0.04642	5.674E+08	10.56					
-40	0.02154	5.133E+08	11.85					
-40	0.01	4.642E+08	15.60					

B-25								
T	*f*	*G**	*δ*		***T***	***f***	***G****	***δ***
[°C]	[Hz]	[Pa]	[°]		**[°C]**	**[Hz]**	**[Pa]**	**[°]**
10	10	1.489E+07	55.92		**10**	**10**	**1.490E+07**	**56.02**
10	4.641	9.052E+06	59.40		**10**	**4.641**	**9.057E+06**	**59.46**
10	2.154	5.353E+06	62.57		**10**	**2.154**	**5.355E+06**	**62.61**
10	1	3.084E+06	65.42		**10**	**1**	**3.085E+06**	**65.44**
10	0.4641	1.739E+06	67.97		**10**	**0.4641**	**1.739E+06**	**67.98**
10	0.2154	9.642E+05	70.21		**10**	**0.2154**	**9.642E+05**	**70.21**
10	0.1	5.290E+05	72.15		**10**	**0.1**	**5.290E+05**	**72.16**
10	0.04641	2.883E+05	73.63		**10**	**0.04641**	**2.883E+05**	**73.63**
10	0.02154	1.572E+05	75.26		**10**	**0.02154**	**1.572E+05**	**75.26**
10	0.01	9.050E+04	77.25		**10**	**0.01**	**9.050E+04**	**77.25**
0	10	7.931E+07	40.24		**0**	**10**	**7.998E+07**	**40.65**
0	4.641	5.532E+07	44.13		**0**	**4.641**	**5.563E+07**	**44.44**
0	2.154	3.749E+07	47.81		**0**	**2.154**	**3.762E+07**	**48.03**
0	1	2.457E+07	51.39		**0**	**1**	**2.462E+07**	**51.55**
0	0.4641	1.561E+07	54.88		**0**	**0.4641**	**1.563E+07**	**54.99**
0	0.2154	9.625E+06	58.19		**0**	**0.2154**	**9.631E+06**	**58.26**
0	0.1	5.782E+06	61.34		**0**	**0.1**	**5.785E+06**	**61.38**
0	0.04641	3.389E+06	64.24		**0**	**0.04641**	**3.390E+06**	**64.26**
0	0.02154	1.941E+06	66.79		**0**	**0.02154**	**1.941E+06**	**66.81**
0	0.01	1.090E+06	69.21		**0**	**0.01**	**1.090E+06**	**69.22**
-10	10	3.033E+08	23.37		**-10**	**10**	**3.154E+08**	**24.36**
-10	4.641	2.468E+08	26.47		**-10**	**4.641**	**2.545E+08**	**27.37**
-10	2.154	1.941E+08	29.88		**-10**	**2.154**	**1.987E+08**	**30.67**
-10	1	1.467E+08	33.30		**-10**	**1**	**1.492E+08**	**33.95**
-10	0.4641	1.088E+08	36.84		**-10**	**0.4641**	**1.101E+08**	**37.36**
-10	0.2154	7.832E+07	40.40		**-10**	**0.2154**	**7.897E+07**	**40.80**
-10	0.1	5.485E+07	43.94		**-10**	**0.1**	**5.515E+07**	**44.24**
-10	0.04641	3.696E+07	47.57		**-10**	**0.04641**	**3.709E+07**	**47.78**
-10	0.02154	2.432E+07	51.46		**-10**	**0.02154**	**2.437E+07**	**51.61**
-10	0.01	1.551E+07	54.82		**-10**	**0.01**	**1.553E+07**	**54.92**
-20	10	5.916E+08	11.63		**-20**	**10**	**6.430E+08**	**12.66**
-20	4.641	5.323E+08	14.11		**-20**	**4.641**	**5.731E+08**	**15.22**
-20	2.154	4.673E+08	16.59		**-20**	**2.154**	**4.981E+08**	**17.71**
-20	1	3.996E+08	19.61		**-20**	**1**	**4.215E+08**	**20.73**
-20	0.4641	3.419E+08	22.12		**-20**	**0.4641**	**3.575E+08**	**23.18**
-20	0.2155	2.798E+08	24.97		**-20**	**0.2155**	**2.899E+08**	**25.94**
-20	0.1	2.237E+08	28.34		**-20**	**0.1**	**2.300E+08**	**29.21**
-20	0.04642	1.747E+08	31.70		**-20**	**0.04642**	**1.783E+08**	**32.45**
-20	0.02154	1.317E+08	34.81		**-20**	**0.02154**	**1.336E+08**	**35.41**
-20	0.01	9.600E+07	38.96		**-20**	**0.01**	**9.700E+07**	**39.44**
-30	10	8.244E+08	5.93		**-30**	**10**	**9.299E+08**	**6.69**
-30	4.641	7.817E+08	7.41		**-30**	**4.641**	**8.756E+08**	**8.30**
-30	2.154	7.304E+08	9.03		**-30**	**2.154**	**8.114E+08**	**10.04**
-30	1	6.654E+08	11.29		**-30**	**1**	**7.313E+08**	**12.43**
-30	0.4641	6.124E+08	12.77		**-30**	**0.4641**	**6.674E+08**	**13.95**
-30	0.2155	5.357E+08	15.08		**-30**	**0.2155**	**5.768E+08**	**16.28**
-30	0.1	4.781E+08	17.69		**-30**	**0.1**	**5.102E+08**	**18.92**
-30	0.04642	4.129E+08	20.81		**-30**	**0.04642**	**4.361E+08**	**22.04**
-30	0.02154	3.424E+08	23.59		**-30**	**0.02154**	**3.579E+08**	**24.72**
-30	0.01	2.794E+08	26.60		**-30**	**0.01**	**2.893E+08**	**27.63**
-40	10	9.823E+08	3.01		**-40**	**10**	**1.137E+09**	**3.48**
-40	4.641	9.633E+08	3.81		**-40**	**4.641**	**1.111E+09**	**4.39**
-40	2.154	9.202E+08	4.68		**-40**	**2.154**	**1.054E+09**	**5.36**
-40	1	8.930E+08	5.76		**-40**	**1**	**1.018E+09**	**6.57**
-40	0.4641	8.453E+08	7.07		**-40**	**0.4641**	**9.563E+08**	**8.00**
-40	0.2155	7.973E+08	8.24		**-40**	**0.2155**	**8.950E+08**	**9.26**
-40	0.1	7.374E+08	10.03		**-40**	**0.1**	**8.196E+08**	**11.16**
-40	0.04642	6.712E+08	11.58		**-40**	**0.04642**	**7.382E+08**	**12.75**
-40	0.02154	6.035E+08	13.79		**-40**	**0.02154**	**6.566E+08**	**15.03**
-40	0.01	5.329E+08	17.08		**-40**	**0.01**	**5.732E+08**	**18.41**

B-26								
T	*f*	*G**	*δ*		***T***	***f***	***G****	***δ***
[°C]	[Hz]	[Pa]	[°]		**[°C]**	**[Hz]**	**[Pa]**	**[°]**
10	10	1.072E+07	49.05		**10**	**10**	**1.073E+07**	**49.12**
10	4.641	7.018E+06	51.68		**10**	**4.641**	**7.022E+06**	**51.72**
10	2.154	4.469E+06	54.34		**10**	**2.154**	**4.470E+06**	**54.37**
10	1	2.789E+06	57.00		**10**	**1**	**2.790E+06**	**57.02**
10	0.4641	1.705E+06	59.57		**10**	**0.4641**	**1.705E+06**	**59.58**
10	0.2154	1.023E+06	61.95		**10**	**0.2154**	**1.023E+06**	**61.96**
10	0.1	5.986E+05	64.15		**10**	**0.1**	**5.986E+05**	**64.15**
10	0.04641	3.470E+05	66.13		**10**	**0.04641**	**3.470E+05**	**66.13**
10	0.02154	2.003E+05	67.69		**10**	**0.02154**	**2.003E+05**	**67.69**
10	0.01	1.181E+05	68.53		**10**	**0.01**	**1.181E+05**	**68.53**
0	10	4.907E+07	36.49		**0**	**10**	**4.934E+07**	**36.72**
0	4.641	3.576E+07	39.11		**0**	**4.641**	**3.590E+07**	**39.29**
0	2.154	2.543E+07	41.65		**0**	**2.154**	**2.550E+07**	**41.79**
0	1	1.770E+07	44.20		**0**	**1**	**1.773E+07**	**44.30**
0	0.4641	1.207E+07	46.81		**0**	**0.4641**	**1.208E+07**	**46.88**
0	0.2154	8.064E+06	49.47		**0**	**0.2154**	**8.070E+06**	**49.51**
0	0.1	5.295E+06	52.16		**0**	**0.1**	**5.298E+06**	**52.20**
0	0.04641	3.410E+06	54.90		**0**	**0.04641**	**3.411E+06**	**54.92**
0	0.02154	2.149E+06	57.99		**0**	**0.02154**	**2.149E+06**	**58.00**
0	0.01	1.317E+06	60.41		**0**	**0.01**	**1.317E+06**	**60.41**
-10	10	1.618E+08	24.80		**-10**	**10**	**1.652E+08**	**25.35**
-10	4.641	1.304E+08	27.19		**-10**	**4.641**	**1.325E+08**	**27.67**
-10	2.154	1.030E+08	29.38		**-10**	**2.154**	**1.043E+08**	**29.79**
-10	1	7.981E+07	31.62		**-10**	**1**	**8.057E+07**	**31.96**
-10	0.4641	6.043E+07	33.87		**-10**	**0.4641**	**6.086E+07**	**34.14**
-10	0.2154	4.513E+07	36.17		**-10**	**0.2154**	**4.535E+07**	**36.38**
-10	0.1	3.308E+07	38.41		**-10**	**0.1**	**3.320E+07**	**38.57**
-10	0.04641	2.377E+07	41.76		**-10**	**0.04641**	**2.383E+07**	**41.89**
-10	0.02154	1.681E+07	43.96		**-10**	**0.02154**	**1.684E+07**	**44.06**
-10	0.01	1.159E+07	46.86		**-10**	**0.01**	**1.160E+07**	**46.93**
-20	10	3.456E+08	16.43		**-20**	**10**	**3.622E+08**	**17.24**
-20	4.641	2.987E+08	18.47		**-20**	**4.641**	**3.108E+08**	**19.25**
-20	2.154	2.536E+08	20.39		**-20**	**2.154**	**2.622E+08**	**21.12**
-20	1	2.156E+08	22.20		**-20**	**1**	**2.217E+08**	**22.86**
-20	0.4641	1.738E+08	24.35		**-20**	**0.4641**	**1.776E+08**	**24.93**
-20	0.2155	1.406E+08	26.23		**-20**	**0.2155**	**1.431E+08**	**26.73**
-20	0.1	1.122E+08	28.42		**-20**	**0.1**	**1.138E+08**	**28.85**
-20	0.04642	8.745E+07	30.13		**-20**	**0.04642**	**8.837E+07**	**30.49**
-20	0.02154	6.887E+07	33.10		**-20**	**0.02154**	**6.942E+07**	**33.40**
-20	0.01	5.204E+07	35.47		**-20**	**0.01**	**5.235E+07**	**35.71**
-30	10	5.447E+08	10.68		**-30**	**10**	**5.883E+08**	**11.55**
-30	4.641	4.968E+08	12.35		**-30**	**4.641**	**5.325E+08**	**13.26**
-30	2.154	4.456E+08	14.03		**-30**	**2.154**	**4.739E+08**	**14.94**
-30	1	3.981E+08	15.64		**-30**	**1**	**4.204E+08**	**16.53**
-30	0.4641	3.404E+08	17.54		**-30**	**0.4641**	**3.564E+08**	**18.39**
-30	0.2155	2.920E+08	19.53		**-30**	**0.2155**	**3.035E+08**	**20.33**
-30	0.1	2.471E+08	21.21		**-30**	**0.1**	**2.553E+08**	**21.94**
-30	0.04642	2.016E+08	19.72		**-30**	**0.02154**	**1.713E+08**	**26.50**
-30	0.02154	1.678E+08	25.91		**-30**	**0.01**	**1.375E+08**	**27.94**
-30	0.01	1.352E+08	27.44		**-40**	**10**	**8.199E+08**	**7.25**
-40	10	7.369E+08	6.52		**-40**	**4.641**	**7.651E+08**	**8.72**
-40	4.641	6.926E+08	7.89		**-40**	**2.154**	**7.105E+08**	**10.06**
-40	2.154	6.477E+08	9.16		**-40**	**1**	**6.515E+08**	**11.53**
-40	1	5.985E+08	10.58		**-40**	**0.4641**	**5.842E+08**	**13.01**
-40	0.4641	5.414E+08	12.05		**-40**	**0.2155**	**5.154E+08**	**15.10**
-40	0.2155	4.821E+08	14.11		**-40**	**0.1**	**4.547E+08**	**16.54**
-40	0.1	4.287E+08	15.57		**-40**	**0.04642**	**3.903E+08**	**18.56**
-40	0.04642	3.712E+08	17.62		**-40**	**0.02154**	**3.456E+08**	**19.65**
-40	0.02154	3.307E+08	18.77		**-40**	**0.01**	**2.903E+08**	**21.43**
-40	0.01	2.798E+08	20.62					

B-27								
T	*f*	*G**	*δ*		***T***	***f***	***G****	***δ***
[°C]	[Hz]	[Pa]	[°]		**[°C]**	**[Hz]**	**[Pa]**	**[°]**
10	10	1.359E+07	52.57		**10**	**10**	**1.360E+07**	**52.65**
10	4.641	8.570E+06	56.26		**10**	**4.641**	**8.576E+06**	**56.32**
10	2.154	5.235E+06	59.63		**10**	**2.154**	**5.237E+06**	**59.67**
10	1	3.116E+06	62.79		**10**	**1**	**3.117E+06**	**62.81**
10	0.4641	1.812E+06	65.71		**10**	**0.4641**	**1.813E+06**	**65.72**
10	0.2154	1.026E+06	68.16		**10**	**0.2154**	**1.026E+06**	**68.17**
10	0.1	5.713E+05	70.30		**10**	**0.1**	**5.714E+05**	**70.30**
10	0.04641	3.178E+05	72.26		**10**	**0.04641**	**3.178E+05**	**72.27**
10	0.02154	1.791E+05	73.88		**10**	**0.02154**	**1.791E+05**	**73.88**
10	0.01	1.045E+05	74.73		**10**	**0.01**	**1.045E+05**	**74.74**
0	10	6.762E+07	37.02		**0**	**10**	**6.813E+07**	**37.35**
0	4.641	4.895E+07	40.27		**0**	**4.641**	**4.920E+07**	**40.52**
0	2.154	3.443E+07	43.61		**0**	**2.154**	**3.455E+07**	**43.80**
0	1	2.353E+07	47.03		**0**	**1**	**2.359E+07**	**47.17**
0	0.4641	1.561E+07	50.49		**0**	**0.4641**	**1.563E+07**	**50.59**
0	0.2154	1.007E+07	53.93		**0**	**0.2154**	**1.008E+07**	**54.00**
0	0.1	6.348E+06	57.29		**0**	**0.1**	**6.351E+06**	**57.33**
0	0.04641	3.906E+06	60.48		**0**	**0.04641**	**3.907E+06**	**60.50**
0	0.02154	2.333E+06	63.47		**0**	**0.02154**	**2.333E+06**	**63.48**
0	0.01	1.366E+06	66.33		**0**	**0.01**	**1.366E+06**	**66.34**
-10	10	2.282E+08	22.57		**-10**	**10**	**2.350E+08**	**23.29**
-10	4.641	1.877E+08	25.00		**-10**	**4.641**	**1.922E+08**	**25.65**
-10	2.154	1.500E+08	27.70		**-10**	**2.154**	**1.528E+08**	**28.26**
-10	1	1.180E+08	30.46		**-10**	**1**	**1.197E+08**	**30.95**
-10	0.4641	8.930E+07	33.37		**-10**	**0.4641**	**9.023E+07**	**33.76**
-10	0.2154	6.656E+07	36.37		**-10**	**0.2154**	**6.705E+07**	**36.69**
-10	0.1	4.859E+07	39.64		**-10**	**0.1**	**4.885E+07**	**39.89**
-10	0.04641	3.428E+07	43.70		**-10**	**0.04641**	**3.439E+07**	**43.89**
-10	0.02154	2.372E+07	46.32		**-10**	**0.02154**	**2.377E+07**	**46.45**
-10	0.01	1.586E+07	50.40		**-10**	**0.01**	**1.588E+07**	**50.50**
-20	10	4.466E+08	12.95		**-20**	**10**	**4.751E+08**	**13.80**
-20	4.641	3.976E+08	14.81		**-20**	**4.641**	**4.199E+08**	**15.66**
-20	2.154	3.486E+08	16.86		**-20**	**2.154**	**3.654E+08**	**17.70**
-20	1	3.020E+08	19.02		**-20**	**1**	**3.144E+08**	**19.83**
-20	0.4641	2.525E+08	21.35		**-20**	**0.4641**	**2.610E+08**	**22.10**
-20	0.2155	2.091E+08	23.63		**-20**	**0.2155**	**2.148E+08**	**24.31**
-20	0.1	1.708E+08	26.24		**-20**	**0.1**	**1.745E+08**	**26.85**
-20	0.04642	1.363E+08	29.86		**-20**	**0.04642**	**1.386E+08**	**30.40**
-20	0.02154	1.058E+08	31.80		**-20**	**0.02154**	**1.072E+08**	**32.25**
-20	0.01	8.039E+07	35.17		**-20**	**0.01**	**8.113E+07**	**35.55**
-30	10	6.425E+08	7.27		**-30**	**10**	**7.046E+08**	**7.98**
-30	4.641	6.031E+08	8.70		**-30**	**4.641**	**6.573E+08**	**9.49**
-30	2.154	5.610E+08	10.16		**-30**	**2.154**	**6.074E+08**	**11.01**
-30	1	5.122E+08	11.81		**-30**	**1**	**5.504E+08**	**12.70**
-30	0.4641	4.570E+08	13.54		**-30**	**0.4641**	**4.869E+08**	**14.44**
-30	0.2155	4.054E+08	14.14		**-30**	**0.1**	**3.738E+08**	**18.35**
-30	0.1	3.562E+08	17.46		**-30**	**0.02154**	**2.643E+08**	**23.64**
-30	0.04642	2.896E+08	17.11		**-30**	**0.01**	**2.197E+08**	**25.09**
-30	0.02154	2.557E+08	22.82		**-40**	**10**	**9.035E+08**	**4.58**
-30	0.01	2.138E+08	24.38		**-40**	**4.641**	**8.690E+08**	**5.50**
-40	10	8.033E+08	4.07		**-40**	**2.154**	**8.358E+08**	**6.52**
-40	4.641	7.760E+08	4.91		**-40**	**1**	**7.856E+08**	**7.68**
-40	2.154	7.496E+08	5.84		**-40**	**0.4641**	**7.341E+08**	**8.89**
-40	1	7.091E+08	6.93		**-40**	**0.1**	**6.169E+08**	**12.11**
-40	0.4641	6.670E+08	8.07		**-40**	**0.04642**	**5.701E+08**	**13.46**
-40	0.2155	6.167E+08	8.23		**-40**	**0.02154**	**5.047E+08**	**15.69**
-40	0.1	5.693E+08	11.16		**-40**	**0.01**	**4.227E+08**	**19.04**
-40	0.04642	5.294E+08	12.48					
-40	0.02154	4.728E+08	14.68					
-40	0.01	4.005E+08	18.01					